Ammonia Removal from Industrial Wastewater - Analysis of Photochemical Reactor Performance

By

Lingling Liu

B. Eng. In Environmental Monitoring

Chengdu University of Science & Technology

A thesis submitted to

the Faculty of Graduate Studies and Research

As partial fulfillment of the requirements for the

Master of Engineering Degree

in Ottawa-Carleton Institute for Civil Engineering

Carleton University

Ottawa, Ontario, Canada

August, 1999

National Library of Canada
Acquisitions and Bibliographic Services
395 Wellington Street
Ottawa ON K1A 0N4
Canada

Bibliothèque nationale du Canada
Acquisitions et services bibliographiques
395, rue Wellington
Ottawa ON K1A 0N4
Canada

Your file Votre référence

Our file Notre référence

0-612-57718-X

Canada

Abstract

Photochemical degradation processes are playing an increasingly important role in industrial wastewater treatment, but most applications reported in the literature mainly relate to the removal of organic contaminants, and very little work is reported on the removal of ammonia nitrogen. An advanced photooxidation process for ammonia removal has been extended from a conventional batch reactor to a custom-modified recirculation reactor and further to a new film-type flow reactor. The primary objective in this work is to establish the performance of these reactors under different operating conditions and to compare the product distribution and relate this information to the possible effect of the flow pattern under different reactor configurations.

Experimental results have indicated that both oxidant type and reactor configuration have significant effect on the course of photooxidation process. Reaction schemes have been proposed to explain the possible pathways of the photooxidation process of ammonia degradation. The overall kinetics model is shown to be in good agreement with the experimental results.

The investigation of various operating variables in the new film-type flow reactor includes UV dose, initial ammonia concentration, reactant molar ratio, pH and flowrate. It is found that pH and flowrate are the most important process parameters. Ammonia degradation occurs significantly only in alkaline solutions, and the larger the residence time, the higher the UV dose, and higher is the removal efficiency.

Acknowledgement

I would like to express my deep gratitude and thanks to my supervisor, Professor S. Sridhar, Carleton University, for his guidance, support, and helpful criticism during the progress of this work. Without the intellectual instructions and patient corrections from Professor Sridhar, I would not have completed the thesis for my Master's degree.

I want to thank Dr. D. Gould, CANMET, for arranging the use of CANMET's laboratories for chemical analysis. I would like to thank Mr. J. Graham and Mr. J. Chaulk in CANMET, for their technical and analytical support with Gas Chromatography. Thanks are also extended to Mr. F. Cassalman and Mr. T. O'Neil, Chemistry Department, Carleton University, for their efficient assistance in the use of Ion Chromatography.

I am indebted to Ms. D. Richardson and Mr. P. Trudel, Civil Engineering Department, Carleton University, and Mr. I. Philips and Mr. L. Boissonneault, Science and Technology Center, Carleton University, for their technical support and assistance in the construction of the experimental apparatus.

I am deeply grateful to my friends P. Kumar, W. Dai and H. Liu, for their invaluable encouragement and endless help on my thesis work.

The financial support for this work provided by ESTAC and NSERC through an industrial research grant to Professor Sridhar is gratefully acknowledged.

Last but not the least, I wish to express my special thanks to my husband, Feijun Ma, for being a constant source of understanding, emotional support and encouragement during the past two years.

Table of Contents

List of Figures

List of Tables

List of Appendices

Glossary

Symbols

A	absorbance of the medium,dimensionless
A	a molecule of reactant
A^*	an electronically excited state of a reactant molecule
B_1, B_2	products of the dissociation of a reactant, which can be atoms or free radicals
c	velocity of light, $m.s^{-1}$
c	molar concentration of the medium, $mol.L^{-1}$ (M),
C, C_i	concentration of the absorbing species, $mol.L^{-1}$
C_0	initial concentration, $mol.L^{-1}$
$C_{i,\ in}$	inlet concentration of substance i in recirculation reactor, $mol.L^{-1}$
$C_{i,\ out}$	outlet concentration of substance i in recirculation reactor, $mol.L^{-1}$
C, D	stable molecules other than the absorbing species
E	activation energy, $kcal.mol^{-1}$
E	energy of a quantum, ergs
E	product molecule
F	fraction of UV light absorbed by hydrogen peroxide, dimensionless
G_0	is the total incident UV light flux, $Einstein.s^{-1}$
h	Planck's constant, 6.6237×10^{-37} erg-s
H	thickness of the water film, m
I_{abs}	intensity of the absorbed light, $Einstein.s^{-1}cm^{-2}$,
I_0	intensity of the incident monochromatic light, $Einstein.s^{-1}cm^{-2}$

I	intensity of the transmitted light, Einstein.$s^{-1}cm^{-2}$
I_a	volumetric rate of light absorption, Einsteins.$s^{-1}cm^{-3}$
I_{r0}	light intensity at the inner radius, Einsteins.$s^{-1}cm^{-2}$
I_r	light intensity at the radial distance of r, Einsteins.$s^{-1}cm^{-2}$
I_λ	incident light intensity, Einsteins.$s^{-1}cm^{-2}$
k_0	frequency factor
k, k_1, k_2, k_3	
k', k_1', k_2', k''	
k_A, k_H, k_r	rate constants, $M^{1-n}s^{-1}$
K_b	basicity constant, the equilibrium constant of a reaction in which a base accept proton from water, dimensionless
l	path length penetrated by the incident light, cm
L	length of the radiating area on the cylinder surface, m
M	a molecule or the surface of the reaction vessel
nm	nanometer, unit of wavelength, 1.0×10^{-9} m
N	a constant given by (2R+H).H.L/2, m^3
Q	recirculation rate, m^3s^{-1}
Q	volumetric flow rate, m^3s^{-1}
r_0	inner radius of the reactor vessel, m
r	radial distance of the reactor vessel, m
r_A	local reaction rate of ammonia in the reactor, mol.$cm^{-3}s^{-1}$
r_1	reaction rate of hydrogen peroxide in the primary process, mol.$cm^{-3}s^{-1}$
r_i	reaction rate of the reacting species

R	radius of the cylinder, m
R	ideal gas law constant, 1.987 $cal.mol^{-1}$ °K
T	temperature, °K
V	total irradiated volume, m^3
X	irradiation time, hr
Y	ammonia removal percentage, %

Greek letters

α, α_λ	molar absorption coefficient or absorptivity, cm^2mol^{-1}
$\bar{\alpha}$	average molar absorption coefficient, cm^2mol^{-1}
ε	molar extinction coefficient, $M^{-1}cm^{-1}$,
λ, λ_1, λ_2	wavelength of light, m
θ_H	hydraulic residence time of the reactor
$\Delta\theta$	radian of the element volume, radian
ΔV	volume of the element volume, m^3
∇C_A	concentration gradient of ammonia, $mol.cm^{-4}$
ϕ	quantum yield, $mol.Einstein^{-1}$
Φ	overall quantum yield, $mol.Einstein^{-1}$
μ, μ_λ	attenuation coefficient which is a function of wavelength λ, cm^{-1}
ν	frequency of light radiation, s^{-1}
v	transportation velocity of reacting fluid, $cm.s^{-1}$
$\bar{\nu}$	wavenumber, cm^{-1}

Abbreviations

APP	Advanced Photo-oxidation Processes
GPM	US gallons per minute
MAP	Modified Advanced Photo-oxidation Processes
NTU	Nephelometric turbidity unit
RPM	Revolutions per minute
RPR	Rotospray Photolytic Reactor
UV	Ultraviolet

Chapter 1

Introduction

1.1 General

The presence of large amounts of ammonia in wastewater can bring about serious environmental problems, such as eutrophication and dissolved oxygen depletion in the receiving water body, leading to the destruction of the living environment of aquatic organisms. The existence of ammonia in drinking water is a danger to human health because of its corrosive alkali nature and toxicity, which have detrimental effects on metabolic processes. As a potential source of nitrate and nitrite, ammonia is further related to serious diseases such as methemoglobinemia, carcinoma etc.[1]

In view of the harmful effects of ammonia, federal and provincial governments have issued various guidelines to regulate the concentration of ammonia in dischargeable industrial wastewater as well as in drinking water. For instance, the Ontario Ministry of Environment, regulates that nitrogen in mine and mill effluents should not exceed 10 mg/L N in the form of ammonia, [5] and the concentration of ammonia nitrogen in surface waters should not exceed 0.02 mg/L. [2]

The removal of ammonia from industrial wastewater prior to its discharge into natural water system is necessary in order to preserve proper water quality for normal aquatic life. Methods for the removal of ammonia proposed by former researchers include air stripping, membrane separation, breakpoint chlorination, ion exchange and

nitrification/denitrification. All these methods have different pros and cons which will be addressed later in detail.

Some pollutants in wastewater can be destroyed by strongly absorbing UV light which degrades them into simple components. This process is called direct photodegradation. However, many of the contaminants absorb UV light weakly and the above process is not effective. In recent years, a set of new technologies, called Advanced Photooxidation Processes (APP) have emerged, which are capable of converting certain types of pollutants in water into environmentally benign substances. APP are based on oxidative reactions initiated by hydroxyl radicals (•OH) which are frequently generated by the photolysis of hydrogen peroxide. [3, 4] UV/H_2O_2 is a typical APP system. The applications of APP as reported in the literature, however, have primarily been focused on the destruction of organic contaminants. In the present study APP is applied to remove ammonia nitrogen in wastewater.

1.2 Objectives and scope

1.2.1 Objectives

An APP developed by Sridhar et al, [67] has been found to be feasible in the destruction of ammonia in the presence of oxidants under certain conditions, and extensive batch reactor data has been obtained earlier.

The overall objective of the work presented here is to extend this method from conventional batch reactor to a custom-modified recirculation reactor and further to a new film-type flow reactor. The primary objective in this work is to establish the performance of these reactors under different operating conditions and to compare the

product distribution and relate this information to the possible effects of the reactor configurations. Particular emphasis is placed on the investigation of the effects of different operating variables. Another important objective of this study is to incorporate the reaction kinetic model developed earlier in the performance evaluation of these reactors, and to establish the performance characteristics of the different reactor systems.

1.2.2 Scope

The original research project, viz, the development of a novel, combined photolytic biological process for the removal of ammonia from industrial wastewater, is divided into two phases:

In phase I, a modified advanced photooxidation process is investigated for the destruction of ammonia by chemical tailoring and photo-oxidation. Highly reactive hydroxyl radicals are produced from photo-dissociation of hydrogen peroxide or other substituted oxidants. Ammonia is then oxidized by the strong oxidant species (•OH).

In phase II, the product distribution from the phase I is studied to determine the necessity of combining the photolytic process with subsequent biological denitrification process in order to reach the complete removal of ammonia. Figure 1.1 illustrates the whole photolytic-biological process.

The present study is focused mostly on phase I, which is the critical step in the combined photolytic-biological process. A new type of flow reactor is designed, assembled and operated to carry out the experimental study. Based on the preliminary work, investigation of the feasibility of the photooxidation process is extended from batch reactor (commercially available Rayox Advanced Oxidation System) to a custom–

modified recirculation reactor system and further to the new type flow reactor system. Current work also includes further studies on the selected oxidants. The effects of different operating variables of the new film-type flow reactor are studied in detail, such

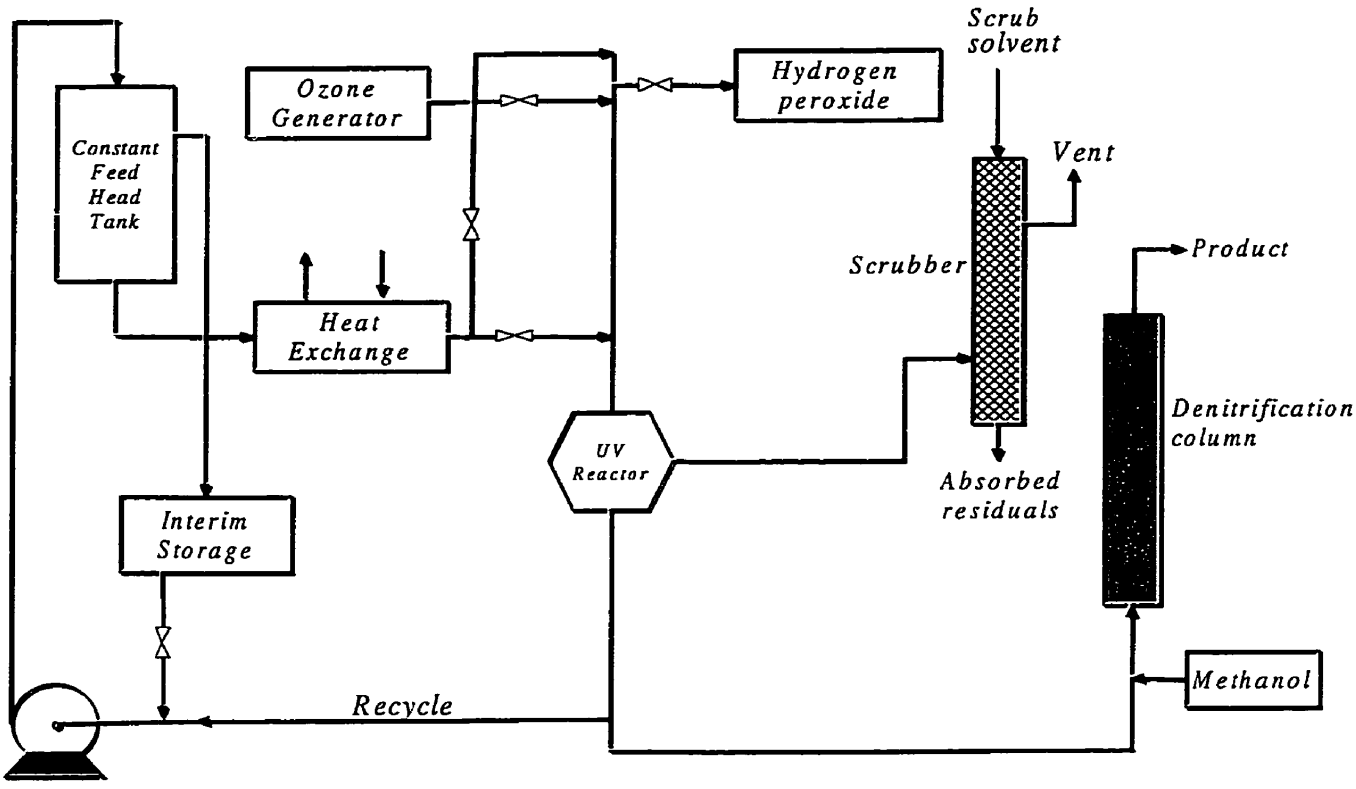

Figure 1.1 Schematic diagram for combined photolytic-biological process: Modified Advanced Photo-oxidation (MAP) Process

as the input power, irradiation time, pH, initial concentration of reactants etc. Finally an overall kinetics reaction model is proposed to illustrate the mechanism of the photooxidation process of ammonia removal and performance comparisons are made on the different reactors.

1.3 Structure of the thesis

The rest of this thesis is comprised of six chapters.

Chapter 2 provides an overview of the basic properties of ammonia, the sources and environmental impact of ammonia, concentration of ammonia in water and wastewater and related guidelines, the existing technologies and their limitations, and the necessity for developing a new methodology to remove ammonia

Chapter 3 presents an overview of the properties of UV radiation and of certain important UV related processes. It also summarizes the photochemical property of several nitrogenous and oxidizing compounds related with the present study.

Chapter 4 discusses different photochemical reactors developed by previous researchers and elucidates the design process of a new film- type flow reactor in this study.

Chapter 5 describes the specific experimental chemicals, apparatus, procedures and sample analysis methods.

Chapter 6 presents the results obtained from this study. A detailed discussion of process variables, reaction schemes and mechanisms, and kinetic models are presented.

Chapter 7 presents the conclusions drawn from the current work. A list of new issues and guidelines for future work are also presented.

Chapter 2

Literature review

2.1 Basic properties of ammonia

Ammonia (NH_3) is a colorless, alkaline gas at ambient temperature and pressure, with a distinct pungent odor. Ammonia is very soluble in water, and the solubility is approximately 90 g per 100 ml of distilled water at 0°C. [1] In aqueous solution, ammonia (un-ionized) exists in equilibrium with ammonium ion (NH_4^+, ionized) according to the following equation:

$$NH_3 + H_2O \longrightarrow NH_4^+ + OH^- \qquad pK_b = 4.75 \qquad (2\text{-}1)$$

Thus, the concentration of ammonia or ammonium ion in water is a function of temperature and pH value. Figure 2.1 is the relative distribution of these two components in water at 25°C. The concentration of unionized ammonia increases with increasing pH at specific temperature.

Ammonia can react with acids vigorously. It can also undergo oxidation in aqueous medium with some common oxidants, such as O_2, O_3, Cl_2, peroxides, etc.

2.2 Ammonia sources

Natural sources of ammonia include groundwater, gas exchange with the atmosphere, chemical and biochemical degradation of nitrogenous substances, and the

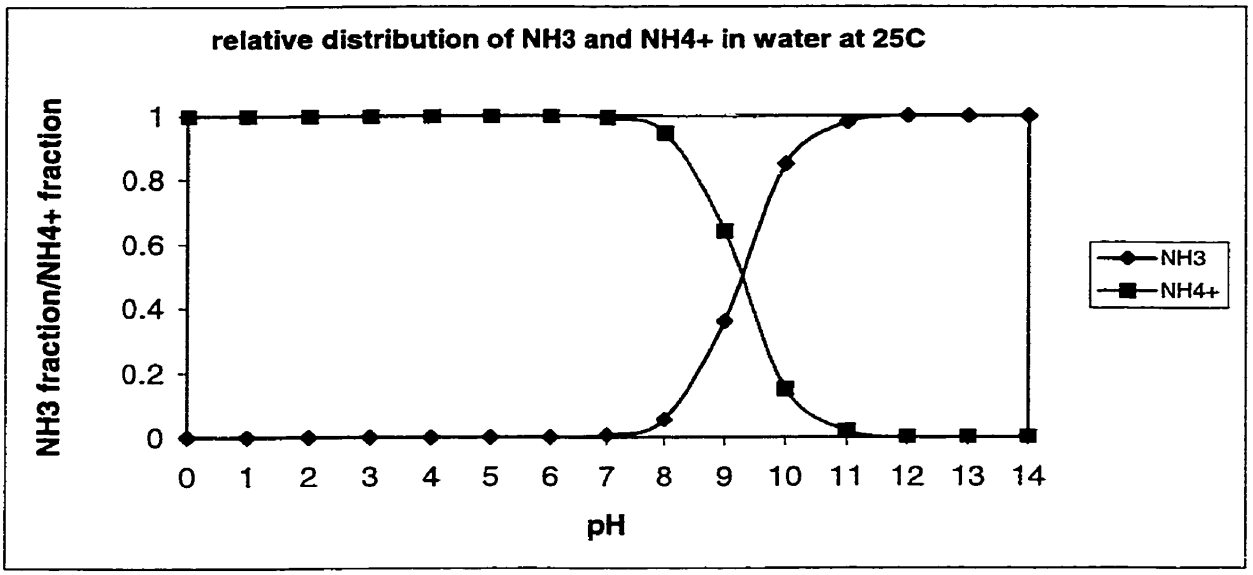

Figure 2.1 Relative distribution of NH_3 and NH_4^+ in water at 25°C

excretion of ammonia by biota. In the metabolism of proteins and amino acids, many heterotrophic bateria, actinomycetes, and fungi present in soil and water excrete the excess nitrogen in the form of ammonia. [5, 6] Ammonia is also produced during the nitrogen fixation processes of dissolved nitrogen gas in water.

Commercially, ammonia is synthesized by the so-called Haber process. In this process, hydrogen and nitrogen react at high temperatures and pressures and in the presence of catalyst according to the reversible reaction:

$$N_2 + 3H_2 \rightleftharpoons 2\,NH_3 \qquad (2\text{-}2)$$

This industrially produced ammonia is extensively used in the manufacturing of chemical products such as fertilizers, explosives, nitric acid and plastics. It is also used in refrigeration plants and petroleum refineries. Ammonium salts are widely used in food

industry such as baked goods, candies, gelatin, fats, oils, jellies, cheese, processed fruits and beverages. As would be expected, the waste discharged from these industries constitute an important source of ammonia. In addition, distillation and combustion of coal also release additional quantities of ammonia into environment.

Mining industry contributes to a large proportion of ammonia produced in the industries. Ammonia in mine and mill water is generated from the degradation of cyanide as in the case of gold mill effluents, from the use of nitrogen-containing reagents as in the ore processing and extractive metallurgy, and from the use of ammonium-containing explosives in mines.

Modern commercial explosives in the mining industry generally contain a fuel and an oxidizer. These oxidizing agents are typically ammonium nitrate, calcium nitrate and sodium nitrate, constituting a great source of ammonia. [7]

2.3 Environmental impact of ammonia

The existence of ammonia in water can cause some challenging environmental problems. Ammonia is toxic to fish and other aquatic life because it reduces the oxygen carrying capacity of the blood. Ammonia toxicity is related to the amount of ammonium ion and is dependent on pH, temperature and dissolved oxygen.

The nutritive properties of ammonia promote excessive growth of algae and other aquatic plants, which in turn decrease the concentration of dissolved oxygen in water and thus deteriorate water quality dramatically.

Ammonia also exerts a high oxygen demand when it is converted to nitrite and nitrate and thus reduces the amount of dissolved oxygen in water. In addition, the nitrite

and nitrate are proven to be health hazards, as they are toxic. The toxicity of nitrate is thought to be due to its reduction to nitrite. Ingestion of nitrite can bring about serious changes in the human body such as methemoglobinemia, carcinoma, and mutation. Some reports suggest that nitrite is associated with congenital malformations. It is also reported that ingesting nitrite-contaminated water lowers down the conditioned motor reflexes of children. [1]

The alkaline nature of ammonia gas is corrosive to eyes, skin and lungs. Ingestion of large dose of ammonia results in headache, insomnia, nausea, diarrhea and a failure in glucose tolerance. A large intravenous dose of ammonia produces immediate hyperventilation and clonic convulsions, followed by either fatal tonic extensor convulsions or gradual onset of coma. Some evidence shows that ammonia could interfere with energy metabolism in the brain. [1]

Ammonia entering the "natural nitrogen cycle" will result in ecosystem nitrogen imbalance leading to soil acidification and nutrient deficiencies, which is the reason for forest dieback.

Guidelines have been proposed to regulate the ammonia discharged in wastewater and the ammonia content in drinking water. Furthermore, removal of ammonia from mine wastewater is considered mandatory before it is discharged as effluent.

2.4 Concentration of ammonia and related guidelines for acceptable limits

Water is a common resource and is widely used in domestic area for drinking, washing, bathing, cooking, waste removal, and yard watering, etc. Water is also used

commercially and industrially, such as coolant in electric-power, steel, oil refining, and chemical industries. Once the water is used, it will ultimately be discharged as wastewater which could destroy the water quality of the receiving water body. Therefore, water quality standards and discharge standards of various wastewater are required in order to maintain the receiving water quality, ensuring its physical, chemical and biological characteristics suitable for intended use. Following is an overview of the related guidelines for the acceptable limits of ammonia and other nitrogenous compounds in water and wastewater.

2.4.1 Municipal effluent quality

The sources of municipal wastewater include water seepage through the collection system pipes and vaults, surface and subsurface storm water entering the collecting system, septage and sludge landfill leachate, and industrial, commercial and institutional wastewater. Domestic wastewater constitutes a large part (about one third) of the municipal wastewater and its quality depends on the lifestyle patterns of the serviced residential customers. For example, minimum domestic flows and pollutant concentrations are observed during the early morning hours while peak flow and pollutant concentrations are typically experienced in the late morning or early afternoon. Table 2.1 displays a typical major pollutant composition of domestic wastewater.

Septage and sludge landfill leachates, which may contain 200 mg/L total nitrogen as N, [9] also contribute to municipal wastewater. Although the municipal plant influent contains high nitrogen concentration, the effluent nitrogen control requirement from municipal treatment plant is site-specific. Typically, the guidelines for nitrogen limits

Table 2.1 Typical major pollutant composition of domestic wastewater [8]

Parameter	Concentration by phase, mg/L		
	Soluble	Particulate	Total
Suspended Solids			
Volatile			190
Inert			50
Total			240
5-day BOD	65	135	200
Chemical oxygen demand	130	260	400
Total nitrogen[1]	20	10	30
Total phosphorus	5	2	7

are based on effluent ammonia concentrations and their objectives are to control dissolved oxygen depletion in the receiving waters due to nitrogenous demand, and to prevent ammonia toxicity to the aquatic life in receiving water.

2.4.2 Industrial effluent quality

The amount of water used in industry constitutes about 42 percent of total municipal water use. [10] It can be assumed that about 85-95 percent of the water used in

[1] 0.02 kg/cap·d (0.04 lb/cap/d) of total nitrogen and 65% soluble, with ammonia nitrogen composing most of the soluble content.

the various industrial operations and processes will become wastewater. This makes it important to stipulate the wastewater effluent from specific industries.

Mining industry

Based on the figures in World Mineral Statistics [11] (1987), the mine productions of minerals and coal in Canada are as follows:

Table 2.2 The production of minerals and coal in Canada (1985)

Category	**Production ($\times 10^3$ kg)**
Nickel	169971
Copper	738637
Zinc	1206683
Lead	284595
Coal	60480000
Total	62879886

The total amount of mine production was reported to be 62,879,886,000 kilograms in 1985. Typically the mine production has to undergo various stages of processing. Amongst them, the processing of ores produces the largest amount of contaminated water. Chemical reagents may be added to separate the minerals from the ground rock, which includes NH_4OH and NH_3 as alkalis. These reagents are then directed to various effluents as inorganic or organic contaminant.

Mine waters also contain ammonia and nitrate resulting from blasting operations. The potential for mixing of ammonia and nitrate into the water system is dependent upon

the specific explosives used, the water conditions, the handling and management of the explosives, and the efficiency of the blasting operation.

Metal Mining Liquid Effluent Regulations of September 20, 1995, issued under the Fisheries Act, restricts deleterious substances in liquid effluents from metal mines. Table 2.3 [12] shows maximum authorized concentrations of certain substances. It should

Tabel 2.3 Authorized levels of substances in mining effluent

Substance	Maximum Authorized Monthly Arithmetic Mean Concentration	Maximum Authorized Concentration in a Composite Sample	Maximum Authorized Concentration in a Grab Sample
Arsenic	0.5 mg/l	0.75 mg/l	1.0 mg/l
Copper	0.3 mg/l	0.45 mg/l	0.6 mg/l
Lead	0.2 mg/l	0.3 mg/l	0.4 mg/l
Nickel	0.5 mg/l	0.75 mg/l	1.0 mg/l
Zinc	0.5 mg/l	0.75 mg/l	1.0 mg/l
Total Suspended Matter	25.0 mg/l	37.5 mg/l	50.0 mg/l
Radium 226	10.0 pCi/l	20.0 pCi/l	30.0 pCi/l

be noted that the concentrations are given as total values with the exception of radium 226 which is a dissolved value after filtration of the sample through a three micron filter. These guidelines are uniformly applied national standards and are intended to provide protection for fish and other aquatic life. Up to date, these regulations do not provide a limit on the concentration of ammonia; however, given the increasing amount of ammonia in the receiving water, it is predicted that new regulations will be enforced in

the near future. Although there are no limits, per se, stated for ammonia, the strict guidelines for the variety of metals imply that pH changes due to ammonia and coordination compounds could cause problems in metal removal processes.

Fertilizer industry

Fertilizer industry produces a large amount of ammonia related compounds. The effluent from fertilizer industry contains mainly three types of nitrogen: ammonia nitrogen, nitrate nitrogen and organic nitrogen. There are 12 nitrogen fertilizer plants in Canada producing around 4.1 billion kilograms of anhydrous ammonia, 1.0 billion kilograms of ammonium nitrate, 2.5 billion kilograms of urea, 0.35 billion kilograms of ammonium sulphate, and 1.0 billion kilograms of nitric acid. The locations and sizes of the fertilizer plant in Canada are shown in Table 2.4. [13] The second column shows the productivity distribution (in percentage) of the different products (present in the first column) in different provinces. The third column is the statistics of productivity.

Table 2.4 Fertilizer plant location and sizes (1987)

Product	Location	Plant size ($\times 10^3$kg/d)
Anhydrous Ammonia	80% Alberta, British Columbia, Manitoba	180-2400
	20% Ontario	225-1100
Ammonium Nitrate	50% Alberta, Manitoba	100-600
	50% Ontario	400-500
Urea	87% Alberta	200-1650
	13% Ontario	300-550
Nitric Acid	37% Alberta, Manitoba	100-600
	63% Ontario	350-850
Ammonium Phosphate	80% Alberta, British Columbia	340-2000
	20% Ontario, New Brunswick	330-800

Because of the potential hazard of these compounds to aquatic life in the receiving stream, effluent limits of these compounds have been established by different provinces, as shown in Table 2.5. [13]

Table 2.5 Effluent limitations for selected pollutants from fertilizer industry

		Limitation		
Industry	Parameter	Alberta	British Columbia	Ontario
Fertilizer And related	Ammonia	35 mg/L Ammonia plants: Existing(2728 L/t) 0.095 kg/454 kg daily average 0.191 kg/454 kg daily maximum grab sample: 0.286 kg/454 kg daily maximum New (1227 L/t) 0.048 kg/454 kg daily average 0.095 kg/454 kg daily maximum grab sample: 0.143 kg/454 kg daily maximum	Marine and fresh water A – 10 mg/L (as N) B – 50 mg/L (as N)	10 mg/L (as N)
	Nitrate	20 mg/L	Marine and freshwaters: A - 10 mg/L B - 50 mg/L	
	Organic nitrogen	10 mg/L	Marine and freshwaters: A - 15 mg/L (Kjeldahl) B - 25 mg/L (Kjeldahl)	

NOTE: Level A is required for all new operations. Level B is required for existing plants within the shortest time technically feasible.

2.4.3 Drinking water quality

The drinking water guidelines recommend limits for physical, chemical, radiological and microbiological characteristics of drinking water in terms of maximum acceptable concentrations. If the concentration of any substance is greater than the limit, drinking water will either produce deleterious health effects or will be aesthetically objectionable. According to the guidelines for Canadian Drinking Water (1978) the maximum acceptable concentration of nitrate as N is 10 mg/L, and that of nitrite as N is 1.0 mg/L. It is recommended that when nitrite and nitrate are present together, the total amount should not exceed 10 mg/L. [14] It should be noted that the concentration of ammonia is not regulated here. One possible reason is that the concentration of ammonia in Canadian drinking water is negligible. Excess nitrate concentration will cause infantile methemoglobinemia because of the conversion from nitrate to nitrite. In addition, nitrate in water can foster undesirable growths of aquatic organisms, such as algae.

2.4.4 Freshwater quality for aquatic life

The freshwater bodies on earth surface constitute an ecosystem, which is comprised of the biological community, the physical and chemical components, and their interactions. Usually the ecosystem reaches equilibrium after evolving over a long period of time and the organisms get adapted to the environment. This ecosystem can become imbalanced by numerous factors. One such factor is the presence of ammonia in the water. A high concentration of ammonia can cause the depletion of dissolved oxygen and the loss of nitrogen balance, thus affecting the ecosystem. To avoid such detrimental

effects, and to protect aquatic life, certain guidelines have been adopted in Canada. Table 2.6 [14] shows the maximum permissible concentration of total ammonia in freshwaters.

The toxicity of un-ionized ammonia varies with pH and temperature, and the portion of total ammonia that is un-ionized also varies with pH and temperature. Table 2.6 gives the equivalent concentration of total ammonia for each combination of temperature and pH to reflect both variations.

Table 2.6 Recommended Guidelines for Total Ammonia (NH_3)

	Ammonia concentration (mg/L) at following temperatures (°C)						
pH	0	5	10	15	20	25	30
6.50	2.5	2.4	2.2	2.2	1.49	1.04	0.73
6.75	2.5	2.4	2.2	2.2	1.49	1.04	0.73
7.00	2.5	2.4	2.2	2.2	1.49	1.04	0.74
7.25	2.5	2.4	2.2	2.2	1.50	1.04	0.74
7.50	2.5	2.4	2.2	2.2	1.50	1.05	0.74
7.75	2.3	2.2	2.1	2.0	1.40	0.99	0.71
8.00	1.53	1.44	1.37	1.33	0.93	0.66	0.47
8.25	0.87	0.82	0.78	0.76	0.54	0.39	0.28
8.50	0.49	0.47	0.45	0.44	0.32	0.23	0.17
8.75	0.28	0.27	0.26	0.27	0.19	0.16	0.11
9.00	0.16	0.16	0.16	0.16	0.13	0.10	0.08

It is recommended that the concentration of nitrite should not exceed 0.06 mg/L. The permissible concentration of nitrate is not specified, but an excessive amount of nitrate is undesirable because it may cause prolific weed growth in fresh water.

2.5 Review of previous studies on ammonia removal

A study of the literature reveals several methods for ammonia removal and some of the more important ones are briefly described below.

2.5.1 Air stripping

This method involves stripping of ammonia gas from wastewater. Normally, the stripping operation is carried out in units similar to those in standard industrial cooling towers. From the top of the tower, water trickles downward over packing materials such as slats, rings, spheres, or corrugated surfaces. Clear air is blown from the bottom counter-currently or cross-currently. Due to a large surface-area-to-volume ratio, ammonia in wastewater is transported to air and the system thus achieves the removal of ammonia from wastewater. [15]

This method is theoretically simple and easy to operate. However, it simply transfers ammonia from one phase to another phase, and the disposal of ammonia remains an issue. This method also has extreme sensitivity to temperature. In addition, because of the equilibrium relationship that exists between the gaseous ammonia (NH_3) and ammonium ion (NH_4^+), ammonia stripping must be done at a relatively high pH, therefore pH adjustment is necessary. The addition of basic substances such as CaO, that

are used to raise pH, may bring about secondary treatment problems and the problem of the cleaning of the stripping tower. An example of this is the reported accumulation of calcium carbonate scale on redwood slats at the South Lake Tahoe advanced wastewater treatment plant (initiated in 1969). The scaling was so severe that treatment process had to be discontinued. [15]

2.5.2 Membrane technologies

In membrane separation, wastewater stream is introduced to the membrane module and is split into two streams, the permeate and the concentrate. The permeate which is the larger part of the two streams by volume, is always a good quality water and can be recycled to the operation or discharged with minimal additional treatment. The concentrate stream contains most of the contaminants.

The removal of ammonium and nitrate ions has been studied [5] from synthetic and actual mine effluents by using nanofiltration (NF) and commercially available reverse osmosis (RO) membranes. RO membranes were found to be more effective in removing these ions as compared to NF membranes and they demonstrated an acceptable performance for the removal of ammonium and nitrate ions from mining effluents.

This method has the advantages of removing both cationic and anionic species to yield good quality water permeate which can be recycled in mining operation. But its degree of separation depends on the size of the ammonia salt molecule. Uncomplexed ammonium hydroxide was not effectively separated while the same membranes can separate larger ammonium complexes (e.g., ammonium iron sulfate complex). Therefore,

the metal constituents and other toxic components concentrated in the retentate stream must be further processed before discharge.

2.5.3 Breakpoint chlorination

Chlorine has found applications in the detoxification of wastewater containing ammonia and other nitrogenous compounds. When chlorine comes in contact with water, hypochlorite (OCl^-) is formed which works as the principal oxidant. The reaction of ammonia with aqueous chlorine results in the formation of mixed chloramines as follows: [16]

$$Cl_2 + H_2O \longrightarrow HOCl + HCl \quad (2\text{-}3)$$

$$NH_3 + HOCl \longrightarrow NH_2Cl + H_2O \quad (2\text{-}4)$$

$$NH_2Cl + HOCl \longrightarrow NHCl_2 + H_2O \quad (2\text{-}5)$$

$$NHCl_2 + HOCl \longrightarrow NCl_3 + H_2O \quad (2\text{-}6)$$

The relative amounts of the three species formed will depend primarily on the pH and the ratio of ammonia to chlorine. At high chlorine-ammonia ratio, Eqn. (2-6) governs the reaction and NCl_3 is the primary product, and when free ammonia is exhausted, chlorine may oxidize the chloramines, for example, according to the following equation:

$$2NH_2Cl + HOCl \longrightarrow N_2(g) + 3H^+ + 3Cl^- + H_2O \quad (2\text{-}7)$$

The above equation illustrates a phenomenon that is called breakpoint chlorination which can be used in ammonia removal. This process can be explained with the help of Fig. 2.2: [16]

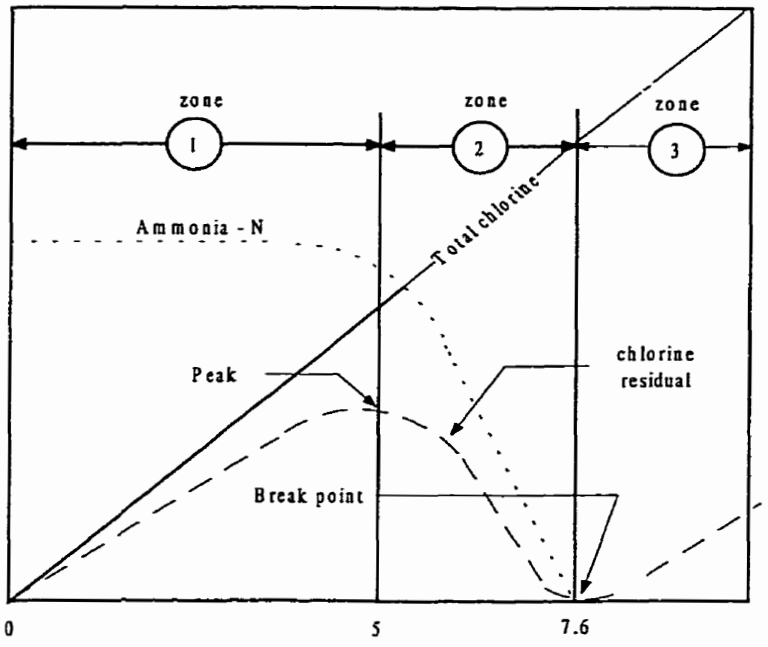

Figure 2.2 Schematic diagram of the breakpoint curve

When the dose of chlorine is in zone 1, which is lower than the peak in the chlorine residual curve, only combined chlorine residuals exist in the system. When dose is in zone 2, which is between peak and valley, the reduction in chlorine residuals is accompanied by the decrease of ammonia. In zone 3, ammonia nitrogen is completely oxidized, and the chlorine residual is composed of only free chlorine. The breakpoint denotes the amount of chlorine to be added into the system in order to achieve complete conversion of ammonia beyond which point free chlorine is obtained.

Although breakpoint chlorination can convert ammonia into environmentally benign substances such as nitrogen, the change in the relative amount of different reacting species with time complicates the process control.

This method requires considerable amount of chlorine. In practice, the dose ratio of Cl_2 : NH_4^+-N, is required to be much higher (mass dose ratio of 15:1) than the theoretical value (mass dose ratio of 7.6:1), resulting in high chemical costs and significant increase in dissolved-solids concentration in wastewater.

A modified method [17] explored is the chlorine-mediated electro-oxidation of ammonia. The procedure consisted of three steps: first ammonia was preconcentrated on an adsorbent such as zeolite or resin, then the loaded adsorbent underwent brine stripping, and finally the strip liquor was electro-oxidized to convert ammonia into nitrogen. This process decreased the chlorine consumption, but disposal of chloride-containing effluent remained a serious environmental concern because residual chlorine is toxic to aquatic organisms, and reactions between chlorine and organic compounds in the receiving water produce a number of known and suspected carcinogens.

2.5.4 Ion exchange

Ion exchange is the process by which ions of a given species are displaced from exchange medium by undesirable ions in wastewater, and thus the removal of undesirable ions is achieved. [10, 15] The exchange medium consists of a solid phase of naturally occurring minerals or a synthetic resin. When the ion exchange system becomes saturated, regeneration is required.

Natural resins, for example zeolites, have been applied in the removal of ammonia from wastewater. The resins are regenerated with lime $Ca(OH)_2$. During regeneration, Calcium ions are re-attached to zeolites and ammonium ions are removed from zeolites.

These ammonium ions are converted to ammonia because of the higher pH of regeneration solution.

The ion exchange process can be expressed by the following equations:

$$CaZ + 2NH_4^+ \rightleftharpoons (NH_4^+)_2Z + Ca^{2+} \quad (2\text{-}8)$$

$$(NH_4^+)_2Z + Ca^{2+} \rightleftharpoons CaZ + 2NH_4^+ \quad (2\text{-}9)$$

$$NH_4^+ + OH^- \rightleftharpoons NH_3 + H_2O \quad (2\text{-}10)$$

Equation (2-8) represents the exchange reaction, Eqn. (2-9) represents elution and regeneration, and Eqn. (2-10) represents the conversion of ammonium ions to ammonia.

The advantage of this system is its performance reliability with fluctuating flow and ammonia concentration. The disadvantages include:

(1) relatively high capital and operating costs.

(2) the formation of calcium carbonate precipitates within the zeolite exchange column, and the disposal of backwash solution if it is utilized to remove the deposits, which is a new problem.

(3) pretreatment such as clarification and filtering of wastewater, if the total suspended solids concentrations are high.

2.5.5 Biological nitrification/denitrification

In this methodology, nitrification and denitrification processes have been coupled together to remove ammonia.

Nitrification

Nitrification is the oxidation of ammonia to nitrate in an aerobic environment by autotrophic ammonia and nitrite oxidizers. The process takes place in two stages:

$$NH_3 \longrightarrow NO_2^- + H^+ \qquad (2\text{-}11)$$

$$NO_{2-} \longrightarrow NO_3^- \qquad (2\text{-}12)$$

The most important factors affecting nitrification in activated sludge [18] are: (1) the retention time of sludge in the aeration tank, which is reciprocal of the specific rate of growth of the nitrifiers, (2) the retention time of sewage, (3) the concentration of dissolved oxygen, (4) the temperature that affects the growth of nitrifiers, (5) the pH value due to the formation of nitrite, producing acid that decreases the buffering capacity of the waste, and (6) inhibitors that increase with the production and use of organic chemicals.

Typical processes for nitrification include [19] (1) trickling filters and rotating biological contactors, in which microbial mass carrying out the nitrification reactions is attached principally to a solid medium, (2) packed-bed systems, in which the bacterial culture is largely attached to the packing column, and (3) suspended-growth nitrification systems, which is based on modified Monod kinetic models.

Denitrification

Denitrification is the reduction of nitrate to nitrogen gas utilizing anaerobic bacteria and an organic food source. [20, 66] The transformation process can be illustrated by the following sequence:

$$2NO_3^- \longrightarrow 2NO_2^- \longrightarrow 2NO \longrightarrow N_2O \longrightarrow N_2 \qquad (2\text{-}13)$$

The energy sources for the denitrification reactions are of two types: exogenous and endogenous. In most of the reported studies on denitrification, methanol has been utilized as both the electron donor and carbon source for bacteria growth. Denitrification requires low oxygen concentration or the absence of oxygen which is contrary to the aerobic condition of nitrification.

Denitrification can remove nitrate over a pH range of 5-10, being most effective in the range of pH 7-8.5. Generally, it is not an unusually pH-sensitive process. Denitrification can occur even at temperature ranges of 5-10 °C, but the rates are slow. The relationship between reaction rate and temperature can be expressed by the Arrhenius equation:

$$k = k_0 e^{-E/RT} \qquad (2\text{-}14)$$

Typical process for denitrification [20] include: (1) packed-bed systems using either coarse-medium as in trickling filters or fine media (2-4 mm), (2) fluidized-bed systems in which the denitrifying bacteria grow on inert-medium particles that are hydraulically kept in a fluidized or suspended state, and (3) suspended growth denitrification processes, which are, in fact, activated-sludge systems operated without aeration.

Nitrification/denitrification process is one of the front-runners. However, the whole process involves living organisms or bacteria, which are sensitive to fluctuations in wastewater conditions. This phenomenon is especially apparent in the nitrification process, where nitrifying bacteria are sensitive to a wide variety of inhibitors such as

organic and inorganic compounds of certain types, concentration of influent ammonia, temperature, pH etc. For example the optimum pH range of nitrification is 8.2-8.6. [21] If pH becomes less than 8.2 or more than 8.6, the process performance drops dramatically. In addition, the organic concentrations must be low for aerobic nitrification reactions, otherwise nitrosomonas and nitrobacter, the primary organisms responsible for the oxidation of ammonia, are not competitive for dissolved oxygen with heterotrophic organisms. Wastewater may require pretreatment to create an environment suitable for biological treatment.

2.5.6 Miscellaneous technologies

Ozonation and ion exchange

Several experiments [22] have been conducted to investigate the combination of ozonation and ion exchange to remove ammonia, nitrite and nitrate. The experimental results indicated that the initial pH of the aqueous solution was crucial to the ammonia removal. The optimal pH range was between 8 and 9.2. They also found that an ozonation process alone was able to completely convert nitrite to nitrate, but could only partially remove ammonia from aqueous solution. To remove nitrate and remaining ammonia, ion exchange resins were found to be necessary and its removal efficiency was found to be high. This method can overcome the limited nitrate removal capabilities of zeolites resin and obtain the simultaneous removal of ammonia and nitrate. However, the disadvantages associated with ion exchange processes are not eliminated.

Ozonation and biofiltering

An improved process [23] was developed for removing ammonia and nitrite by treating the wastewater with ozone and then biofiltering it on a bed of granular carbon. It was shown that the ozonation/granular carbon biofilter were able to remove a quantity of ammonia and nitrite several times larger than that of conventional biofiltration systems employing gravel media. However, the performance of this method was strongly dependent on the fluidization of the carbon bed and the action of ozone on contaminants existing in the wastewater.

2.6 Motivation for the current work

As discussed in the preceding section, each of the ammonia removal processes has one or more limitations. Relatively speaking, nitrification/denitrification seems to be the most promising method because of its high potential removal efficiency and moderate cost. However, in this method, the growth of nitrifying bacteria is rather slow and is often suppressed by heterotrophic competitor, and thus it is difficult to maintain these bacteria in the nitrification process.

A new method reported [24] was to develop a biological ammonia removal process that combined the control of ion exchange and the economy of nitrification. An enriched culture of nitrifying bacteria was co-immobilized with clinoptilolite, a naturally occurring mineral that preferentially exchanged the ammonium ion. This nitrifier/clinoptilolite system took up ammonia in an ion-exchange column and held it for biological recharge during a subsequent aeration cycle. It was demonstrated that the co-immobilized bed remained active through numerous cycles. Although this system improves the efficiency

of nitrification, it is only a modified biological process and it complicates the process operation significantly.

In the work presented here, a new methodology is proposed. It incorporates the development of advanced photo-oxidation processes, which employ a high-energy source to induce hydroxyl radical, initiating a series of chemical reactions that attack and ultimately destroy ammonia in wastewater. Ultraviolet light is used as the high-energy source in this process. In this process, under certain conditions, most of ammonia can be converted into nitrogen. However, if a part of ammonia gets converted to nitrite and nitrate, then the proposed new process will be combined with the denitrification process to obtain complete removal of ammonia. A schematic diagram of the whole process has been presented in Fig. 1.1.

Chapter 3

Principles of photochemistry

A brief review of the principles of photochemistry is necessary to obtain a better understanding of the theoretical background and main principles of the study presented here. This chapter presents an overview of the nature of light, photochemical reactions induced from light absorption, and various light sources to initiate photochemical reaction. Specific emphasis is placed on the UV light applications and photochemical properties of various nitrogenous compounds related to this work.

3.1 Nature of light

It is well known that light is a form of energy. It neither possesses mass nor takes up space. It can be detected only by its effect on matter. Many of the characteristics of light can be explained if light is assumed to travel as an electromagnetic wave.

Different types of light (e.g. radio, infrared, visible light etc.) are distinguished by their wavelength, as are different colors of light in the visible part of the electromagnetic spectrum. For example, red light has a wavelength of about 700 nanometers (nm)[1]. The wavelengths of green and violet lights are approximately 540 nm and 400 nm, respectively. Wavelength can be expressed by the following equation:

---

[1] A nanometer (nm) is 1.0×10^{-9} meters

$$\lambda = \frac{c}{\nu} \tag{3-1}$$

where, c is the velocity of light ($m.s^{-1}$), and ν is the frequency of light radiation (s^{-1}).

A complete electromagnetic spectrum is shown in Table 3.1 and displayed in Fig. 3.1. [71]

Although light can be characterized as a wave, it also behaves like a particle. The elementary particle of light is called photon. Both the wave and particle concepts of light are necessary to explain all the properties.

There is a relationship between the wavelength of a light beam and the amount of energy it carries. As wavelength decreases, the amount of energy it carries, increases. For example, light with a wavelength of 250 nm (ultraviolet light) carries more energy than light of 680 nm (red light). Ultraviolet radiation has enough energy to damage skin cells. It is the ultraviolet component of sunlight that causes sunburn.

The UV spectrum can be divided into three categories: the UVA, that refers to wavelength range of 320 to 400 nm; the UVB, that refers to wavelengths from 280 to 320 nm; and the UVC, that refers to shorter UV wavelengths, usually between 180 to 280 nm.

3.1.1 Planck's quantum theory

Planck's quantum theory provides a relationship between the energy of a quantum and the characteristics of the light radiation, given by the following equation [25]

$$E = h\nu = hc/\lambda \tag{3-2}$$

where,

E = energy of a quantum, ergs

Table 3.1 a complete electromagnetic spectrum table [70]

Region	Approx Range (meters/hertz)	Specific Range
Radio Waves	$10^{8} - 10^{-3}$ m/3 - 10^{10} Hz	
	Ultra-low (ULF)	3 - 30 Hz
	Extremely low (ELF)	30 - 300 Hz
	Voice frequencies (VF)	300 Hz - 3 kHz
	Very low (VLF)	3 - 30 kHz
	low (LF)	30 - 300 kHz
	Medium (MF)	300 kHz - 3 MHz
	High (HF)	3 - 30 MHz
	Very high (VHF)	30 - 300 MHz
	Ultra high (UHF)	300 MHz - 3 GHz
	Super high (SHF)	3 - 30 GHz
	Extremely high (EHF)	30 - 300 GHz
	Shortwave	see MF, HF
	Television	see VHF, UHF
	Microwave	30 cm - 1 mm/1-300 GHz
Infrared	$10^{-3} - 10^{-6}$ m/10^{11} - 10^{14} Hz	
	Far	1000-30 um
	Middle	30-3 um
	Near	3-.75 um
Visible	$5x10^{-7}$ m/$2x10^{14}$ Hz	
	Red	770-622 nm
	Orange	622-597 nm
	Yellow	597-577 nm
	Green	577-492 nm
	Blue	492-455 nm
	Violet	455-390 nm
Ultraviolet	$10^{-7} - 10^{-8}$ m/10^{15} - 10^{16} Hz	
	UV-A	400-320 nm
	UV-B	320-280 nm
	vacuum UV	less than 200 nm
X ray	$10^{-9} - 10^{-11}$ m/10^{17} - 10^{19} Hz	
Gamma ray	$10^{-11} - 10^{-13}$ m/$10^{19} - 10^{21}$ Hz	

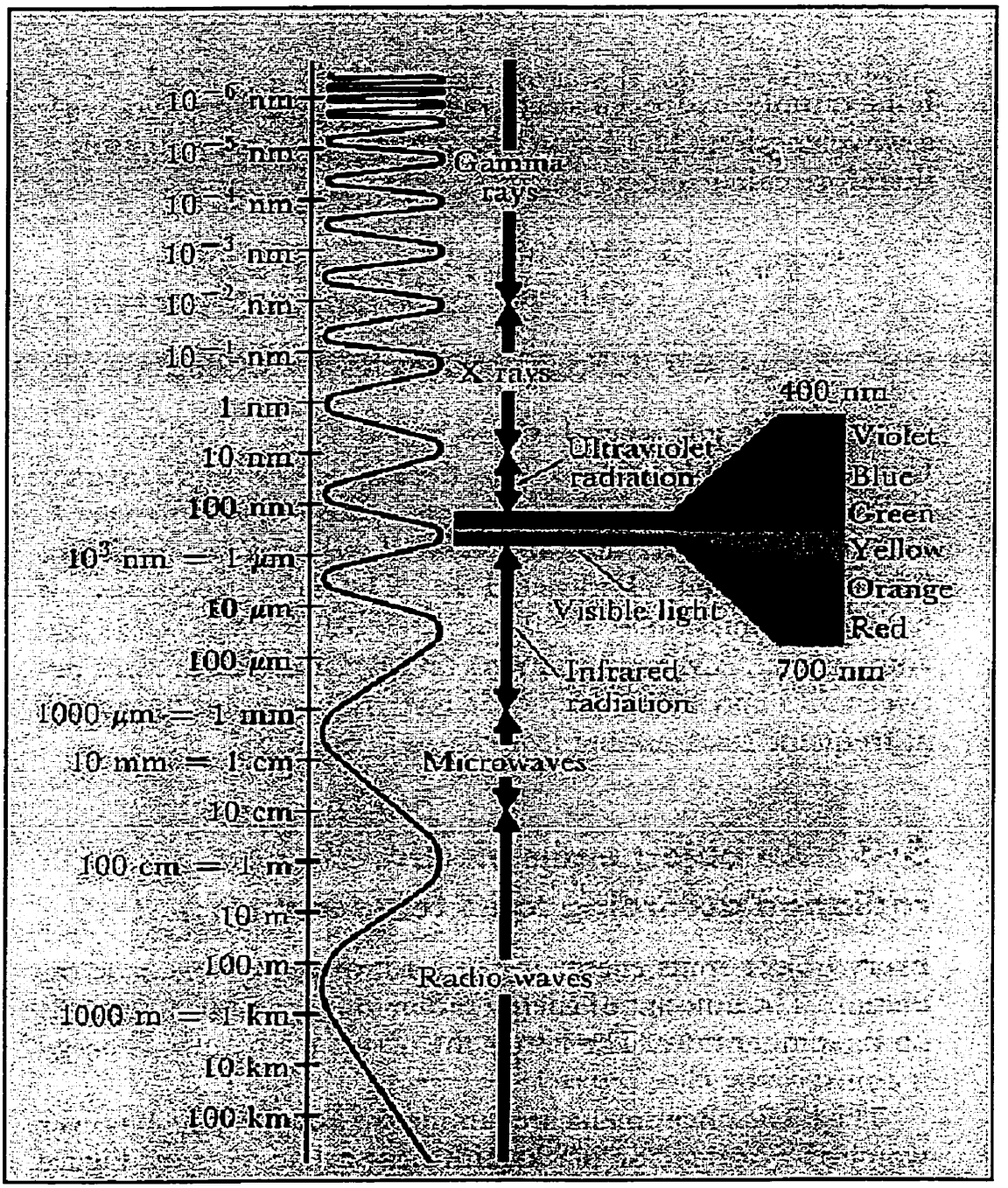

Figure 3.1 The electromagnetic spectrum

h = Planck's constant, 6.6237×10^{-37} erg-s

ν = frequency of the light radiation, s^{-1}

An Einstein is defined as the energy corresponding to one mole of quanta, that is 6.0203×10^{23} quanta. It is given by

$$\text{energy of one Einstein (kcal)} = \frac{2.86\times10^{4}}{\lambda} \qquad (3\text{-}3)$$

where, λ is expressed in nanometer (nm).

Table 3.2 shows the energy contained in one mole of quanta, expressed in kcal, for the spectrum ranging from radio waves to gamma rays.

Table 3.2 Energy spectrum of light radiation [26]

Name	Average wavelength	Energy (kcal/Einstein)
Radio	1000 m	2.86×10^{-8}
Microwave	1 cm	2.86×10^{-3}
Infrared	1-10 μm	28.6-2.86
Visible light		
Red	700 nm	40.8
Orange	620 nm	46.1
Yellow	580 nm	49.3
Green	530 nm	53.9
Blue	470 nm	60.8
Violet	420 nm	68.1
Ultraviolet	230 nm	142.9-95.3
Long X-Ray	30 nm	953
Short X-Ray	0.1 nm	2.86×10^{5}
Gamma Ray	1×10^{-3} nm	2.86×10^{7}

3.1.2 Absorption of light energy

When the light of wavelength λ enters a medium, its incident radiant energy is absorbed according to the Beer-Lambert law given by

$$I_{abs} = I_0 - I = I_0(1 - 10^{-\varepsilon cl}) \quad (3\text{-}4)$$

$$A = \log_{10} I_0/I = \varepsilon cl \quad (3\text{-}5)$$

where,

I_{abs} is the intensity of the absorbed light, Einstein.sec^{-1}cm^{-2}

I_0 is the intensity of the incident monochromatic light, Einstein.sec^{-1}cm^{-2}

I is the intensity of the transmitted light, Einstein.sec^{-1}cm^{-2}

ε is the molar extinction coefficient, M^{-1}cm^{-1}

c is the molar concentration of the medium, M

l is the path length penetrated by the incident light, cm

A is absorbance of the medium

The molar extinction coefficient, ε, is a function of wavelength and of the nature of the chemical species. It controls the probability of quantum-molecule interaction leading to absorption. For a chemical bond to be broken in a molecule, the energy E of a photon must be greater than the bond energy. The relevant photochemical laws are presented next.

3.1.3 Photochemical laws

There are two photochemical laws that describe the basic principles of photochemical processes. The first law of photochemistry [26] states that only the light absorbed by a molecule can be effective in producing photochemical change. It implies that the emitting spectra of the light source must coincide with the absorption spectra for the reactant molecule, at least in the wave length region where emission and absorption are significant.

The second law of photochemistry [27] states that the primary process involved, when a molecule takes part in a light-induced chemical reaction, is the absorption of a single quantum of radiation. That is, the absorption of one quanta of light causes one molecule to react.

3.1.4 Processes after light absorption

When an atom or molecule absorbs light energy in the primary process, the energy can be emitted with a return to the lower energy level, or one of the following processes can occur: [25, 26, 27]

(1) Luminescence, fluorescence or phosphorescence are the two particular aspects, in which the absorbed radiant energy is remitted as UV or visible radiation, usually with a change in wavelength to lower energies.

(2) Physical quenching to a ground state by transferring energy to an inert quencher, which in turn decays to inactive quencher by radiationless processes, for example, by wall collisions.

(3) Chemical quenching or activation by exciting a molecule to higher energy level. This high-energy molecule then undergoes further reactions to form new products. These are called photosensitized reactions,

(4) Chemical quenching by dissociation,

(5) Chemical dissociation of excited molecules, this is the primary process of conventional photoreactions.

As stated by Planck's quantum theory, different light radiations have different energy levels, which cause different changes. For example, energy in the infrared region can cause changes in rotational levels but not in electronic energy levels; in the near infrared, changes in vibrational and rotational energy levels can occur, but this is still inadequate for photoreactions. In electromagnetic spectrum, only the energy levels in the visible and ultraviolet region are sufficient to cause electronic excitation of the light absorber and then initiate photoreactions.

3.2 Photochemical reactions

The photochemical process involves two distinct steps: the absorption of light by a reactant (primary process) and the subsequent chemical reactions, as dictated by the two photochemical laws mentioned earlier.

3.2.1 Primary quantum yield

The primary process of photochemistry is considered to be inclusive of the initial act of absorption and the processes that immediately follow it. The nature of these

following processes is determined by the properties of the initially-excited electronic state. In most cases, the process followed is a dissociation of the absorbing molecule if light radiation ultimately induces chemical reactions: [29]

$$A + h\nu \rightarrow A^* \quad (3\text{-}6)$$

$$A^* \rightarrow B_1 + B_2 \quad (3\text{-}7)$$

where,

A represents a molecule of reactant

A^* represents an electronically excited state

B_1 and B_2 are the products of dissociation, they can be atoms or free radicals.

Primary quantum yield (ϕ) is defined as the number of molecules of reactant consumed for each quanta of light absorbed. ϕ reflects the efficiency of the primary photochemical process and it can not exceed a maximum value of 1.0, which can be derived easily from the second photochemical law.

3.2.2 Overall quantum yield

The secondary process in photochemistry is subsequent chemical reactions. It may include any possible reactions including B_1 and B_2: [29, 25]

(1) Recombination or regeneration producing A

$$B_1 + B_2 + M \rightarrow A + M \quad (3\text{-}8)$$

$$B_1 + C \rightarrow A + D \quad (3\text{-}9)$$

(2) Non-chain reactions

$$B_1 + B_1 \rightarrow C + D \quad (3\text{-}10)$$

$$B_1 + B_1 \rightarrow C \quad (3\text{-}11)$$

$$B_2 + B_2 \rightarrow D \quad (3\text{-}12)$$

$$B_1 + C \rightarrow D \quad (3\text{-}13)$$

$$B_1 + A \rightarrow C + D \quad (3\text{-}14)$$

(3) Chain reactions

$$B_1 + C \rightarrow E + B_2 \quad (3\text{-}15)$$

$$B_2 + D \rightarrow E + B_1 \quad (3\text{-}16)$$

$$B_1 + A \rightarrow C + B_2 \quad (3\text{-}17)$$

$$B_2 + A \rightarrow D + B_1 \quad (3\text{-}18)$$

where,

M represents another molecule or the surface of the reaction vessel,

C and D represent stable molecules other than the absorbing species,

E represents product

Overall quantum yield (Φ) is defined as follows to reflect the extent of secondary reaction:

Φ = number of molecules decomposed or formed/number of quanta absorbed

A large overall quantum Φ indicates chain reactions, whereas a small one indicates recombination or deactivation.

3.2.3 Comparison of photochemical and thermochemical reactions

In photochemical reactions, light of a definite wavelength is absorbed as an energy source. Accordingly, a definite energy level of a molecule is selectively excited and the energy distribution is narrow. Whereas in thermochemical systems, the energy distribution is broad, obeying the Maxwell-Boltzmann distribution. Thus, photochemical reactions possess the property of better selectivity, better feasibility, and fewer side reactions.

In addition, the number of active molecules per unit of absorbed energy in the photochemical systems is greater than that in thermochemical systems, thus high temperature and high pressure are not required in the photochemical reactions. Because of these advantages, photochemical reactions have been applied in many areas such as industrial synthesis which include photochlorination and pharmaceutical preparation, disinfection of air and water, and sterilization of the surfaces of materials. It has also been widely used in photodegradation of pollutants in contaminated water. [27, 29, 30]

3.3 Light sources

A light source for photochemical use must have the following characteristics:

(1) high intensity of the desired wavelength,

(2) long life,

(3) proper physical dimensions for the process under consideration,

(4) stability,

(5) low-cost, minimum amount of necessary auxiliary equipment

(6) facility of operation

As mentioned earlier, UV light has sufficient energy to cause various types of photochemical effects and therefore they find extensive applications. A few sources of UV light are discussed here.

3.3.1 Mercury lamps

When an electrical current is passed between electrodes separated by a gas or vapor, UV radiation is generated. The intensity and wavelength distribution of this radiation are largely dependent upon both the nature of the gas and its pressure. The most widely used gas is mercury, which has following characteristics:

(1) its spectrum is rich in UV region

(2) it is relatively inert and does not react with electrode materials nor attack glass

(3) its vapor pressure lies in a convenient range for lamps which operate near room temperature

A wide variety of mercury lamps are available commercially, which are characterized by gas pressures, determining the kind of radiation generated by the discharge.

Low-pressure mercury lamp

Low-pressure mercury lamps operate at low pressures (about 10^2 torr) and temperatures. The operating temperature is typically 40 °C. These lamps have low power inputs in the range of 20-120 W and long lifetimes ranging from 4,000 to 10,000 h. [28]

About 90 percent of the light output falls around 254 nm, with an electrical efficiency of around 30 percent. There is also a significant output at 185 nm which can be absorbed completely by a thin film of water. Low-pressure lamps are not effective for treatment systems that require light of wavelengths below 254 nm to dissociate. Its major limitation is the low power available, which means that a very large number of lamps would be required to treat wastewater at reasonable flow rates. Thus it will increase the size of system, the capital cost and lamp replacement costs.

Medium-pressure mercury lamp

Medium-pressure mercury lamps operate with more mercury in the bulb, thus they produce higher pressures and temperatures than low-pressure lamps. The bulb temperature is typically in the range of 400-600 °C or higher. Their lifetime is in the range of 3,000-4,000 h. The emitting spectra of medium-pressure lamps spread over a wide range, from UV, visible to IR regions. Typical lines are at 254 nm, 313 nm, 365 nm, 405 nm, 546 nm, 578 nm etc. [27] However, the efficiency in the UV range 200-300 nm is only about 5-20 percent, which is lower than that of low-pressure lamps. This is reflected in the higher electrical power operation costs. The medium-pressure lamp powers available are in a quite large range, from 100 to 60,000 W, thus a smaller number of lamps are required than in low-pressure lamp systems.

High-pressure mercury lamp

As the pressure increases, the spectral lines in medium-pressure lamp systems are broadened and a continuous background appears. The spectral distributions approach that of a continuum type. Typical high-pressure lamp has operating pressure normally ranging from 2 to 110 atm. [27] The operating temperature is so high that water-cooling is necessary. High-pressure mercury lamp has high-energy output, but suffers from limitations such as availability, optimum arc length, necessary cooling methods etc.

3.3.2 Other lamps

Other types of lamps that are available with significant output between 200 nm and 300 nm include pulsed xenon flashlamps and proprietary lamps.[4]

Pulsed xenon flashlamps operate differently from mercury lamps. They are pulsed rapidly by applying a short intense burst of energy, followed by an off time. Under the current technology, the practical lamp output falling in the wavelength range of 200-300 nm, is around 20 percent for a plasma temperature of about 15,000°K. Since xenon flashlamps must operate at very high current densities, this reduces the lifetime of lamps to 50-500 h, which greatly limits their application.

Proprietary lamps are kinds of modified medium-pressure mercury lamps. They are operated on higher power densities which results in an improved efficiency and spectral emission. The operating temperatures are between 700 to 1,000°C. These lamps have efficient output in the range of 200-300 nm.

3.4 Application of ultraviolet radiation

3.4.1 Advanced Photo-oxidation Processes

Most of the current remediation technologies in wastewater treatment are hampered by the disposal problems because the final products and/or by-products are not environmentally benign substances. Recently, Advanced Photo-oxidation Processes (APP) have emerged as new technologies that are capable of converting the pollutants into harmless chemicals. The APP are defined as the oxidation processes in which hydroxyl radicals work as the primary oxidant. They are called oxidation processes because they promote reactions that bring about a nearly complete oxidation of the pollutants to mineral substances. For example, hydrocarbon organic substance can be oxidized into CO_2 and H_2O.

APP processes rely on the generation of hydroxyl radicals (•OH) induced by high-energy sources. UV light photoexcitation has been selected most frequently as the high-energy source. UV light can be used in the following ways.

3.4.2 Direct photolysis

In direct photolysis, the contaminant to be destroyed in wastewater must absorb the incident light and then degrade in its photochemically excited state. This can only occur when the contaminant efficiently absorbs the light and has a reasonable quantum yield. One such example is photodissociation of N-nitrosodimethylamine (NDMA), which has a strong absorption band at 227 nm ($\varepsilon = 7{,}000\ M^{-1}cm^{-1}$). [4] However, in most

cases, the required situation is difficult to achieve under practical conditions, especially when the contaminant absorbs UV light weakly and is present at very low concentration.

In the research work presented here, the direct photolysis of ammonia compounds such as ammonium hydroxide (NH_4OH), ammonium nitrate (NH_4NO_3), and ammonium sulfate ($(NH_4)_2SO_4$) have been studied both in a batch reactor and in a continuous reactor.

3.4.3 Homogeneous photooxidation - UV/oxidant combination

The combination of UV and oxidants is a kind of APP system mentioned earlier. When the wastewater subjected to UV photolysis contains oxidants, hydroxyl radicals (•OH) are formed, which in turn attack pollutants to initiate oxidation. The two major oxidants that are commonly used are hydrogen peroxide and ozone.

UV/H_2O_2 combination

Hydrogen peroxide (H_2O_2) solutions are clear, colorless, water-like in appearance, and can be mixed with water in any proportion. At high concentrations, they have a slightly pungent or acidic odor. Hydrogen peroxide has a molecular weight of 34.02. Other physical and chemical properties of the two standard industrial strengths are shown in Table 3.3. [72]

Table 3.3 Properties of hydrogen peroxide

Property	Industrial strength(wt%)	
	16.5	23.5
Active oxygen content, wt.%	16.5	23.5
Density @ 68°F:		
Specific gravity	1.132	1.196
lbs per gallon	9.45	9.98
gms-100% per mL	0.397	0.598
Apparent pH	2-3	1-2
Acidity, mg/L (as H_2SO_4)	< 50	< 50
Total heavy metals, mg/L	< 1	< 1
Freezing point, °F	-27	-62
Boiling point, °F	226	237
Vapor pressure @ 86°F, mm Hg	23	18
Viscosity:		
@ 32°F, cp	1.81	1.87
@ 68°F, cp	1.11	1.17
Heat of decomposition, cal/gm	233	335
Mole fraction	0.22	0.346

Hydrogen peroxide is unstable, it decomposes into water and oxygen under sunlight or heat. Increasing temperature, increasing pH and the existence of transition metals such as copper, manganese or iron will promote its decomposition.

Hydrogen peroxide absorbs light in the ultraviolet region, with the absorption increasing exponentially as the wavelength decreases from 300 nm to 200 nm. The variation of extinction coefficient (ε) is plotted against the wavelength of UV spectra in Fig. 3.2. It is evident from the graph that the molar extinction coefficient (ε) is 18 $M^{-1}cm^{-1}$ at a wavelength of 254 nm, whereas at a wavelength of 200 nm, the value of ε is 190 $M^{-1}cm^{-1}$, depicting an increase of about ten times.

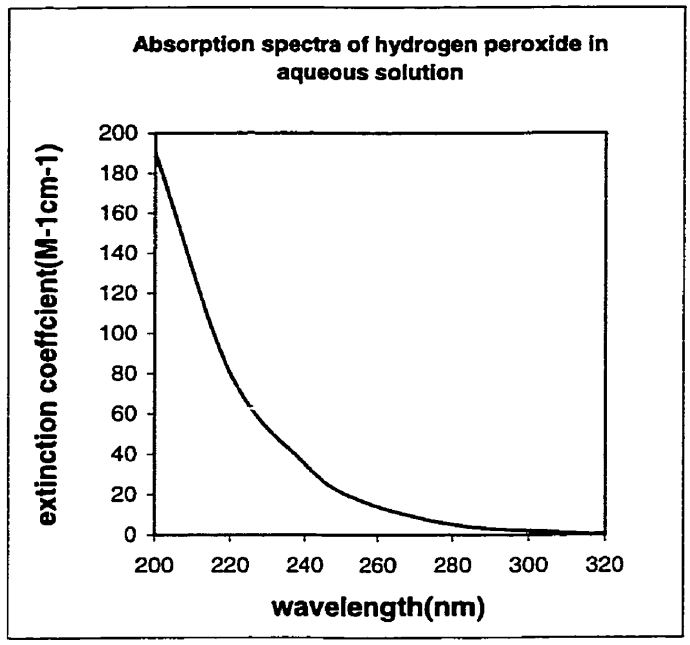

Figure 3.2 Absorption spectra of hydrogen peroxide in aqueous solution

Hydrogen peroxide may experience the following two photolytical decomposition processes:

$$H_2O_2 \xrightarrow{h\nu} 2 \bullet OH \qquad (3\text{-}19)$$

$$H_2O_2 \xrightarrow{h\nu} \bullet H + \bullet HO_2 \qquad (3\text{-}20)$$

The bond energy of HO-OH is 51.0 kcal.mol^{-1}, corresponding to the energy of a radiation of wavelength 560.6 nm. The bond energy of HOO-H is 90.1 kcal.mol^{-1}, corresponding to the energy of radiation of wavelength 317.7 nm. [31] Thus, reaction (3-19) is advantageous from the energy point of view. The subsequent processes may include radical chain reactions in which the propagation cycle gives high quantum yields as follows: [31]

$$\bullet OH + H_2O_2 \rightarrow H_2O + \bullet HO_2 \qquad (3\text{-}21)$$

$$\bullet HO_2 + H_2O_2 \rightarrow O_2 + H_2O + \bullet OH \quad (3\text{-}22)$$

The following termination processes have been suggested [31]:

$$\bullet OH + \bullet HO_2 \rightarrow H_2O + O_2 \quad (3\text{-}23)$$

$$2\bullet HO_2 \rightarrow H_2O_2 + O_2 \quad (3\text{-}24)$$

$$2\bullet OH \rightarrow H_2O + O \quad (2O \rightarrow O_2) \quad (3\text{-}25)$$

$$2\bullet OH \rightarrow H_2O_2 \quad (3\text{-}26)$$

$$\bullet OH + X \rightarrow \text{interruption of the chain} \quad (3\text{-}27)$$

The produced hydroxyl radical (•OH) is a powerful oxidant which has the following properties: [4]

Table 3.4 Properties of aqueous hydroxyl radical (•OH)

Property	Value
Absorption wavelength (maximum) Molar extinction coefficient	230 nm 530 $M^{-1}cm^{-1}$
PK_a	11.9
E°	1.77 V
Diffusion coefficient	2.3×10^{-5} cm^2s^{-1}
ΔG_f°	13 $kJ.mol^{-1}$
ΔH_f°	-7 $kJ.mol^{-1}$
S_{298}°	96 $J.mol^{-1}K^{-1}$

Through hydrogen abstraction or multiple bond addition, hydroxyl radical can react with many inorganic pollutants and most of the organic pollutants with rate constants ranging from 10^7 to 10^{10} $M^{-1}s^{-1}$. [4] Because of the extreme reactivity of hydroxyl radical (•OH), hydrogen peroxide photochemically reacts with a wide variety of substances, such as aromatic compounds, sulfur and its compounds, halogen derivatives, phosphorus compounds etc. Thus UV/ H_2O_2 combination has found extensive applications in wastewater treatment, such as the treatment of boiler feed makeup water and sugar-containing effluent from bottling plant. In a previous work [32] researchers have studied the kinetics and mechanism of the degradation and mineralization of acetone in dilute aqueous solution sensitized by the UV photolysis of hydrogen peroxide. It can be expected that at a sufficient concentration of hydrogen peroxide and for a sufficiently long irradiation time, the final product from the organic pollutants will be carbon dioxide, water and other inorganic substances. However, only a few studies have reported the application of UV/ H_2O_2 on ammonia removal. Ogata et al [33] have investigated the photooxidation of ammonia with aqueous hydrogen peroxide and proposed a mechanism for the oxidation processes.

UV/O_3 combination

Ozone (O_3) is a very powerful disinfecting and deodorizing gas. It consists of oxygen (O_2) with an extra attached oxygen atom. Ozone is created when oxygen is exposed to a high intensity ultraviolet radiation. In fact, the ozone layer in atmosphere has been formed by a similar mechanism.

Ozone reacts with other compounds by giving up and attaching its extra oxygen atom to the compound. Once this happens, the ozone molecule is converted into oxygen ($O_3 - O = O_2$). Thus, the only by-product of ozone is pure oxygen.

In fact, ozone reverts to pure oxygen quite rapidly and naturally. The half life of ozone in air is of the order of hours and of the order of minutes when dissolved in water. Additionally, ozone dissolves over 12 times more readily into water than pure oxygen, then reverts to oxygen, providing high concentration of dissolved oxygen in water.

Ozone has a strong absorption band centered at a wavelength of 254 nm with a molar extinction coefficient of 3300 $M^{-1}cm^{-1}$. Its absorption spectrum is shown in Fig. 3.3. [4]

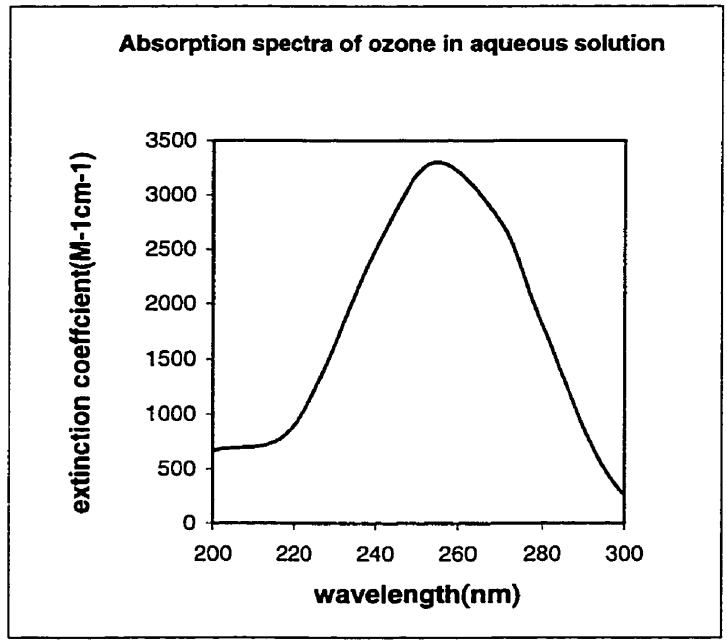

Figure 3.3 Absorption spectra of ozone in aqueous solution

The bond energy of OO-O is 66 kcal.mol^{-1}, thus theoretically, O_3 can dissociate below light of wavelength of 410 nm. The absorption of light by ozone leads to formation of hydrogen peroxide as follows:

$$O_3 \xrightarrow{h\nu} O + O_2 \quad (3\text{-}28)$$

$$O + H_2O \rightarrow H_2O_2 \quad (3\text{-}29)$$

Hydroxyl radicals are then formed by reactions of ozone as follows:

$$H_2O_2 + H_2O \rightarrow H_3O^+ + HO_2^- \quad (3\text{-}30)$$

$$HO_2^- + O_3 \rightarrow \bullet HO_2 + O_3^- \quad (3\text{-}31)$$

$$H_2O + O_3^- \rightarrow \bullet HO_3 + OH^- \quad (3\text{-}32)$$

$$\bullet HO_3 \rightarrow \bullet OH + O_2 \quad (3\text{-}33)$$

The subsequent processes are very similar to those in UV/H_2O_2 system. Hydroxyl radicals are more effective oxidants than ozone. Their oxidizing potentials are 2.87 V, as compared to that for ozone as 2.07 V. The UV/O_3 has been found to be very effective in removing contaminants from wastewater. Under proper conditions, it is possible even to convert refractory species. The usage includes the removal of EDTA from plating plants, polynuclear aromatic hydrocarbons, pesticides, polychlorinated biphenyls etc.

Comparison of UV/H_2O_2 and UV/O_3

Both UV/H_2O_2 and UV/O_3 are APP processes that generate hydroxyl radicals. Table 3.5 presents a comparison of the primary photochemical processes of H_2O_2 and O_3. [4, 39]

It should be noted that the threshold wavelength is the maximum wavelength for which the photon energy matches the bond energy.

Table 3.5 Primary photochemical processes of H_2O_2 and O_3

Absorber	Primary Products	Threshold wavelength(nm)	ε at 254nm ($M^{-1}cm^{-1}$)	Quantum Yield
H_2O_2	2•OH	560.6	18	0.50 at 254 nm 0.30 at 313 nm
O_3	$•O + O_2$	410	3300	0.61 at254 nm

As shown in Table 3.5, ozone has strong absorption in UV region and thus is applicable when contaminants in water also absorb the energy significantly in the UV region.

However, the net result of ozone photolysis is the conversion of ozone into hydrogen peroxide, thus UV/O_3 appears to be an expensive method to prepare hydrogen peroxide. Normally, UV/H_2O_2 is preferred for the generation of hydroxyl radicals.

Although the molar extinction coefficient of hydrogen peroxide is relatively low, it is photolytically active even under long wavelength irradiation (560.6 nm). The other advantages of using hydrogen peroxide over ozone in photooxidation are as follows:

(1) Hydrogen peroxide is available as solution that can be easily added into the aqueous wastewater to give a wide range of accurate, reproducible concentrations. On the other hand, it is not possible to achieve a high concentration of ozone in water, which makes UV/O_3 useful for the treatment of only small quantity of water and wastewater.

(2) There is no gas generation during photodissociation of hydrogen peroxide, as opposed to UV/O_3 system where O_2 gas is released. This can be a serious problem for UV/O_3 system, especially in the treatment of volatile substances, where air stripping of these substances can occur.

(3) The photodissociation of hydrogen peroxide can generate hydroxyl radicals with a high quantum yield and relative cost efficiency.

Based on the above reasons, hydrogen peroxide is selected as oxidant in the present study.

UV/$K_2S_2O_8$ combination

Potassium persulphate has molecular weight of 270.31. Its physical and chemical properties are given in Table 3.6. [73]

Table 3.6 Physical and chemical properties of potassium persulphate

Property	Unit	Value or description
Appearance	-	white powder
Odor	-	odorless
Solubility	g/g	4.7/100 in water
Specific gravity	-	2.48
pH	-	acidic(aqueous solution)
% Volatiles by volume	-	0
@ 21°C (70°F):		
Boiling point	-	not applicable
Melting point	-	100°C (212°F) decomposes completely
Vapor density (Air = 1)	-	9.30
Vapor pressure	mmHg	-
Evaporation rate (BuAc=1)	-	-

Potassium persulphate is unstable. It gradually decomposes to lose oxygen. Decomposition occurs more rapidly at higher temperatures as follows:

$$S_2O_8^{2-} + 2H_2O \rightarrow SO_4^{2-} + 2H^+ + H_2O_2 \quad (3\text{-}34)$$

$$2H_2O_2 \rightarrow 2H_2O + O_2 \quad (3\text{-}35)$$

Potassium persulphate is a strong oxidizing agent in acid medium, the half-cell reaction is:

$$S_2O_8^{2-} + 2e \rightarrow 2SO_4^{2-} \qquad E = +2.0V \quad (3\text{-}36)$$

Potassium persulphate can react with powdered metals, phosphorus, hydrides, organic matter, halogens, acids, alkalis etc. It can oxidize manganese(IV) to permanganate(VII), chromium(III) to dichromate(VI) and vanadium to vanadate. At a very high temperature and pressure, ammonia can be oxidized by potassium persulphate.

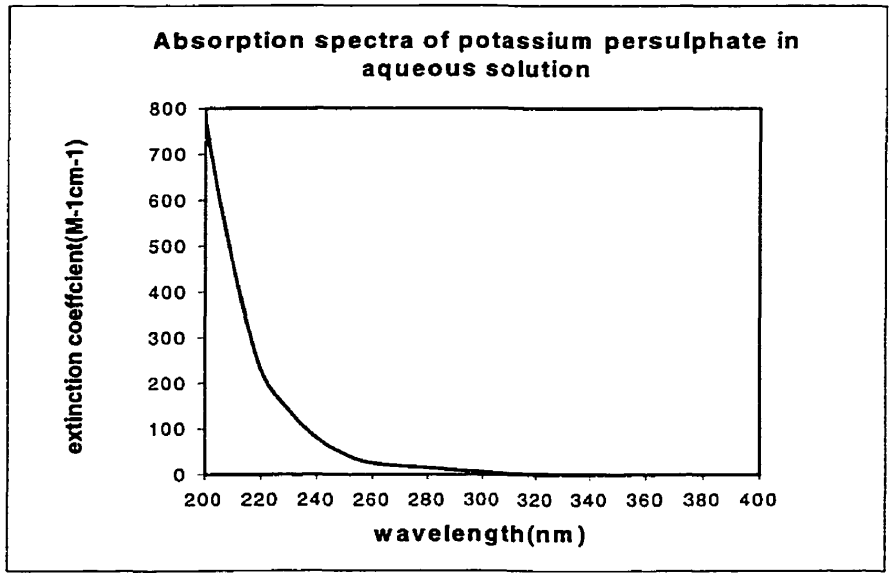

Fig. 3.4 Absorption spectra of potassium persulphate in aqueous solution

Under UV irradiation, potassium persulphate shows an exponentially increasing absorption curve when wavelength decreases from 300 to 200 nm as shown in Fig. 3.4.

The absorption of UV irradiation by potassium persulphate leads to a reaction as follows:

$$S_2O_8^{2-} \xrightarrow{h\nu} 2 \cdot SO_4^- \qquad (3\text{-}37)$$

Persulphate ion dissociates into sulfate anion radical ($\cdot SO_4^-$). In aqueous solution, sulfate anion radical is a very strong oxidant ($E° \cong 2.6V$). It is capable of hydrogen abstraction from water to generate hydroxyl radicals as shown by Eqn. (3-38), and also capable of oxidizing hydroxide ion through electron-transfer to give hydroxyl radicals as shown by Eqn. (3-39).

$$\cdot SO_4^- + H_2O \rightarrow HSO_4^- + \cdot OH \qquad (3\text{-}38)$$

$$\cdot SO_4^- + OH^- \rightarrow SO_4^{2-} + \cdot OH \qquad (3\text{-}39)$$

The subsequent processes are more or less similar to those in UV/H_2O_2 and UV/O_3 system. Hydroxyl radical will further attack the contaminants in wastewater and initiate chain reactions.

In addition, the redox reaction between potassium persulphate and water also occurs upon UV irradiation which generate certain products as expressed by Eqns. (3-34) and (3-35).

Potassium persulphate is chosen as another oxidant in the present study because of the following reasons:

(1) It has relatively strong absorption in UV region compared to that of hydrogen peroxide.

(2) It is commercially available in powdered form and easy to obtain in any concentration in aqueous solution.

(3) The final photodegration products of persulphate are sulfate salts which are environmentally benign substances.

3.4.4 Heterogeneous photocatalytic oxidation

A photocatalytic oxidation system is a heterogeneous system in which dispersed solid particles, that are usually metal oxide or other insoluble inorganic semiconductor powder, can absorb large fractions of the UV spectrum efficiently. The light excitation promotes an electron form of a bonding or non-bonding level in the solid to a highly delocalized level, creating a localized oxidizing site - a hole and a mobile reducing site - an electron. This electron-hole pair can be captured by reagents present on the surface of the solid particle. For example, the hole can be filled by electron transferred from water to give hydroxyl radicals as in UV/H_2O_2 and UV/O_3 system. On the other hand, the electron can be captured by oxygen adsorbed on the surface of the particle, then further forming superoxide radical anion, hydroperoxide radical, hydrogen peroxide, or hydroxyl radicals. These species can induce subsequent oxidative degradation of contaminants. This is why heterogeneous processes are considered to be APP.

The most commonly used photocatalysts are TiO_2 and ZnO because they can efficiently absorb long-wavelength UV light and are chemically stable to the reaction conditions. The pollutants that can be photocatalytically degraded include carboxylic acid, monoaromatics, halogen-containing compounds, sulfur- and phosphorous-

containing compounds, etc. [4] Some researchers have studied the photo-assisted oxidation of aqueous ammonia with and without iron-doped titanium dioxide. Since the introduction of catalyst results in additional preparations and extra costs, photocatalytic oxidation is not investigated in the present study.

3.5 Photochemistry of nitrogenous compounds

As discussed in Sections 3.1 and 3.2, the absorption of UV light can cause different activated states, depending upon the type of molecule and the wavelength, and can subsequently initiate different reaction paths. Therefore a detailed analysis of the molecular structure, physical and chemical properties, and absorption characteristics of the nitrogenous compounds that may be present in the photolytical system, is necessary in providing valuable information for the quantitative study of the system.

3.5.1 Ammonia (NH_3)

Physical and chemical properties

Ammonia is a colorless, nonflammable liquefied gas with a strong smell. It has molecular weight of 17.03 and specific gravity of 0.597 at 70°F. Ammonia is highly soluble in water, forming an alkaline solution called ammonium hydroxide, which has been discussed earlier, in Section 1.2.

Ammonia becomes highly reactive when dissolved in water and readily combines with many chemicals. Hydrogen halides (e.g., HCl) and carboxylic acids (e.g., CH_3COOH) react with ammonia to form ammonia salts.

Ammonia can be oxidized by hypochlorite or hypobromite. The mechanism is essentially the same as that of breakpoint chlorination of ammonia removal. The oxidation of ammonia with oxygen, ozone or hydrogen peroxide is also feasible. [36]

Photochemical properties

The UV absorption spectrum of ammonia has been reported in the region of 195 – 243 nm with discrete bands.

The bond energy of NH_2-H is approximately 102 kcal.mol^{-1}, and that of NH-H_2 is approximately 91.7 kcal.mol^{-1}. There are two primary reactions that are possible under UV irradiation: [37, 40]

$$NH_3 \xrightarrow{h\nu} \bullet NH_2 + H \qquad (3\text{-}40)$$

$$NH_3 \xrightarrow{h\nu} \bullet NH + H_2 \qquad (3\text{-}41)$$

Reaction (3-40) is energetically possible for UV radiation of wavelength below 280 nm, while reaction (3-41) is possible for a wavelength below 311 nm.

The following secondary reactions are probable:

Imide radicals (•NH) can react with ammonia to produce hydrazine:

$$\bullet NH + NH_3 \rightarrow N_2H_4 \qquad (3\text{-}42)$$

Two •NH radicals can combine to give nitrogen and hydrogen atoms:

$$\bullet NH + \bullet NH \rightarrow N_2 + 2H \quad (3\text{-}43)$$

The reaction of amino radicals ($\bullet NH_2$) with NH_3 is too slow to be observed but the $\bullet NH_2$ radicals disappear by combining to produce hydrazine:

$$\bullet NH_2 + \bullet NH_2 \rightarrow N_2H_4 \quad (3\text{-}44)$$

The hydrogen atoms in the system disappear by:

$$H + NH_3 \rightarrow NH_2 + H_2 \quad (3\text{-}45)$$

$$H + H \rightarrow H_2 \quad (3\text{-}46)$$

In APP systems, photolytically produced hydroxyl radicals can attack an ammonia molecule and abstract hydrogen atom from ammonia:

$$\bullet OH + NH_3 \rightarrow \bullet NH_2 + H_2O \quad (3\text{-}47)$$

The products, amino radicals ($\bullet NH_2$) and hydrogen atoms are the same as that obtained from reaction (3-40). However, comparing the dissociation energy of 51.0 kcal.mol^{-1} of hydrogen peroxide (HO-OH) with 102 kcal.mol^{-1} for ammonia (NH_2-H), it can be estimated that if hydrogen peroxide exists in the system, the generation of hydroxyl radicals will be the dominant primary process and Eqn. (3-47) will be a secondary process.

$\bullet NH_2$ radicals can undergo further reactions as Eqn. (3-44) or as follows to give hydroxylamine:

$$\bullet OH + \bullet NH_2 \rightarrow NH_2OH \quad (3\text{-}48)$$

Because hydrazine and hydroxylamine are produced as intermediates in APP systems as shown in Eqns. (3-44) and (3-48), it is important to review their properties.

3.5.2 Hydrazine (N_2H_4)

Physical and chemical properties

Hydrazine (N_2H_4) is a colourless, oily, flammable liquid for a temperature range of 2.0°C to 113.5°C. It is miscible in water and has a molecular weight of 32.05 g/mol. At 20°C, Hydrazine has a density of 1.00 g/cm^3.

Commercially, hydrazine is prepared in two steps. In the first step, chloramine is prepared by the reaction of ammonia and hypochlorite solution: [38]

$$NH_3 + OCl^{-1} \rightarrow OH^{-1} + NH_2Cl \qquad (3\text{-}49)$$

then chloramine reacts with ammonia to form hydrazine:

$$NH_3 + NH_2Cl + OH^{-1} \rightarrow N_2H_4 + Cl^{-1} + H_2O \qquad (3\text{-}50)$$

The over-all reaction is obtained by summarizing the above two equations:

$$2NH_3 + OCl^{-1} \rightarrow N_2H_4 + Cl^{-1} + H_2O \qquad (3\text{-}51)$$

At room temperature, pure hydrazine and its aqueous solutions are stable. However, it decomposes in the presence of catalysts such as platinum or nickel:

$$N_2H_4 \rightarrow N_2 + 2H_2 \qquad (3\text{-}52)$$

$$3N_2H_4 \rightarrow N_2 + 4NH_3 \quad (3\text{-}53)$$

Hydrazine is a weak base ($K_b = 8.5 \times 10^{-7}$ at 25°C), more reactive than ammonium sulphide, but less alkali than ammonia:

$$N_2H_4 + H_2O \rightarrow N_2H_5^+ + OH^{-1} \quad (3\text{-}54)$$

Hydrazine is a powerful reducing agent. It is attractive as a reducing agent due to its high hydrogen content, and by-product nitrogen. It may be oxidized by a wide variety of oxidzing agents, including molecular oxygen.

$$N_2H_4 + O_2 \rightarrow N_2 + 2\,H_2O \quad (3\text{-}55)$$

Table 3.7 lists three important half-cell reactions for the oxidation of hydrazine together with their oxidation potentials.

Table 3.7 Half-cell reactions and oxidation potentials of hydrazine [38]

Solution	Half-cell reaction		Potential (E°)
Acid	$N_2H_5^+ \rightarrow N_2 + 5H^+ + 4e^-$	(3-56)	+0.23
Acid	$2N_2H_5^+ \rightarrow 2NH_4^+ + N2 + 2H^+ + 2e^-$	(3-57)	+1.74
Acid	$2N_2H_5^+ \rightarrow HN_3 + NH_4^+ + 5H^+ + 4e^-$	(3-58)	-0.11
Basic	$N_2H_4 + 4OH^- \rightarrow N_2 + 4H_2O + 4e^-$	(3-59)	+1.16
Basic	$2N_2H_4 + 2OH^- \rightarrow 2NH_3 + N_2 + 2H_2O + 2e^-$	(3-60)	+2.42
Basic	$2N_2H_4 + 5OH^- \rightarrow N_3^- + NH_3 + 5H_2O + 4e^-$	(3-61)	+0.92

Hydrazine reacts with chemicals such as nitrates, permanganates, chromic acid, hydrogen peroxide, nitric acid, sodium peroxide, halogens, or persulphate, oxidizing materials, and highly oxygenated or halogenated solvents. [34, 38]

$$N_2H_4 + 2H_2O_2 \rightarrow N_2 + 4H_2O \quad (3\text{-}63)$$

$$N_2H_4 + 2NO_2^- + 2H^+ \rightarrow N_2 + N_2O + 3H_2O \quad (3\text{-}64)$$

$$N_2H_4 + 2S_2O_8^{2-} \rightarrow N_2 + 4SO_4^{2-} + 4H^+ \quad (3\text{-}65)$$

Photochemical properties

The N-N bond energy in hydrazine is 60 kcal.mol^{-1}, compared to 102 kcal.mol^{-1} for NH_2-H in ammonia, the dissociation of hydrazine is energetically possible below the wavelength of 470 nm. Hydrazine decomposes into two amino radicals as follows: [38]

$$N_2H_4 \xrightarrow{h\nu} \bullet NH_2 + \bullet NH_2 \quad (3\text{-}66)$$

The formation of hydrazyl radicals ($\bullet N_2H_3$) occurs as:

$$N_2H_4 + \bullet NH_2 \xrightarrow{h\nu} NH_3 + \bullet N_2H_3 \quad (3\text{-}67)$$

The generated hydrazyl radicals probably decompose:

$$2\bullet N_2H_3 \xrightarrow{h\nu} 2NH_3 + N_2 \quad (3\text{-}68)$$

As mentioned in Section 3.5.1, upon UV irradiation, ammonia may dissociate directly by photolysis or attacked by hydroxyl radicals through secondary reaction to give amino radicals:

$$NH_3 \xrightarrow{h\nu} \bullet NH_2 + H \quad (3\text{-}40)$$

$$\bullet OH + NH_3 \rightarrow \bullet NH_2 + H \quad (3\text{-}47)$$

Two amino radicals combine to give hydrazine:

$$\bullet NH_2 + \bullet NH_2 \rightarrow N_2H_4 \quad (3\text{-}44)$$

If there are hydrogen atoms in the system, the following reactions may occur:

$$N_2H_4 + H \rightarrow \bullet N_2H_3 + H_2 \quad (3\text{-}69)$$

$$N_2H_4 + H \rightarrow \bullet NH_2 + NH_3 \quad (3\text{-}70)$$

3.5.3 Hydroxylamine (NH_2OH)

Physical and chemical properties

50% hydroxylamine (NH_2OH) solution is a colorless liquid with a molecular weight of 33.03. It freezes at 9 °C and boils at 107 °C. At 20 °C, it has a density of 1.12 g/cm^3.

One preparation method of hydroxylamine involves hydrogenation of nitric oxide in aqueous acid catalyzed by platinum:

$$2NO + 3H_2 + 2H^+ \rightarrow 2NH_3OH^+ \quad (3\text{-}71)$$

Pure hydroxylamine is very unstable and decomposes into a mixture of ammonia, nitrogen, nitrous oxide and water when temperature is above 15 °C.

Hydroxylamine in aqueous solution is much more stable because the free hydroxylamine is under equilibrium with protonated hydroxylammonium ion NH_3OH^+ ($K_b = 6.6 \times 10^{-9}$ at 25°C), the solution is a weak base:

$$NH_2OH + H_2O \rightarrow NH_3OH^+ + OH^- \quad (3\text{-}72)$$

Hydroxylamine is a strong reducer. The oxidation state of the nitrogen in the final product depends on the oxidant type, oxidant and hydroxylamine molar ratio, specific reaction etc.

Table 3.8 [34] lists certain half-cell reactions for the oxidation of hydroxylamine together with their oxidation potentials.

Table 3.8 Half-cell reactions and oxidation potentials of hydroxylamine

Half-cell reaction		Potential (E°)
$NH_3OH^+ + 2H^+ + 2e \rightarrow NH_4^+ + H_2O$	(3-73)	+1.35
$2NH_3OH^+ + H^+ + 2e \rightarrow N_2H_5 + 2H_2O$	(3-74)	+1.46
$NH_2OH + 2H_2O + 2e \rightarrow NH_4OH + 2OH^-$	(3-75)	+0.42
$2NH_2OH + 2e \rightarrow N_2H_4 + 2OH^-$	(3-76)	+0.74

Hydroxylamine reacts with chemicals such as permanganates, perchloric acid, dichromate, cerium(IV), bromate, hydrogen peroxide and persulphate etc. [33, 34]

$$2OH^- + 4NH_2OH + 6H_2O_2 \rightarrow N_2 + NO_2^- + NO_3^- + 13H_2O \quad (3\text{-}73)$$

$$2NO_2^- + 2NH_2OH + 2H^+ \rightarrow 2NO + N_2 + 4H_2O \quad (3\text{-}74)$$

$$6NH_2OH + 12S_2O_8^{2-} \rightarrow 2N_2 + NO_2^- + NO_3^- + 24SO_4^{2-} + H_2O + 14H^+ \quad (3\text{-}75)$$

Photochemical properties

The NH_2-OH bond energy in hydroxylamine is 66 kcal.mol^{-1}, compared to 102 kcal.mol^{-1} of NH_2-H in ammonia, the dissociation of hydroxylamine is energetically possible below the wavelength of 430 nm. Hydroxylamine decomposes into amino radical and hydroxyl radical as follows: [38]

$$NH_2OH \xrightarrow{h\nu} \bullet NH_2 + \bullet OH \qquad (3\text{-}76)$$

Hydroxylamine can be oxidized by electrons in aqueous solution to give amino radical and hydroxyl anion: [40]

$$NH_2OH + e_{aq}^- \rightarrow \bullet NH_2 + OH^- \qquad (3\text{-}77)$$

$$NH_3OH^+ + e_{aq}^- \rightarrow NH_3 + \bullet OH \qquad (3\text{-}78)$$

As mentioned in Section 2.5.1, upon UV irradiation, ammonia may dissociate directly by photolysis or attacked by hydroxyl radicals through secondary reaction to give amino radicals:

$$NH_3 \xrightarrow{h\nu} \bullet NH_2 + H \qquad (3\text{-}40)$$

$$\bullet OH + NH_3 \rightarrow \bullet NH_2 + H \qquad (3\text{-}47)$$

The amino radical combines with hydroxyl radical to give hydroxylamine:

$$\bullet OH + \bullet NH_2 \rightarrow NH_2OH \qquad (3\text{-}48)$$

Because nitrogen compounds have wide oxidation states from -3 to +5, a number of products are possible. They include N_2, N_2O, NO, NO_2^-, NO_2 and NO_3^-. A brief review of their properties is presented next.

3.5.4 Nitrogen gas (N_2)

Physical and chemical properties

Nitrogen (N_2) constitutes 78.03% of the air, has a gaseous specific gravity of 0.967, and has a boiling point of -320.5 °F (-195.8 °C) at atmospheric pressure. It is colorless, odorless, and tasteless.

There are two methods that are commonly used to prepare nitrogen in the laboratory: the decomposition of sodium azide, and the decomposition of ammonium dichromate under controlled conditions.

$$NaN_3\ (300°C) \rightarrow 2Na + 3N_2 \qquad (3\text{-}79)$$

$$(NH_4)_2Cr_2O_7 \rightarrow N_2 + Cr_2O_3 + 4H_2O \qquad (3\text{-}80)$$

Large quantities of nitrogen can be produced by the liquefaction and fractional distillation of the resulting liquid air, by separating out oxygen and other gases.

Nitrogen is an inert gas. It is nonreactive with many materials. However, when nitrogen is heated, it combines directly with magnesium, lithium, and calcium. When mixed with oxygen and subjected to electric sparks, it forms nitric oxide (NO) and then the dioxide (NO_2). When heated with hydrogen under pressure, in the presence of a suitable catalyst, ammonia is formed. This is known as the Haber process.

Photochemical properties

Nitrogen shows no absorption in the UV region. Its absorption becomes prominent only below a wavelength of 100 nm.

The N-N bond energy of nitrogen is 226 kcal.mol^{-1}, the dissociation of nitrogen is energetically possible below the wavelength of 127 nm. Nitrogen decomposes under 61.7 nm as follows: [41]

$$N_2 \xrightarrow{h\nu} N(^4P) + N(^4S^\circ) \qquad (3\text{-}81)$$

Obviously, the above process can not happen under UV irradiation, furthermore, only 1% of the total nitrogen participates in the above process. However, nitrogen may exist as a final photolytical product as discussed in Sections 3.5.1 through 3.5.3.

3.5.5 Nitrous oxide (N_2O)

Physical and chemical properties

Nitrous oxide (N_2O), is also called dinitrogen monoxide, or laughing gas. It is a colorless gas with pleasant, sweetish odor and taste. When inhaled it produces insensibility to pain preceded by mild hysteria, and sometimes laughter. This is where the nickname laughing gas comes from. Nitrous oxide is comprised of 2 parts nitrogen and one part oxygen (36% oxygen by weight) with a molecular weight of 44.0.

It can be prepared by the reaction of hydroxylamine hydrochloride (NH_2OH HCl) with sodium nitrite ($NaNO_2$), or by the decomposition of ammonium nitrate (NH_4NO_3).

Nitrous oxide is relatively inert compared to the other nitrogen oxides. It can only react slowly with some oxidizing and reducing agents. When temperature is above 600 °C, it decomposes into nitrogen and oxygen.

Photochemical properties

There are two regions of continuous absorption in the absorption curve of nitrous oxide. One extends from 170 to 220 nm, the other begins at 158 nm and extends far into the UV region. Its total absorption in UV region is weak.

The N_2-O bond energy in nitrous oxide is 40 kcal.mol^{-1}, N-NO bond energy 115 kcal.mol^{-1}, accordingly, two dissociation process of nitrous oxide are energetically possible below the wavelength of 250 nm. [41]

$$N_2O \xrightarrow{h\nu} N_2 + O \qquad (3\text{-}82)$$

$$N_2O \xrightarrow{h\nu} NO + N \qquad (3\text{-}83)$$

The final photolytical decomposition products of nitrous oxide are known to be N_2, O_2, NO and NO_2, which can be explained by the following secondary processes:

$$O + N_2O \rightarrow N_2 + O_2 \qquad (3\text{-}84)$$

$$O + N_2O \rightarrow 2NO \qquad (3\text{-}85)$$

$$2NO + O_2 \rightarrow 2NO_2 \qquad (3\text{-}86)$$

If O_3 exists in the system, following secondary reactions will occur similar to the processes that occur in the upper atmosphere:

$$O_3 \xrightarrow{h\nu} O_2 + O \qquad (3\text{-}28)$$

$$O + N_2O \rightarrow N_2 + O_2 \quad (3\text{-}84)$$

$$O + N_2O \rightarrow 2NO \quad (3\text{-}85)$$

$$NO + O_3 \rightarrow NO_2 + O_2 \quad (3\text{-}87)$$

3.5.6 Nitric oxide (NO)

Physical and chemical properties

Nitric oxide (NO) is colorless, poisonous gas with a slight odor. Its molecular weight is 30.

Nitric oxide is generated by catalytic oxidation of ammonia (Eqn. 3-88) or by the reaction of nitrous acid and iodide (Eqn. 3-89):

$$4NH_3 + 5O_2 \rightarrow 4NO + 6H_2O \quad (3\text{-}88)$$

$$2HNO_2 + 2I^- + 2H^+ \rightarrow 2NO + I_2 + 2\ H_2O \quad (3\text{-}89)$$

Nitric oxide is soluble in water to some degree and reacts with water to form nitric acid. It reacts with fluorine, chlorine, and bromine to form the corresponding nitrosyl halide. It is also used in the preparation of metal nitrosyl carbonyls and related compound.

Nitrous oxide reacts rapidly with oxygen to form nitrogen dioxide (NO_2) as shown in Eqn. (3-86).

Photochemical properties

In the region of wavelength 135 nm to 230 nm, the absorption curve of nitric oxide is composed of many discrete bands. There is no strong absorption in UV region.

The N-O bond energy in nitric oxide is 151 $kcal.mol^{-1}$, the dissociation process of nitric oxide is energetically possible below the wavelength of 191 nm.

When incident wavelength is above 191 nm, a probable mechanism of photochemistry of nitric oxide is: [41]

$$NO \xrightarrow{h\nu} NO^* \quad (3\text{-}90)$$

$$NO^* + NO \rightarrow 2NO \quad (3\text{-}91)$$

$$NO^* + NO \rightarrow N_2 + O_2 \quad (3\text{-}92)$$

$$NO^* + NO \rightarrow N_2O + O \quad (3\text{-}93)$$

$$2NO + O_2 \rightarrow 2NO_2 \quad (3\text{-}86)$$

$$O + NO + M \rightarrow NO_2 + M \quad (3\text{-}94)$$

When incident wavelength is below 191 nm, nitric oxide may dissociate as:

$$NO \xrightarrow{h\nu} N + O \quad (3\text{-}95)$$

$$N + NO \rightarrow N_2 + O \quad (3\text{-}96)$$

$$O + NO + M \rightarrow NO_2 + M \quad (3\text{-}97)$$

$$O + O + M \rightarrow O_2 + M \quad (3\text{-}98)$$

Where M is another molecule or the surface of the reaction vessel.

3.5.7 Nitrogen dioxide (NO_2)

Physical and chemical properties

Nitrogen dioxide (NO_2) is an acidic, pungent smelling gas. At low pressures or at high temperatures, it has a deep brown color, but at low temperatures the color almost completely disappears as it dimerizes to form dinitrogen tetroxide (N_2O_4). At room temperature an equilibrium between the two molecules exists. Nitrogen dioxide has molecular weight of 46.0.

Nitrogen dioxide is prepared commercially by oxidizing NO with air. It can be prepared in the laboratory by heating the nitrate of a heavy metal, as shown in the following equation,

$$2Pb(NO_3)_2 + \text{heat} \rightarrow 2PbO + 4NO_2 + O_2 \qquad (3\text{-}99)$$

or by adding copper metal to concentrated nitric acid.

Nitrogen dioxide is a very reactive gas. It reacts with water in two ways. In cold water, a mixture of HNO_2 and HNO_3 is formed, while at higher temperatures HNO_3 and NO are formed. Upon heating, nitrogen dioxide decomposes to form nitrogen and oxygen. In addition, nitrogen dioxide undergoes extensive oxidation-reduction reactions because it is a strong oxidizing agent with nitrogen in the valence of +4.

Photochemical properties

The absorption spectrum of nitrogen dioxide is the combined spectrum of NO_2 and N_2O_4. The mixture (NO_2+N_2O_4) absorbs over the full range from the visible to the short UV.

The spectrum of NO_2 is quite complex with a minimum absorption value at a wavelength of about 250 nm.

The ON-O bond energy in nitrogen dioxide is 73 $kcal.mol^{-1}$, the dissociation process of nitrogen dioxide is energetically possible below the wavelength of 390 nm.

The main photochemical reactions of nitrogen dioxide are the production of oxygen atoms and the rapid reaction of O atoms with NO_2:

$$NO_2 \xrightarrow{h\nu} NO + O \quad (3\text{-}100)$$

$$O + NO_2 \rightarrow NO + O_2 \quad (3\text{-}101)$$

The produced O atoms can combine with oxygen molecules to form O_3. Further reactions of O atoms, OH radicals and O_3 with hydrocarbons initiate photochemical air pollution.

3.5.8 Nitrite (NO_2^-)

Nitrite (NO_2^-) is the intermediate product in the breakdown of ammonia to nitrate, for example, in the nitrification process or in the other oxidation processes of ammonia:

$$NH_3 \rightarrow NO_2^- + H^+ \quad (2\text{-}11)$$

$$NH_3 + O_3 \rightarrow NO_2^- + H_2O + H^+ \quad (3\text{-}102)$$

Because the nitrogen is in the valence of +3, nitrite can be oxidized into nitrate by a wide variety of oxidants, such as ozone, manganate, persulphate, bromate etc.

$$3NO_2^- + O_3 \rightarrow 3NO_3^- \quad (3\text{-}103)$$

$$5NO_2^- + 2MnO_4^- + 6H^+ \rightarrow 5NO_3^- + 2Mn^{2+} + 3H_2O \quad (3\text{-}104)$$

Nitrite can also work as an oxidizer and is reduced to the low oxidation state of nitrogen when it meets a strong reducing agent, such as hydrazine or hydroxylamine:

$$N_2H_4 + 2NO_2^- + 2H^+ \rightarrow N_2 + N_2O + 3H_2O \quad (3\text{-}64)$$

$$2NO_2^- + 2NH_2OH + 2H^+ \rightarrow 2NO + N_2 + 4H_2O \quad (3\text{-}74)$$

Nitrite absorbs light in the ultraviolet region, with the absorption curve increasing continuously as the wavelength decreases from 280 to 220 nm.

3.5.9 Nitrate (NO_3^-)

The nitrogen is in the valence of +5, hence nitrate represents the most highly oxidized form of nitrogen and it is relatively stable compared with other nitrogenous compounds. Nitrate (NO_3^-) is the final product in the breakdown of ammonia, for example, in the nitrification process:

$$NH_3 \longrightarrow NO_2^- + H^+ \quad (2\text{-}11)$$

$$NO_2^- \longrightarrow NO_3^- \quad (2\text{-}12)$$

Nitrate is a strong oxidant, especially in the acid solution. It can be reduced to nitrite, nitric oxide or nitrogen dioxide depending on different reducing agents. The reducers can be ferrous ion(ii), titanous ion (ii) compounds, sodium thiosulphate, chromium (ii) chloride etc. In biological denitrification process, nitrate is reduced to nitrogen gas. Table 3.9 [34] lists certain half-cell reactions for the redox reactions of nitrite and nitrate together with their oxidation potentials.

Nitrate absorbs light in the ultraviolet region, with the absorption curve increasing continuously as the wavelength decreases from 320 to 200 nm.

Table 3.9 Half-cell reactions and oxidation potentials of nitrite and nitrate

Half-cell reaction		Potential (E°)
$NO_2^- + H_2O + e \rightarrow NO + 2OH^-$	(3-105)	-0.46
$2NO_2^- + 3H_2O + 4e \rightarrow N_2O + 6OH^-$	(3-106)	+0.15
$2HNO_2 + 4H^+ + 4e \rightarrow N_2O + 3H_2O$	(3-107)	+1.29
$N_2O_4 + 2e \rightarrow 2NO_2$	(3-108)	+0.88
$N_2O_4 + 2H^+ + 2e \rightarrow 2HNO_2$	(3-109)	+1.07
$NO_3^- + H_2O + 2e \rightarrow NO_2^- + 2OH^-$	(3-110)	+0.01
$2NO_3^- + 3H^+ + 2e \rightarrow N_2O_4 + 2H_2O$	(3-111)	+0.81
$NO_3^- + 3H^+ + 2e \rightarrow HNO_2 + H_2O$	(3-112)	+0.94
$NO_3^- + 4H^+ + 3e \rightarrow NO + 2H_2O$	(3-113)	+0.96

Chapter 4

Design of photochemical reactors

4.1 Overview of the type of photochemical reactors

Any practical application of UV radiation requires that the radiation from the source must be efficiently absorbed by the material to be irradiated. This necessitates a proper design of the photochemical reactor. The early studies on photochemical reactors have provided useful descriptions of various kinds of available lamps and arrangements of equipment for large-scale photochemical processes. Various reactor configurations can be classified into two main categories: the batch reactors, and the continuous flow reactors. An overview of both the types of reactors is presented here and the relevant design issues are discussed.

4.1.1 Batch reactor

A typical batch reactor essentially consists of the reactants, an agitation device, and the light source. Since the UV light source generates heat and attains high temperature, it must be cooled in order to maintain efficient operation. Thus, gas cooling in low-energy lamp systems or water cooling in high-energy lamp systems may be required. Figure 4.1 [28] shows a simple batch photoreactor. The lamp, surrounded by a cooling jacket, is immersed in the vessel containing the reacting fluid. In this system, all the radiation from the lamp is available to be absorbed by the reacting fluid. Hence, there

are no light rays lost to the surroundings and there is no need for the installation of a reflector. However, the light intensity decreases very rapidly with increasing distance from the lamp because of the absorption of reactants and the divergence of the light rays.

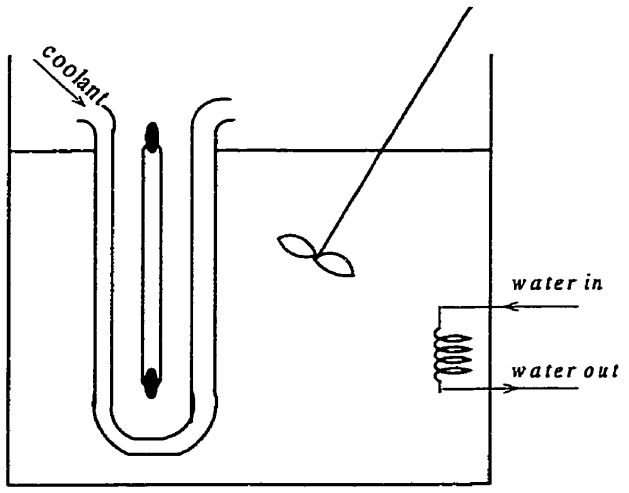

Figure 4.1 Batch photoreactor

Therefore, it is necessary to install an efficient agitating system in order to reach uniform irradiation of the reactants and at the same time prevent local overheating if

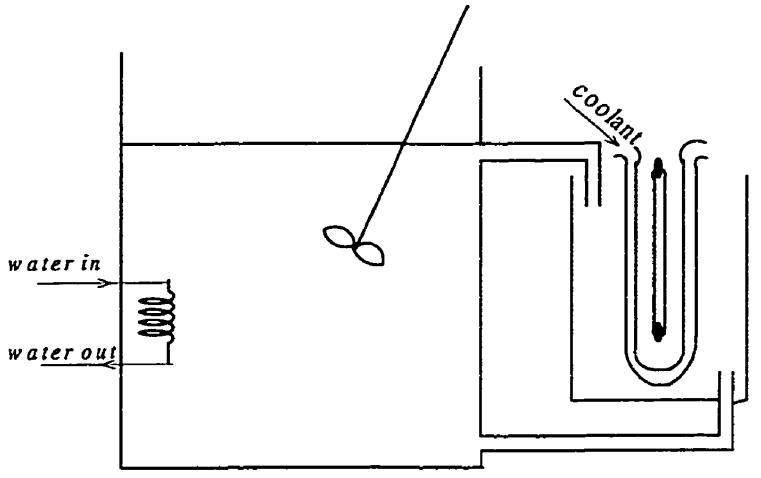

Figure 4.2 Batch photoreactor with recirculation

the reaction is exothermic.

Figure 4.2 shows a different version of the batch photoreactor. The lamp is separated from the vessel and is put in another irradiation jacket. The reacting fluid circulates from the vessel and flows through the irradiation jacket, then back into the vessel. For this kind of reactor configuration, it is important to keep a high circulation flow rate to assure turbulent flow through the reactor. The other critical factor in design is to ensure a proper path between the lamp and the inner wall of the irradiation jacket. If the path is too long, the UV radiation will be completely extinguished in partial length of the path due to the absorption of reacting fluid. If the path is too short, the radiation will reach the jacket wall, and is absorbed by the jacket material or escapes from the jacket wall, thus causing the loss of radiation energy.

4.1.2 Continuous reactor

Figure 4.3 [28] shows a continuous flow reactor of the annular type. The reactor

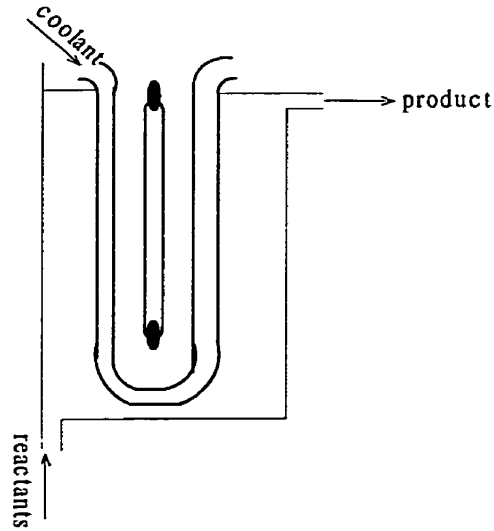

Figure 4.3 Continuous annular flow photoreactor

consists of an annular space between two concentric cylinders. The reacting fluid contained in this space is irradiated by the light source mounted along the axis of the inner cylinder. This system requires complete mixing of the reacting fluid.

Figure 4.4 [30, 42] shows a continuous flow reactor of elliptical type. A tubular reactor

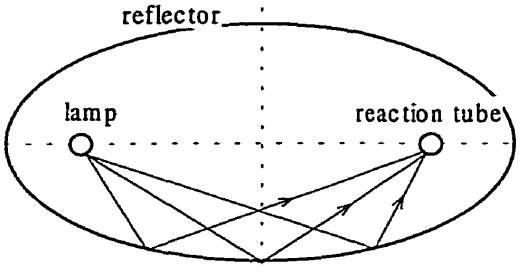

Figure 4.4 Continuous elliptical photoreactor

through which reacting fluid flows is situated at one focus of the elliptical reflector, and the light source is placed at the other focus. An internal cooling tube can be fitted to remove the excess heat from the tubular reactor. The advantage of this system is that the light emitting from the light source will converge towards the center of the tubular reactor.

Figure 4.5 shows another configuration of a continuous flow reactor. The light source is mounted at the focus axis of a parabolic reflector, hence the cylindrical reactor is irradiated from the bottom. The advantage of this system is that the reacting fluid is

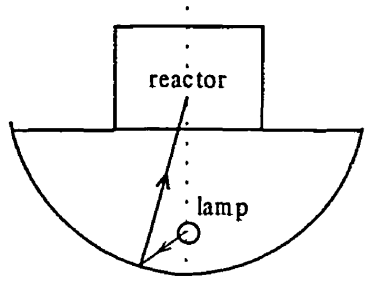

Figure 4.5 Continuous parabolic reactor

separated from the light source. Thus operation control is easy to achieve. For example, the cylindrical reactor can be perfectly mixed when vigorous mixing is needed.

4.1.3 Selection of the reactor type

Some of the operational characteristics of the different reactors are as follows:

(1) The operating conditions of batch process are time varying, which could make it difficult to control the operating conditions. In continuous reactors, operating conditions can be held constant.

(2) The initial conditions are very important in the operation of batch processes. Continuous processes have more flexibility and are more controllable during operation.

(3) Batch processes are normally used for the manufacturing of low-volume, high value products.

(4) Batch processes are operated for a definite time period which is the mean hydraulic residence time, while the true hydraulic residence time in continuous processes varies with the longitudinal length and flow conditions of the reactor.

In photochemical engineering, batch reactors are employed almost exclusively for low-quantum-yield reactions where long irradiation time is required. Batch processes have certain specific applications, such as the irradiation of viscous reacting fluids. [27]

Batch reactor and recirculation reactor

Batch reactors as shown in Fig. 4.1, are commercially available and are suitable for general purpose. One example is the Rayox Advanced Oxidation System provided by Calgon Carbon Oxidation Technologies of Markham, Ontario, Canada. This system was chosen for the previous study. The equipment configuration will be presented in Chapter 5. The previous study evaluated the process feasibility of an advanced photo-oxidation process for ammonia removal. It involved a study of the chemical tailoring of various precursor ammonia compounds and the study of process operating variables. In the present work, the study is extended to a recirculation reactor using a custom-modified Rayox system, which is schematically illustrated in Fig. 4.6. This reactor is similar to the batch reactor with circulation as shown in Fig. 4.2. There are two tanks in the system: one is the reactor, and the other is the recycling tank. Light source and agitating equipment are incorporated in the same reactor. Reacting fluids are irradiated in the reactor. Part of the reacting fluid circulates from the reactor, flows through the recycling tank, and then flows back into the reactor. The reactor has the following characteristic: Mixing

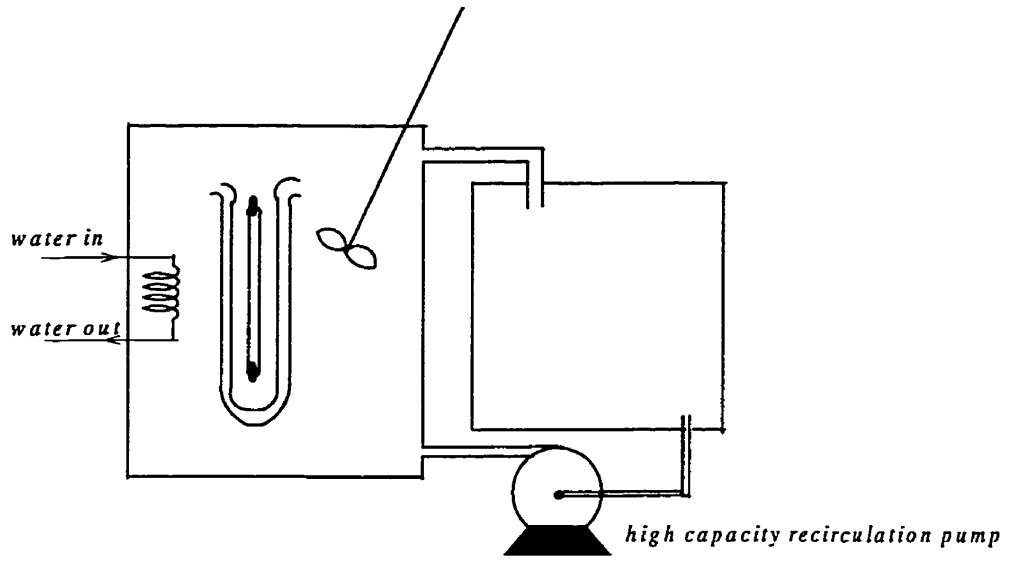

Figure 4.6 Recirculation reactor

is a very important aspect in photochemical reactor design, especially when reacting fluid has strong absorption of UV light. Because the effective path length of a photochemical reaction is quite small, it is very important to exchange the treated water near the UV source with the untreated water near the reactor wall. Complete mixing means that the concentrations of the photolytically activated species would be uniform throughout the reactor. It was reported [44] that the efficiency of treatment can dramatically decrease if the reacting fluid is not adequately mixed. With a high circulation flow rate, complete mixing can be more easily achieved in the recirculation reactor, the schematic of which is shown in Fig. 4.6.

New film-type continuous flow reactor

In photochemical engineering, high-quantum-yield reactions are usually run in continuous flow systems, which provide for short contact irradiation time. New film-type

reactor in this study is designed as a continuous plug-flow like system based on the following considerations:

(1) It is evident from the first law of photochemistry that only the light absorbed by the reacting materials can be effective in initiating photochemical changes. Furthermore, Beer-Lambert law states that the light absorption is directly proportional to the concentration of absorbing media. In a plug-flow like system, the concentrations of absorbing reactants are maintained at a value higher than that in a batch or a mixed reactor system. Thus the light absorption is greater, leading to a higher reaction rate.

(2) Since the products continually flow from the reaction tank, sampling from the system is convenient. This facilitates the study of process kinetics greatly.

(3) Continuous flow system enables on-line treatment, so a large volume of wastewater can be treated without excessive requirement of reactor space. This is very advantageous to the industrial scale-up of the system.

(4) The problem of deposits on the outer wall of the lamp well is reduced in a flow system. Deposit formation is a serious problem in photochemical reactor design, which will be discussed in detail in Section 4.2.

(5) Because the reacting fluids are in continuous movement through the light radiation area, no additional mixing device is necessary.

4.2 Design of the new film-type continuous flow reactor

- the Rotospray Photolytic Reactor (RPR)

The annular flow reactor as shown in Fig. 4.3 is not a good choice for continuous processes operation. The reason is that this kind of reactor has a relatively large cross-

sectional area that requires large volumetric flow rate of reacting fluid. This puts a severe limitation on design. The continuous elliptical photoreactor as shown in Fig. 4.4 is suitable for laboratory work but is not recommended for industrial scale-up because its capacity of concentrating the energy within the tubular reactor boundary is not high. For the reasons cited above, the continuous parabolic photoreactor is chosen as the prototype reactor in this study.

After the reactor prototype is selected, the design of a photochemical reactor needs to address a wide variety of aspects: the configuration of the reactor, the choice of UV source, shielding materials, reflector, and reactor construction materials, etc. Quantitative design processes are closely related with mass balance and radiation balance.

4.2.1 Mass balance equation

For a photochemical reaction, the rate of reaction term in the mass balance equation, depends upon the composition and volumetric rate of light absorption, I_a. The quantity I_a is a function of wavelength. Thus, if the rate constants are also dependent on wavelength, complete mass balance expressions must be written not only for each species, but also for each wavelength interval for a given reacting species. In addition, the complex kinetics of a photochemical reaction may introduce further complication of the mass balance equation. Hence some simplification is required. Taking the UV/H_2O_2 system as an example, a simplified form of mass balance for ammonia removal is written as follows: consists

$$-v\nabla C_A + r_A = dC_A/dt \qquad (4\text{-}1)$$

where v is the transportation velocity of reacting fluid ($cm.s^{-1}$)

∇C_A is the concentration gradient of ammonia ($mol.cm^{-4}$)

r_A is the local reaction rate of ammonia in the reactor ($mol.cm^{-3}s^{-1}$)

The above equation is based on the following assumptions:

(1) The transportation property of reacting fluid is constant.

(2) The radiation of UV source is monochromatic.

(3) Mixing in the cross-section of flow is complete.

(4) There is no molecular diffusion.

(5) Fluid flow is incompressible.

4.2.2 Radiation balance equation

The intensity of light radiation will decrease as the light passes through the reacting medium. It is the light absorption that is responsible for the chemical reaction. No photochemical reaction can occur without light absorption. As mentioned earlier, light intensity is a function of wavelength. Hence, there is one radiation equation for each wavelength and each direction of radiation, as expressed by Eqn. (4-2): [46]

$$\nabla I = -\mu_\lambda I = -I_a \qquad (4\text{-}2)$$

where,

I is incident light intensity ($Einsteins.s^{-1}cm^{-2}$)

I_a is volumetric rate of light absorption ($Einsteins.s^{-1}cm^{-3}$)

μ_λ is the attenuation coefficient which is a function of wavelength λ (cm^{-1})

The attenuation coefficient is directly proportional to the molar concentration of the absorbing species:

$$\mu_\lambda = \alpha C \tag{4-3}$$

where,

α is the molar absorption coefficient (cm^2mol^{-1}), or absorptivity, which is a function of wavelength and of the nature of the chemical species

C is the concentration of the absorbing species ($mol.cm^{-3}$)

Generally the mass balance Eqn. (4-1) and the radiation balance Eqn. (4-2) are coupled because the reacting species is also the absorbing species. Therefore it is very difficult to find analytical solution for the two equations even for monochromatic light. However, the practical system model can be simplified.

As discussed above, the reaction rate will depend on the intensity of UV light in the reacting system and molar absorption coefficient of absorbing species. The former factor depends on the light distribution inside the photochemical reactor, and is further related to the light emission model. The latter depends on the spectral output distribution of UV light source and absorption spectral distribution of absorbing species, and further related to the choice of light source. The following sections discuss this in detail.

4.2.3 Emission models of light source

To predict light profiles inside photochemical reactors, emission models are most commonly used. Such models are built from the source of the light and are based on the following hypotheses:

(1) The light emitted by the source is assumed to be monochromatic.

(2) The phenomena of reflection, refraction, diffusion and diffraction of the light are ignored.

(3) The light source follows the Beer-Lambert law, and it emits in all directions of space, with the same probability.

(4) The absorption coefficient of the absorbing species is assumed to be independent of the direction of propagation of the light rays.

There are three kinds of emission models: radial model (LSPP model), two-dimensional model (LS model), three-dimensional model (ES model). [47] Among these, the radial model is the simplest and it is chosen as the emission model in this study. In the radial model, the lamp is assumed to be of infinite length and all the rays are radial with respect to the lamp axis. At a distance of r from the axis of the lamp, the differential equation for light intensity is given by, [48]

$$\frac{1}{r}\frac{d}{dr}(rI_r) = -\mu I_r \qquad (4\text{-}4)$$

The above equation can be integrated from the inner radius of the reactor r_0 where the light intensity is I_{r0}, to any point within the reactor. Thus

$$I_r = \frac{r_0 I_{r0}}{r} e^{-\mu(r-r_0)} \qquad (4\text{-}5)$$

The nomenclature used, is illustrated in Fig. 4.7.

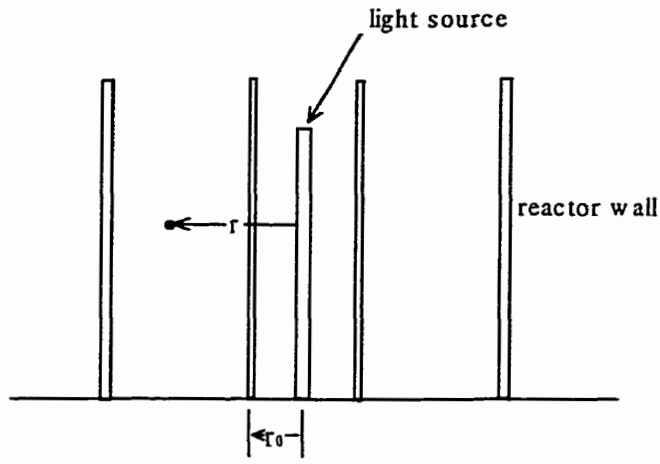

Figure 4.7 Nomenclature used in radial model

Equation (4-5) is schematically illustrated in Fig. 4.8. Obviously, the intensity

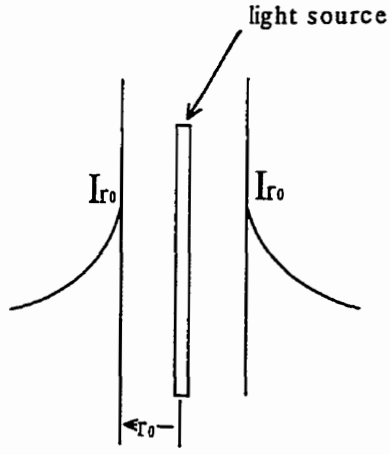

Figure 4.8 Profile of the distribution of the light

at the inner wall has the largest value and will diminish dramatically with the increase of the distance from the lamp axis. The depletion rate will depend on the attenuation coefficient μ of the absorbing species. Based on this principle, a new reactor is designed as a film-type reactor. [69] The basic configuration is shown in Fig. 4.9. Essentially the

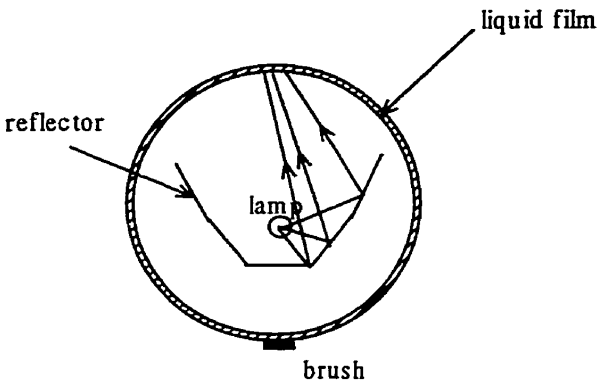

Figure 4.9 Schematic illustration of new film-type reactor configuration

reactor consists of a cylindrical space, with the UV light source located along the central axis. A reflector may be mounted if necessary. The cylindrical space is constructed by a certain specific UV penetrating material that will be discussed later in detail. Radiation emitting from UV light will impinge on the cylindrical surface, with the maximum intensity on the surface. Reacting fluid flows through the reactor from top inlet and leaves reactor from bottom outlet, forming a liquid film around the cylindrical surface. During the flow path, the liquid film absorbs the high-intensity UV light and a series of photochemical reactions occur. This new reactor is called Rotospray Photolytic Reactor (RPR), and will be discussed in detail in Chapter 5.

4.2.4 Choice of the light source

Although monochromatic light is perfect for building simple theoretical models in photo kinetic analysis, it is very difficult to produce on an industrial scale. In addition, the insertion of monochromators between lamp and reactor, to introduce monochromatic

light, will result in problems. For example, the intensity of the transmitted light is reduced by monochromators, and the size and geometry of the reactor are severely limited because the monochromators produce a direct beam in a small area. Hence, monochromators are used only if the narrow wavelength band is required to obtain high selectivity for bench scale research.

Therefore, polychromatic light will normally be employed in engineering applications. There are quite a few manufacturers of UV lamps, such as Hanovia Limited, Aquionics Inc, General Electric Co., Osram Sylvania Inc., Philips Electronics, and Westinghouse Electric Corp. [74] The commercially available UV lamps include Deuterium, Tungstan, Xenon and Mercury lamps. Mercury lamps are usually chosen in industrial photochemistry because of their attractive long lifetime and other favourable characteristics as discussed in Section 3.3. Life of the lamp is an important parameter not just because it is related to economy, but also because it affects the performance of the lamp. As a lamp experiences continuous use, its intensity degrades over time and thus its overall output also degrades.

In this study, medium-pressure mercury lamp is selected because of its relatively longer lifetime, higher energy output and better spectrum distribution. To compare the effects of different radiation sources on the photochemical reaction kinetics and on the product distribution, two different medium-pressure mercury lamps are employed in this study. The first kind of lamp is provided by the Hanovia Limited, New Jersey, USA, and the second one, a Rayox lamp, is provided by Calgon Carbon Oxidation Technologies of Markham, Canada. Their spectral distributions of energy output are shown in Figs. 4.10 and 4.11, respectively.

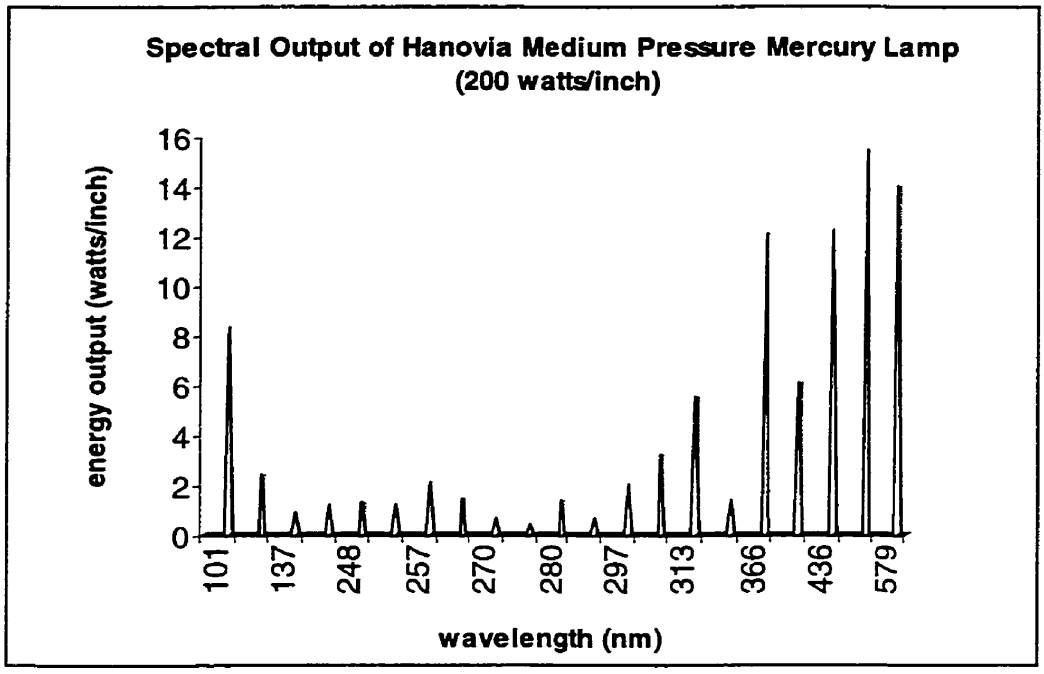

Figure 4.10 Spectral output of Hanovia medium pressure mercury lamp (200 watts/inch)

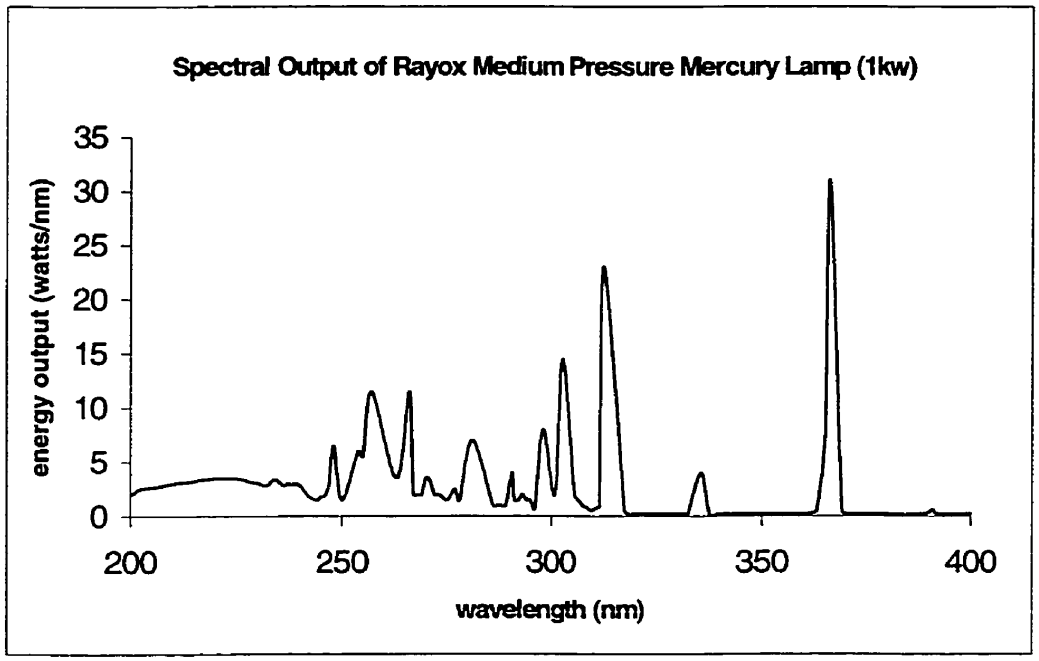

Figure 4.11 Spectral output of Rayox medium pressume mercury lamp in Rayox system (1kw)

Polychromatic light has its energy distributed over a range of wavelengths. To evaluate the absorptivity over a range of wavelength, the effect of polychromatic light is evaluated by using an average absorption coefficient calculated by the following equation:

$$\bar{\alpha} = \frac{\int_{\lambda_1}^{\lambda_2} \alpha_\lambda I_\lambda d\lambda}{\int_{\lambda_1}^{\lambda_2} I_\lambda d\lambda} \tag{4-6}$$

where,

$\bar{\alpha}$ is average molar absorption coefficient

α_λ is molar absorption coefficient at wavelength of λ

λ_1 and λ_2 are the limiting absorption wavelengths

I_λ is the incident light intensity at wavelength of λ

It is assumed that the emission spectra of the lamp and the molar absorption coefficient for the absorbing species have been known when applying Eqn. (4-6). If a further assumption is made that the rate constants are the same for different wavelengths, the derived $\bar{\alpha}$ can be substituted into Eqn. (4-3).

4.2.5 Choice of the construction materials

Inner cylinder

For the photochemical reactor shown in Fig. 4.9, the radiation from light source travels first through the air gap between light source and the surrounding cylinder, then

penetrates through the cylinder wall, and finally reaches the thin film of the reacting fluid. Thus the choice of proper material for the cylinder is important, in order to ensure maximum light intensity impinging on reacting fluid.

Obviously, it is desirable that the cylinder material has small wall thickness and small absorbing coefficient. However, there are not many materials available commercially which have both proper mechanical strength and optical transparency to UV light. Pyrex-brand glass (borosilicate glass) and fused silica (quartz) are the two possible choices among the materials available in the market.

An important factor to be considered here is the effect of solarization, which is observed as the changes in the physical properties of glass, after prolonged exposure to UV light. It was reported that under the radiation of 253.7 nm mercury emission, the percent transmission of pyrex-brand glass decreased from 69 to 54 percent after 50 h of exposure. However, there is no significant decrease for fused silica. [25, 49] In addition, fused silica is generally considered to be good even for transmission of spectrum with low wavelengths of about 200 nm. Depending on trace element composition, different grades and types of fused silica are available to meet the diverse ultraviolet radiation requirements of the lamps. Thus fused silica is chosen as the inner cylinder material in the new photochemical reactor.

Reactor shielding material

UV radiation is dangerous to the skin. It can cause photochemical effects in mammalian tissues at considerable depths below skin. Short exposure to UV results in erythema, while moderate exposure causes reddening of skin, and excessive exposure

may cause blistering or even bleeding in extreme cases. [28] In addition, UV light can have immediate or long-term effects on the eyes. Photokeratitis is an example of an immediate effect that causes painful feeling on the front surface of the eyes. Long term effects include cataract formation, and possibly macular degeneration. The damaging effects of exposure to UV radiation can be cumulative, with the consequences not immediately apparent.

To prevent UV radiation escaping from the reactor, the outer wall of a reactor should work not only as a container of the flow fluid, but also as a UV shield. In this study, acrylic is chosen as the outer material of reactor because it allows negligible transmission of UV light through it. The light transmission through a 3 mm thick layer of the commercially available Plexiglass-brand acrylic is shown in Table 4.1. [75]

Table 4.1 Measurement of light transmission through Plexiglass-brand acrylic (3 mm thickness)

Wavelength (nm)	**% transmission**
400	89
375	69
350	9
325	0
300	0

In the present work, the reactor front is covered by two pieces of Sellstrom green vinyl curtain for additional safety. This curtain, which is 4' × 5' and 1.4 mm thick, is 100 percent UV protective.

4.2.6 Choice of reflector

The most desirable reflector material has a high reflectivity in the UV region, and it can maintain this kind of reflectivity for long periods. Among different reflecting materials, aluminum is the only anti-corrosion material that is capable of providing such a high level of specular reflectance throughout the UV region with wavelength range of 200 nm – 400 nm. It is expected that higher the purity of the aluminum, the higher its specular reflectivity is. [28] Keeping all of these in mind, commercially available alzak aluminum reflector is selected for the present study. The length of the reflector is chosen to be longer than the UV lamp and almost the same as the length of irradiated surface formed by the liquid film. The shape of the reflector is shown in Fig. 4.9, and its cross section is similar to that of the parabolic reflector described in Section 4.1.2. As illustrated in Fig. 4.9, the position of the reflector is chosen to be close to the UV lamp, so that the reflected rays fall more closely on the top of the cylinder, which is the radiated area. If the reflector is placed far from the lamp, a large fraction of the reflected energy will not be concentrated on the top of cylinder, thereby reducing the light intensity at the radiated area.

A complete analysis of the reflectance characteristics of the reflector requires the knowledge of the angular distribution of the reflected light for every possible angle of incidence and for every possible wavelength. This kind of analysis is almost not feasible. To overcome this, a simple method has been employed in the present study. An investigation of ammonia removal efficiency is conducted for two cases, with and without the reflector. The conclusions drawn, give a good qualitative as well as semi-quantitative understanding of the effect of the reflector.

4.2.7 Control of temperature

Theoretically, the effect of temperature on the overall rate of reaction is determined by the activation energies of all the important reaction steps and by the effect of temperature on the volumetric rate of light absorption, I_a. The latter is related to the change of molecular absorptivity α with the change in temperature, which is normally negligible. In addition, the overall activation energy is believed to be very low in photochemical reactions. [46, 48] If it is further assumed that the reaction path does not change with temperature, then it can be stated that for most practical cases, the energy added to a molecule at a given wavelength by an increase in the temperature, is small compared to the energy rise upon the absorption of a light quantum. Hence the temperature does not have a significant effect on the primary process. In this study, it was found that the temperature of the reacting fluid experienced only small fluctuations under natural ventilation. Therefore, there is no specific temperature control device employed in the new reactor system.

4.2.8 Control of wall deposit

Wall deposits are the opaque layers that deposite on the reactor walls transmitting the effective light radiation. It has been reported in the literature [26, 46, 50, 51] that they are the common experimental problems in photochemistry. Unfortunately, the mechanisms of their formation are not very clear. However, some of the characteristics of wall deposit can be described as follows:

(1) Wall deposits can be caused by the impurities in feed solution or by the side reactions during the photochemical processes.

(2) The significance of the wall deposits is influenced by system characteristics. For example, they are a more serious problem in gas phase reacting system than in a liquid phase reacting system.

(3) Wall deposits reduce the light intensity reaching the reacting fluid and thus cause a decrease in the reaction rate. The decrease in the light intensity depends upon the transmission characteristics of the wall deposits.

(4) Wall deposits may affect the rate and the nature of the wall termination steps, thus further affecting the overall equation.

One possible solution [50] to overcome these problems, is to divide the whole reactor into two zones that are separated by a Teflon grid with low optical transparency. The first zone is used to carry out primary reactions. The free radicals produced in the first zone then transport to the second zone, and thus initiate subsequent secondary reactions. This design prevents deposit-forming constituents from interacting at the light transmitting surfaces of the reactor, and thereby avoiding the deposition. However, the success of this method depends on the transportation of free radicals through the separating grid. Thus the type and geometry of the grid and the length of first zone need to be carefully designed. The use of low concentrations and conversions may be another choice [51] to avoid the formation of wall deposits, but this method does not solve the design and scale-up problem ultimately.

In the present study, a wiping blade is installed at the bottom of the inner cylinder as shown in Fig. 4.9. To provide an efficient scraping action, the cylinder is rotated continuously so that the wiping blade maintains continuous contact with the whole surface of the cylinder wall and removes any deposit formed there. The position of the wiping blade is adjustable to provide flexibility. With this design, a fully replenished clear reacting surface is provided for irradiation. This is one of the novel features of the Rotospray Photolytic Reactor.

4.3 Initial kinetics reaction model

In UV/H_2O_2 system, hydrogen peroxide is the principal absorber of UV light. For example, at $\lambda = 220$ nm, the molar extinction coefficients for hydrogen peroxide and ammonia, are 80 $M^{-1}cm^{-1}$ and 2 $M^{-1}cm^{-1}$ respectively. The spectral distributions of molar extinction coefficients of hydrogen peroxide and ammonia in aqueous solution are illustrated in Fig. 4.12.

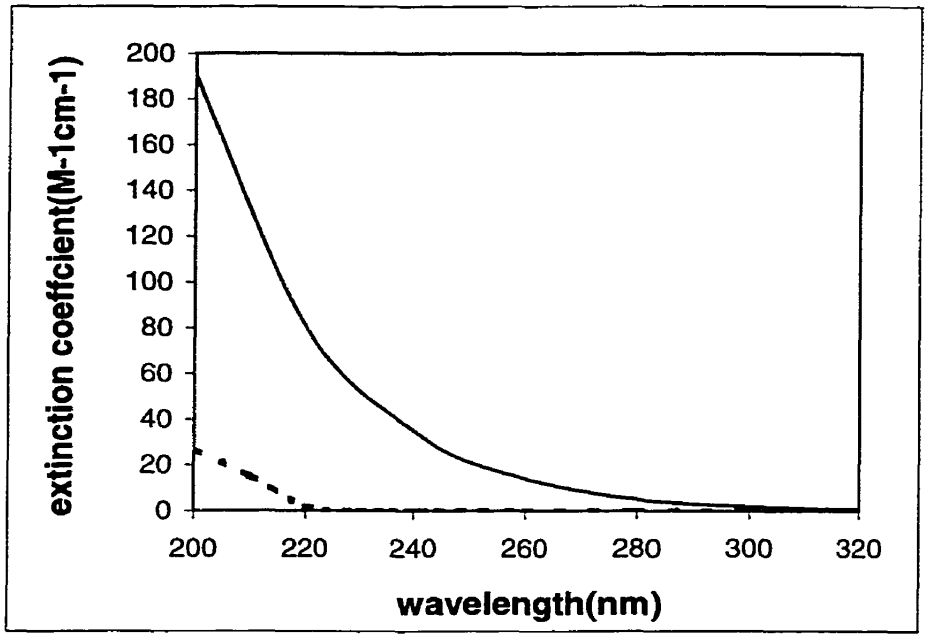

Figure 4.12 Spectral distribution of molar extinction coefficients of hydrogen peroxide and ammonia in aqueous water. (-) H_2O_2, (.) NH_4OH

The direct photolysis of ammonia can be ignored because of its weak absorption compared to hydrogen peroxide, thus hydrogen peroxide is considered as the only species involved in the primary process. Hence in UV/H_2O_2 system, for short irradiation times, the reaction schemes can be illustrated by the equations given below. It should be noted that ammonia and hydrogen peroxide are considered to be the only effective •OH radical scavengers here. [42, 52]

$$H_2O_2 \xrightarrow{h\nu} 2{\bullet}OH \qquad (3\text{-}19)$$

$${\bullet}OH + NH_3 \xrightarrow{k_A} {\bullet}NH_2 + H_2O \qquad (3\text{-}47)$$

$${\bullet}OH + H_2O_2 \xrightarrow{k_H} H_2O + {\bullet}HO_2 \qquad (3\text{-}21)$$

Where k_A and k_H are rate constants of Eqn. (3-47) and (3-21) respectively.

Supposing the quantum yield is Φ, the rate expression for Eqn. (3-19) can be written as:

$$r_I = \Phi I_a \tag{4-7}$$

Where Φ is quantum yield (mol/Einstein) of hydrogen peroxide.

The differential equations describing the concentrations of ammonia, hydrogen peroxide and hydroxyl radicals deduced from Eqns. (2-19), (2-47) and (2-21) are:

$$\frac{d[NH_3]}{dt} = -k_A[NH_3][\bullet OH] \tag{4-8}$$

$$\frac{d[H_2O_2]}{dt} = -\Phi I_a - k_H[H_2O_2][\bullet OH] \tag{4-9}$$

$$\frac{d[\bullet OH]}{dt} = 2\Phi I_a - k_A[NH_3][\bullet OH] - k_H[H_2O_2][\bullet OH] \tag{4-10}$$

To simplify the above differential equations, the steady-state hypothesis can be used. It states that the concentrations of intermediates are low and constant because the lifetimes of the intermediate species are very short. Hence,

$$\frac{d[\bullet OH]}{dt} = 0 \tag{4-11}$$

Equation (4-10) becomes,

$$2\Phi I_a - k_A[NH_3][\bullet OH] - k_H[H_2O_2][\bullet OH] = 0 \tag{4-12}$$

hence,

$$[\bullet OH] = \frac{2\Phi I_a}{k_A[NH_3]+k_H[H_2O_2]} \quad (4\text{-}13)$$

By substituting Eqn. (4-13) into (4-8),

$$\frac{d[NH_3]}{dt} = (-k_A[NH_3])\left[\frac{2\Phi I_a}{k_A[NH_3]+k_H[H_2O_2]}\right] \quad (4\text{-}14)$$

To use the above reaction model for predicting the initial reaction rate of ammonia, the values of the concentrations of various reacting species are replaced by their initial concentrations, indicated by the subscript 0:

$$\left.\frac{d[NH_3]}{dt}\right|_{t=0} = (-k_A[NH_3]_0)\left[\frac{2\Phi I_a}{k_A[NH_3]_0+k_H[H_2O_2]_0}\right] \quad (4\text{-}15)$$

Practically I_a is calculated by the following equation:

$$I_a = FG_0/V \quad (4\text{-}16)$$

where,

F is the fraction of UV light absorbed by hydrogen peroxide

G_0 is the total incident UV light flux

V is the total irradiated volume

Substituting Eqn. (4-16) into (4-15),

$$\left.\frac{d[NH_3]}{dt}\right|_{t=0} = (-2\Phi FG_0/V)\left[\frac{k_A[NH_3]_0}{k_A[NH_3]_0+k_H[H_2O_2]_0}\right] \quad (4\text{-}17)$$

The above equation can also be written as:

$$\frac{d[NH_3]}{dt}\Big|_{t=0} = (-2\Phi FG_0/V)\left[\frac{k_A}{k_A + k_H[H_2O_2]_0/[NH_3]_0}\right] \quad (4\text{-}18)$$

As indicated by the above equation, the initial rate of ammonia degradation depends on incident UV light flux, initial concentration ratio of hydrogen peroxide and ammonia and the fraction of UV light absorbed by hydrogen peroxide. F is further influenced by the total absorbed light flux and the relative absorbance of ammonia and hydrogen peroxide.

If incident light intensity (I) is known, the incident light flux, I_a can be calculated by the following equation:

$$I_a = \alpha CI = \alpha I\,[H_2O_2] \quad (4\text{-}19)$$

where,

α is the molar absorption coefficient

C is the concentration of hydrogen peroxide

Substituting Eqn. (4-19) into (4-15) at initial conditions,

$$\frac{d[NH_3]}{dt}\Big|_{t=0} = (-2k_A\Phi\alpha I)\left[\frac{[NH_3]_0[H_2O_2]_0}{k_A[NH_3]_0 + k_H[H_2O_2]_0}\right] \quad (4\text{-}20)$$

The above equation can be written as:

$$\frac{d[NH_3]}{dt}\Big|_{t=0} = (-2\Phi\alpha I)\left[\frac{k_A}{\frac{k_A}{[H_2O_2]_0} + \frac{k_H}{[NH_3]_0}}\right] \quad (4\text{-}21)$$

Eqn. (4-21) illustrates that both the initial concentration of ammonia and hydrogen peroxide will affect the initial rate of ammonia removal.

4.4 Overall kinetic reaction model

The photochemical process of ammonia removal with the help of UV radiation is quite complex. It involves a series of reactions including photo-initiating step, propagation steps and termination steps. Even if the rate expression for every individual step is known, it is almost impossible to derive a complete kinetics model because the number of variables is too large. Thus it is necessary to find a simple but reliable model to describe the performance of different photochemical reactors. Based on the results obtained in a previous study, [34] it is known that nitrite (NO_2^-), nitrate (NO_3^-), and nitrogen gas (N_2) are the primary products in photochemical oxidation processes of ammonia removal. Hence an overall kinetics is proposed to model the whole photochemical process as given by the following equations:

$$NH_3 \xrightarrow{k1} NO_2^- \xrightarrow{k2} NO_3^- \qquad (4\text{-}22)$$

$$NH_3 \xrightarrow{k3} N_2 \qquad (4\text{-}23)$$

In photochemistry, the reaction rate is a function of the concentration of the reacting species, the individual kinetic constants of each reacting step, and the volumetric rate of light absorption. It can be expressed by the following equation:

$$r_i = k' I_a^m C_i^n \qquad (4\text{-}24)$$

For simplification, I_a is assumed to be constant for a specific incident light intensity and n is taken as 1. The first two parameters are constants and can be combined into one constant k. Hence Eqn. (4-24) becomes

$$r_i = kC_i \tag{4-25}$$

k_1, k_2 and k_3 in Eqns. (4-22) and (4-23) have the same meaning as that of rate constant k in the above equation.

The differential equations describing the concentration changes of ammonia (C_1), nitrite (C_2), nitrate (C_3) and nitrogen (C_4) are:

$$r_{c1} = -k_1C_1 - k_3C_1 = -(k_1 + k_3)C_1 = -kC_1 \tag{4-26}$$

$$r_{c2} = k_1C_1 - k_2C_2 \tag{4-27}$$

$$r_{c3} = k_2C_2 \tag{4-28}$$

$$r_{c4} = k_3C_1 \tag{4-29}$$

In a recirculation reactor, the mass balance is schematically shown in Fig. 4.13 and is expressed by Eqn. (4-30):

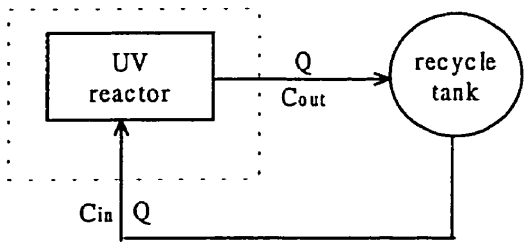

Figure 4.13 Schematic diagram of mass balance of recirculation reactor

$$\frac{dC_i}{dt} V = QC_{i,in} - QC_{i,out} + r_{ci}V \quad (4\text{-}30)$$

where,

V is the volume of reactor (m^3)

Q is the recirculation rate (m^3/s)

$C_{i,\,in}$ and $C_{i,\,out}$ are the inlet and outlet concentrations of substance i (mol/L)

When recirculation rate is high, $C_{i,\,in}$ can be considered equal to $C_{i,\,out}$, thus Eqn. (4-30) can be simplified as:

$$\frac{dC_i}{dt} = r_{ci} \quad (4\text{-}31)$$

Substituting Eqn. (4-26) to (4-29) into (4-31) gets,

$$\frac{dC_1}{dt} = -k_1C_1 - k_3C_1 = -(k_1 + k_3)C_1 = -kC_1 \quad (4\text{-}26)$$

$$\frac{dC_2}{dt} = k_1C_1 - k_2C_2 \quad (4\text{-}27)$$

$$\frac{dC_3}{dt} = k_2C_2 \quad (4\text{-}28)$$

$$\frac{dC_4}{dt} = k_3C_1 \quad (4\text{-}29)$$

Where $k = k_1 + k_3$. According to the principle of mass balance, the total concentration of nitrogen-containing substances is constant, hence

$$C_{1_0} + C_{2_0} + C_{3_0} + C_{4_0} = C_1 + C_2 + C_3 + C_4 \quad (4\text{-}30)$$

The initial concentrations of nitrite, nitrate and nitrogen are zero, thus the initial conditions are:

$$C_{2_0} = 0,\ C_{3_0} = 0,\ C_{4_0} = 0 \quad (4\text{-}31)$$

Solving Eqn. (4-26) through (4-31),

$$C_1 = C_{1_0} e^{-kt} \quad (4\text{-}32)$$

$$C_2 = \frac{k_1 C_{1_0}}{k_2 - k}(e^{-kt} - e^{-k_2 t}) \quad (4\text{-}33)$$

$$C_3 = C_{1_0} - C_{1_0} e^{-kt} - \frac{k_1 C_{1_0}}{k_2 - k}(e^{-kt} - e^{-k_2 t}) - \frac{k_3 C_{1_0}}{k}(1 - e^{-kt}) \quad (4\text{-}34)$$

$$C_4 = \frac{k_3 C_{1_0}}{k}(1 - e^{-kt}) \quad (4\text{-}35)$$

The conversion percentage of ammonia can be obtained by rewriting Eqn. (4-32) in the following format:

$$\frac{C_{1_0} - C_1}{C_{1_0}} = 1 - e^{-kt} \quad (4\text{-}36)$$

Equation (4-32) through (4-36) can be used to predict the final product distribution and the conversion percentage in photooxidation system of ammonia removal

under proper values of k_1, k_2, k_3 and k. In recirculation reactor system, the time t is the mean hydraulic detention time. In the continuous plug-flow like system, the time t is the true hydraulic residence time. It can be predicted that longer the residence time, the greater the conversion percentage is. Thus if several photochemical reactors constitute a cascade series as shown in Fig. 4.14, the ammonia will be degraded while the reacting

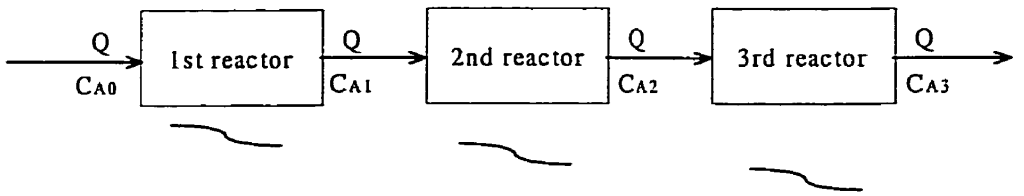

Figure 4.14 Schematic diagram of a cascade series of connected reactors

fluid passes through the reactor. The ammonia concentration will form a reverse s-type curve as shown in Fig. 4.14. It should be noted that the ammonia conversion percentage may not strictly satisfy Eqn. (4-36) for the second and subsequent reactors because of the product interference and concentration effects, etc. In the present study, the reacting fluid is completely recycled back to the reactor for the next pass to simulate the reactor cascades.

Chapter 5

Details of experimental set-up and procedures

This chapter describes the chemicals and apparatus used in this study. The experimental procedures employed on both the recirculation reactor and the new film-type flow reactor (RPR) are outlined here. The chemical analysis methods and protocols for the various compounds, involved in this study, are presented.

5.1 Materials

5.1.1 Water

In all the experiments carried out, distilled water has been used for feed preparation. For analytical determinations, deionized water and distilled water have been used. The water was prepared using the Barnstead Distillation System.

5.1.2 Chemicals

Nitrogen precursor

Ammonia hydroxide (29.8%, aqueous, certified ACS plus), ammonia nitrate (certified ACS granular) and ammonia sulfate (certified ACS), supplied by Fisher Scientific, were used.

Oxidants

Hydrogen peroxide (30%, aqueous) has been used as received from Fisher Scientific. Potassium persulphate (certified ACS), provided by VWR Scientific, has been used.

Other chemicals

Catalase from bovine liver, (60 000 units mg^{-1}, 1 unit decomposes 1 μmol H_2O_2/min at pH 7.0 and 25 °C) was obtained from Sigma. It was used to decompose the remaining hydrogen peroxide in the course of sample analysis. Bentonite from Fisher Scientific was used to synthesize feed solutions with turbidity.

All the other reagents, such as hydrochloric acid, sulfuric acid, sodium hydroxide, pH buffer solutions and various chemicals used in the sample analysis were obtained from Fisher Scientific, Sigma or Anachemia. They were certified ACS grades and were used in experiments directly without further purification.

5.2 Apparatus

5.2.1 Recirculation reactor system

The recirculation reactor system is a custom-modified Rayox advanced oxidation system provided by Calgon Carbon Oxidation Technologies of Markham, Ontario, Canada. The major components of the system are a UV reactor, a UV lamp, reactor control panel, a recycle tank, recycle control panel and other auxiliary equipment. Figure 5.1 presents a setup of the complete system.

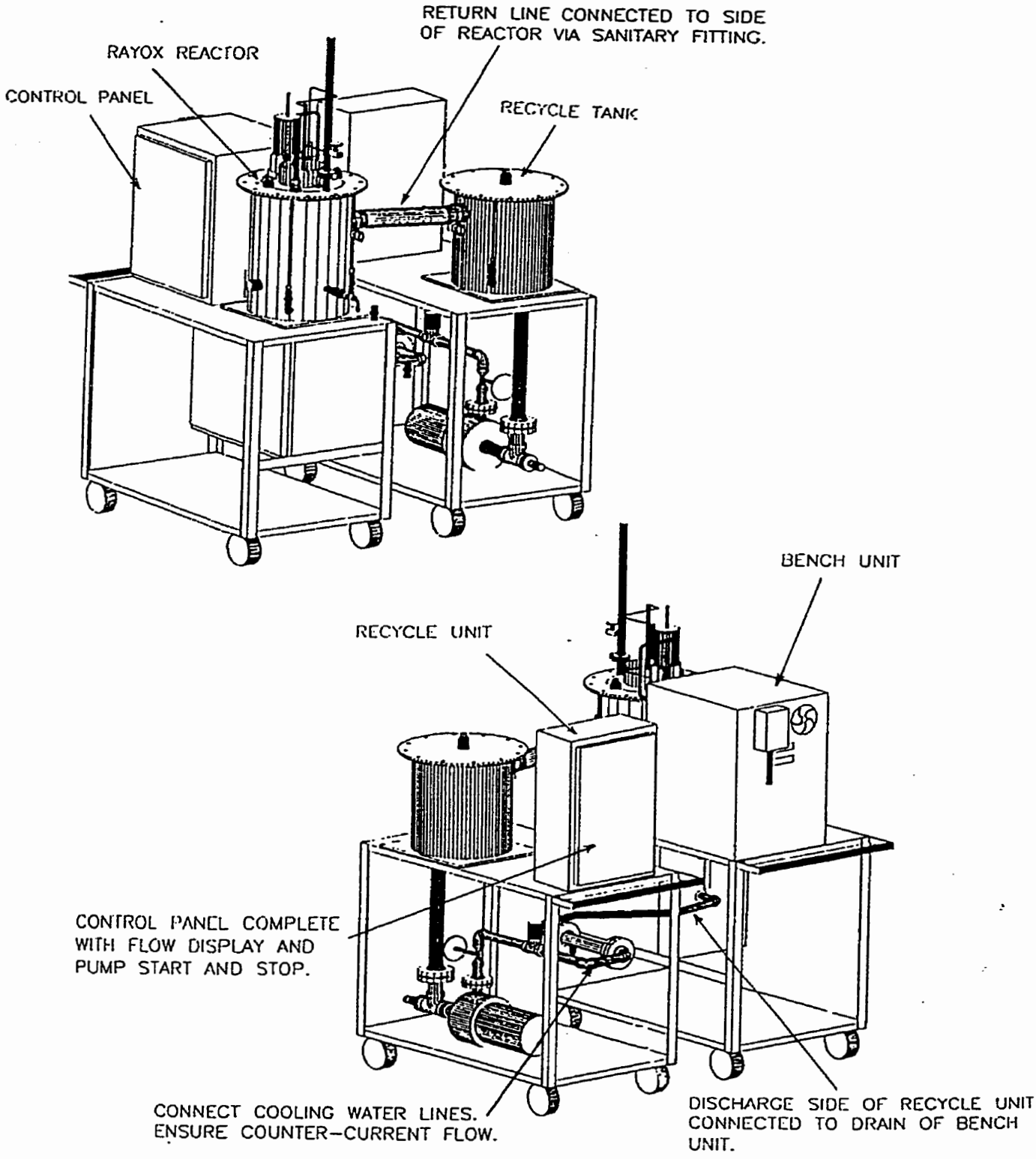

Figure 5.1 Complete setup of the recirculation photoreactor

UV Reactor

The UV reactor is a cylindrical stainless steel vessel where the treatment of wastewater takes place. It has an outer diameter of 36 cm and height of 50 cm, with a capacity of 40 L. A high power lamp is installed in the center of the reactor to emit light in the UV spectrum into the wastewater contained in the reactor chamber.

A mixer is mounted on the top plate of the reactor to provide agitation within the reactor. Its control is provided by a variable speed controller on the control panel.

A pH-sensing probe can be inserted into the reactor from the top port. The pH readout is displayed on the control panel. This pH probe is stored in pH 4.01 buffer solution when not in use.

Other parts inside the reactor include a shutter to block the UV light during the lamp startup stage, ensuring the system to be operated at the maximum output of the lamp at time zero of the experiment; a transmittance controller to provide air driven automatic cleaning of the lamp tube; and a cooling water loop through which cooling water can flow in and out ensuring the system to be operated at a constant temperature. Sample port is on the side of the reactor. Water filling port and reagent supply port are on the top of the reactor.

UV lamp

The UV lamp is separated from the water by a quartz tube of 4.2 cm outer diameter. This UV lamp is a 1kw medium pressure mercury lamp with total length of 20 cm and arc length of 8.0 cm. Its operating voltage is 250 $\pm$ 25 volts and amperage is 4 $\pm$ 0.4 amps. The output values of the lamp are shown in Table 5.1. [53] The spectral output

curve has been drawn in Fig. 4.11. The energy output of the Rayox lamp in the range of 200 to 500 nm is 482 W, among which 267 W are in the range of 200 to 300 nm, showing UV efficiency of more than 25%. For 30 L of water inside the reactor, the UV dose per minute is estimated to be 2.1 kwh/1000 gal.

Table 5.1 Output values of the Rayox medium pressure mercury lamp

Wavelength (nm)	**Light Output (watts)**	**Light Output (Einstein/s)**
200-249	159	3.0×10^{-4}
250-299	108	2.5×10^{-4}
300-349	39	1.1×10^{-4}
350-399	66	2.1×10^{-4}
400-449	49	1.7×10^{-4}
450-500	61	2.4×10^{-4}

Reactor control panel

The reactor control panel provides control over the operation of the UV reactor. There are various switches and indicators to control and display various operating conditions such as the voltage and current of the UV lamp, pH and temperature of the reacting fluid, mixing motor, shutter and the transmittance controller.

Recycle tank

The recycle tank is a cylindrical stainless steel vessel with a capacity of 25 L. It is

connected to one side of the UV reactor via a sanitary fitting by means of a 5.08 cm stainless steel braided hose. The discharge line of the recycle tank is connected to the drain line of the UV reactor through a centrifugal pump. The pump draws reacting fluid out of the UV reactor, pumps it through the flexible hose to the recycle tank and then back to the UV reactor all at a controlled flow rate. The recycle loop between the UV reactor and the recycle tank contains a manual flow control valve, a flow meter, a sample port and a heat exchanger/static mixer, to ensure a counter-current flow of cooling water and reacting fluid.

Recycle control panel

The recycle control panel provides control over the operation of system recycling. It has a flow indicator and an on-off control button for recycle.

Other equipment

Other equipment used in recirculation reactor system include Nalgene HDPE tanks, supplied by Fisher Scientific, for preparation and storage of the feeding solution; and a Masterflex peristaltic pump, from Barnant company, to pump the synthesized wastewater from the feeding tank to the reactor. The sampling device and the analytical instrument will be discussed later in this chapter.

5.2.2 Continuous film-type flow reactor - the Rotospray Photolytic Reactor (RPR)

The continuous film-type flow reactor called the Rotospary Photolytic Reactor

(RPR) has been designed by Sridhar [69] and fabricated at Carleton University, Ottawa, Canada. The design of this new system has been discussed in Chapter 4. In this section, the essential features of the apparatus constructed are described. The major components of the system are a UV reactor, a UV lamp, UV lamp control panel, a gas scrubber column and other auxiliary equipment. A schematic drawing of the apparatus is given in Fig. 5.2.

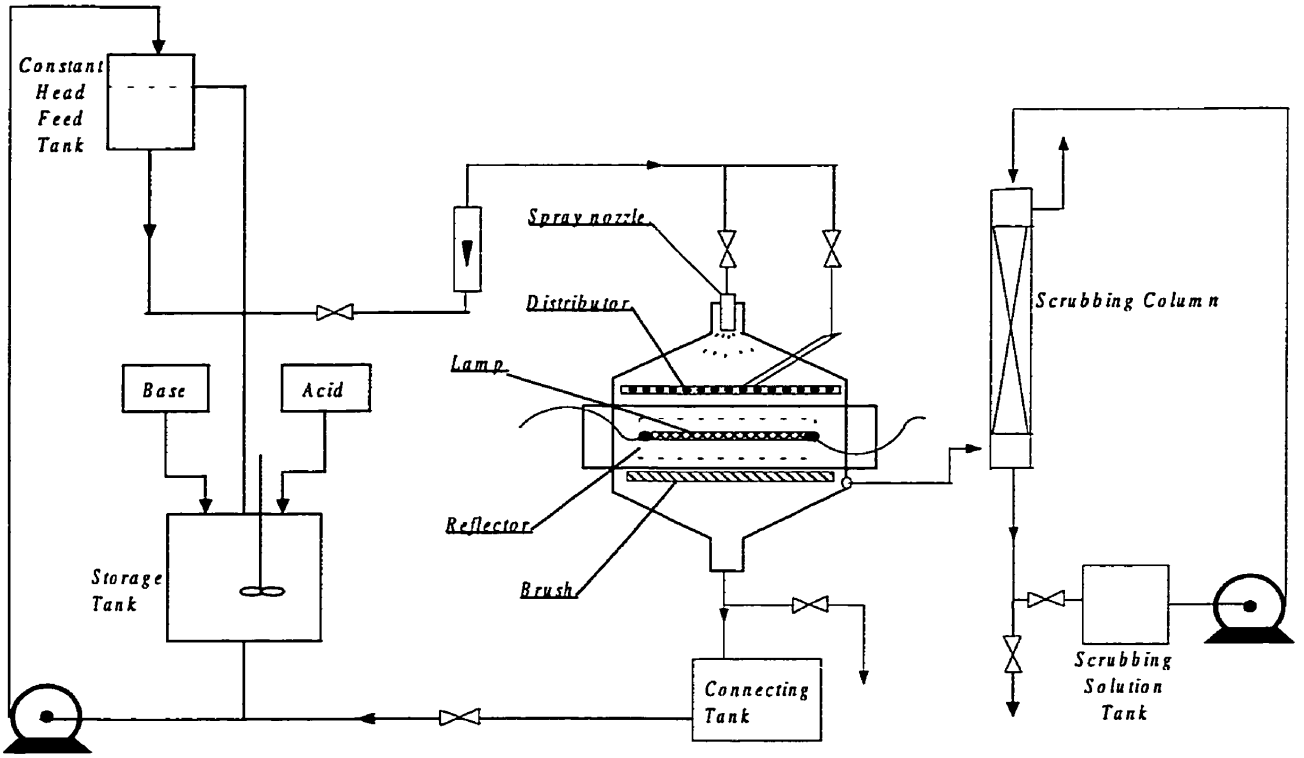

Figure 5.2 Complete setup of the RPR system

UV Reactor

The UV reactor is a vessel made out of Lexan, through which the wastewater continuously flows and the photochemical reactions take place. The vessel consists of

three sections. The top section is for the injection of wastewater into the reactor. It has a prismatic shape with increasing dimension from 12 to 40 cm with an entrance at the top, in which a spray nozzle is held, and the reacting fluid can be atomized and sprayed from the nozzle. The bottom section is for the collection of wastewater from the reactor. It also has a prismatic shape, with a dimension reducing from 40 to 12 cm, ending up with a collecting tube. The middle cubical section is the main reactor section connecting the top section and the bottom section, and has a uniform dimension of 40 cm each side.

The reactor section carries in the middle a cylindrical tube made of quartz material which has good transmission characteristics for UV light. It has an outer diameter of 21.6 cm, and an overall length of 60 cm. The cylinder passes into the acrylic wall through a compressible seal and is rotated by means of a belt drive connected to a motor. There are two advantages of this rotation: Firstly, it evenly distributes the water drops on the cylinder surface to provide a continuous film for the light absorption; Secondly, it provides a continuously replenished radiating area and prevents local overheating of the cylinder surface. The two ends of the cylinder are open to provide natural ventilation for the UV lamp. This design is important because too small an opening leads to overheating of the lamp and shortened life, whereas too large an opening may lead to excessive cooling that may prevent lamp from heating and working.

A high power UV lamp is mounted on the central axis of the cylinder so that the entire arc length of the lamp is well inside the cylinder ends. A removable aluminum reflector is installed just below the UV lamp to focus the UV rays on to the top portion of the rotating cylinder. The reflector has an opening of 10.5 cm width at the top, and 5.0 cm width at the bottom and a length of 46 cm.

A distributor tube is also provided about 1 cm from the cylinder surface at the top, for feed distribution over the rotating cylinder. The distributing tube is 32 cm long and has small apertures punched at the bottom that are 0.32 cm in diameter and are 2.12 cm apart. The configuration is horizontal, and the reacting fluid discharges from the distributor through the apertures as small water drops and forms a continuous thin film on the rotating surface of the cylinder. In addition to the distributor, the reactor is also provided with a spray nozzle (supplied by Lechler) at the top, through which additional feed can be added continuously onto the film. The spray is in the form of a fine mist which can also absorb any UV radiation not absorbed in the thin film. Upon UV light radiation, photochemical reactions occur mainly in this thin film.

An adjustable rubber brush with a length of 30 cm is provided in the six o'clock position of the rotating cylinder to keep the reaction surface free of deposits that could affect the UV transmittance.

UV lamp

Different types of UV lamps can be accommodated in the RPR system. In this study, two types of UV lamp are employed. One is the Rayox medium pressure mercury lamp as used in recirculation reactor system. The other is LL-189A UV lamp manufactured by Hanovia, Inc. This lamp is a 1.2 kw medium pressure mercury lamp with total length of 44.2 cm and arc length of 30.48. Its operating voltage is 285 volts and amperage is 4.7 amps. The output values of the lamp are shown in Table 5.2. The spectral output curve is presented in Fig. 4.10. The total energy output of the important mercury lines in the wavelength range of 200 to 300 nm, is 182.6 W, which is more than 15% of

the total energy output.

Table 5.2 Spectral energy distribution of radiated mercury lines of the Hanovia medium pressure mercury lamp

Wavelength (nm)	**Light Output (W)**
101.4	31.6
112.87	6.93
136.73	10.15
222.4	9.2
232	7.65
236	6.2
238	8.4
240	7.3
248.2	10.15
253.7	24.1
257.1	6.3
265.2	27.8
270	4.85
275.3	4.2
280.4	13.9
289.4	4.41
296.7	15.2
302.5	32.9
313	50.6
334.1	6.93
366	97.1
404.5	24.2
435.8	53
546.1	40.52
578.5	69.35

UV lamp control panel

The lamp control panel (LK-9802-01) provides control over the operation of the UV lamp. The "Start" and "Stop" buttons are provided to switch on and switch off the lamp, respectively. There are three control buttons for the input energy level of the lamp. "High" indicates full energy input, while "Medium" and "Low" indicate 66 and 33% of full energy input, respectively. There are two indicators to display the input voltage and current of the UV lamp.

Scrubbing column

A scrubbing column is provided to continuously scrub the gas exiting the reactor to trap any trace of ammonia that could become airborne in the course of the experiments. It is an acrylic column that is 15 cm in outer diameter and is 175 cm long. The column is divided into three sections which are connected by flanges to provide flexibility in installation. The bottom section is 20 cm long and contains an effluent tube that is 4 cm in outer diameter, and is the outlet for the scrubbing solution. On the side of the bottom section is an inlet for the gas coming out of the UV reactor. The top section is of the same size as the bottom section and contains a vertical inlet tube for liquid solution and a side outlet for scrubbed gas. A nozzle at the end of the inlet tube provides an even distribution of scrubbing liquid over the whole cross section of the column.

The packing material inside the column consists of two types. One is polyethlyene tubing segments with 0.64 cm i.d., 0.95 cm o.d. and 2.54 cm in length. The other material is structured cubic elements with dimension of 3.18 cm. These elements are made of stainless steel strips which have many punched holes to provide a larger surface area. The

packing materials are filled into the middle section of the column alternately, layer by layer, to improve the contact between liquid and gas. In this study, water has been chosen as the scrubbing solution because ammonia has good solubility in it. Water is pumped into the top of the column and removed from the bottom of the column. Gas enters into the column from the bottom, flows upwards through the column and leaves from the top. Inside the column, the counter-current flow of the liquid and gas contact with each other and mass transfer occurs between these two phases. If there is ammonia contained in the exit gas from UV reactor, it will transfer from gas to water. The amount of the scrubbed ammonia can be determined by sampling the scrubbing water. If necessary, spot checks for gaseous ammonia can be made directly on this exiting gas from the scrubber, by bubbling it in a mild acid solution and back titrating the acid solution.

Other equipment

Other equipment used in the RPR system include a 12-channel scanning thermocouple thermometer (692-8010) provided by Bernant company, which is used for real-time monitoring on the temperature of the cylinder surface; a PHCN-440 pH controller with peristaltic metering pump that is used to adjust the pH of the feeding solution; a mixer with propeller shaft and Nalgene HDPE tanks, used for synthesizing the feeding solution; Masterflex peristaltic pumps, to pump the synthesized wastewater from storage tank to feed tank and to pump the scrubbing solution into the scrubbing column; and various tubes and stopcocks to connect the piping system. The other sampling device and analytical instrument will be discussed later in this chapter.

5.3 Experimental procedures

5.3.1 Recirculation reactor

Dark reaction

In the study presented here, a typical experiment of dark reaction in the recirculation reactor was conducted as follows: First, 57.2 L of distilled water were pumped into the recirculation system through the filling port of the UV reactor. Then the mixer inside the UV reactor was turned on and the pump of the recycle tank was switched on and adjusted to 10 GPM of recirculation speed. This was done to ensure a complete mixing of the solution. Ammonium hydroxide with proper concentration was then introduced into the reactor through the reagent supply port. Then the selected oxidant, hydrogen peroxide or potassium persulphate, was added into the reactor and the pH of the combined solution was adjusted to 10 by pH buffer solution and proper acidic or basic solution. The total volume of the solution was then adjusted to 60 L and initial sample was taken from the sampling port of the UV reactor. The reacting fluid was recirculated for several hours as designed and samples were taken from the UV reactor every half hour and analyzed.

Photooxidation reaction

In the study presented here, a typical experiment of photooxidation reaction in the recirculation reactor was performed as follows: First, 57.2 L of distilled water were pumped into the recirculation system through the filling port of the UV reactor. Then the mixer inside the UV reactor was turned on and the pump of the recycle tank was also

switched on and adjusted to the designed recirculation speed to ensure a complete mixing of the solution. Ammonium hydroxide with proper concentration was then introduced into the reactor through the reagent supply port. Then the selected oxidant, hydrogen peroxide or potassium persulphate, was added into the reactor and the pH of the combined solution was adjusted to the designed value by pH buffer solution and proper acidic or basic solution. The total volume of the solution was then adjusted to 60 L and an initial sample was taken from the sampling port of the UV reactor. The lamp pushbutton was pressed to ignite the lamp after the shutter was closed. When the voltmeter on the control panel indicated a stable value around 220 V, it meant that the ignition of the lamp was complete and the shutter could be withdrawn. This was the starting point of the photochemical reaction and the beginning of the experimental run. The reacting fluid was then irradiated and recirculated for several hours as planned and samples were taken from the UV reactor at designed intervals and analyzed.

The operating steps in the corresponding experiments in batch reactor were similar to the above procedure except that the total volume of the reacting solution taken was 30 L instead.

5.3.2 RPR system

Direct photolysis

In the study presented here, a typical experiment of direct photolysis in the RPR system was carried out as follows. First, 10 L of distilled water were added into the storage tank. Ammonium hydroxide with the desired concentration was then introduced

into the tank with the mixer switched on, to ensure complete mixing of the solution. The pH of the solution was then adjusted to 10 by pH controller by the addition of acidic or basic solution. Then the solution was pumped from the storage tank to the top feed tank. The solution was fed by gravity and entered into the UV reactor at a set flowrate (e.g., 85 ml/min). The flowrate could be easily controlled by the adjustment of the rotameter valve installed on line. The motor controller was then turned on and the cylinder rotation speed was adjusted to 7.5 rpm. The solution was then allowed to flow through the whole system for a few minutes, to rinse the piping system and the reactor. Then the lamp was powered on at the required power level and this was the beginning of the experimental run. After the UV lamp came to a steady state, the samples were collected every five minutes and analyzed.

Photooxidation reaction

In the study presented here, a typical experiment of photooxidation reaction in the RPR system was run as follows: First, 10 L of distilled water were added into the storage tank. Then ammonium hydroxide with the desired concentration was introduced into the tank with the mixer switched on, to ensure complete mixing of the solution. Then the selected oxidant, hydrogen peroxide or potassium persulphate, was added into the tank and the pH of the combined solution was adjusted to the desired value by pH controller, through the addition of acidic or basic solution. This solution was then pumped from the storage tank to the top feed tank. The solution was fed by gravity and entered into the UV reactor at a regulated flowrate. The flowrate could be easily controlled by the adjustment of the rotameter valve installed on line. The motor controller was then turned on and the

cylinder rotation speed was adjusted to 7.5 rpm. The solution was let to flow through the whole system for a few minutes to rinse the piping system and the reactor. Then the lamp was powered on at the required power level and this was the beginning of the experimental run. After the UV lamp came to a steady state, the samples were collected every five minutes and analyzed.

The operating steps in the multi-pass photooxidation were similar to the above procedures except that the reacting solution was pumped back into the top feed tank, for the next pass.

5.4 Sample analysis

The aqueous samples in this study were taken from the reactor sampling port and collected in Nalgene HDPE bottles. Samples were analyzed immediately. If prompt analysis was not possible, samples were stored at 4 °C and analyzed within the next 24 hours. Catalase was added to remove the remaining hydrogen peroxide in the sample. Gaseous samples in this study were collected through gas sampling nipples provided in the reactor vessel into Tedlar sampling bag by the Gilian air sampling pump.

The compounds analyzed in the aqueous solution included ammonia, nitrite, nitrate, hydrazine, hydroxyamine, hydrogen peroxide, persulphate and sulphate. The compounds analyzed in the gaseous sample included nitric oxide, nitrous oxide, nitrogen dioxide, nitrogen and ammonia. The analytical methods are outlined below.

5.4.1 Reactant

Colorimetric analysis of ammonia [56]

Ammonia can react with Nessler reagent (K_2HgI_4), which is a complex of mercury iodide and potassium iodide in strong alkaline solution, to produce a yellow-brown colloid, mercury amino iodide (Hg_2OINH_2). This complex absorbs strongly over a wide wavelength range from 400 to 425 nm and its absorbance is a linear function of the ammonia concentration according to Beer-Lambert law. This method can be applied to natural water and purified effluents that are low in color. The detection range of this method is 0.02 to 5 mg/L.

In this study, samples were diluted to make the concentration of ammonia fall in the detection range. Then 0.5 mL Nessler reagent was added and completely mixed. The reaction was allowed to proceed for 40 minutes. Then the absorbance was measured at 410 nm for 1-cm light path with a UV/Vis spectrophotometer. Blank solution and standard ammonium solutions of 1, 2, 3 and 4 mg/L were reacted with Nessler reagent at the same temperature and reaction time used for samples. Calibration curve was obtained by plotting the absorbance of standard ammonium solutions versus their concentration. Therefore given the absorbance of the sample solution, the concentration of ammonia could be obtained directly from the calibration curve.

Iodometric titration of hydrogen peroxide [58, 59]

Hydrogen peroxide can react with iodide in acidic solution to produce iodine. The iodine generated can then be quantitatively titrated by sodium thiosulphate (NaS_2O_3) solution. Using starch as indicator, the titrated solution will change from blue to colorless

at end point. The consumed amount of thiosulphate is directly proportional to the concentration of hydrogen peroxide existing in the samples. This method can be applied to water, free of turbidity and low in color.

In this study, first 5 mL 20% KI and 5 mL 1M H_2SO_4 were added into a 125 mL Erlenmyer flask containing 50 mL water. Then an appropriate sample aliquot was added and mixed completely. The solution was allowed to stand for 15 minutes. Then the solution was titrated with 0.1 N sodium thiosulphate. When the solution turned to a straw yellow color, 2 mL 2% starch solution was added and the titration was continued till a clear endpoint.

Ceric titration of persulphate [58]

Persulphate can react with ferrous ion (Fe^{2+}) in acidic solution in the presence of bromide to give sulphate and ferric ion (Fe^{3+}). The excess ferrous ion is further titrated by ceric sulphate solution. Using ferroin as indicator, the titrated solution will change from orange to yellow. The consumed amount of ferrous is directly proportional to the concentration of persulphate existing in the samples. This method can be applied to water free of turbidity and low in color.

In this study, first 7 mL 5M NaBr and 2 mL 3M H_2SO_4 were added into a 125 mL Erlenmyer flask containing 50 mL water. Then 10 mL sample was added and mixed completely. 10 mL 0.05 N $Fe(NH_4)_2(SO_4)_2$ was then added and mixed. The solution was allowed to stand for 20 minutes. Then 1 mL 0.001 M ferroin indicator was added and the solution was titrated with 0.02 N ceric sulphate solution till the color is changed from orange to yellow.

5.4.2 Reaction intermediate

Colorimetric analysis of hydrazine [60]

Hydrazine can react with P-dimethylaminobenzaldehyde to produce a yellow-colored azine that rearranges in the presence of strong acid to form an intensely red-orange quinonoid structure. This complex absorbs strongly at 458 nm and its absorbance is a linear function of the hydrazine concentration according to Beer-Lambert law. This method can be applied to water free of turbidity and low in color. The upper detection limit of this method is 0.77 mg/L.

In this study, samples were diluted to make the concentration of hydrazine fall in the detection range. Then 0.5 mL of 2% P-dimethylaminobenzaldehyde solution was added and completely mixed. The reaction was allowed to proceed for 40 minutes. Then the absorbance was measured at 458 nm for 1-cm light path with a UV/Vis spectrophotometer. Blank solution and standard hydrazine solutions of 0.1, 0.3, 0.5 and 0.7 mg/L were reacted with P-dimethylaminobenzaldehyde reagent at the same temperature and reaction time used for samples. Calibration curve was obtained by plotting the absorbance of standard hydrazine solutions versus their concentration. Therefore given the absorbance of the sample solution, the concentration of hydrazine could be obtained directly from the calibration curve.

Colorimetric analysis of hydroxylamine [57]

Hydroxylamine can react with Nessler reagent (K_2HgI_4) to produce a yellow-colored complex as that in ammonia analysis. This complex absorbs five times greater

than ammonia. To overcome the interference with ammonia, hydrochloric acid is added after the formation of the colored complex, in order to decompose ammonium mercuriiodide complex, while the complex of hydroxylamine and Nessler reagent remained unchanged. This complex absorbs strongly at 420 nm and its absorbance is a linear function of the hydroxylamine concentration according to Beer-Lambert law. This method can be applied to water free of turbidity and low in color. The detection range of this method is from 0.1 to 1.65 mg/L.

In this study, samples were diluted to make the concentration of hydroxylamine fall in the detection range. Then 4 mL 4% perchloric solution was added and completely mixed. After 2 minutes, 0.5 mL Nessler reagent was added and mixed. When precipitation was formed after 5 minutes, 1 mL 6N HCl was added and completely mixed. The reaction was allowed to proceed for 60 minutes. It was observed that the precipitation was dissolved and the color formation reached to its maximum. Then the absorbance was measured at 420 nm for 1-cm light path with a UV/Vis spectrophotometer. Blank solution and standard hydroxylamine solutions of 0.25, 0.5, 0.75 and 1.0 mg/L were reacted with Nessler reagent at the same temperature and reaction time used for samples. Calibration curve was obtained by plotting the absorbance of standard hydroxylamine solutions versus their concentration. Therefore given the absorbance of the sample solution, the concentration of hydroxylamine could be obtained directly from the calibration curve.

5.4.3 Final products of the reactions

Colorimetric analysis of nitrite [61]

Nitrite can react with sulfanilamide in acidic solution to produce diazo compound. The generated diazo can further react with N-(1-naphthyl)-ethylenediamine dihydrochloride to give a reddish purple azo dye. This complex absorbs strongly at 543 nm and its absorbance is a linear function of the nitrite concentration according to Beer-Lambert law. This method can be applied to water free of turbidity and low in color. The detection range of this method is from 10 to 200 μg/L.

In this study, samples were diluted to make the concentration of nitrite fall in the detection range. Then 0.5 mL 1% sulfanilamide solution was added and completely mixed. After 5 minutes, 0.5 mL 0.1% N-(1-naphthyl)-ethylenediamine dihydrochloride solution was added and mixed. The reaction proceeded for 30 minutes. Then the absorbance was measured at 543 nm for 1-cm light path with a UV/Vis spectrophotometer. Blank solution and standard hydroxylamine solutions of 50, 100, 150 and 200 μg/L were reacted with the two reagents at the same temperature and reaction time used for samples. Calibration curve was obtained by plotting the absorbance of standard nitrite solutions versus their concentration. Therefore given the absorbance of the sample solution, the concentration of nitrite could be obtained directly from the calibration curve.

Ion chromatographic analysis of nitrite, nitrate and sulphate [56.62]

A water sample was injected into a stream of carbonate-bicarbonate eluent and

passed through a series of ion exchange columns. The anions were separated according to their relative affinities for the low capacity, strongly basic anion exchanger. Then the separated anions were directed through a suppressor column in which the anions were converted to their highly conductive acid forms and the carbonate-bicarbonate eluent was converted to weakly conductive carbonic acid. The separated anions, in their acid forms, were measured by conductivity. They were identified on the basis of retention time as compared to their standards and quantified by the measurement of peak area. In this method the lower limits of detection for nitrite, nitrate and sulphate were 0.1, 0.1 and 0.25 mg/L, respectively.

In this study, a Dionex Ion Chromatograph equipped with a conductivity detector and a linear UV/Vis detector was used. The operating conditions were as follows:

Sample loop volume	50 μL
Eluent pressure	7-10 psi
Eluent flowrate	20 $ml.min^{-1}$
AMMS suppressor solution pressure	10 psi
AMMS suppressor solution flowrate	4 $ml.min^{-1}$
Conductivity detector operating range	3
UV detector (λ)	215 nm

Samples were diluted to make the concentration of anions fall in the detection range. The standard solutions of 1, 5, 10 and 15 $mg.L^{-1}$ were injected to the column first. Calibration curve was obtained by plotting the peak area of standard solutions versus their concentrations. After the correlation coefficients of the calibration curves were larger than 0.999, samples were injected. Therefore given the peak area of the sample

solution, the concentration of anion could be obtained directly from the calibration curve.

Gas chromatographic analysis of nitrogen and nitrous oxides [60, 63, 64]

A gas sample was injected into a stream of carrier gas (helium) and passed through a teflon chromatographic column. Different gaseous components have different retention time in the column. Hence they emerged from the column sequentially and were detected, recorded and integrated to give a gas chromatogram. The peaks were identified on the basis of the retention time as compared to their standards, and were quantified by the measurement of peak area. This method was applied to analyze nitrogen and nitrous oxide.

In this study, a Varian Vista 6000 gas chromatograph equipped with a teflon column (packed with porapak Q, 8' × 1/8", 80/100 mesh) and a thermal conductivity detector were used. The operating conditions were as follows:

Carrier gas flowrate	20 $ml.min^{-1}$
Injection temperature	150°C
Column temperature	25°C
Thermal conductivity detector temperature	200°C

First, carrier gas (helium) was passed through the column. When the baseline reached stable state, the mixture of standard gases was injected. After the calibration curve was prepared by plotting the peak area of standard gases versus their percentage, samples were injected. Therefore given the peak area of the sample gas, the percentage of sample could be obtained directly from the calibration curve.

Gas detector tube monitoring of nitrogen oxides [65]

Gastec Detector Tube is a rapid, fully quantitative analysis of the concentration of nitrogen oxides in air using Gastec Multi-Stroke Gas Sampling Pump. Nitric oxide is oxidized to nitrogen dioxide by chromic acid in the tube. The generated nitrogen dioxide and the original nitrogen dioxide possibly existing in the sample are then oxidized by o-tolidine ($C_{14}H_{16}N_2$) to form nitroso-o-tolidine ($C_{14}H_{14}N_2O$). The processes are expressed by Eqns. (5-1) and (5-2). This method can be applied to analyze nitrogen dioxide in the range of 0.2 to 16.5 ppm.

$$NO + CrO_3 + H_2SO_4 \rightarrow NO_2 \qquad (5\text{-}1)$$

$$NO_2 + C_{14}H_{16}N_2 \rightarrow C_{14}H_{14}N_2O \qquad (5\text{-}2)$$

In this study, one end of the detector tube was inserted into the rubber inlet of the sampling pump with the arrow on the tube pointing toward the pump, while the other end of the tube was connected to the outlet of the UV reactor. The gas was pumped into the tube by pulling the pump handle all the way out until it locked on 1 pump stroke. A waiting period of 2 minutes was observed, until the staining stopped. The above sampling procedure was then repeated once. The concentration of nitrogen dioxide could be read directly at the interface of the stained-to-unstained reagent.

Chapter 6

Experimental results and discussions

In the present research work, a study of the photochemical oxidation of ammonia has been carried out for two different reactor systems: the recirculation reactor, and the RPR system. Hydrogen peroxide and potassium persulphate have been used as oxidizing species in the reactor systems. A detailed discussion of the process variables, reaction schemes, reaction mechanisms, and kinetics models for different reactor configurations is presented here.

6.1 Review of the previous studies on photochemical oxidation

A comprehensive study of the photochemical oxidation was conducted recently by Sridhar, 1998, [35] which included the selection of ammonia precursors and oxidants, the study of the direct photolysis, and the advanced photo-oxidation of the different ammonia precursors. The effects of the major process parameters were also studied in the Rayox batch reactor system. The conclusions drawn in the above-mentioned study, that are relevant to the present work are described below:

(1) Nitrogen precursor: Ammonium hydroxide had a higher removal efficiency compared to other ammonia precursors, such as ammonium nitrate, ammonium oxalate, ammonium acetate, etc. The performance of the ammonium sulphate was close to that of the ammonium hydroxide. Hence both ammonium hydroxide and ammonium sulphate could be chosen as precursors in photochemical oxidation of ammonia.

(2) Oxidants: Hydrogen peroxide and potassium persulphate were used as the oxidants in the photochemical oxidation of ammonia. It was shown that the destruction of ammonia was more rapid with potassium persulphate as oxidant. The product distributions also showed significant difference for the two oxidants. In UV/H_2O_2 system, the main products were nitrite, nitrate and nitrogen with nitrate as the predominant product. In $UV/K_2S_2O_8$ system, the main products were nitrate and nitrogen with nitrogen as the predominant product.

(3) Reactant ratio: In a UV/H_2O_2 system, different molar ratio of hydrogen peroxide over ammonia (2, 4, 8, 16, and 64) indicated no significant variation on ammonia removal efficiency. In a $UV/K_2S_2O_8$ system, for molar ratios of potassium persulphate over ammonia equal to 1.04, 1.56, and 2.07, there was no significant difference in ammonia removal. However, when the ratio was 0.52, the ammonia removal efficiency was low suggesting insufficient persulphate amount.

(4) pH: In both UV/H_2O_2 and $UV/K_2S_2O_8$ systems, it was found that ammonia removal is significant only when pH was in the basic range.

(5) Reaction temperature: In both UV/H_2O_2 and $UV/K_2S_2O_8$ system, it was found that ammonia removal efficiency indicated no obvious change under the temperatures of 20, 25, 35, and 40°C.

Based on the above results, ammonium hydroxide was chosen as the precursor of ammonia in the present study. A value of pH equal to10 and an ambient temperature of 25 °C were chosen as the control pH and temperature, respectively, in the study of the recirculation reactor system. The present study is focused on the performance comparison between the batch reactor and recirculation reactor. In addition, for the RPR system, the

roles of various operating parameters on the reaction kinetics and on the product distribution are examined thoroughly in order to provide a complete description of the system. Performance comparison with other reactor configurations has also been carried out.

6.2 Study of the recirculation reactor

6.2.1 UV/H_2O_2 recirculation system

Dark reaction

There are two reasons for carrying out dark reaction. Firstly, it is needed to check if ammonia is stripped out from the bulk recirculating solution by a pumping effect. Secondly, it is required to examine the possible reaction between ammonia and hydrogen peroxide in the absence of the light radiation. In this study, 60 L reacting fluid containing 3.57 mM ammonia nitrogen and 28.9 mM hydrogen peroxide was recirculated at a flow rate of 10 gallons per minute (GPM). Samples were taken from the UV reactor every 30 min and were analyzed. The analytical results indicated that ammonia concentration showed no obvious change and nitrite/nitrate were not detected in the samples even after 6 h. This suggested that no significant degradation of ammonia occurred under dark condition.

Degradation of ammonia sensitized by hydrogen peroxide under UV light

The direct photolysis of ammonia has been studied by previous researchers and it has been found that the ammonia removal is not comparable to that of the photochemical degradation of ammonia by hydrogen peroxide under light irradiation. In this study, to elucidate the photooxidation of ammonia in the recirculation reactor, 60 L of feed solution was prepared and fed into reactor system which contained 3.67 mM ammonia nitrogen and 29.4 mM hydrogen peroxide. The solution was then irradiated and recirculated for 6 h. Samples were taken every half hour of the exposure time and then analyzed. The change in concentration of ammonia is plotted against irradiation time in Fig. 6.1. It shows that ammonia nitrogen concentration decreases from 3.67 mM to

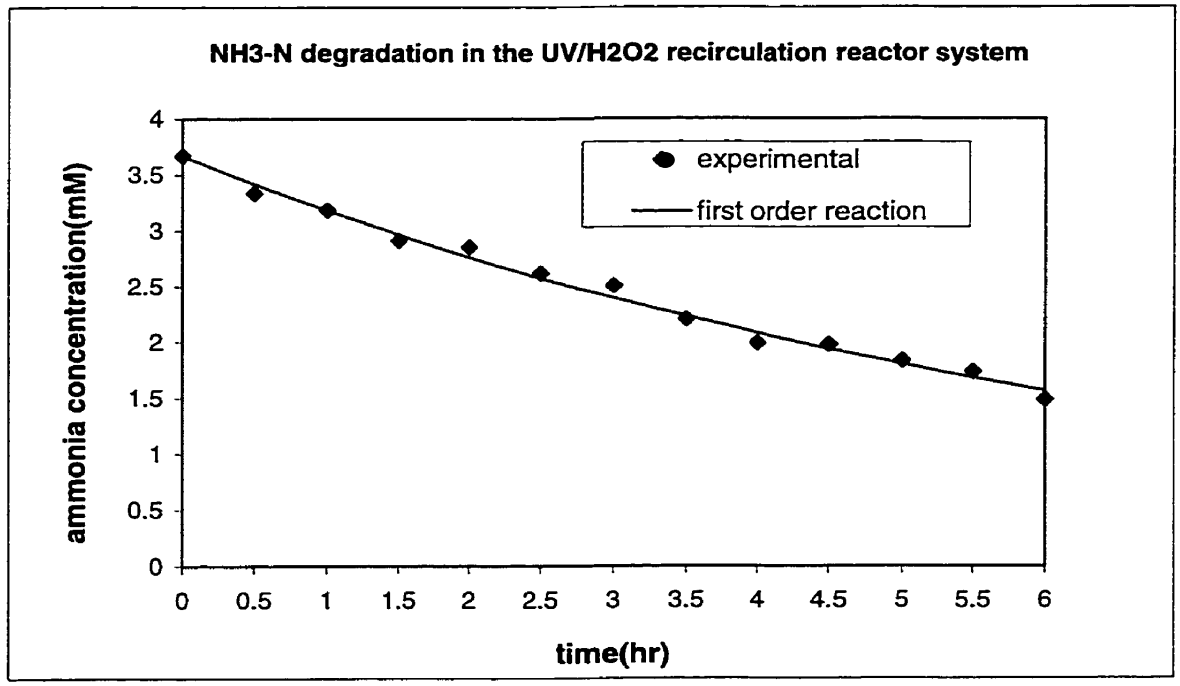

Figure 6.1 NH_3-N degradation by UV/H_2O_2 treatment in the recirculation reactor system

1.49 mM which accounts for ~60% removal efficiency. The least-squares method was applied to the experimental data and it was found that the degradation followed first order kinetics with a reaction rate constant of 0.14 hr^{-1} (correlation coefficient 0.9943). The diamonds in Fig. 6.1 represent the actual experimental data, and the solid line is the first order fitted line. This is consistent with the observation made by previous researchers. [35]

Effect of variation in UV dose

One primary parameter of the UV oxidation system is the UV power radiated per unit volume of the wastewater treated, which is commonly referred to as UV dose. For a given electrical energy input, the longer the irradiation time, the greater is the UV dose. In the recirculation reactor used in this study, the power of UV lamp is 1 kw and the volume of the reacting fluid is 60 L, thus each minute of the time corresponds to a UV dose of 0.278 kWh/m^3.

To observe the effect of UV dose on the ammonia removal efficiency, the ammonia removal efficiency is plotted against the irradiation time in Fig. 6.2, for time periods of 0 to 6 h.

As the irradiation time (UV dose) increases, the ammonia removal percentage increases. The relationship of the two parameters can be described by the following function which is represented by the solid line in Fig. 6.2:

$$Y = 100 - 101e^{-0.14X} \quad (6\text{-}1)$$

Where,

Y is the ammonia removal percentage (%)

X is the irradiation time (hr)

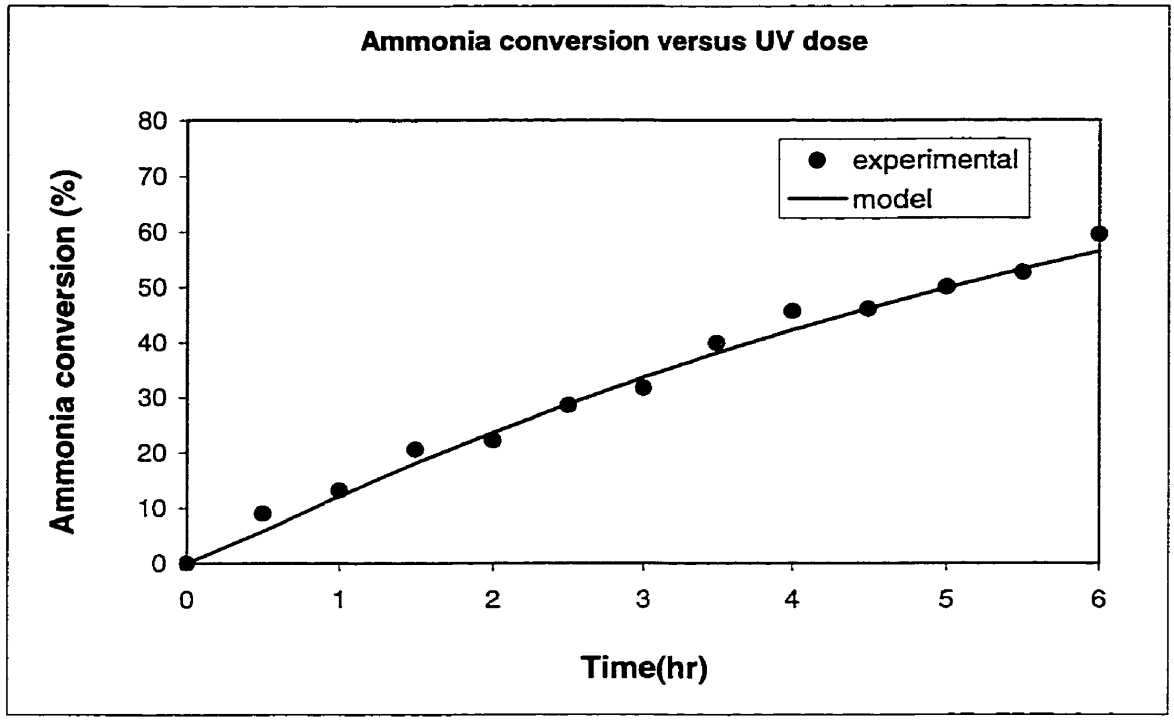

Figure 6.2 Ammonia conversion versus UV dose curve in the UV/H_2O_2 recirculation reactor system ($[NH_3\text{-}N]_0$ = 3.67 mM, pH = 10). Each minute of the time corresponds to a UV dose of 0.278 kWh/m^3

Effect of variation in initial ammonia concentration

As described earlier in Section 3.3, in UV/H_2O_2 system, hydroxyl radical produced from photodecomposition of hydrogen peroxide will attack ammonia and initiate further reactions. This suggests that ammonia concentration will have a significant effect on the ammonia removal. In order to compare the ammonia degradation at different initial concentrations, three experiments were run under the same operating conditions with ammonia nitrogen feed concentrations of 1.59, 3.67, 5.33 mM. The experiment results are displayed in Fig. 6.3 where the squares, diamonds and triangles represent the ammonia conversion for initial concentration of 1.59 mM, 3.67 mM, and 5.33 mM, respectively. It is observed that ammonia removal percentage is higher at lower

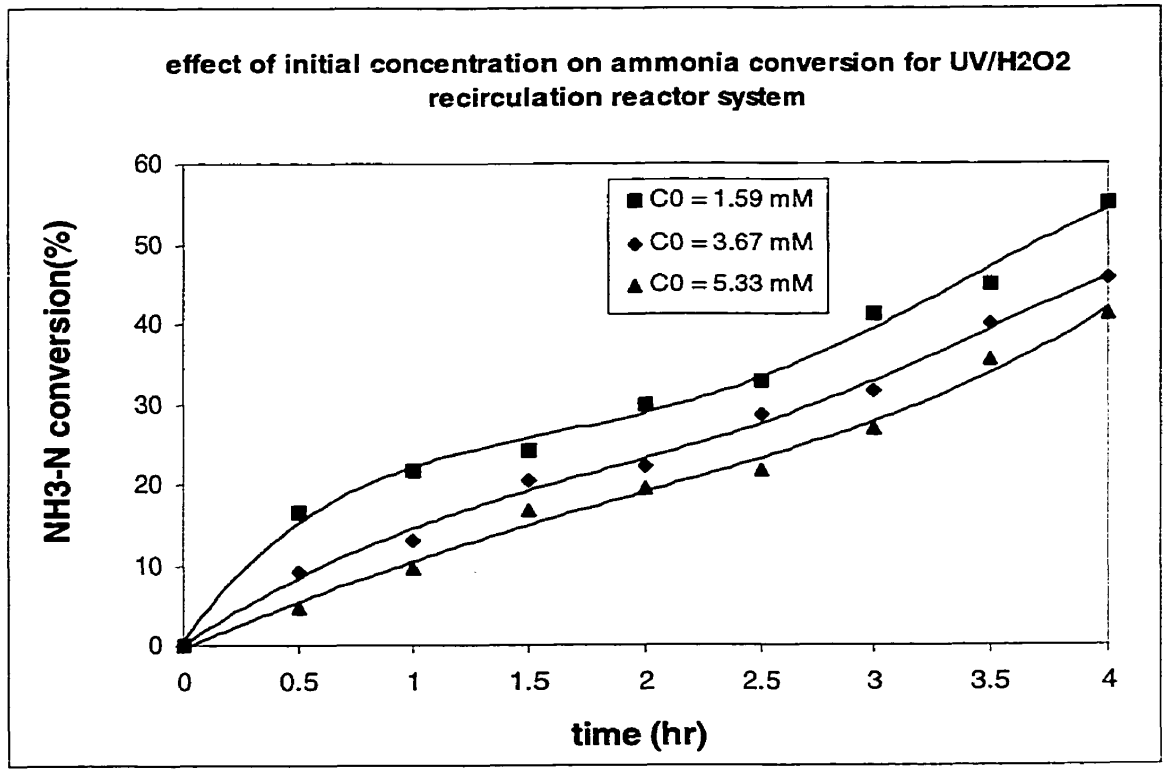

Figure 6.3 Effect of initial concentration on ammonia conversion in the UV/H_2O_2 recirculation reactor system

initial concentration of ammonia but the total amount of ammonia removed is greater at higher concentration. This is consistent with the results obtained in previous studies for the batch reactor and is explainable by the first order reaction model as discussed earlier.

Effect of variation in recirculation flow rate

To test the effect of the recirculation flow rate on the degradation of ammonia, three experiments were conducted at flow rates of 10, 15, 25 gallons per minute (GPM). The experimental results shown in Fig. 6.4 indicate that there is no significant difference in ammonia conversion for different values of the recirculation flow rate.

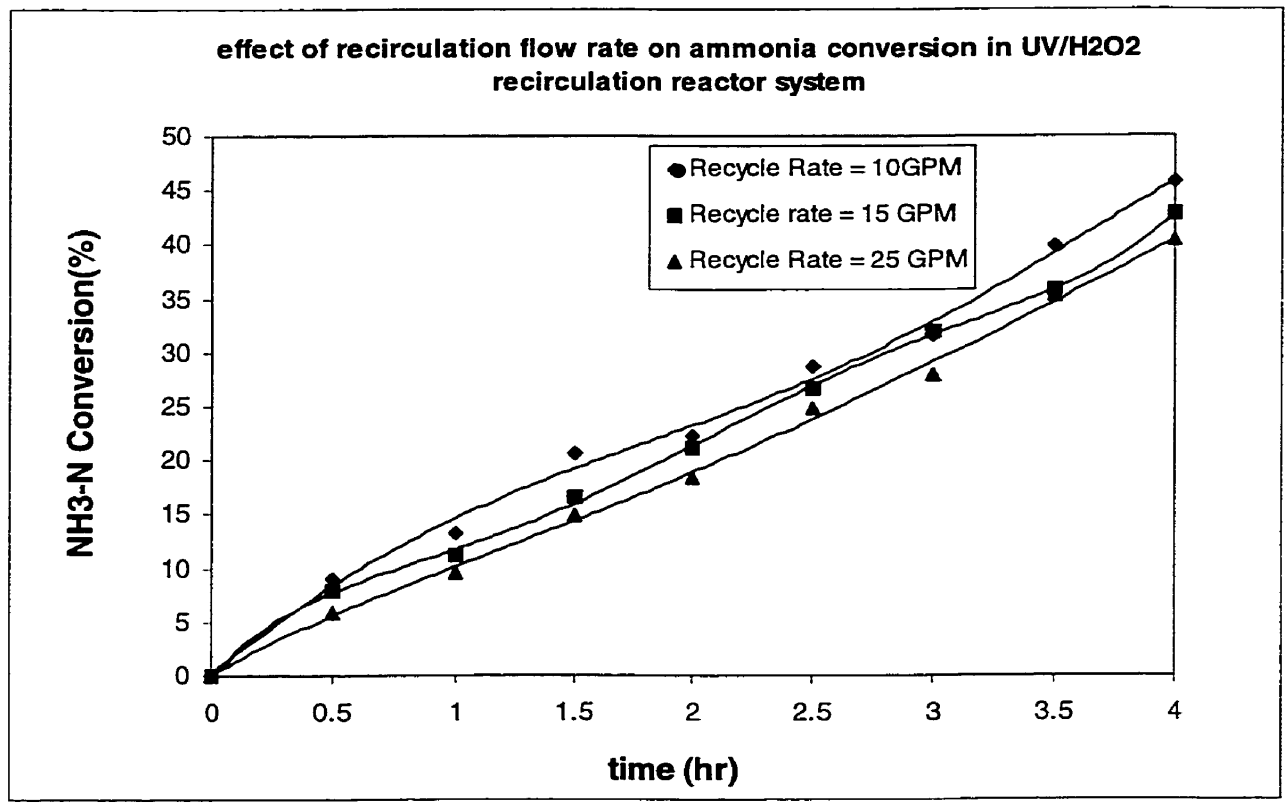

Figure 6.4 Effect of recirculation flow rate on ammonia conversion in the UV/H_2O_2 recirculation reactor system

Product identification and quantification

In all the experiments carried out in the UV/H_2O_2 recirculation reactor system, samples were taken every half hour and analyzed in order to identify and quantify various possible intermediates and final products. It was observed that nitrite, nitrate and nitrogen were the primary products. Table 6.1 gives a typical product distribution of the nitrogenous compounds detected in the system after 6 h of UV irradiation and recirculation.

Table 6.1 A typical product distribution of the nitrogenous compounds in the UV/H_2O_2 recirculation system

Time (hr)	Nitrogen concentration of different species							
	Aqueous (mM)					Gas (mM)		
	NH_3	NO_2^-	NO_3^-	N_2H_4	NH_2OH	N_2	NO + NO_2	N_2O
0	3.67	0	0	0	0	0	0	0
6	1.49	0.44	0.16	0	0	1.57	0.0087	0
P[1]	40.6	12.0	4.36	0	0	42.8	0.24	0

The data in Table 6.1 show that nitrite, nitrate and nitrogen are the products in the UV/H_2O_2 recirculation system. Amongst these, the concentration of nitrogen is more than

[1] P is the percentage of the concentration of various nitrogenous compounds after 6 hours

42%, while those of nitrite and nitrate are 12 and 4.36% respectively. Hydrazine and hydroxylamine were not detected in the aqueous sample. In the gas sample, trace amounts of nitric oxide and nitrogen dioxide were found. Based on the experimental results obtained and the relevant knowledge of photochemistry, presented in Chapter 3, following reaction schemes are proposed in order to explain the mechanisms of ammonia photodegradation in the presence of hydrogen peroxide.

Reaction mechanism

The initial photochemical step in the UV/H_2O_2 system is the photolysis of hydrogen peroxide which generates hydroxyl radicals (•OH) as shown in reaction (3-19). Hydroxyl radicals may also react with hydrogen peroxide as shown in reaction (3-21).

$$H_2O_2 \xrightarrow{h\nu} 2\,\bullet OH \qquad (3\text{-}19)$$

$$\bullet OH + H_2O_2 \xrightarrow{k_H} H_2O + \bullet HO_2 \qquad (3\text{-}21)$$

The perhydroxyl radicals ($\bullet HO_2$) produced are significantly less reactive than hydroxyl radicals. Hydroxyl radicals are highly reactive and will initiate the decomposition of ammonia by hydrogen abstraction:

$$\bullet OH + NH_3 \xrightarrow{k_A} \bullet NH_2 + H_2O \qquad (3\text{-}47)$$

The amino radicals ($\bullet NH_2$) produced from the above reaction can react in the following two ways: (1) two amino radicals may combine to produce hydrazine as

illustrated by Eqn. (3-44); (2) amino radicals may combine with hydroxyl radical to produce hydroxylamine as illustrated by Eqn. (3-48).

$$\bullet NH_2 + \bullet NH_2 \rightarrow N_2H_4 \qquad (3\text{-}44)$$

$$\bullet OH + \bullet NH_2 \rightarrow NH_2OH \qquad (3\text{-}48)$$

Therefore, hydrazine and hydroxylamine are two possible intermediates generated during the photooxidation of ammonia by UV/H_2O_2 treatment. However, both hydrazine and hydroxylamine are strong reducing agents and will react with the oxidants existing in the system, such as hydroxyl radical, and hydrogen peroxide as shown in the following equations:

$$N_2H_4 + 2H_2O_2 \rightarrow N_2 + 4H_2O \qquad (3\text{-}63)$$

$$2OH^- + 4NH_2OH + 6H_2O_2 \rightarrow N_2 + NO_2^- + NO_3^- + 13H_2O \qquad (3\text{-}73)$$

Once hydrazine or hydroxylamine is produced in the system the above two reactions proceed rather quickly, which is why hydrazine and hydroxylamine disappear rapidly and could not be detected in the sample. These observations are in good agreement with the results reported in the literature [33] and the previous study on the reaction between hydrazine/hydroxylamine and hydrogen peroxide. Nitrite and nitrate produced by reaction (3-73) may convert between each other under UV radiation. Nitrite can be oxidized into nitrate while nitrate can be reduced to nitrite. [34]

In addition, hydrazine and hydroxylamine can also undergo the reactions given by Eqns. (3-64) and (3-74), in the presence of nitrite to liberate nitrogen, nitrous oxide and

nitric oxide. This explains the detection of nitric oxide and nitrogen dioxide in the sample of the UV/H_2O_2 recirculation reactor system:

$$N_2H_4 + 2NO_2^- + 2H^+ \rightarrow N_2 + N_2O + 3H_2O \quad (3\text{-}64)$$

$$2NO_2^- + 2NH_2OH + 2H^+ \rightarrow 2NO + N_2 + 4H_2O \quad (3\text{-}74)$$

Other probable mechanisms could have the following pathways: first, the amino radicals generated in Eqn. (3-47) may react with perhydroxyl radical ($\bullet HO_2$) generated in Eqn. (3-21) to produce active species NH_2OOH:

$$\bullet NH_2 + \bullet HO_2 \rightarrow NH_2OOH \quad (6\text{-}2)$$

NH_2OOH may be photochemically decomposed to give $\bullet NH_2O$ and •OH radicals as follows:

$$NH_2OOH \rightarrow \bullet NH_2O + \bullet OH \quad (6\text{-}3)$$

The $\bullet NH_2O$ radical can then be oxidized to give final products of nitrite and nitrate.

It should be noticed that hydrogen peroxide is unstable and may decompose to release oxygen:

$$2H_2O_2 \rightarrow 2H_2O + O_2 \quad (3\text{-}35)$$

The above reaction explains the observation of the gas bubbles inside the UV reactor and also illustrates the importance of using high initial concentration of hydrogen peroxide to maintain sufficient amounts during the whole process.

Initial kinetics reaction model

The initial kinetics reaction model for the UV/H_2O_2 system has been proposed in Section 4.3. Eqn. (4-21) predicts that given incident light intensity, the initial rate of ammonia degradation is dependent on both the initial concentrations of ammonia and hydrogen peroxide:

$$\left.\frac{d[NH_3]}{dt}\right|_{t=0} = (-2\Phi\alpha I)\left[\frac{k_A}{\frac{k_A}{[H_2O_2]_0}+\frac{k_H}{[NH_3]_0}}\right] \qquad (4\text{-}21)$$

The validity of the above model could be tested with the experimental data obtained under different initial concentrations of ammonia and hydrogen peroxide as follows.

The full development of the above rate model is given in Chapter 4. It may be noted that the first term in the RHS of Eqn. (4-21) consists of the quantum yield and the intensity factors, while the second term in the square brackets consists of the purely kinetic rate constants k_A and k_H for the following two reactions:

$$\bullet OH + H_2O_2 \xrightarrow{k_H} H_2O + \bullet HO_2 \qquad (3\text{-}21)$$

$$\bullet OH + NH_3 \xrightarrow{k_A} \bullet NH_2 + H_2O \qquad (3\text{-}47)$$

For the test of the above model, it would be reasonable to use the values of the kinetic rate constants reported for the above reactions in the literature. The values of k_A and k_H are $9.0\times10^7\ M^{-1}s^{-1}$ and $2.7\times10^7 M^{-1}s^{-1}$, respectively [4]. The value of the Φ (quantum yield of hydrogen peroxide) is taken as 1.0 which has been well

established. [32, 52] The value of the α is taken as 47.07 $M^{-1}cm^{-1}$, which is a representative molar absorption coefficient value of hydrogen peroxide in the range of 200 to 300 nm [52]. The value of I is an estimation, and is calculated as follows: The data of the energy output from the lamp have been provided by the manufacturer. The total light flux entering the reactor from the UV lamp was found to be 12.8×10^{-4} Einstein s^{-1} in the wavelength range of 200-500 nm and 5.5×10^{-4} Einstein s^{-1} from 200-300 nm. [53] By dividing the latter value by the cross-sectional area of the UV reactor, the incident light intensity was calculated to be 2.56×10^{-7} Einstein cm^{-2} s^{-1}. Therefore, the initial rate of ammonia degradation can be calculated from Eqn. (4-21) under different initial concentrations of ammonia and hydrogen peroxide, and the results are presented in Table 6.2. The first and second columns show the initial concentration of ammonia and hydrogen peroxide, respectively. The third column is the experimental result obtained from the graphical analysis of the degradation curve of ammonia. The fourth column

Table 6.2 Initial rate of ammonia degradation at different initial concentrations of ammonia and hydrogen peroxide

Initial concentration (mM)		**Initial rate of ammonia degradation ($M\ s^{-1}$)**	
NH_3	**H_2O_2**	**Experimental**	**Model**
5.33	50.1	3.36×10^{-7}	3.16×10^{-7}
3.67	29.4	1.89×10^{-7}	2.08×10^{-7}
1.59	14.8	9.63×10^{-8}	9.40×10^{-8}

is the model data calculated from the initial kinetics model.

From Table 6.2, it can be reasonably concluded that experimental data are in good agreement with the model data, given the uncertainties in the literature for the values of the reaction rate constants. It is also noticed that the initial rate is higher when initial concentrations of ammonia and hydrogen peroxide are higher, which is explainable by the reaction kinetics.

Overall kinetics reaction model

To study the kinetics of the photochemical oxidation of ammonia in the UV/H_2O_2 recirculation reactor system, a typical experiment was designed as follows: The initial concentration of ammonia nitrogen was 3.67 mM while that of hydrogen peroxide was

Table 6.3 The concentration of various components at different radiation time in the UV/H_2O_2 recirculation reactor system

Time (hr)	**Nitrogen concentration of different species**			
	NH_3	**NO_2^-**	**NO_3^-**	**N_2**
0	3.67	0	0	0
1.0	3.18	0.26	0.082	0.18
2.0	2.85	0.28	0.089	0.68
3.0	2.5	0.38	0.098	0.85
4.0	1.99	0.44	0.19	1.05
5.0	1.83	0.44	0.18	1.2
6.0	1.49	0.44	0.16	1.57

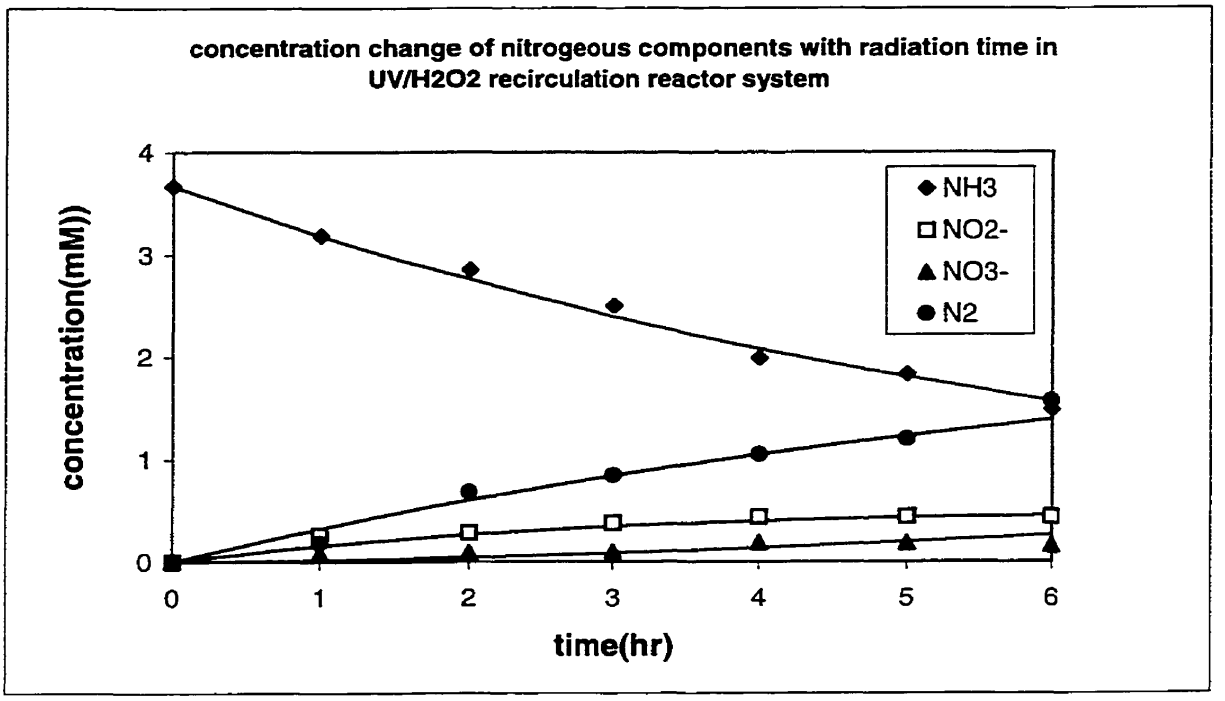

Figure 6.5 The concentration change of the nitrogeous components with radiation time in the UV/H_2O_2 recirculation reactor system

29.4 mM. The total volume of the reacting fluid was 60 L. The operating conditions were pH of 10.0 and temperature of 25°C. The reacting fluid was irradiated for 6 h with the recirculation rate of 10 GPM. To monitor the concentration change of ammonia and those of the products of nitrite, nitrate and nitrogen in the system, samples were taken every hour and analyzed. Table 6.3 presents the analytical results of various components at different radiation time. Figure 6.5 plots the concentration changes of these components with radiation time.

In Fig. 6.5, the diamonds represent experimentally measured concentrations of ammonia, while the circles, the squares and the triangles represent those of nitrogen,

nitrite and nitrate respectively. Recalling the overall kinetics model presented in Section 4.4, the whole photochemical process of ammonia removal can be represented by the following equations:

$$NH_3 \xrightarrow{k1} NO_2^- \xrightarrow{k2} NO_3^- \qquad (4\text{-}22)$$

$$NH_3 \xrightarrow{k3} N_2 \qquad (4\text{-}23)$$

The concentrations of ammonia, nitrite, nitrate and nitrogen can be expressed by Eqn. (4-32) to (4-35):

$$C_1 = C_{1_0} e^{-kt} \qquad (4\text{-}32)$$

$$C_2 = \frac{k_1 C_{1_0}}{k_2 - k}(e^{-kt} - e^{-k_2 t}) \qquad (4\text{-}33)$$

$$C_3 = C_{1_0} - C_{1_0} e^{-kt} - \frac{k_1 C_{1_0}}{k_2 - k}(e^{-kt} - e^{-k_2 t}) - \frac{k_3 C_{1_0}}{k}(1 - e^{-kt}) \qquad (4\text{-}34)$$

$$C_4 = \frac{k_3 C_{1_0}}{k}(1 - e^{-kt}) \qquad (4\text{-}35)$$

The solid lines in Fig. 6.5 represent the data obtained from the kinetics model. It can be seen that model data fits the experimental data well based on the values of k = 0.14 hr^{-1}, k_1 = 0.048 hr^{-1}, k_2 = 0.14 hr^{-1} and k_3 = 0.094 hr^{-1}.

Performance comparison of the UV/H_2O_2 recirculation/batch reactor system

To compare the performance of the recirculation reactor and batch reactor, a typical experiment in the UV/H_2O_2 batch reactor system was designed as follows: The initial concentration of ammonia nitrogen was 3.85 mM while that of hydrogen peroxide was 30.9 mM. The total volume of the reacting fluid was 30 L. The operating conditions were pH of 10.0 and temperature of 25 °C. The reacting fluid was irradiated for 6 h. Samples were taken every hour and analyzed for ammonia, nitrite, nitrate and nitrogen. Figure 6.6 plots the concentration changes of these components with radiation time. The

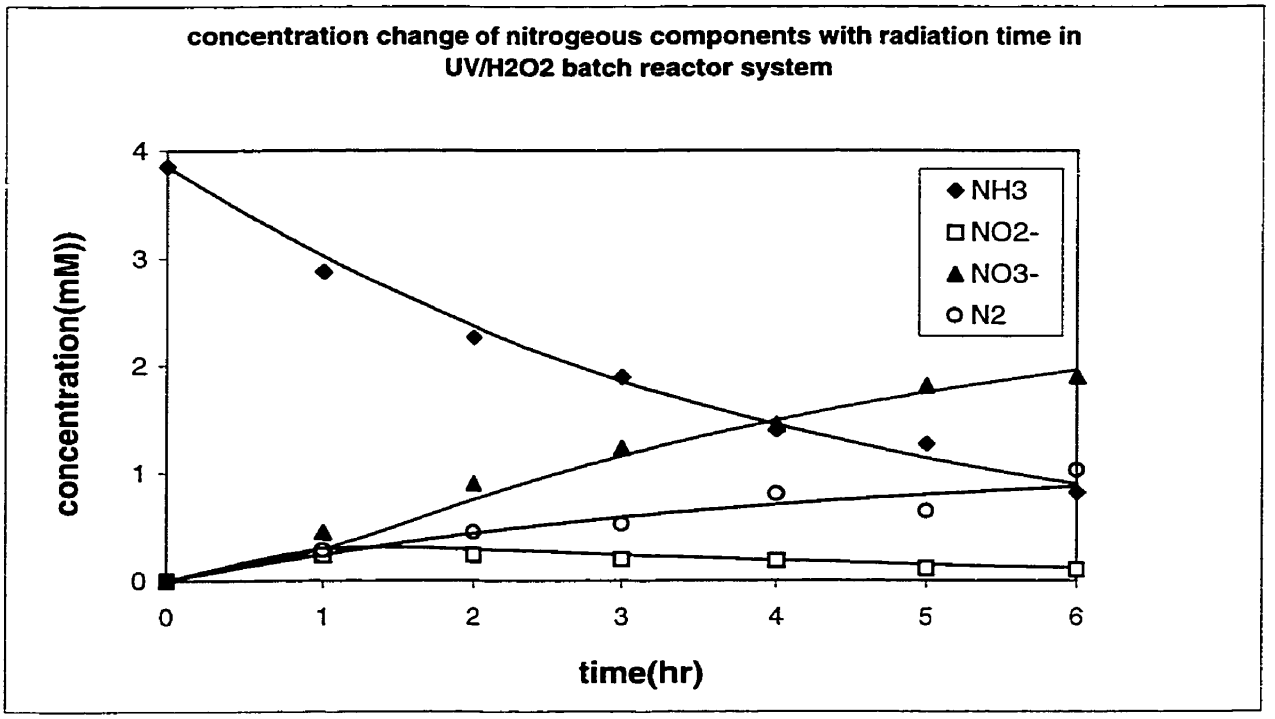

Figure 6.6 The concentration change of the nitrogenous components with radiation time in the UV/H_2O_2 batch reactor system

discrete value points are experimental results, while the solid lines are the model data when applying the same overall kinetics model as in the recirculation reactor system with $k = 0.24\ hr^{-1}$, $k_1 = 0.17\ hr^{-1}$, $k_2 = 1.53\ hr^{-1}$ and $k_3 = 0.072\ hr^{-1}$.

From Figs. 6.5 and 6.6, it is evident that product distributions in the two reactor systems are different. In the recirculation reactor, nitrogen is the predominant product, nitrite is the intermediate, and nitrate is the lowest amount. In the batch reactor, nitrate is the predominant product, while nitrogen is second and nitrite is the lowest. It is speculated that this significant difference in product distribution between the recirculation reactor and the batch reactor may be attributed to the flow pattern. In contrast to the batch reactor in which the products of the irradiation remain in the reactor, in the recirculation reactor, some of the highly reactive species are moved out of the reactor into the recirculation loop where they are not exposed to further UV attack until the next pass. This possibly inhibits the $NO_2^- \rightarrow NO_3^-$ transformation, accounting for the higher NO_2^- concentration observed. In the batch reactor, the above transformation seems to be facilitated. [34]

It is also found that ammonia degradation in the recirculation reactor is slower than that in the batch reactor. After 6 h of radiation, the removal percentage of ammonia is ~60% in the recirculation reactor, while that in the batch reactor is close to 80%. This difference is also reflected in the rate constants of the first-order degradation model, which are $0.14\ hr^{-1}$ in the recirculaton reactor and $0.24\ hr^{-1}$ in the batch reactor, respectively. One possible explanation is that the volumetric rate of light absorption (I_a) is higher in the batch reactor, because of its small reacting volume, and therefore the overall reaction rate is higher.

Table 6.4 summarizes the performance of the recirculation reactor and batch reactor, which includes the overall kinetic rate constant, the volume of the reacting fluid and the amount of ammonia removed in 6 h.

Table 6.4 Summary of the performance comparison between the recirculation reactor and batch reactor

Reactor type	**Overall rate constant (hr^{-1})**	**Reaction time (hr)**	**Volume of the reacting fluid (L)**	**Amount of ammonia removed (mmol)**
Recirculation reactor	0.14	6	60	130.87
Batch reactor	0.24	6	30	90.97

From Table 6.4, it is evident that the amount of ammonia removed in the recirculation reactor is higher than that of the batch reactor in the same period of reaction time, which suggests that the treatment of ammonia in the recirculation reactor is more energy efficient. As discussed in Section 4.1.3, this can be attributed to mixing in the recirculation reactor, which results in performance improvement.

6.2.2 UV/$K_2S_2O_8$ recirculation system

Dark reaction

To check if there is reaction between ammonia and potassium persulphate under dark conditions, a blank experiment was performed as follows: 60 L of aqueous solution containing 3.57 mM ammonia nitrogen and 5.54 mM potassium persulphate was fed into

the recirculation reactor system. The solution was then recirculated for 4 h at a flow rate of 10 GPM. Samples were taken from the UV reactor, once every 30 minutes, and analyzed. It was observed that ammonia concentration exhibited no obvious decrease, and nitrite or nitrate was not detected in the sample even after 4 h, suggesting no significant reaction between ammonia and potassium persulphate under dark conditions. These results are consistent with the observations in reference [55], which stated that very high temperature and pressure were needed to oxidize ammonia by potassium persulphate.

Degradation of ammonia sensitized by potassium persulphate under UV light

As discussed in Section 3.4.3, potassium persulphate absorbs UV light in the wavelength range of 200-300 nm and can dissociate to give sulfate anion radical ($\bullet SO_4^-$), which is a very strong oxidant in aqueous solution. Therefore it can be expected that photooxidation of ammonia will occur to a significant degree in the presence of potassium perfulphate. To confirm this, 60 L solution was prepared and introduced into the recirculation reactor system containing 3.64 mM ammonia nitrogen and 5.78 mM potassium persulphate. The reacting fluid was then irradiated and recirculated for 2 h. During the first half hour, samples were taken every five minutes, to compare with the observations made in the batch reactor. Then, samples were taken every half hour. The identification and quantification of the components in the products will be presented later. Figure 6.7 presents the concentration change of ammonia as a function of the light

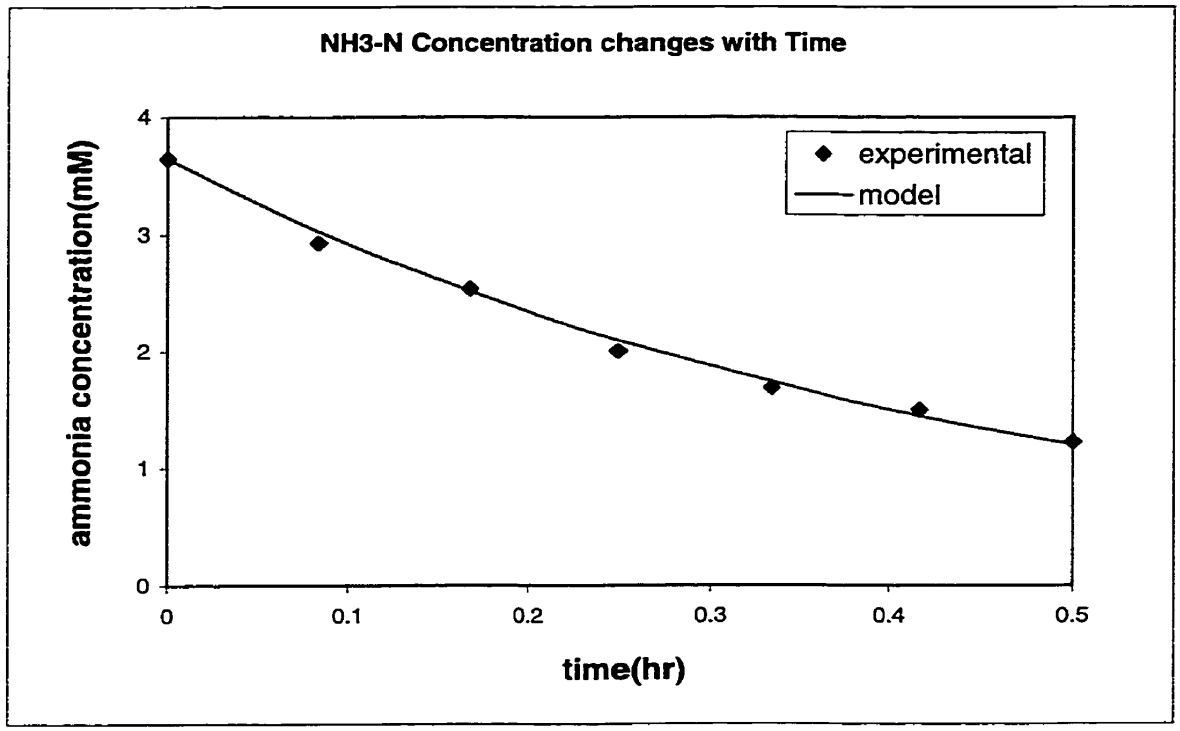

Figure 6.7 NH_3-N degradation by UV/$K_2S_2O_8$ treatment in the recirculation reactor system

exposure time in one half hour. Ammonia exhibited high removal efficiency of about 66%, in the first half hour, with concentration decreasing from 3.64 mM to 1.23 mM. The ammonia removal efficiency rose to 97% in about two h.

As in the case of the UV/H_2O_2 system, the experimental results of the [–ln (C/C_0)] versus radiation time were analyzed by the least-squares method. Here, C is the measured ammonia concentration at different radiation time, and C_0 is the initial concentration. It was found that the first-order model provides an adequate fit to the experimental data as shown in Fig. 6.7. The diamonds are the actual experimental data, and the solid line shows the first-order fitted line. The correlation coefficient is 0.9969. The first-order

reaction rate constant is 2.21 hr^{-1}, which is 15.6 times greater than that in the UV/H_2O_2 system. It can be concluded that potassium persulphate is a more efficient oxidant than hydrogen peroxide in the destruction of ammonia under UV irradiation. It is conceivable that far more reactive radicals are formed in the photooxidation of persulphate leading to very effective destruction of ammonia.

Effect of variation in UV dose

As discussed earlier, a longer radiation time refers to a greater UV dose. To elucidate the influence of UV dose on the ammonia removal efficiency, ammonia removal efficiency was plotted against the irradiation time. Figure 6.8 presents the relationship between these two parameters. It is evident that ammonia removal efficency increases with increasing irradiation time (UV dose).

The dependence of ammonia removal efficiency on the irradiation time can be represented by Eqn. (6-4):

$$Y = 100 - 101e^{-2.21X} \qquad (6\text{-}4)$$

Where,

Y is the ammonia removal percentage (%)

X is the irradiation time (hr)

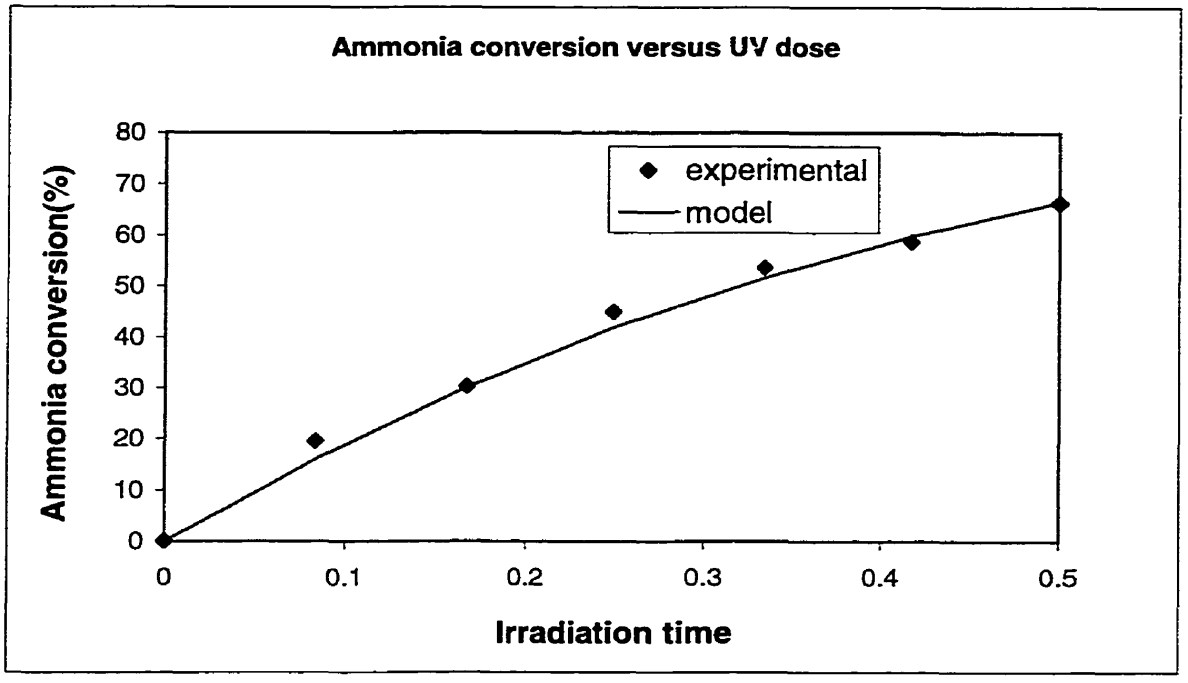

Figure 6.8 Ammonia conversion versus UV dose curve in the UV/$K_2S_2O_8$ recirculation reactor system ($[NH_3\text{-}N]_0$ = 3.64 mM, pH = 10). Each minute of the time corresponds to a UV dose of 0.278 kWh/m^3

Effect of variation in initial ammonia concentration

In the UV/$K_2S_2O_8$ system, the sulfate anion radical ($\bullet SO_4^-$) generated from primary process will further react with water or hydroxide ion in aqueous solution to release hydroxyl radical. Both sulfate anion radical and hydroxyl radical will attack ammonia and initiate a chain of photochemical reactions as in the UV/H_2O_2 system, suggesting that ammonia concentration will affect the removal efficiency significantly. To confirm this, the degradation of ammonia was studied for 2 h under three different

initial concentrations of ammonia nitrogen, 1.57, 3.64 and 5.34 mM while keeping the other operating parameters constant. Figure 6.9 presents the experimental results where

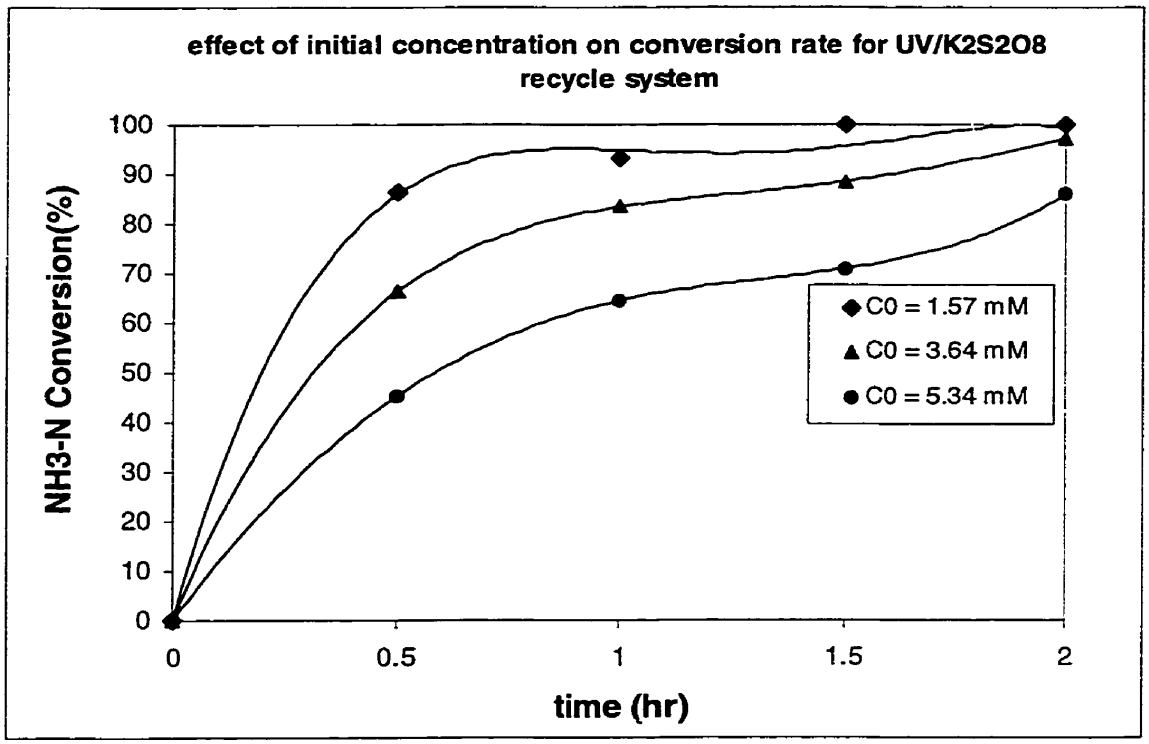

Figure 6.9 Effect of the initial concentration on ammonia conversion in the UV/$K_2S_2O_8$ recirculation reactor system

the ammonia removal percentage at different initial concentrations is plotted against the radiation time. From Fig. 6.9, it is evident that to obtain same level of removal efficiency, less irradiation time is needed at lower initial concentration, which means less input energy is needed. However, the amount of ammonia removed is greater at higher concentration which is consistent with the first-order kinetics, especially at higher radiation time.

Effect of variation in recirculation flow rate

To examine the effect of recirculation flow rate on the degradation of ammonia, three experiments were run for 2 hours each at flow rates of 10, 15, and 25 GPM, respectively, while keeping other operating parameters constant. Samples were taken every half hour and analyzed. The experimental results are plotted in Fig. 6.10. It is observed that recirculation flow rate appears to have no significant effect on the removal efficiency of ammonia.

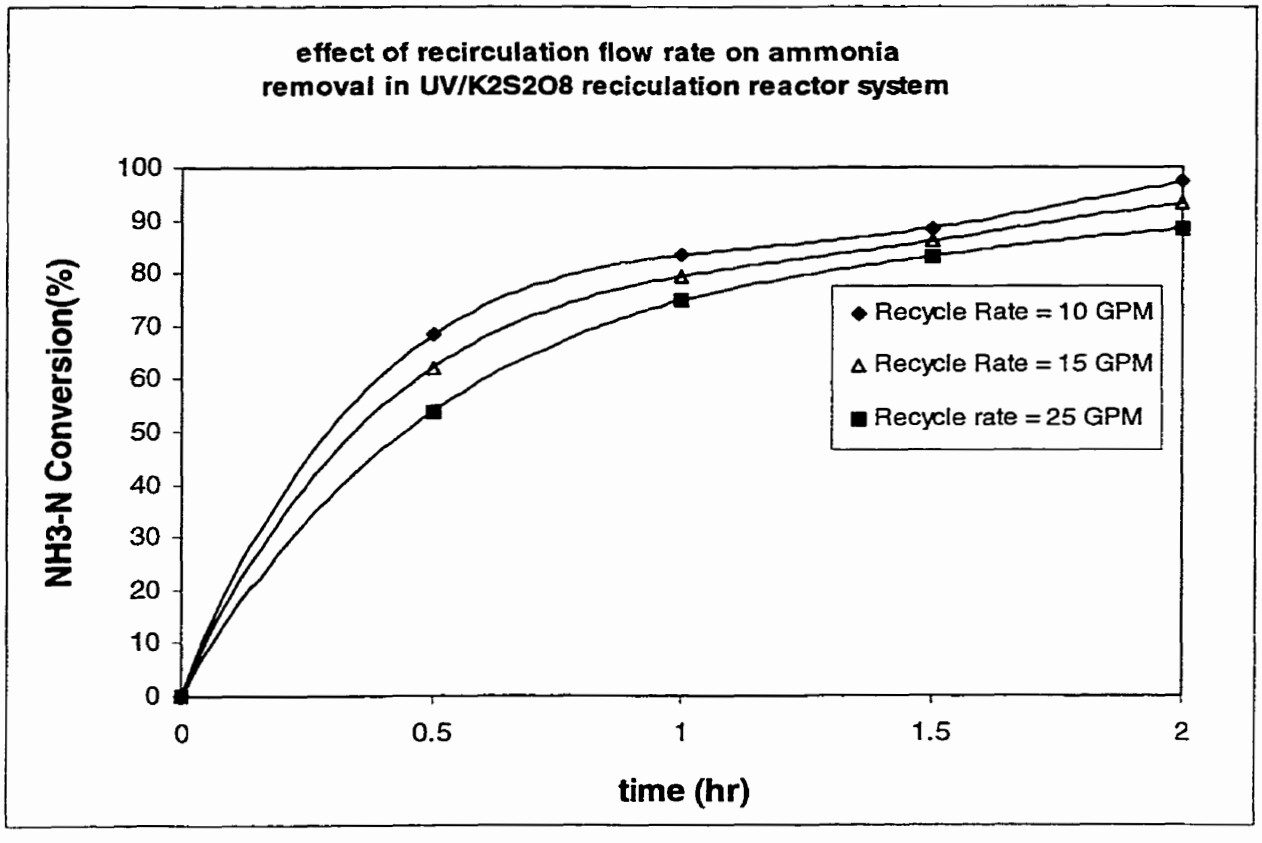

Figure 6.10 Effect of the recirculation flow rate on ammonia conversion in the $UV/K_2S_2O_8$ recirculation reactor system

Product identification and quantification

To facilitate the comparison between the recirculation reactor and batch reactor, samples were taken every five minutes and analyzed in order to identify and quantify various possible intermediates and final products. As in the UV/H_2O_2 system, nitrite, nitrate and nitrogen are found to be primary products in the UV/$K_2S_2O_8$ recirculation system after half hour of UV irradiation and recirculation. Table 6.5 presents a typical product distribution of various nitrogenous compounds measured in the sample.

Table 6.5 A typical product distribution of the nitrogenous compounds in the UV/$K_2S_2O_8$ recirculation system

Time (hr)	Nitrogen concentration of different species							
	Aqueous (mM)					Gas (mM)		
	NH_3	NO_2^-	NO_3^-	N_2H_4	NH_2OH	N_2	NO + NO_2	N_2O
0	3.64	0	0	0	0	0	0	0
0.5	1.23	0.28	1.43	0	0	0.7	0.011	0
P[2]	33.7	7.67	39.0	0	0	19.2	0.3	0

From Table 6.5, it can be seen that nitrite, nitrate and nitrogen are the primary products in the UV/$K_2S_2O_8$ recirculation system. Nitrate is the largest amount among the products, which is about 39%. The concentrations of nitrogen and nitrite are 19.2 and

[2] P is the percentage of the concentration of various nitrogenous compounds after 30 minutes

7.67% respectively. The intermediate hydrazine and hydroxylamine are not detected in the aqueous sample. In addition, trace amounts of nitric oxide and nitrogen dioxide (~0.3%) are detected in gas sample. The above experimental results provide important information on the mechanisms of ammonia degradation. If they are further combined with the photochemical processes as discussed in Chapter 3, a set of reaction schemes may be proposed to explain the mechanisms of ammonia photodegradation when potassium persulphate is used as the oxidant.

Reaction mechanism

As in general advanced photooxidation process, the treatment of ammonia in the UV/$K_2S_2O_8$ system also relies on the generation of highly reactive radicals, such as hydroxyl radicals. Potassium persulphate has a relatively strong absorption of UV light from 200 to 300 nm. It can then experience the following primary process in which persulphate decomposes into sulfate anion radicals ($\bullet SO_4^-$).

$$S_2O_8^{2-} \xrightarrow{h\nu} 2\,\bullet SO_4^- \qquad (3\text{-}37)$$

Sulfate anion radicals are powerful oxidants in aqueous solution. They can react with water through hydrogen abstraction, or oxidize hydroxide ion through electron-transfer. Both the processes generate hydroxyl radicals and can be expressed by Eqn. (3-38) and Eqn. (3-39).

$$\bullet SO_4^- + H_2O \rightarrow HSO_4^- + \bullet OH \qquad (3\text{-}38)$$

$$\bullet SO_4^- + OH^- \rightarrow SO_4^{2-} + \bullet OH \quad (3\text{-}39)$$

Both sulfate anion radicals and hydroxyl radicals produced are very strong oxidants and will further attack ammonia and initiate the following reactions by hydrogen abstraction:

$$\bullet SO_4^- + NH_3 \rightarrow \bullet NH_2 + HSO_4^- \quad (6\text{-}5)$$

$$\bullet OH + NH_3 \rightarrow \bullet NH_2 + H_2O \quad (3\text{-}47)$$

The amino radicals ($\bullet NH_2$) produced will combine with each other to form hydrazine or combine with hydroxyl radicals to form hydroxylamine. Eqn. (3-44) and Eqn. (3-48) express the two reactions:

$$\bullet NH_2 + \bullet NH_2 \rightarrow N_2H_4 \quad (3\text{-}44)$$

$$\bullet OH + \bullet NH_2 \rightarrow NH_2OH \quad (3\text{-}48)$$

Therefore, as in the UV/H_2O_2 treatment, hydrazine and hydroxylamine are the two possible intermediates during the process of ammonia degradation in the UV/$K_2S_2O_8$ treatment. Both hydrazine and hydroxylamine will undergo further reactions in the presence of the strong oxidants in the system. For example, hydrazine will react with persulphate ion to release nitrogen, while hydroxylamine will react with persulphate ion to generate nitrogen, nitrite and nitrate as per the following unbalanced reactions:

$$N_2H_4 + 2S_2O_8^{2-} \rightarrow N_2 + 4SO_4^{2-} + 4H^+ \quad (3\text{-}65)$$

$$6NH_2OH + 12S_2O_8^{2-} \rightarrow 2N_2 + NO_2^- + NO_3^- + 24SO_4^{2-} + H_2O + 14H^+ \qquad (3\text{-}75)$$

The above two reactions proceed rather easily. Therefore, the absence of hydrazine and hydroxylamine during the photodegradation of ammonia can be attributed to their complete consumption by the rapid reaction with the oxidants as discussed earlier. Similarly, nitrite and nitrate generated from reaction (3-75) may change into each other in the presence of UV radiation. Nitrite can be oxidized to form nitrate while nitrate can be reduced to form nitrite. [34] It is also noticed that hydrogen ion is produced in both Eqn. (3-65) and Eqn. (3-75). Besides the destruction of ammonia, this explains the decrease of the pH value during the photooxidation process of ammonia. Thus, the real-time adjustment of the pH value is necessary.

Hydrazine and hydroxylamine can also react with nitrite to release nitrogen, nitrous oxide and nitric oxide. Nitric oxide can easily be oxidized into nitrogen dioxide. These reactions explain the existence of nitric oxide and nitrogen dioxide in the products of the UV/$K_2S_2O_8$ recirculation reactor system:

$$N_2H_4 + 2NO_2^- + 2H^+ \rightarrow N_2 + N_2O + 3H_2O \qquad (3\text{-}64)$$

$$2NO_2^- + 2NH_2OH + 2H^+ \rightarrow 2NO + N_2 + 4H_2O \qquad (3\text{-}74)$$

In addition, Under UV radiation, potassium persulphate will react with water to generate sulfate ion and hydrogen peroxide. Hydrogen peroxide is not stable and may decompose into water and oxygen as shown in Eqn. (3-34) and Eqn. (3-35). This explains the generation of the gas bubbles observed during the ammonia degradation.

$$S_2O_8^{2-} + 2H_2O \rightarrow SO_4^{2-} + 2H^+ + H_2O_2 \qquad (3\text{-}34)$$

$$2H_2O_2 \rightarrow 2H_2O + O_2 \quad (3\text{-}35)$$

Because oxygen is produced, one possible reaction is between amino radical and oxygen as follows to give $\bullet NH_2OO$ radical:

$$\bullet NH_2 + O_2 \rightarrow \bullet NH_2OO \quad (6\text{-}6)$$

Two $\bullet NH_2OO$ radicals can undergo bimolecular decomposition to give $\bullet NH_2O$ radical and O_2:

$$\bullet NH_2OO + \bullet NH_2OO \rightarrow \bullet NH_2O + O_2 \quad (6\text{-}7)$$

Then the $\bullet NH_2O$ radical produced can be oxidized to give final products of nitrite and nitrate.

Overall kinetics reaction model

Because of the lack of values for quantum yield and reaction rate constants in the literature, the initial kinetics reaction model could not be applied to the UV/$K_2S_2O_8$ treatment. A discussion of the overall kinetics of the photochemical oxidation of ammonia in the UV/$K_2S_2O_8$ recirculation reactor system, is presented here.

A typical experiment was carried out as follows: 60 L of synthetic wastewater containing 3.64 mM ammonia nitrogen was introduced into the reactor, then 5.78 mM potassium persulphate was added. Under the operating conditions of the pH value of 10.0 and temperature of 25 °C, the reacting fluid was irradiated and recirculated for half an hour. The recirculation rate was 10 GPM. To be able to compare with the experiments in

the batch reactor, samples were taken every five minutes and analyzed, to trace the concentration change of ammonia and those of the primary products of nitrite, nitrate and nitrogen in the reacting system. Table 6.6 presents the measured concentration of various components at different radiation time. Figure 6.11 plots the data presented in Table 6.6.

Table 6.6 The concentration of various components at different radiation time in the $UV/K_2S_2O_8$ recirculation reactor system

Time (min)	**Nitrogen concentration of different species**			
	NH_3	**NO_2^-**	**NO_3^-**	**N_2**
0	3.64	0	0	0
5	2.93	0.23	0.060	0.43
10	2.54	0.27	0.62	0.21
15	2.01	0.32	0.83	0.48
20	1.69	0.34	1.13	0.49
25	1.50	0.26	1.15	0.73
30	1.23	0.28	1.43	0.70

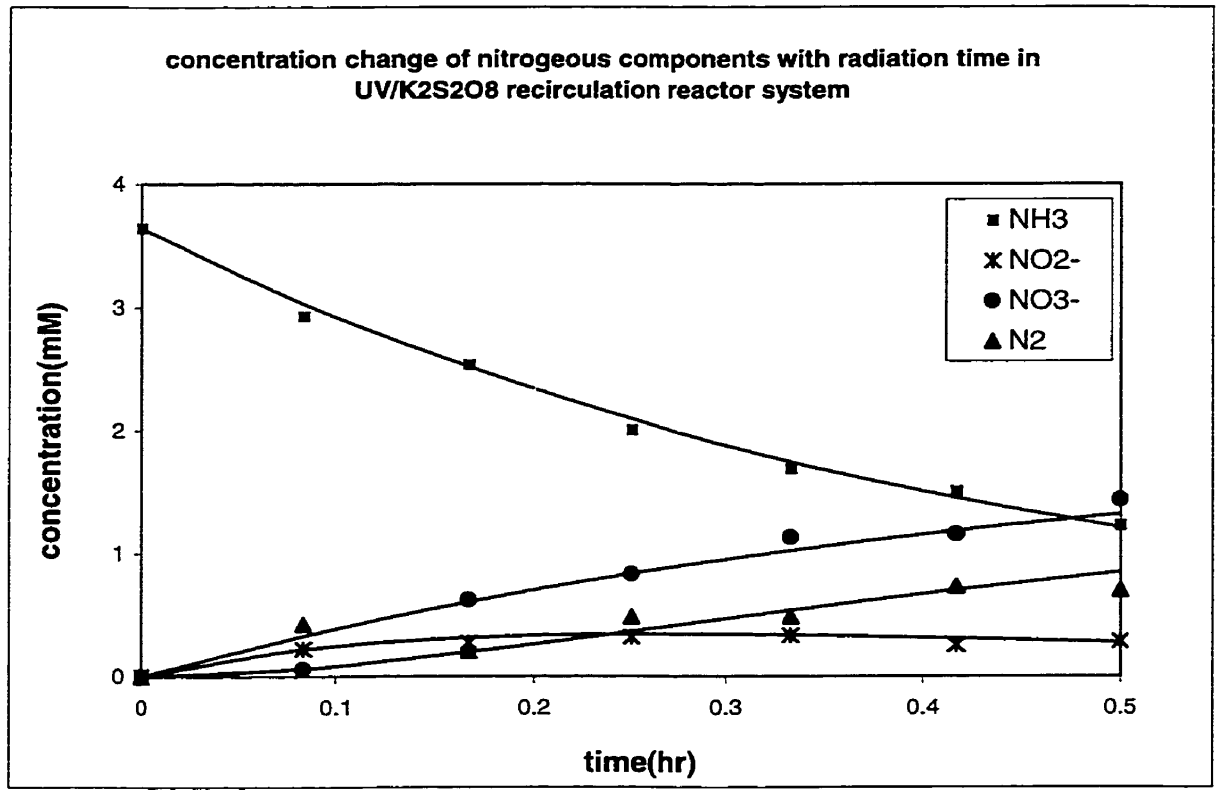

Figure 6.11 The concentration change of the nitrogeous components with radiation time in the UV/$K_2S_2O_8$ recirculation reactor system

It can be seen from Fig. 6.11 that the concentration of ammonia decreases and the concentrations of nitrate and nitrogen increase in proportion to the increase in the UV irradiation time. It is also observed that there are no significant changes in the concentration of nitrite. This may have been due to the conversion of nitrite into nitrate. Since nitrite, nitrate and nitrogen are major products, the overall kinetics model discussed earlier can be applied here. The overall photooxidation process of ammonia can be represented by the following equations:

$$NH_3 \xrightarrow{k1} NO_2^- \xrightarrow{k2} NO_3^- \quad (4\text{-}22)$$

$$NH_3 \xrightarrow{k3} N_2 \quad (4\text{-}23)$$

Similarly, applying Eqn. (4-32) to Eqn. (4-35), the concentration of ammonia, nitrite, nitrate and nitrogen can be derived from the kinetics model. These calculated concentrations are plotted in Fig. 6.11 and are represented by the four solid lines. From Fig. 6.11, it is evident that the model is in good agreement with the experimental data. The kinetics rate constants employed in the model are as follows: $k = 2.21\ hr^{-1}$, $k_1 = 1.02\ hr^{-1}$, $k_2 = 5.98\ hr^{-1}$ and $k_3 = 1.19\ hr^{-1}$.

Performance comparison of the UV/$K_2S_2O_8$ recirculation/batch reactor system

To compare the performances of the recirculation and batch reactors, a typical experiment in the UV/$K_2S_2O_8$ batch reactor system was designed as follows: 30 L of synthetic wastewater containing 3.62 mM ammonia nitrogen was introduced into the reactor, followed by an addition of 5.80 mM potassium persulphate. Under the operating conditions of the pH value at 10.0 and temperature at 25°C, the reacting fluid was irradiated in the batch reactor for a half hour. Samples were taken every five minutes and analyzed for ammonia, nitrite, nitrate and nitrogen. Figure 6.12 shows the variation in the concentration of these components with respect to radiation time. The squares represent measured concentration of ammonia, while the triangles and circles represent those of nitrogen and nitrate, respectively. It is noticed that nitrogen and nitrate are primary products while the concentration of nitrite is negligible. Therefore the overall kinetics

model has to be modified to simulate this case. Following is the proposed competitive-parallel model as shown in Eqn. (6-8) and Eqn. (6-9):

$$NH_3 \xrightarrow{k1'} NO_3^- \qquad (6\text{-}8)$$

$$NH_3 \xrightarrow{k2'} N_2 \qquad (6\text{-}9)$$

As in Section 4.4, applying the principles of mass balance and same initial conditions, the concentrations of ammonia (C_1), nitrate (C_2') and nitrogen (C_3') can be expressed by Eqn. (6-10) to (6-12):

$$C_1 = C_{1_0} e^{-k't} \qquad (6\text{-}10)$$

$$C_2' = \frac{k_1' C_{1_0}}{k'}(1 - e^{-k't}) \qquad (6\text{-}11)$$

$$C_2' = \frac{k_2' C_{1_0}}{k'}(1 - e^{-k't}) \qquad (6\text{-}12)$$

Where, k', k_1' and k_2' are rate constants and $k' = k_1' + k_2'$. The above equations are kinetics expressions in the UV/$K_2S_2O_8$ batch reactor system. The model data are plotted in Fig. 6.12 as solid lines. It can be seen that the model fits the experimental results well. The values of k', k_1' and k_2' are 4.04 hr^{-1}, 0.15 hr^{-1}, and 3.89 hr^{-1}.

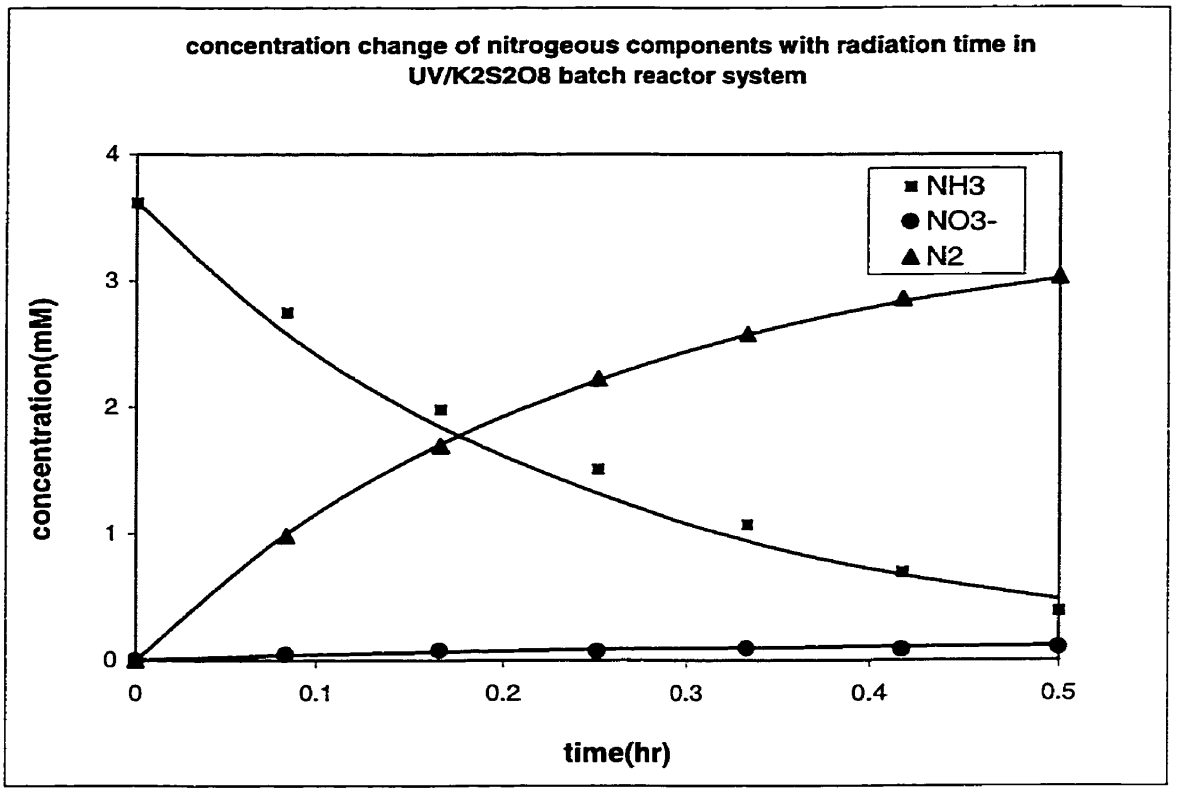

Figure 6.12 The concentration change of the nitrogenous components with radiation time in the UV/$K_2S_2O_8$ batch reactor system

A comparison of Figs. 6.11 and 6.12 indicates a significant difference in the product distributions in these two reactor systems. In the recirculation reactor, nitrate is the predominant component, followed by nitrogen and then nitrite. In the batch reactor, nitrogen is the predominant product, while only a small amount of nitrate is formed and nitrite is negligible. In explaining the product distribution, there are two aspects to consider. One could be that the flow pattern in the recirculation reactor which inhibits the $NO_2^- \rightarrow NO_3^-$ transformation which results in the existence of the remaining nitrite. The other may involve the relative proportion of hydrazine and hydroxylamine generated

during the process. If there is more hydrazine produced, final product will tend to consist of more nitrogen. Further study on the possible change of the reaction pathways in different reactor configurations may be required to further elucidate the reasons.

As in UV/H_2O_2 system, it is also noticed that ammonia degradation in the recirculation reactor is slower than that in the batch reactor for the $UV/K_2S_2O_8$ system. The kinetic rate constants of the first-order degradation model are 2.21 and 4.04 hr^{-1} in the recirculaton and batch reactor, respectively. After a half hour of irradiation, the removal percentage of ammonia is found to be ~66% in the recirculation reactor, while that in the batch reactor, it is observed to be more than 89%. It can be stated that the higher volumetric rate of light absorption (I_a) in the batch reactor due to the smaller reacting volume, resulted in a higher reaction rate. Table 6.7 summarizes the performance of the recirculation reactor and batch reactor for the $UV/K_2S_2O_8$ system.

Table 6.7 Summary of the performance comparison between the recirculation reactor and batch reactor in the $UV/K_2S_2O_8$ system

Reactor type	**Overall rate constant (hr^{-1})**	**Reaction time (hr)**	**Volume of the reacting fluid (L)**	**Amount of ammonia removed (mmol)**
Recirculation reactor	2.21	0.5	60	145.07
Batch reactor	4.04	0.5	30	96.87

From Table 6.7, it is evident that the amount of ammonia removed in the recirculation reactor is greater than that in the batch reactor, suggesting that the ammonia

removal is more energy efficient in the recirculation reactor. As discussed earlier, one possible explanation is that the recirculation in the latter reactor improves the mixing of the reacting fluid resulting in a much improved performance.

6.3 Study of the RPR system

The RPR system is a continuous plug-flow like system, and it is quite different from the recirculation and batch reactors. A detailed investigation of the operating conditions and process parameters are therefore necessary. Various operating conditions including input power, initial concentration of ammonia, pH, flowrate of the reacting fluid and cylinder rotation speed were varied and their effects were assessed. This section presents the experimental results obtained from direct photolysis of ammonia compounds, the process parameter studies of the single pass UV/H_2O_2 and UV/$K_2S_2O_8$ systems, and the study of the product distribution. Results are also presented from the studies that compare the ammonia removal efficiency between single pass and multi-pass processes, reactor systems with and without reflector, and systems with Hanovia and Rayox lamps.

6.3.1 Direct photolysis

As described earlier, researchers in the previous study found that the direct photolysis of ammonia in the batch reactor was quite low compared to the photochemical degradation of ammonia under light irradiation in the presence of the oxidants. To examine the effect of the direct photolysis of ammonia in the RPR, three experiments

were conducted following the experimental procedures presented in Section 5.2.2. After UV lamp came to a steady operating output, samples were taken every five minutes and analyzed. Table 6.8 shows the combination of the operating conditions for three runs that were carried out. Figure 6.13 presents the ammonia removal efficiency under three different input powers. It can be seen that for all the energy input conditions, the removal percentage of ammonia is quite low. The removal percentage is less than 20% even under the high-energy input. The removal percentages are as low as16 and 11%, for medium and low energy inputs, respectively. This suggests that the direct photolysis is not an effective method for ammonia removal. Hence in the RPR system, advanced photooxidation processes using hydrogen peroxide and potassium persulphate as the oxidants were studied in detail.

Table 6.8 Operating conditions of the direct photolysis of ammonia in the RPR system by UV/H_2O_2 treatment

Run number	**Input voltage (V)**	**Input current (A)**	**Initial concentration (mM)**	**pH**	**Flowrate (ml/min)**	**Rotation speed (rpm)**
1	250	3.8	3.92	10	85	7.5
2	250	2.5	3.92	10	85	7.5
3	250	1.35	3.92	10	85	7.5

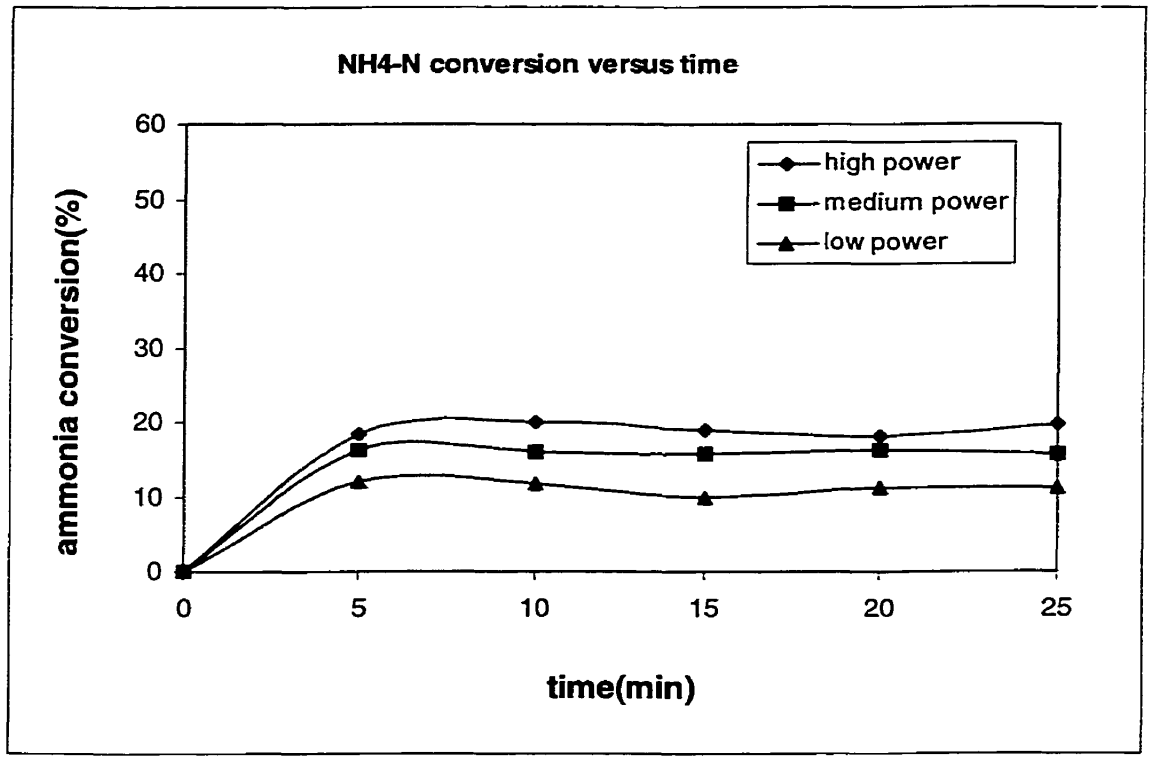

Figure 6.13 Direct photolysis of ammonia in the RPR system by UV/H_2O_2 treatment

6.3.2 Single pass UV/H_2O_2 system

The experiments presented in this section were carried out with the reacting fluid flowing through the reactor in a single pass, without any recycling.

Photoxidation of different ammonia percursors

The photooxidation of three different ammonia precursors were examined as follows: Three feed solutions were prepared containing ammonium hydroxide, ammonium sulphate and ammonium nitrate, respectively. All the three solutions had the

same initial concentration of ammonia nitrogen, 3.5 mM and hydrogen peroxide of 7.0 mM. Experimental results are shown in Fig. 6.14, which represent the removal efficiency of the different ammonia precursors. It can be seen that ammonium hydroxide

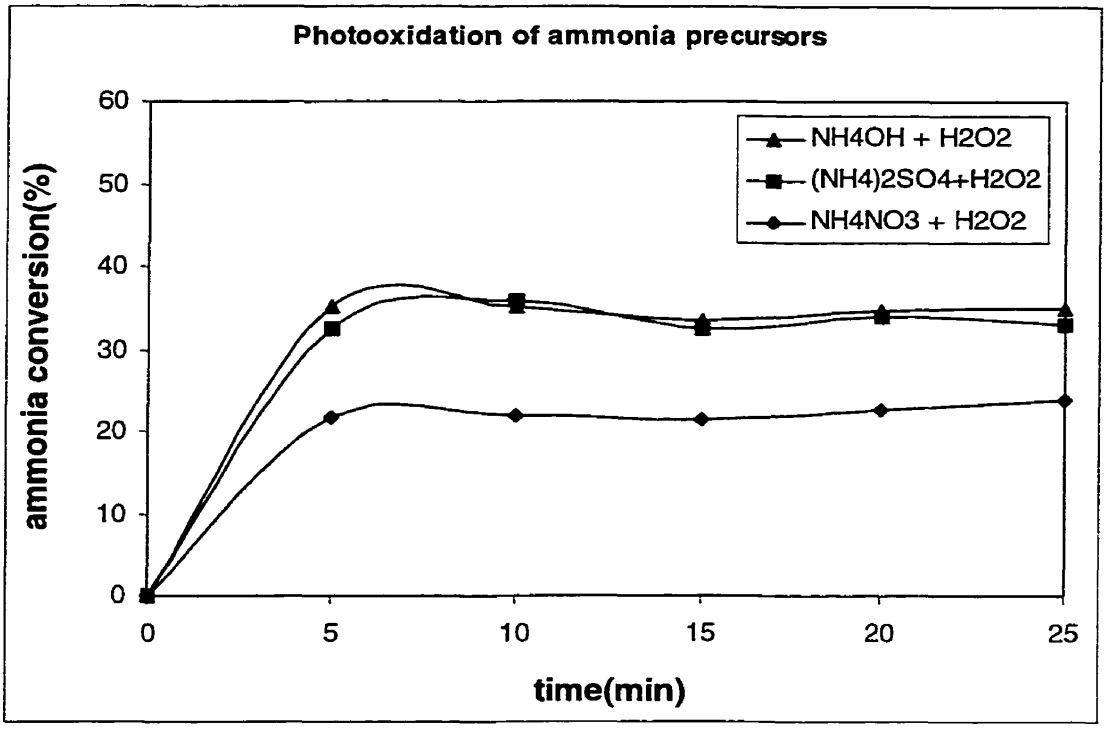

Figure 6.14 Photooxidation of ammonia precursors in the UV/H_2O_2 RPR system

and ammonium sulphate have higher degradation than ammonium nitrate. Thus both ammonium hydroxide and ammonium sulphate can be selected as the ammonia precursors. However, considering the fact that no extra ions are introduced into the system from its oxidation, ammonium hydroxide was chosen as the precursor in further experiments.

Effect of variation in UV input power

To investigate the photooxidation of ammonia under different power inputs, three experiments were run under the same operating conditions as those in direct photolysis. The initial concentration of ammonia nitrogen was 3.47 mM, while that of hydrogen peroxide was 7.0 mM. Figure 6.15 presents the removal percentage of ammonia versus the sampling time for each input power level.

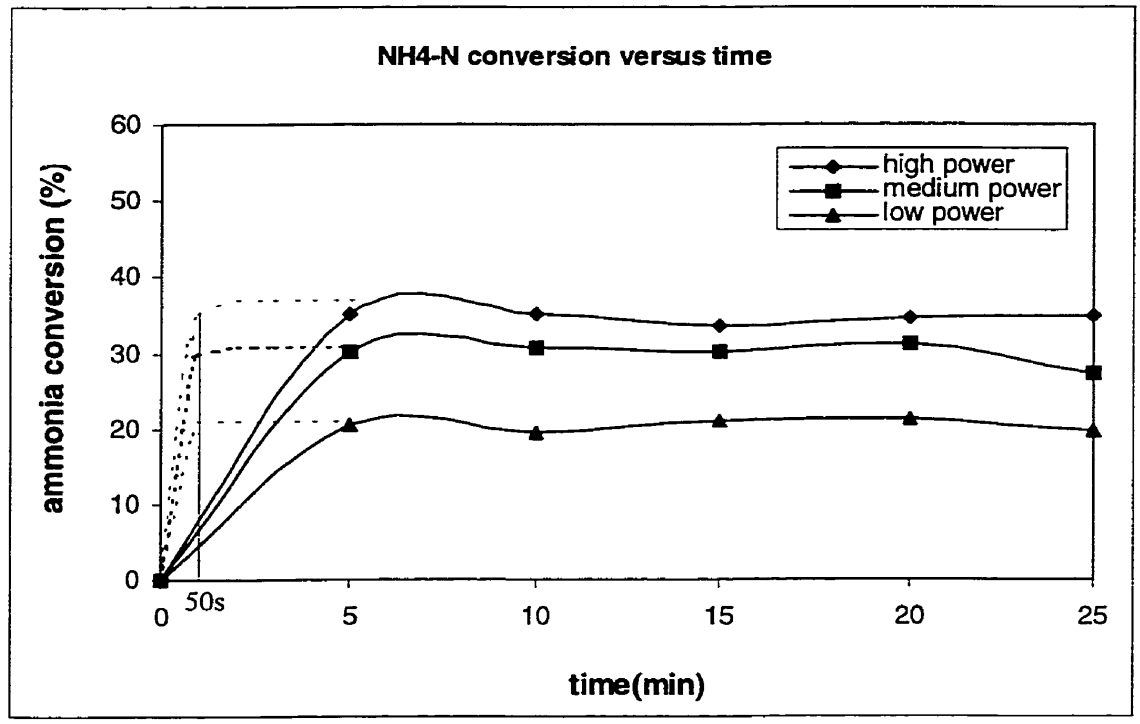

Figure 6.15 Ammonia conversion under different levels of input power in the UV/H_2O_2 RPR system

From Fig. 6.15, it can be seen that for higher input power, the removal efficiency of ammonia is higher. The removal percentages are 20, 30 and 35%, for low, medium and high input power, respectively. This can be explained as follows: varying the power input

to the lamp means varying the light intensity. It has been reported that the relative light intensity has positive relationship with the power input. [49] Suppose that the light intensity 100% corresponds to the full energy input of the lamp, half the input power will result in light intensity decreasing more than 25%. According to the principles of photochemistry, reaction rate will be greater at higher light intensity, thus resulting in higher removal efficiency.

A comparison of Figs. 6.13 and 6.15, also reveals that the removal efficiency in the photooxidation process of ammonia is significantly higher compared to that in direct photolysis of ammonia, suggesting that the former process is much more effective for ammonia removal.

The other characteristics to be noted in Fig. 6.15 are the shape of the curves. It is apparent that all the three curves tend to be flat after five minutes. In other words, for each experiment, the samples taken after five minutes tend to have same concentration of ammonia. This can be attributed to the plug-flow like property of the reactor. Because the irradiating area on the cylinder surface is small, the actual exposure time of the reacting fluid is quite short (<60 s) while fluid flows through the reactor. Due to the limitations on the equipment arrangement and analytical method involved, samples could not be taken at a shorter interval of time. Therefore even the first sample taken at 5 minutes is well above the actual residence time of the fluid in the reacting surface and for all practical purposes, maximum conversion and steady state are reached within the first minute of the stable operation. The same removal efficiencies in different samples demonstrate that the flowing fluids have stable residence time inside the reactor. The initial rise in the shape of the curves in Fig. 6.15 from 0 minute to 5 minute is just an abstraction of the warm-up

period of the lamp. However, the true shape of the curve in this time span is undetermined because of the lack of the information on lamp warm-up period, and it is likely that the initial part of the curves follow the dotted lines shown in the figure, with the maximum concentration change of ammonia occurring within 50 seconds.

Effect of variation in initial ammonia concentration

As discussed in Section 6.2, initial ammonia concentration has significant effect on ammonia removal. To examine this, experiments were conducted with ammonia nitrogen feed concentrations of 3.47, 4.92 and 7.47 mM. The reactant ratio of hydrogen peroxide to ammonia was taken as 2.0. Other operating conditions were input voltage = 250 V, input current = 3.8 A, pH = 10, flow rate of the fluid = 85 ml/min, and the

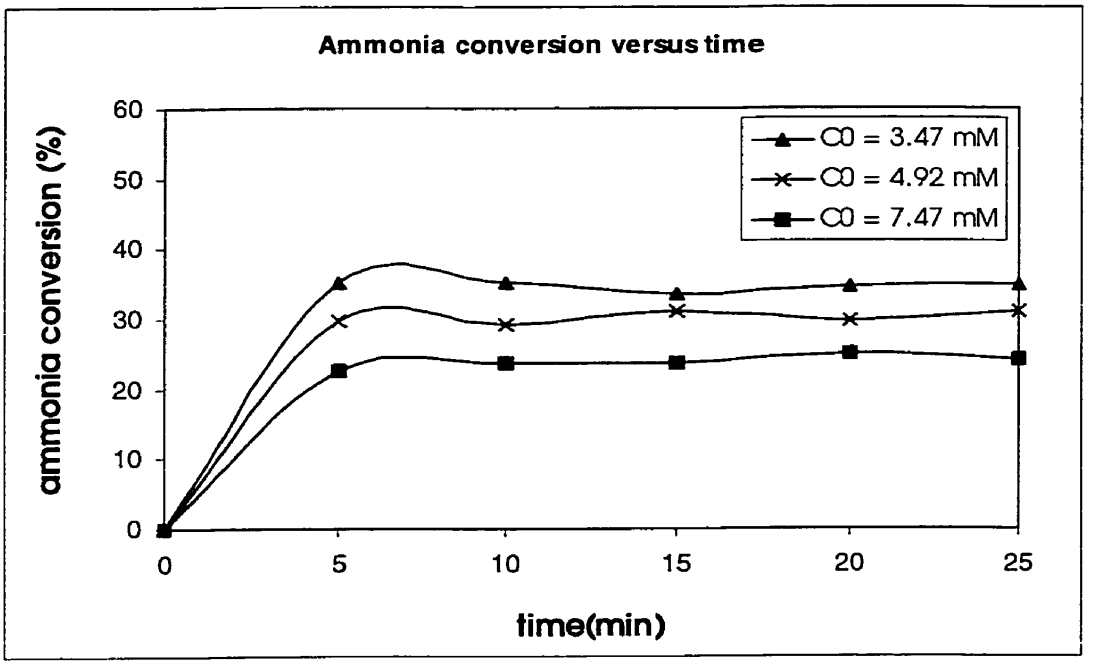

Figure 6.16 Ammonia conversion at different initial ammonia concentration in the UV/H_2O_2 RPR system

cylinder rotation speed = 7.5 rpm. Figure 6.16 presents the experimental results. It is evident that ammonia removal efficiency (~35%) is higher for initial ammonia nitrogen concentration of 3.47 mM, than those for 4.92 and 7.47 mM, which are 30 and 24%, respectively.

Effect of variation in reactant ratio

The previous studies on batch reactor concluded that different molar ratio of hydrogen peroxide over ammonia had no significant effect on ammonia removal efficiency. However, because hydrogen peroxide decomposes easily, its initial

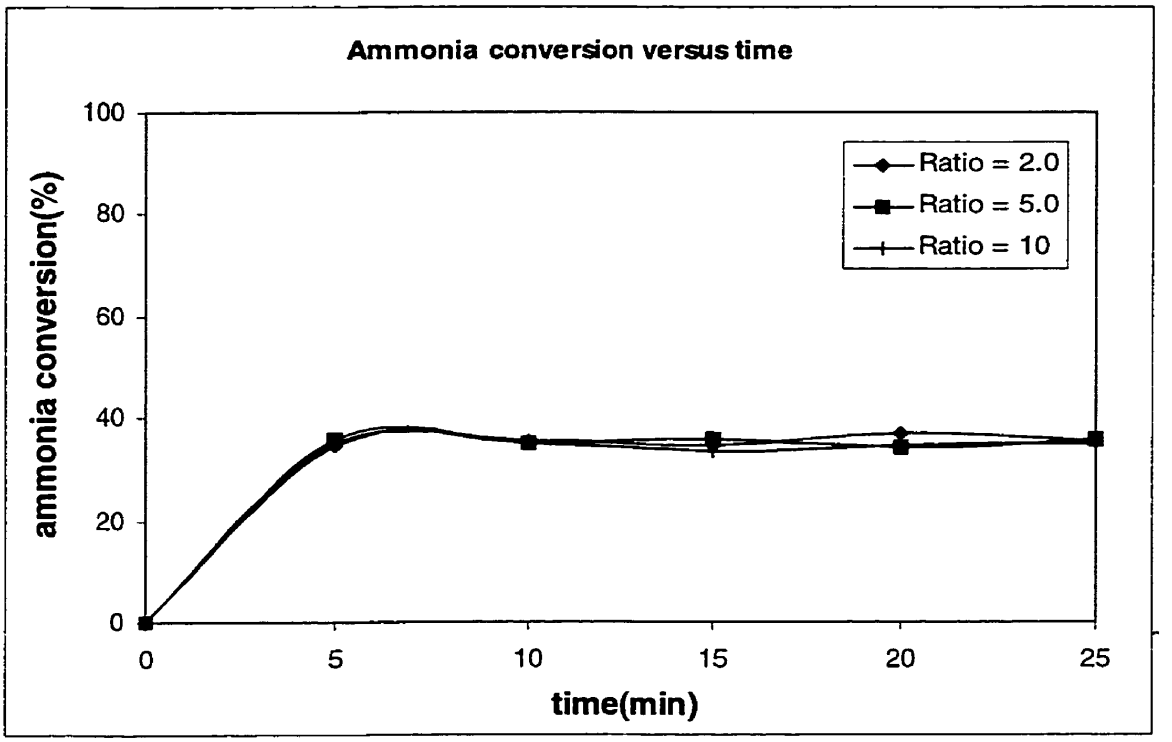

Figure 6.17 Ammonia conversion at different molar ratio in the UV/H_2O_2 RPR system

concentration has to be kept high. This is why in the recirculation reactor, the reactant ratio in all the experiments described in previous sections, was kept at about 8~9. In the RPR system, the effect of the reactant ratio is studied again. In this study, three different molar reactant ratios 2.0, 5.0, and 10.0 were obtained by varying the concentration of hydrogen peroxide, while keeping the initial concentration of ammonia nitrogen consistent. The experiments were carried out under the same operating conditions as earlier. Figure 6.17 plots the removal efficiencies against the sampling time at different reactant ratios. It is observed that there is no significant difference in removal efficiency when molar ratio is 2.0, 5.0 and 10.0. This may be explained by the short exposure time of the reacting fluid in the UV irradiating area. This suggests that the changes in molar ratio do not have any obvious effect. Considering both the efficiency and the cost of the reagent, molar ratio of 2.0 is chosen in this study. This value is significantly lower than the molar ratio of 8-9 in the recirculation reactor.

Variation of pH

To study the effect of pH on the ammonia degradation, the acidity of three feed solutions containing ammonia and hydrogen peroxide were adjusted to be 3.0, 7.0, 10.0, respectively. The pH controlling reagents were buffer solutions, sodium hydroxide and sulphuric acid. Figure 6.18 demonstrates ammonia removal efficiency. It is apparent from Fig. 6.18 that the removal efficiency of ammonia is very low at pH = 3. The removal efficiency of ammonia is significantly improved as the pH of the feed solution is increased from 7 to 10. Recalling the dissociation equilibrium between unionized ammonia (NH_3) and ionized ammonia (NH_4^+), when the solution is in basic region, most

of ammonia is unionized. The above observations suggest that unionized ammonia is oxidized much more easily than ionized ammonia.

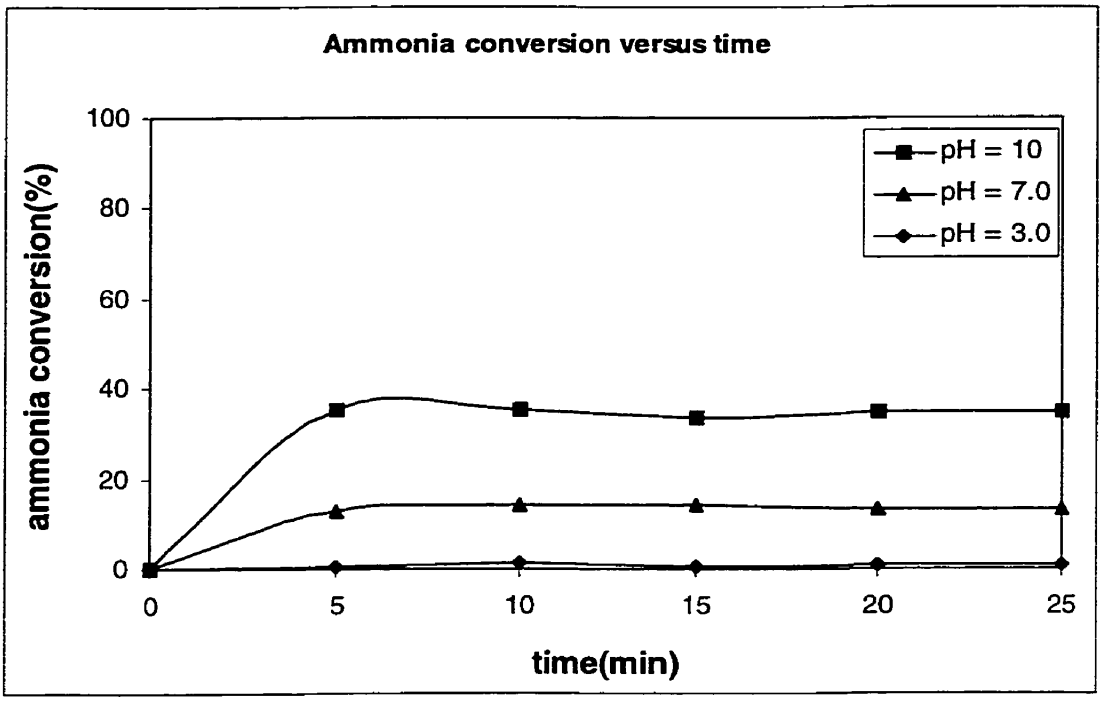

Figure 6.18 Ammonia conversion at different pH in the UV/H_2O_2 RPR system

This may be explained by the reactivity between ammonia and hydroxyl radicals. Ammonia can be attacked by hydroxyl radical through hydrogen abstraction at a high rate ($9.0\times10^7\ M^{-1}\ s^{-1}$). On the contrary, the ammonium ion is uncharged and may not undergo the same process easily. These observations suggest that the photooxidation process of ammonia must be run in the basic range to obtain high removal efficiency, which is the reason why pH = 10 was chosen as the operating pH in this study. It was also noticed that the pH of the solution decreased very slightly from 10.0 to 9.9 after the reacting fluid flowed through the reactor for one pass, and this decrease was smaller than that in the

recirculation reactor. Hence, there was no need to have any prompt adjustment of pH, as was required in the case of the recirculation reactor, in which the fall in pH was drastic.

Effect of variation in feed flow rate

The effect of the flow rate of the reacting fluid on ammonia degradation was studied by adjusting flowrate monitored by a rotameter. Three experiments were run under different flow rates of 48, 85, 195 ml/min, which corresponded to rotameter

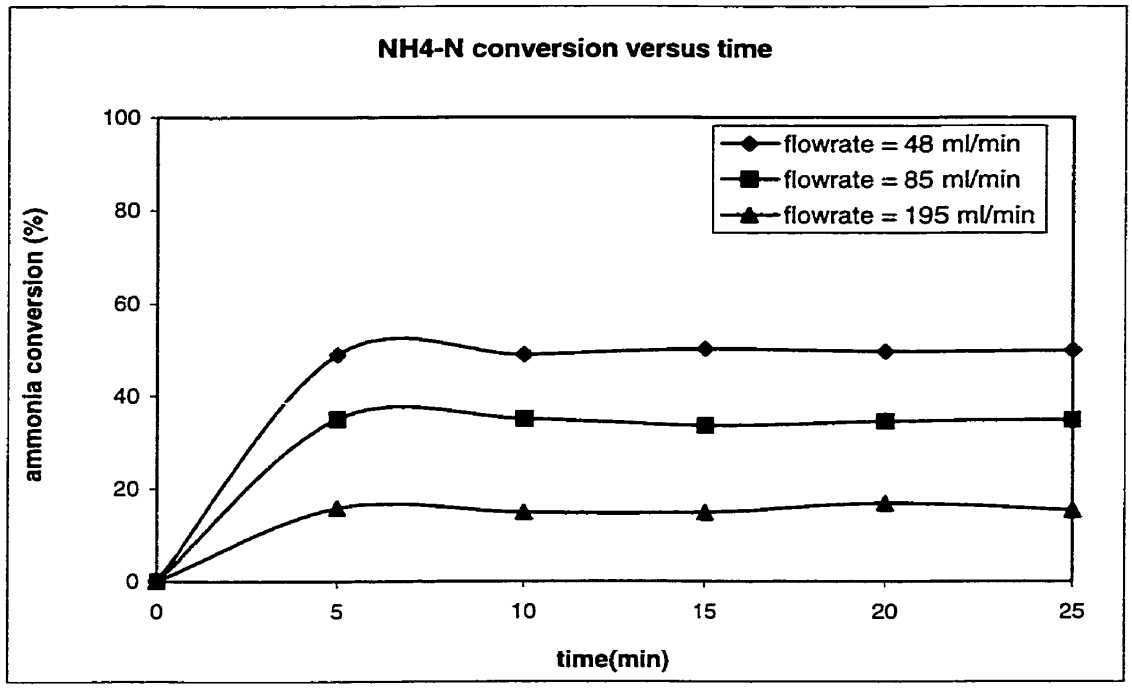

Figure 6.19 Ammonia conversion under different flow rate in the UV/H_2O_2 RPR system

readings of 20, 30 and 60. The initial concentration of ammonia nitrogen was 3.47 mM and other operating conditions are kept constant. Figure 6.19 presents the experimental results. It can be seen that the ammonia removal efficiency increases significantly when

flow rate decreases from 195 ml/min to 48 ml/min. There are two possible explanations for this result: One is the hydraulic residence time. When the flowrate is lower, the residence time is greater. Therefore the removal efficiency is higher in this plug-flow like reactor system. The quantitative relationship between the two parameters will be discussed later in detail. The other reason is related to the light absorption. It is obvious that at lower flow rate, the amount of the light absorption per unit volume of the reacting fluid is higher. Thus the overall reaction rate is higher.

Effect of variation in cylinder rotation speed

The macro-process of the reacting fluid flowing through reactor is as follows: First, the reacting fluid entering the top distributor tube redistributes inside the distributor. Because the apertures located at the bottom of the distributor tube have very small diameters, the water drops leave out of the distributor tube as spray-like flow. The small water drops hit the cylinder surface at a low point on the right side of the top central line. The gravity forces of the drops tend to pull the drops down the cylinder surface directly from the right side. However, the rotation of the cylinder will carry the drops to rotate, form a thin film and pass the UV light radiating area. From the above description, it can be predicted that the rotation speed will have an effect on the ammonia degradation. To verify this prediction, three cylinder rotation speeds are examined while keeping other operating conditions constant. Figure 6.20 plots the ammonia removal efficiency against time curves at rotation speed of 1.46, 4.29 and 7.50 revolutions per minute (rpm) that correspond to motor controller readings of 20, 50 and 80, respectively.

From Fig. 6.20, it is evident that there is no significant difference on ammonia removal between the rotation speed 4.29 and 7.50 rpm. However, when the rotation speed is

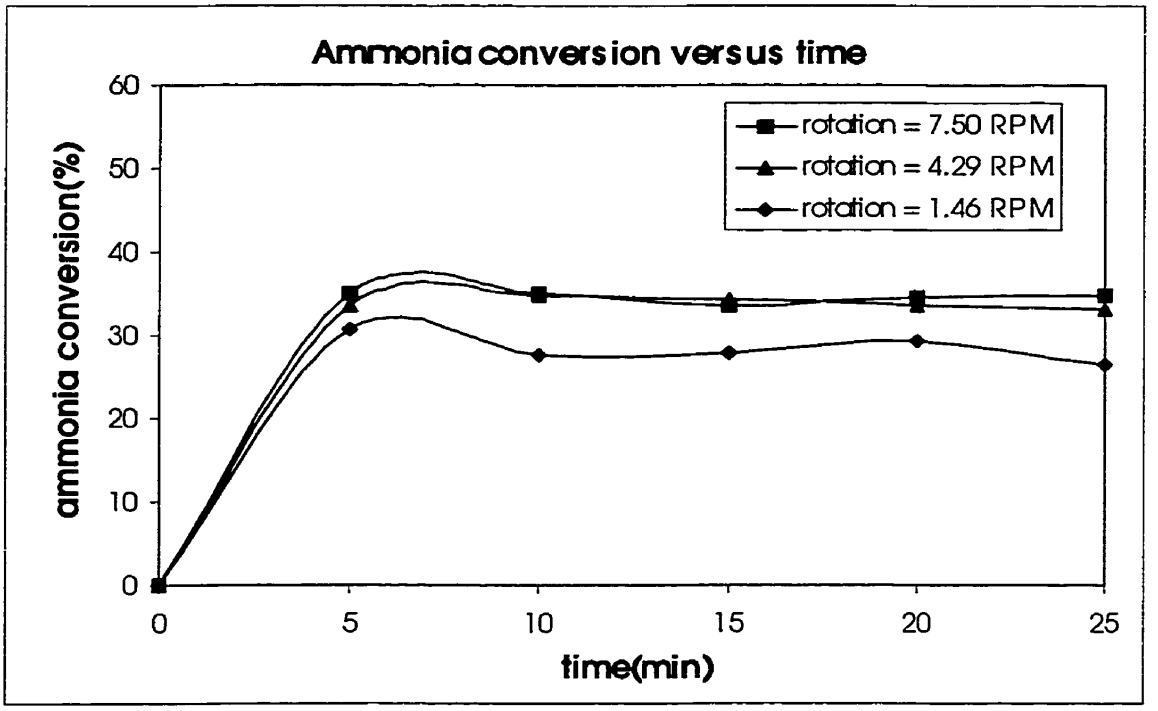

Figure 6.20 Ammonia conversion under different rotation speed in the UV/H_2O_2 RPR system

1.46 rpm, the ammonia removal efficiency is lower than that for higher speed. The possible explanation is as follows: When the rotation speed is too slow, water drops flow down the cylinder because of the gravity force and can not be carried to the irradiating area, resulting in the decrease of the removal efficiency. Hence it is important to maintain the rotation speed high enough. In this study, 7.5 rpm was chosen as the operating speed.

Interference effect

The interference effect refers to the absorption of UV light by components other than the light sensitizing substance such as hydrogen peroxide, which undergoes the desired light-initialized dissociation to produce hydroxyl radicals. These components can be intermediates, products or by products generated during the photochemical process. From the previous studies, it has been concluded that the products of ammonia photodegradation in aqueous solution were nitrite and nitrate. Therefore, the effect of nitrite and nitrate on ammonia removal was studied as follows: Three feed solutions were prepared containing 3.5 mM (50 ppm) ammonia nitrogen (NH_3-N), while two of them

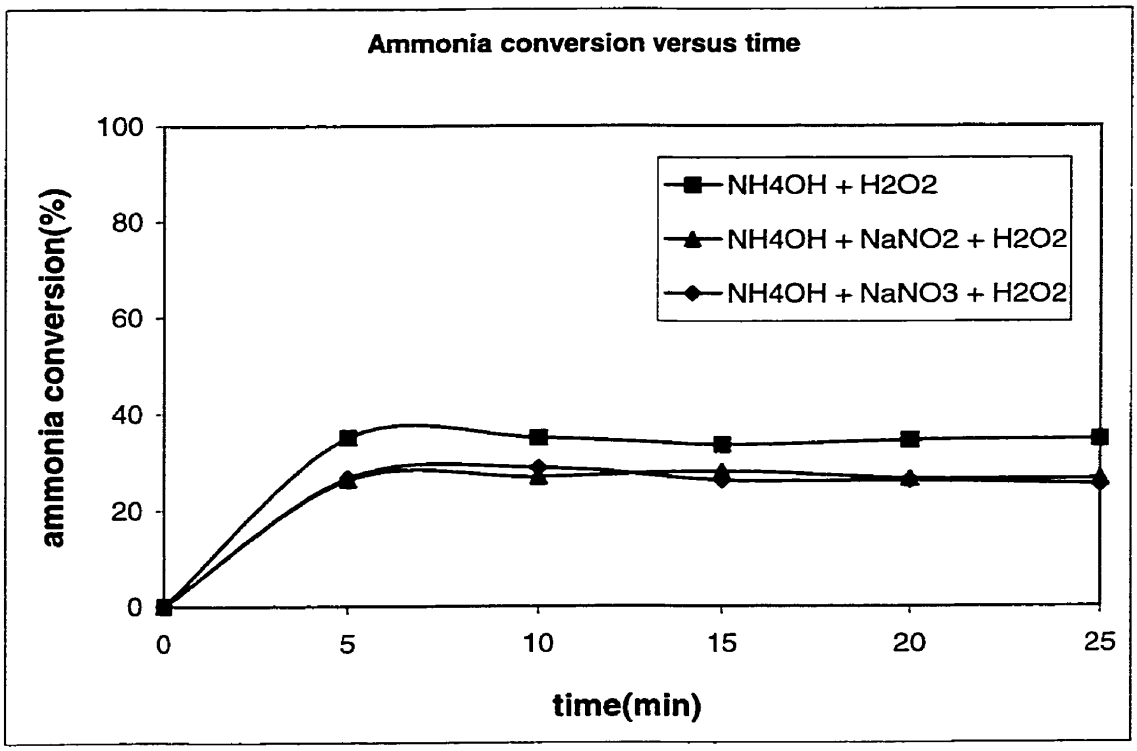

Figure 6.21 Effect of the interference in the UV/H_2O_2 RPR system

were added 1.79 mM (25 ppm) nitrite nitrogen (NO_2-N) and 0.79 mM (11 ppm) nitrate nitrogen, respectively.

Figure 6.21 presents the experimental results of the three feed solutions under the same operating conditions. It can be seen that the removal efficiency is somewhat decreased when the concentration of nitrite or nitrate is relatively high in the system. However, it can be predicted that if nitrite or nitrate is at a low concentration among the products, the interference effect can be ignored. As will be discussed later, there is only very small amount of nitrite and nitrate produced in the RPR system, thus interference effect is negligible, which is an advantage of the RPR system over other reactor systems.

Effect of reflector

As discussed in Chapter 4, theoretical analysis of the effect of reflector will be very difficult because of the lack of the information on the reflectance characteristics of the reflector. Hence, in this study, the effect of the reflector was investigated by the comparison of the reactor performance with and without the reflector. A typical experiment was conducted as follows: initial concentration of ammonia nitrogen was 3.54 mM, the reactant molar ratio was 2. The other operating conditions were input voltage = 250 V, input current = 3.8 A, pH = 10, flow rate of the fluid = 85 ml/min, the cylinder rotation speed = 7.5 rpm. Figure 6.22 presents the removal efficiency of ammonia with and without the reflector. It is found that there is no significant difference between these two cases. The explanation involves two aspects: light intensity and exposure time. The light intensity is decreased when the reflector is removed. However, removing the reflector makes the whole cylinder surface irradiated by the UV light. Hence, the

exposure time of the reacting fluid becomes longer. Because the photo-oxidation reaction rate depends on both the light intensity and exposure time, the effect of using reflector is not obvious in this study.

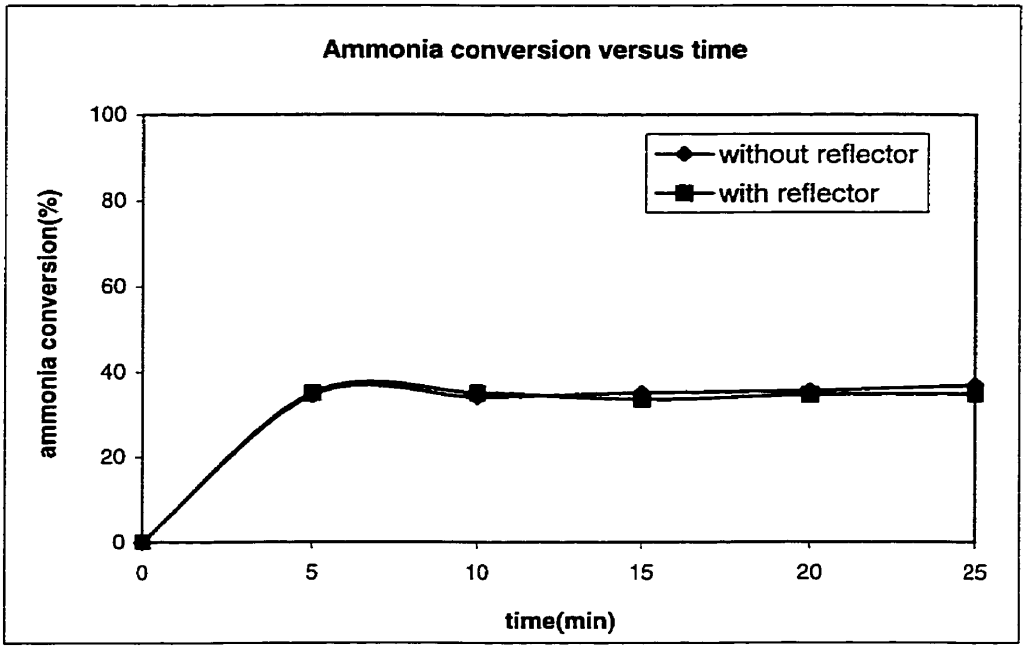

Figure 6.22 Ammonia conversion with/without reflector in the UV/H_2O_2 RPR system

Product identification and quantification

In this study, samples were taken every five minutes after UV lamp came to a steady state and analyzed to identify and quantify various possible intermediates and final products. Table 6.9 presents a typical product distribution of the nitrogenous compounds detected in the samples. The operation conditions were input voltage = 250 V, input current = 3.8 A, pH = 10, flow rate of the fluid = 85 ml/min, the cylinder rotation speed = 7.5 rpm.

Table 6.9 A typical product distribution of the nitrogenous compounds in the UV/H_2O_2 RPR system

	Nitrogen concentration of different species							
	Aqueous (mM)					**Gas (mM)**		
	NH_3	**NO_2^-**	**NO_3^-**	**N_2H_4**	**NH_2OH**	**N_2**	**NO + NO_2**	**N_2O**
Inlet	3.47	0	0	0	0	0	0	0
Outlet	2.27	0.014	0.0064	0	0	1.18	0	0
P[3]	65.3	0.41	0.18	0	0	34.1	0	0

From Table 6.9, it is evident that nitrogen is the only primary product in the UV/H_2O_2 RPR system, after the reacting fluid flows through the reactor for one pass. There are small amounts of nitrite and nitrate produced, which are 0.41 and 0.18%, respectively. Hydrazine and hydroxylamine are possible intermediates but they are not detected in the aqueous sample, suggesting that they get completely oxidized. In addition, there are no other components detected in the gas sample. The study of the product distribution, suggests that the reaction schemes in the RPR system are the same as those discussed in the Section 6.2.1. However, since this RPR system is a plug-flow like reactor, a detailed analysis of the reactor model is given below.

[3] P is the percentage of the concentration of various nitrogenous compounds

Reactor model

Figure 6.23 illustrates the schematic diagram of the water flow in the RPR system. The water influent enters into the reactor from the top, forms a thin film around the surface of the cylinder, and leaves the reactor out of the bottom. Assuming the

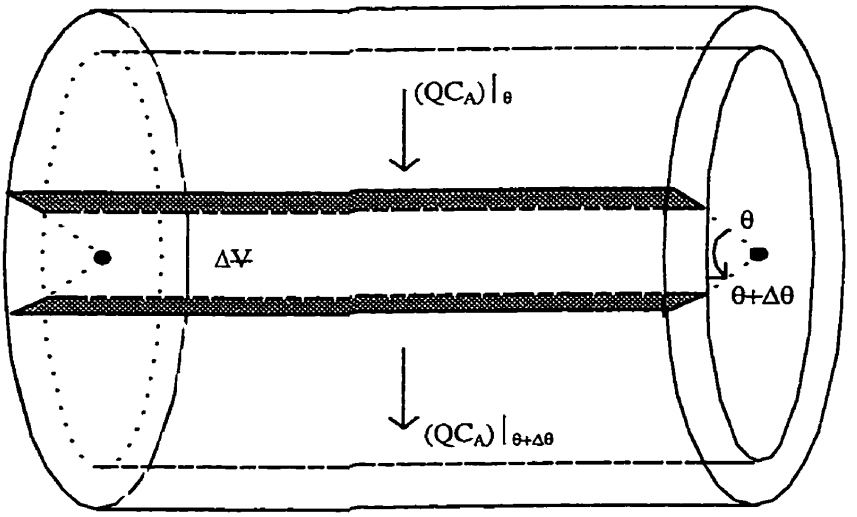

Figure 6.23 Schematic diagram of the water flow in the RPR system

reacting flow is ideally unmixed in the longitudinal direction and mixed radially, this reactor can be considered as a plug flow reactor. The mass balance of ammonia on the incremental volume ΔV can be given as follows:

$$\frac{\partial C_A}{\partial t}\Delta V = QC_A|_\theta - QC_A|_{\theta+\Delta\theta} + r_A \Delta V \qquad (6\text{-}13)$$

(Accumulation) (Inflow) (Outflow) (Generation)

Where,

C_A is the concentration of ammonia in the volume element, mol/m^3

Q is the volumetric flow rate, m^{3}s^{-1}

r_A is the rate of the reaction of ammonia, mol.m^{-3}s^{-1}

Referring to Fig. 6.23, the term $QC_A\big|_{\theta+\Delta\theta}$ can be given as follows:

$$QC_A\big|_{\theta+\Delta\theta} = Q(C_A + \frac{\Delta C_A}{\Delta\theta})\Delta\theta \tag{6-14}$$

Substituting the above equation into Eqn. (6-13),

$$\frac{\partial C_A}{\partial t}\Delta V = -Q\frac{\Delta C_A}{\Delta\theta}\Delta\theta + r_A\Delta V \tag{6-15}$$

Dividing the above equation by ΔV results in,

$$\frac{\partial C_A}{\partial t} = -\frac{Q}{\Delta V}\frac{\Delta C_A}{\Delta\theta}\Delta\theta + r_A \tag{6-16}$$

The volume of the element ΔV is calculated as follows:

$$\Delta V = \frac{R\cdot\Delta\theta + (R+H)\cdot\Delta\theta}{2} H\cdot L = \frac{(2R+H)\cdot\Delta\theta}{2} H\cdot L \tag{6-17}$$

Where,

R is the radius of the cylinder (m)

L is the length of the radiating area on the cylinder surface (m)

H is the thickness of the water film (m)

Suppose constant N is equal to $\frac{(2R+H)}{2} H\cdot L$, Eqn. (6-17) can be expressed as:

$$\Delta V = N \cdot \Delta\theta \tag{6-18}$$

Substituting above equation into Eqn. (6-16) results in Eqn. (6-19) and it can be further simplified as equation (6-20):

$$\frac{\partial C_A}{\partial t} = - \frac{Q}{N\Delta\theta} \frac{\Delta C_A}{\Delta\theta} \Delta\theta + r_A \tag{6-19}$$

$$\frac{\partial C_A}{\partial t} = - \frac{Q}{N} \frac{\Delta C_A}{\Delta\theta} + r_A \tag{6-20}$$

Taking the limit as $\Delta\theta$ approaches zero results in,

$$\frac{\partial C_A}{\partial t} = - \frac{Q}{N} \frac{\partial C_A}{\partial \theta} + r_A \tag{6-21}$$

Under steady state conditions $dC_A/dt = 0$. Also for the thin film conditions prevailing in this reactor, the variation of radiation intensity, dI/dr across the thickness of the film would be negligible. The rate constant k for ammonia destruction under irradiation is simply $k_r(I)$, where k_r is the kinetic reaction rate constant and I is the intensity of radiation. Under these conditions, if the rate of ammonia degradation is assumed to be first-order ($r_A = kC_A$) then the above equation can be integrated between the limits $C_A = C_{A0}$ and $C_A = C_A$, $\theta = 0$ and $\theta = \theta$ and Eqn. (6-23) is obtained:

$$\int_{C_{A_0}}^{C_A} \frac{dC_A}{kC_A} = - \frac{N}{Q} \int_0^{\theta} d\theta \tag{6-22}$$

$$- \frac{1}{k} \ln \frac{C_A}{C_{A_0}} = \frac{N}{Q} \theta \tag{6-23}$$

Comparing Eqn. (6-23) with the typical tubular plug flow reactor, the RHS of the Eqn. (6-23) can be considered as the hydraulic residence time of the reactor θ_H. Hence the relationship between C_A and C_{A0} is given as follows:

$$\frac{C_A}{C_{A_0}} = e^{-k\theta_H} \tag{6-24}$$

From the above reactor model, it can be predicted that if the first-order reaction is assumed, the output of the C_A/C_{A0} will have exponential dependence on the residence time. To verify this, the experimental studies were carried out for different flow rates. The results are summarized in Table 6.10.

Table 6.10 Summary of the experimental results under different flowrates in the UV/H_2O_2 RPR system

Flowrate (mls-1)	**Resid-ence Time θ_H (s)**	**Nitrogen concentration of different species**			
		NH_3	**NO_2^-**	**NO_3^-**	**N_2**
0	0	3.47	0	0	0
195	13.98	2.93	0.0065	0.0029	0.53
85	32.06	2.27	0.014	0.0064	1.18
48	56.78	1.75	0.023	0.014	1.69

The residence time in Table 6.10 was calculated by the RHS of the Eqn. (6-23) with the measured values of L, H, R as 0.4 m, 0.001 m, 0.108 m respectively. Figure 6.24 plots the values of C_A/C_{A0} against the hydraulic residence time θ_H. It can be seen from Fig. 6.24

that the first-order model fits the experimental results well, with the value of the reaction rate constant as 0.0122 s^{-1} (43.92 hr^{-1})

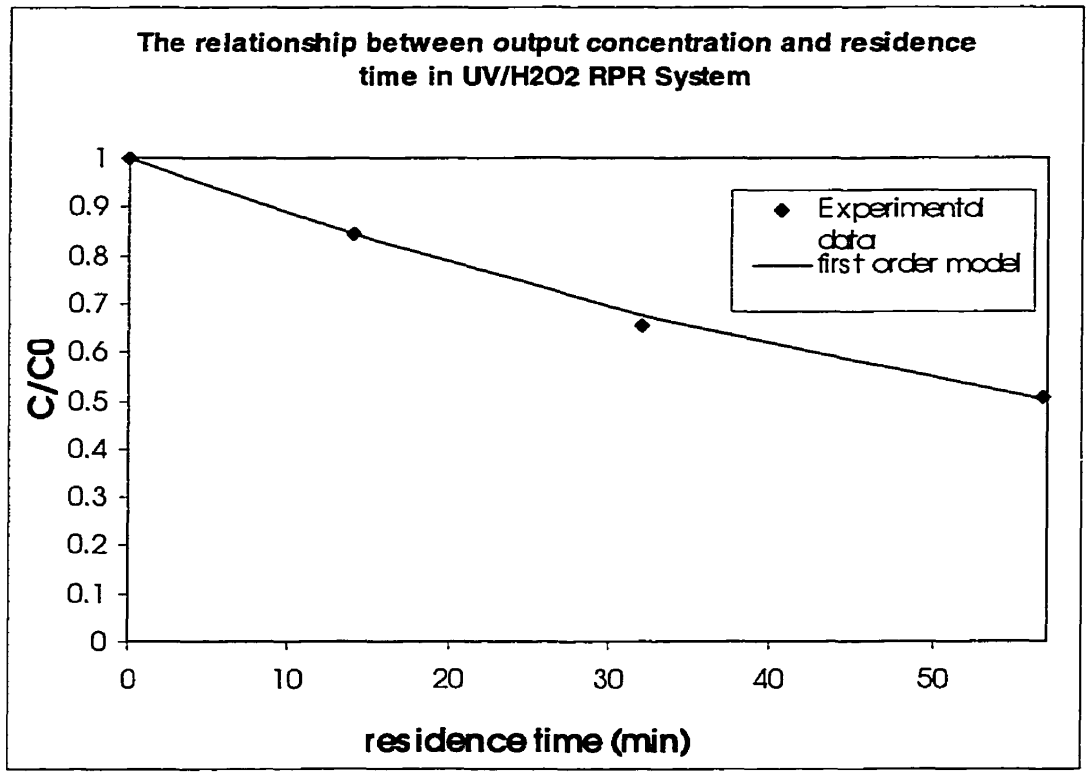

Figure 6.24 The relationship between output concentration and residence time in the UV/H_2O_2 RPR system

Overall kinetics model

It has been noticed that only nitrogen is the primary product while the concentrations of nitrite and nitrate are negligible. Hence a simple overall kinetics model is postulated by the following equation:

$$NH_3 \xrightarrow{k''} N_2 \qquad (6\text{-}25)$$

As in Section 4.4, applying the principles of mass balance and same initial conditions, the concentrations of ammonia (C_1) and nitrogen (C_2") can be expressed by Eqns. (6-26) and (6-27):

$$C_1 = C_{1_0} e^{-k'' t} \tag{6-26}$$

$$C_2'' = C_{1_0}(1 - e^{-k'' t}) \tag{6-27}$$

Where k″ is rate constant. The above equations are the kinetics expressions in

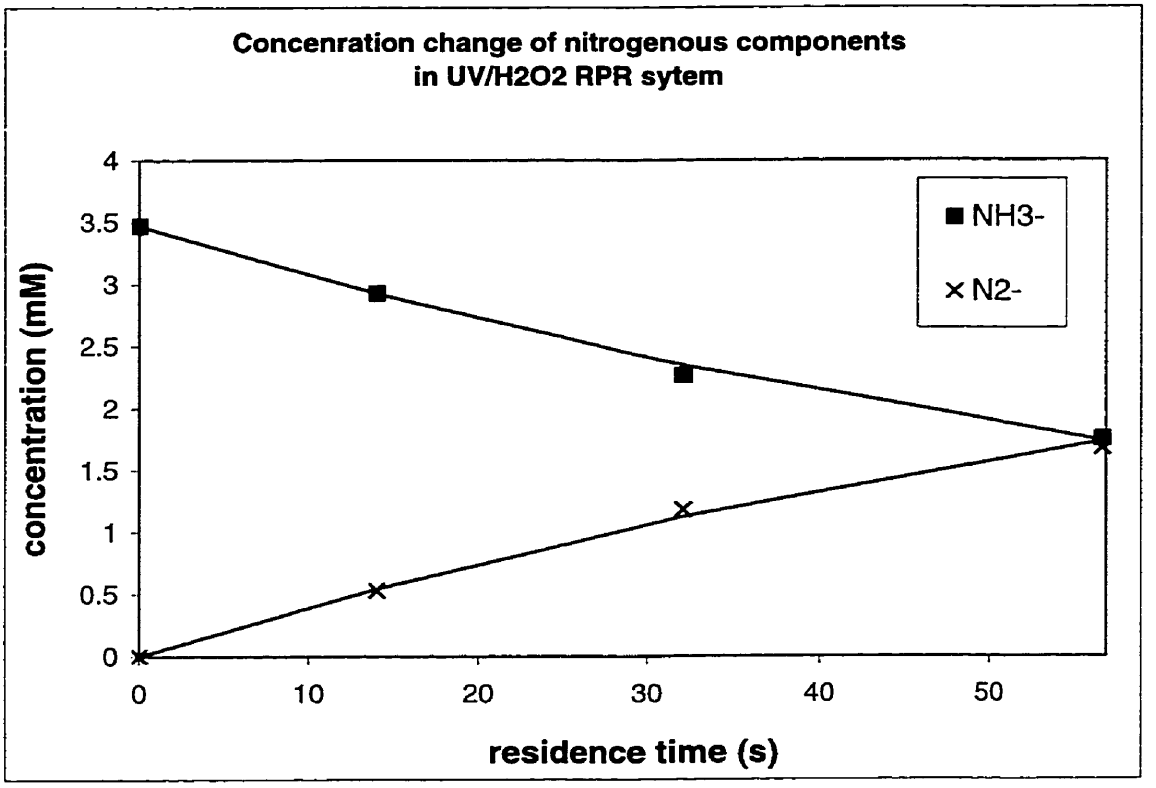

Figure 6.25 The concentration change of the nitrogenous components in the UV/H_2O_2 RPR system

the UV/H_2O_2 RPR system and their calculated model data are plotted in Fig. 6.25 as solid lines. It can be seen that the model data are in good agreement with the experimental results.

Performance comparison of the UV/H_2O_2 recirculation and RPR systems

Table 6.11 summarizes the performance parameters of the recirculation reactor and RPR system, which includes the overall kinetic rate constant, the volume of the reacting fluid and the amount of ammonia removed in 6 h.

Table 6.11 Summary of the performance of the recirculation reactor and RPR system in the UV/H_2O_2 treatment

Reactor type	**Overall rate constant (hr^{-1})**	**Reaction time (hr)**	**Volume of the reacting fluid (L)**	**Amount of ammonia removed (mmol)**
Recirculation reactor	0.14	6	60	130.87
RPR	43.92	6	30.6	36.83

From Table 6.11, it is evident that the overall rate constant in the RPR system is much higher than that in the recirculation reactor. However, the amount of ammonia removed in the RPR system is much lower than that in the recirculation reactor, which suggests that the energy efficiency may not be high in the RPR system. In addition, it is also noticed that a significant difference exists on product distribution. In the RPR system, nitrogen is the only primary product, which is desirable, as it needs no further treatment.

6.3.3 Product distribution and reactor configurations in the UV/H_2O_2 system

The product distributions in the different reactor systems are compared in the following table.

Table 6.12 Product distribution in different reactors in the UV/H_2O_2 system

Reactor type	Reaction time (hr)	Percentage in the products (%)		
		NO_2^--N	NO_3^--N	N_2-N
Batch	6	3.39	62.75	33.86
Recirculation	6	20.21	7.38	72.41
RPR	0.0089	1.18	0.54	98.28

As can be seen from Table 6.12, for the same oxidant H_2O_2, and for the same UV lamp system, the product distribution is not identical with each other. The amount of nitrate formed is very significant in the case of the batch reactor at 62.75% while in the recirculation reactor and RPR system it is very low. Indeed in the recirculation reactor and the RPR system, the amount of nitrogen formed is very high, 72.41 and 98.28%, respectively.

The differences in product distribution can possibly be explained as follows. Besides the free radicals, many other reactive species are formed in the UV reactor, which proceed to further absorb UV and take part in other transformations and subsequent reactions. Between the three reactors, in the batch reactor, whatever active

species formed are further bombarded by the UV radiation, whereas in the case of the recirculation reactor and the RPR system the active intermediates and free radicals that are as yet unreacted are transported out of the reactor. It is speculated that the continued bombardment of the active species and the active intermediates in the batch reactor possibly favors the oxidation of the nitrogen species to their highest oxidation state, namely, nitrate, whereas, in the recirculation reactor and the RPR system, the oxidation of the active nitrogen intermediates does not proceed beyond the intermediate state of oxidation, namely the nitrogen product.

Further, it could be stated that from the overall ammonia removal process point of view, it would be advantageous not to go beyond the oxidation state of nitrogen, as nitrogen is an environmentally benign product, which can be safely released to the atmosphere. This also means that no further denitrification step would be necessary, as the amounts of nitrate and nitrite are very low in the products.

6.3.4 Multi-pass UV/H_2O_2 system

From the discussions carried out in previous sections, it can be predicted that the longer the residence time, the greater the removal percentage is. To verify this, the reacting effluent flowing out of the reactor after one pass was recycled back into the reactor for the second pass, and then further recycled for the third pass. Every pass lasted for 30 minutes. Samples were taken every five minutes after the UV lamp came to steady working state. The operation conditions for all passes were consistent at input voltage = 250 V, input current = 3.8 A, flow rate of the fluid = 85 ml/min, and the cylinder rotation speed = 7.5 rpm. Figure 6.26 demonstrates the change of ammonia removal percentage with sampling time. Table 6.13 lists the initial ammonia concentration, average exiting concentration, average overall removal percentage and average removal percentage per pass.

From Table 6.13, it can be seen that the ammonia removal remains more or less the same for the first two passes, but shows an obvious decrease on the third pass. This can be attributed to the consumption of hydrogen peroxide and the decrease of pH in the system with the increase in the number of passes. The drop in pH per pass is about 0.1 to 0.2.

Table 6.13 Experimental data in the multi-pass UV/H_2O_2 RPR system

	Ammonia nitrogen concentration (mM)	**Overall removal percentage (%)**	**Removal percentage per pass (%)**
Initial	4.0	0	0
One pass	2.62	34.41	34.41
Two pass	1.67	58.19	36.26
Third pass	1.26	68.51	24.69

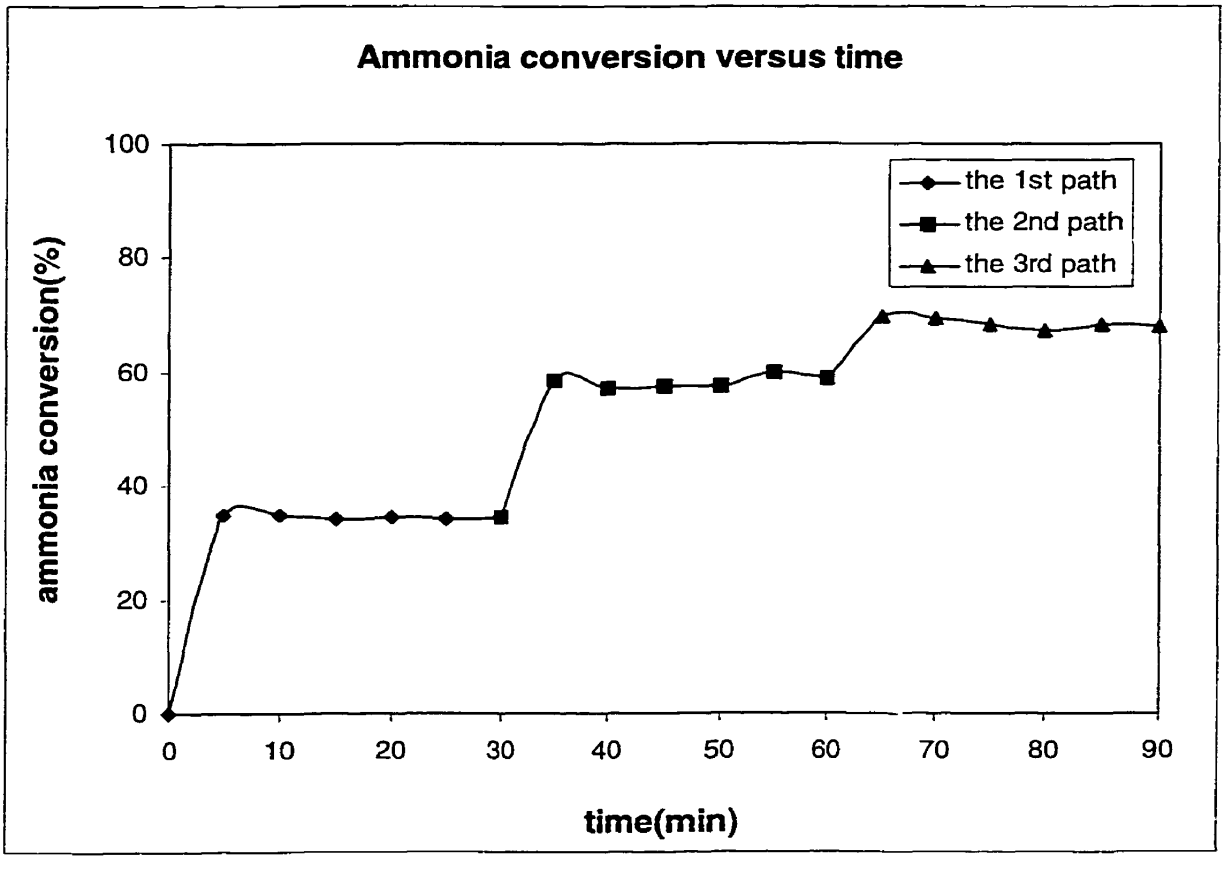

Figure 6.26 Ammonia conversion versus time in the UV/H_2O_2 RPR system

6.3.5 Alternative UV lamp in the UV/H_2O_2 RPR system

Product identification and quantification

The effect of the radiation source on the photodegradation of ammonia was investigated by employing an alternative Rayox medium-pressure mercury lamp substituting existing Hanovia medium-pressure mercury lamp. The experiments were run at different flowrates under the same operating conditions as those in the Hanovia lamp, except for the input voltage = 212 V, and input current = 4.11 A. The concentrations of the nitrogenous compounds detected in the samples are summarized in Table 6.14.

Table 6.14 Summary of the experimental results under different flowrates (Rayox lamp)

Flowrate (ml/min)	**Resid-ence Time θ_H (s)**	**Nitrogen concentration of different species**			
		NH_3	**NO_2^-**	**NO_3^-**	**N_2**
0	0	3.95	0	0	0
195	13.98	3.42	0.0091	0.0066	0.51
85	32.06	2.78	0.088	0.041	1.04
48	56.78	2.29	0.18	0.14	1.33
P[4]		70.4	2.23	1.05	26.3

Comparing Table 6.14 and 6.9 and 6.10, it is found that there is some difference in the

[4] P is the percentage of the concentration of various nitrogenous compounds under the flowrate of 85ml/min

product distribution. In the Rayox system, the concentrations of nitrite and nitrate are slightly higher than those for the Hanovia system. This may explained as due to the influence of the differences in the spectral distribution on the reaction pathways. For example, if there is more hydroxylamine produced during the process, the product may turn out to have more nitrite and nitrate. Considering nitrogen as the only primary product, the same overall kinetics model as shown by Eqn. (6-25) can be applied here. Figure 6.27 presents the experimental data and calculated model data ($k'' = 0.01\ s^{-1} = 36\ hr^{-1}$). It can be seen that the experimental data are in good agreement with the model data.

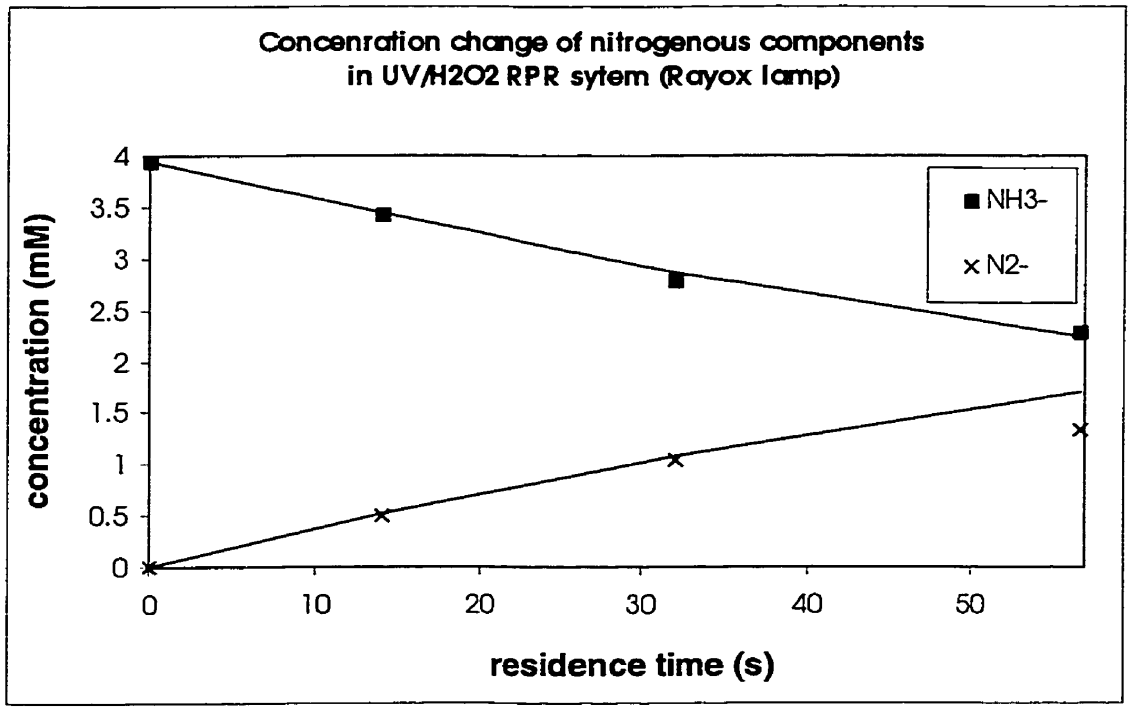

Figure 6.27 The concentration change of the nitrogenous components in the UV/H_2O_2 RPR system (Rayox lamp)

Performance comparison of the Hanovia/Rayox lamp in the UV/H_2O_2 RPR system

To compare the performance of the Hanovia lamp and Rayox lamp in the UV/H_2O_2 RPR system, the performance parameters are presented in Table 6.15.

Table 6.15 Summary of the performance of the Hanovia lamp and Rayox lamp in the UV/H_2O_2 RPR system

Lamp type	**Overall rate constant (hr^{-1})**	**Reaction time (hr)**	**Volume of the reacting fluid (L)**	**Amount of ammonia removed (mmol)**
Hanovia lamp	43.92	6	30.6	36.83
Rayox lamp	36.0	6	30.6	35.68

From the above table, it can be seen that the rate constant of ammonia degradation is higher and the amount of ammonia removed is greater in the Hanovia lamp system than that in the Rayox lamp system. The possible explanation is that the input power in the former system is higher. The input power of the Hanovia lamp is 250×3.8 = 950 w, while that of the Rayox lamp is 212×4.11 (= 871 w).

Effect of nozzle

As discussed earlier, the amount of ammonia removed in the RPR system is relatively low, which suggests that the energy efficiency may not be high. To trap the UV radiation that possibly escapes the reacting film on the cylinder surface, a spray nozzle is incorporated and additional feed solution can be atomized and sprayed on to the reacting

surface. Four experiments were conducted under different flow rates (via the nozzle) of 85, 157, 236, 317 ml/min, which corresponded to rotameter readings of 30, 50, 70, and 90, respectively. Other operating conditions were: initial concentration of ammonia nitrogen = 3.94 mM, input voltage = 212 V, input current = 4.11 A, pH = 10, flow rate via distributor tube = 85 ml/min, and cylinder rotation speed = 7.5 rpm. Table 6.16 summarizes the volume of the reacting fluid and the amount of ammonia removed under different flowrates in six hours. The last column of Table 6.16 is the amount of ammonia removed after the reflector is removed from the reactor system, which will be discussed later.

Table 6.16 Summary of the experimental results under different flowrates in the UV/H_2O_2 RPR system (Rayox lamp)

Distributor flowrate (ml/min)	**Nozzle flowrate (ml/min)**	**Reaction time (hr)**	**Volume of the reacting fluid (L)**	**Amount of ammonia removed (mmol)**	
				With reflector	**Without reflector**
85	0	6	30.6	35.68	37.84
85	85	6	61.2	47.60	50.71
85	157	6	87.12	48.14	52.77
85	236	6	115.56	55.08	56.79
85	317	6	144.72	57.49	59.55

From Table 6.16, it is found that the amount of ammonia removed increases with the feed spray. It is likely that the escaping UV radiation is absorbed by the reacting fluid spray, resulting in better utilization of the UV.

Effect of reflector

As in the Hanovia lamp system, the effect of the reflector was studied by removing reflector and then comparing the performance between with and without the reflector. The operating condition were initial concentration of ammonia nitrogen = 3.90 mM, input voltage = 212 V, input current = 4.11 A, pH = 10, flow rate via distributor tube = 85 ml/min, and cylinder rotation speed = 7.5 rpm. The flow rate via the nozzle was adjusted as 85, 157, 236, 317 ml/min, respectively. The experimental results obtained from without reflector has been presented in the last column of Table 6.16.

Comparing the last two columns of Table 6.16, it can be seen that the amount of ammonia removed is slightly increased after the reflector is removed. Two factors are related to the explanation of this observation. One is the effect of light intensity, which is reduced when the reflector is removed. The other is the effect of exposure time, which is increased when the reflector is removed. The obtained results suggest that the latter factor counterbalance the former in the Rayox lamp system.

6.3.6 Single pass UV/$K_2S_2O_8$ system

This section presents the results obtained in the series of experiments conducted with potassium persulphate as the oxidant. The reacting fluid passed through the reactor for one pass, without any recycling.

Photoxidation of different ammonia percursors

The photooxidation of three different ammonia precursors: ammonium hydroxide, ammonium sulphate and ammonium nitrate were studied. The initial concentrations of ammonia nitrogen in the three solutions were 3.4 mM, and the concentrations of

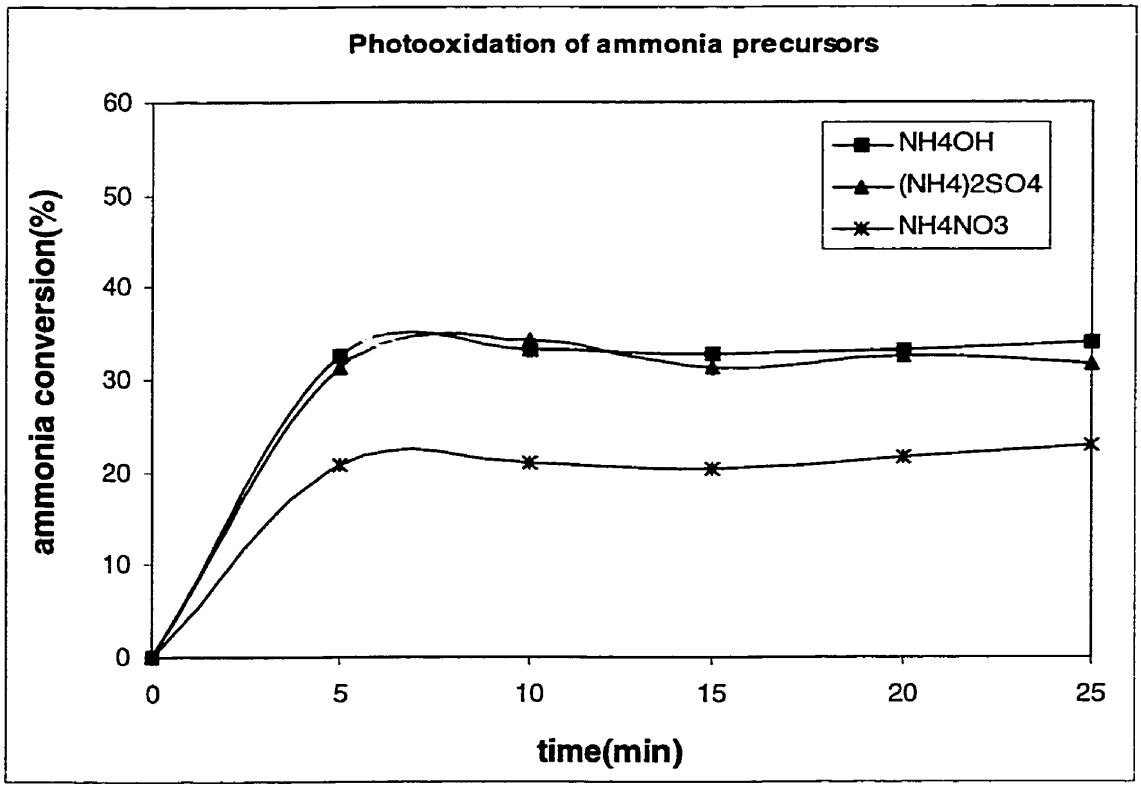

Figure 6.28 Photooxidation of ammonia precursors in the UV/$K_2S_2O_8$ RPR system

potassium persulphate were 5.30 mM. Figure 6.28 presents the variation of the removal efficiency of the different ammonia precursors with time. As can be seen, the average removal efficiencies of ammonium hydroxide, ammonium sulphate and ammonium nitrate are ~33.1, ~32.1 and 21.3%, respectively. As in the UV/H_2O_2 system, ammonium hydroxide was chosen as the precursor for further study.

Effect of variation in UV input power

The effect of input power on the photoxidation of ammonia was studied by varying the input current as 3.8, 2.5, and 1.35 amps., while keeping the input voltage constant at 250 V. The other operation conditions were as follows: the initial

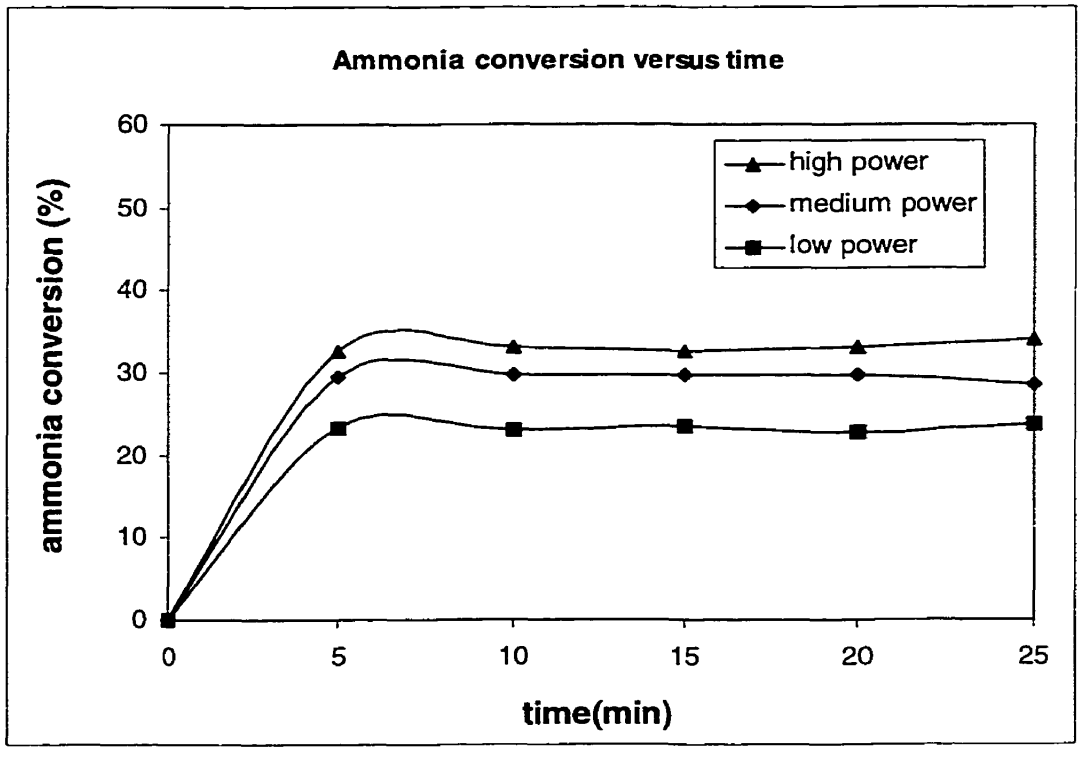

Figure 6.29 Ammonia conversion under different levels of the input power in the UV/$K_2S_2O_8$ RPR system

concentration of ammonia nitrogen = 3.42 mM, the reactant ratio $[K_2S_2O_8]/[NH_3\text{-}N]$ = 1.55, the flowrate of the fluid = 85 ml/min, and the cylinder rotation speed = 7.5 rpm. Figure 6.29 plots the removal efficiency of ammonia against time under three input power levels. As expected it is found that the removal efficiency of ammonia increases as the input power increases, which can be explained by the photochemical principles as discussed earlier.

Effect of variation in initial ammonia concentration

The effect of initial ammonia concentration on ammonia removal was examined by varying the initial concentration as 3.42, 5.51, and 7.47 mM. The molar ratio

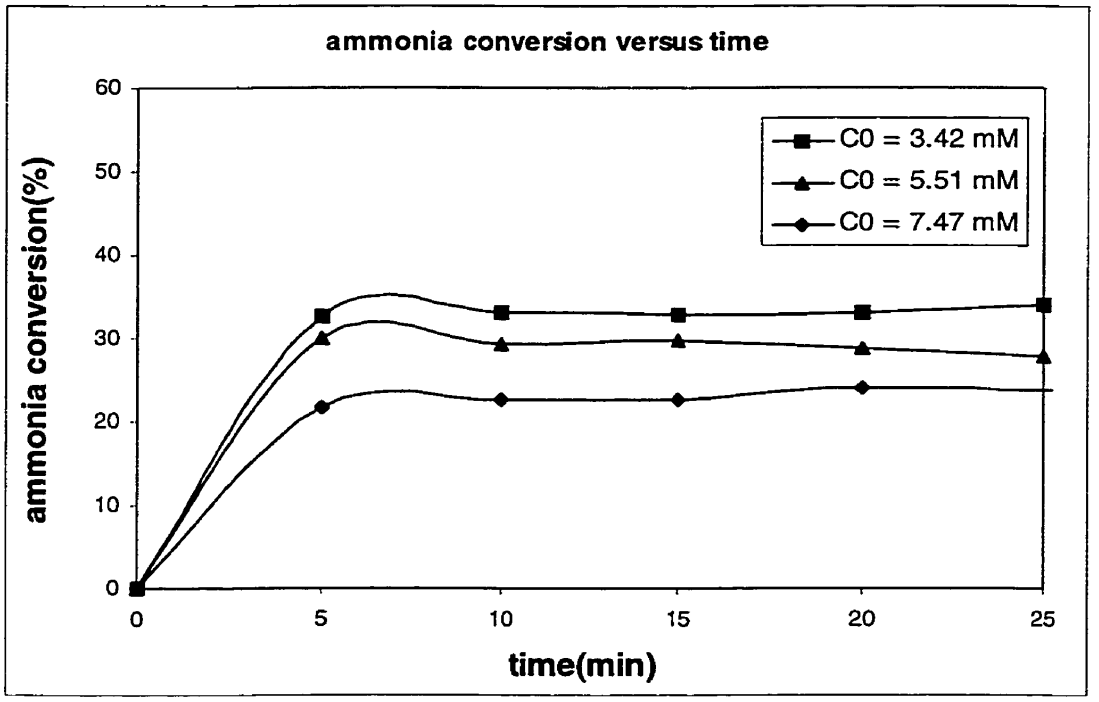

Figure 6.30 Ammonia conversion at different initial ammonia concentration in the UV/$K_2S_2O_8$ RPR system

of potassium persulphate over ammonia was taken as 1.55. Other operating conditions were input voltage = 250 V, input current = 3.8 A, pH = 10, flow rate of the fluid = 85 ml/min, and the cylinder rotation speed = 7.5 rpm. Experimental results are plotted in Fig. 6.30 and it is evident that ammonia removal efficiency is higher at lower concentration. This observation is consistent with that in the UV/H_2O_2 RPR system.

Effect of variation in reactant ratio

In this study, the reactant molar ratio of potassium persulphate to ammonia was studied at four different values: 0.67, 1.05, 1.55 and 2.15. The initial concentration of ammonia and other operating conditions were kept the same. The concentration of

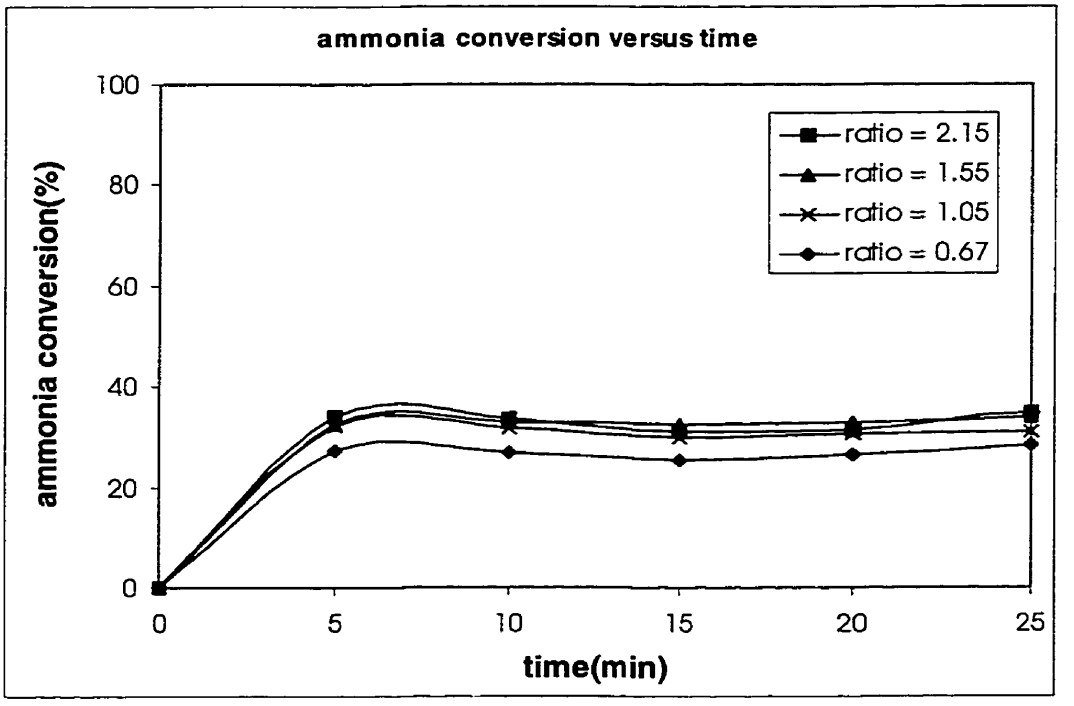

Figure 6.31 Ammonia conversion at different molar ratio in the $UV/K_2S_2O_8$ RPR system

potassium persulphate was adjusted to obtain the designed ratio. Figure 6.31 presents the removal efficiencies at different reactant ratios. It can be seen that when molar ratio is 1.05, 1.55 and 2.15, there is no significant variation on removal efficiency. However, when the molar ratio is as low as 0.67, the removal efficiency is slightly lower, which suggests that the amount of potassium persulphate is not enough in the reacting system. Hence 1.55 is chosen as the reactant molar ratio in this study.

Effect of variation in pH

As in the UV/H_2O_2 system, to study the effect of pH on the ammonia degradation,

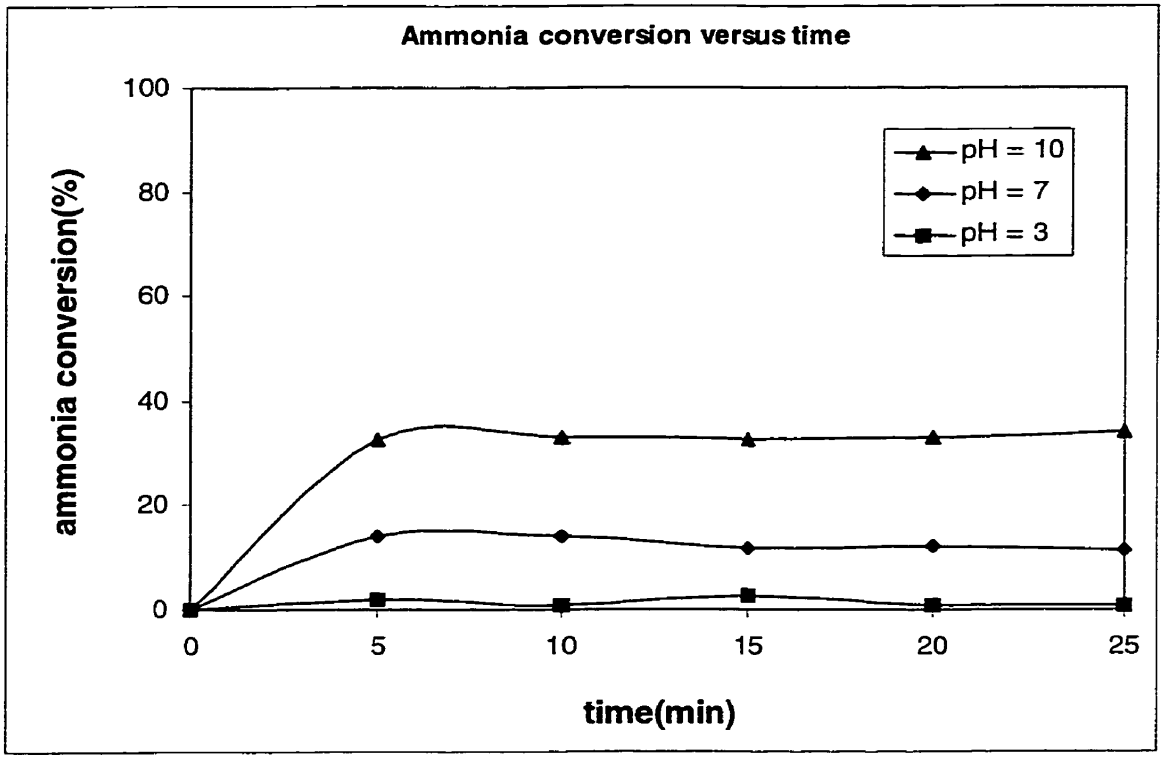

Figure 6.32 Ammonia conversion at different pH in the UV/$K_2S_2O_8$ RPR system

pH buffer solutions, sodium hydroxide and sulphuric acid were employed to adjust the acidity of the feed solutions. The initial concentration of ammonia nitrogen was 3.42 mM and the molar reactant ratio $[K_2S_2O_8]/[NH_3\text{-}N]$ was 1.55. Other operating conditions remained the same. The experimental results are shown in Fig. 6.32. It is evident that the removal efficiency of ammonia is negligible when pH is 3. However, as pH increases from 7 to 10, the removal efficiency of ammonia is significantly improved from 12.7 to 33.1%. This observation is similar to that obtained in the UV/H_2O_2 system and the explanations given earlier hold true here as well. Hence, pH 10 was chosen as the operating pH in this study to obtain high removal efficiency.

It was also observed that the pH of the solution decreased from 10.0 to 9.5 after the reacting fluid passed through the reactor in one pass. However, this change was much smaller than that in the recirculation reactor and thus it was decided that no on-line adjusting of pH was needed.

Effect of variation in feed flow rate

To examine the effect of the flow rate of the reacting fluid on ammonia photo-degradation, three experiments were carried out at different flow rates of 48, 85, and 195 ml/min. The corresponding rotameter readings were 20, 30, 60, respectively. In all three experiments, the initial concentration of ammonia nitrogen was 3.42 mM and other operating conditions were constant. Figure 6.33 plots the removal efficiency against time. The removal efficiency is 41.0% when the flowrate is 48 ml/min. This value is significantly higher than 33.1 and 17.1%, which are the removal efficiencies under

flowrates of 85, and 195 ml/min, respectively. The possible explanation is related to the residence time and the quantitative analysis will be presented later.

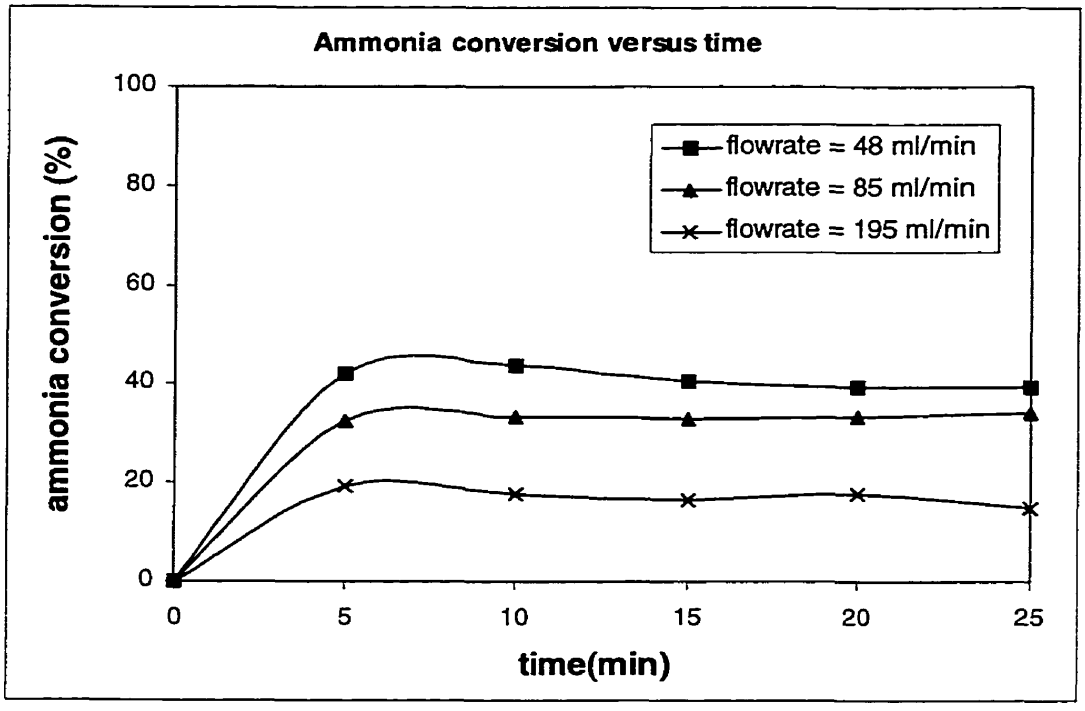

Figure 6.33 Ammonia conversion under different flow rate in the UV/$K_2S_2O_8$ RPR system

Effect of variation in cylinder rotation speed

The effect of the cylinder rotation speed on ammonia removal was studied for three different speeds, while keeping other operating conditions constant. Figure 6.34 presents the experimental results in which removal efficiencies are plotted against time. The rotation speeds are 1.46, 4.29 and 7.50 revolutions per minute (rpm), which correspond to motor controller readings of 20, 50 and 80, respectively. It can be seen

from Fig. 6.34 that when the rotation speeds are 4.29 and 7.50 rpm, there is no obvious difference on ammonia removal. However, when the rotation speed is 1.46 rpm, the average ammonia removal efficiency decreases to 27.6%, which is in good agreement with the observation

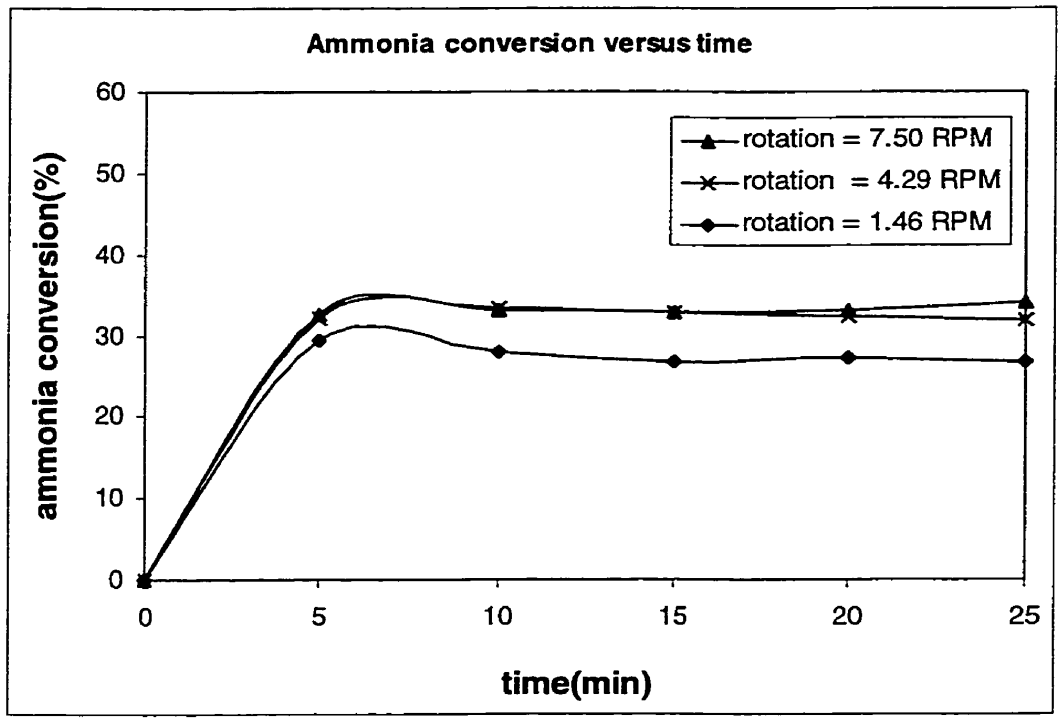

Figure 6.34 Ammonia conversion under different rotation speed in the UV/$K_2S_2O_8$ RPR system

made for the UV/H_2O_2 system. This suggests that a high rotation speed is necessary to obtain high removal efficiency. This is why 7.5 rpm is chosen as the operating speed in experiments conducted in the present study.

Interference effect

It has been observed that nitrite and nitrate existing in the UV/H_2O_2 system will have undesirable effects on the ammonia removal. Therefore the effect of these products was re-studied in the UV/$K_2S_2O_8$ system. Three feed solutions were prepared. One contained 3.5 mM (50 ppm) ammonia nitrogen (NH_3-N) only, while the other two solutions also contained 1.79 mM (25 ppm) nitrite nitrogen and 0.71 mM (10 ppm) nitrate nitrogen, respectively. Figure 6.35 are the experimental results of the three feed solutions under the same operating conditions. It is evident that when nitrite or nitrate exists in the system with relatively high concentration, the ammonia removal efficiency is decreased.

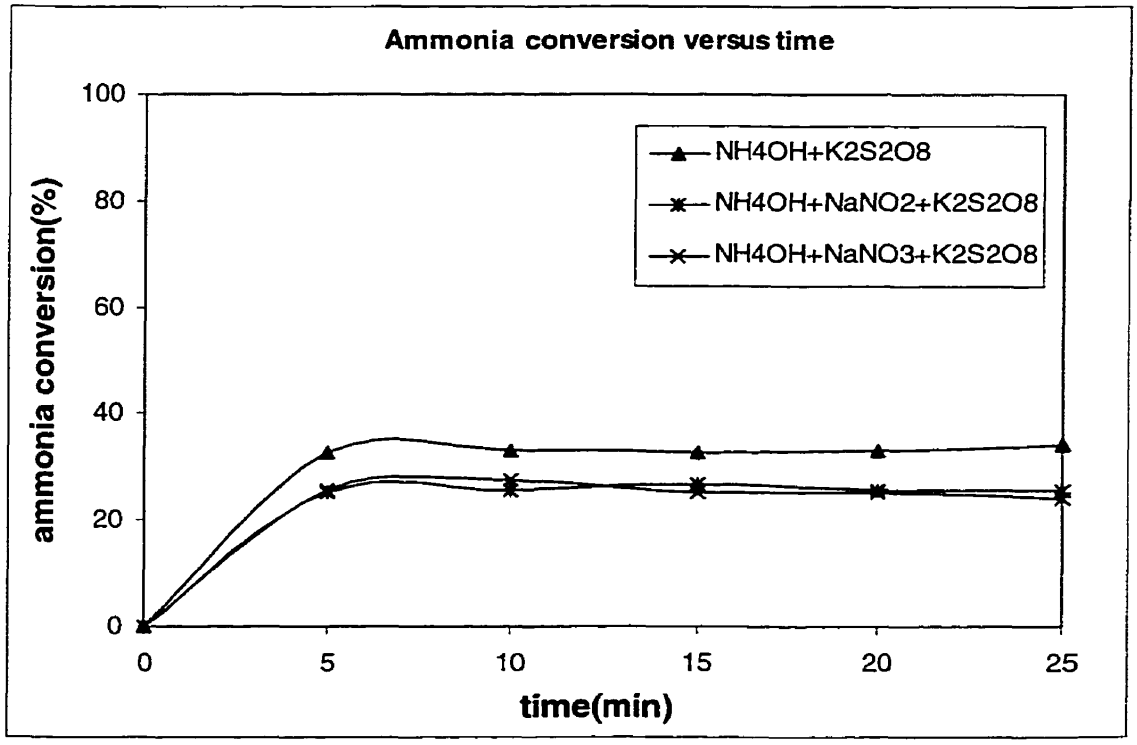

Figure 6.35 Effect of the interference in the UV/$K_2S_2O_8$ RPR system

Effect of reflector

The effect of the reflector was studied by carrying out experiments with and without the reflector. A typical experiment was carried out with an initial concentration of ammonia nitrogen as 3.64 mM, and the reactant molar ratio of potassium persulphate over ammonia as 1.55. The other operating conditions were input voltage = 250 V, input current = 3.8 A, pH = 10, flow rate of the fluid = 85 ml/min, and the cylinder rotation speed = 7.5 rpm. From Fig. 6.36, it can be seen that there is no significant difference in

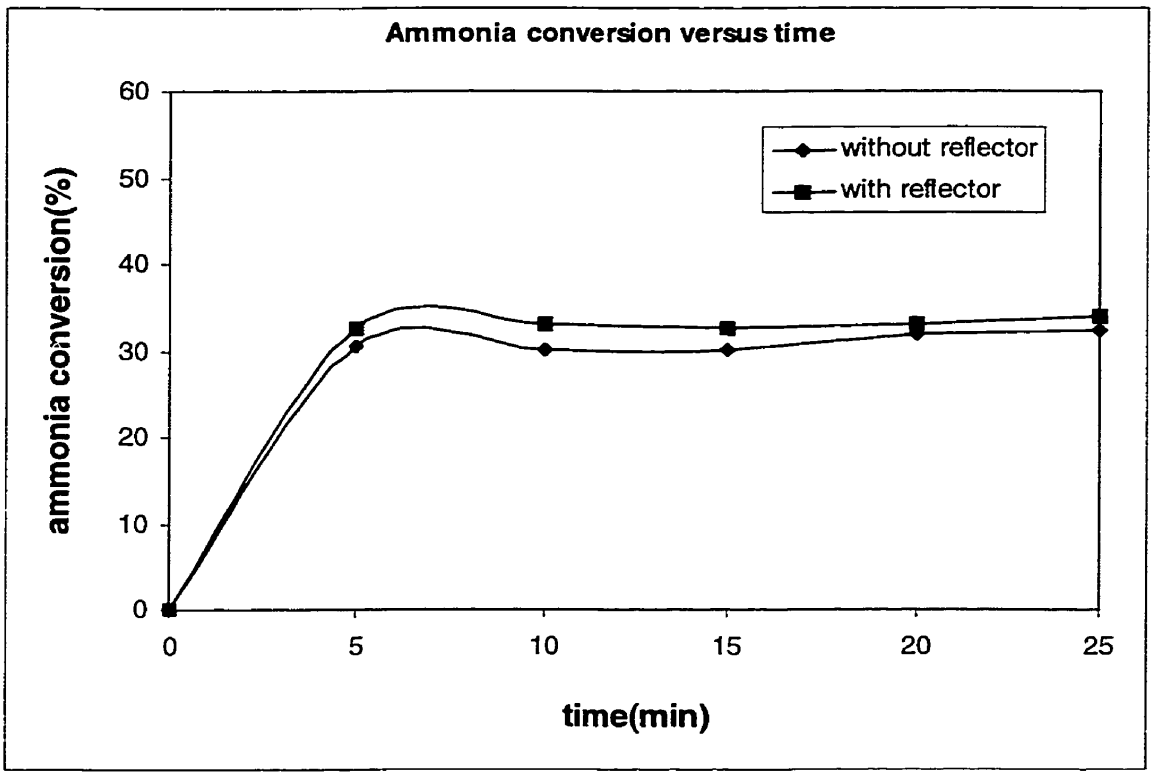

Figure 6.36 Ammonia conversion with/without reflector in the UV/$K_2S_2O_8$ RPR system

the ammonia removal efficiency between the systems with and without the reflector. As discussed earlier for the UV/H_2O_2 systems, this involves a tradeoff between two factors: light intensity and exposure time.

Product identification and quantification

To identify and quantify various possible intermediates and final products, samples were taken every five minutes and sent to analysis after lamp reached steady working condition. Typical operating conditions were reactant molar ratio [$K_2S_2O_8$]/[NH_3-N] =1.55, input voltage = 250 V, input current = 3.8 A, pH = 10, flow rate of the fluid = 85 ml/min, the cylinder rotation speed = 7.5 rpm. Table 6.17 lists a typical product distribution of the nitrogenous compounds detected in the sample.

Table 6.17 A typical product distribution of the nitrogenous compounds in the UV/$K_2S_2O_8$ RPR system

	Nitrogen concentration of different species							
	Aqueous (mM)					**Gas (mM)**		
	NH_3	**NO_2^-**	**NO_3^-**	**N_2H_4**	**NH_2OH**	**N_2**	**NO + NO_2**	**N_2O**
Inlet	3.42	0	0	0	0	0	0	0
Outlet	2.28	0.020	0.0063	0	0	1.11	0	0
P[5]	66.9	0.58	0.18	0	0	32.4	0	0

[5] P is the percentage of the concentration of various nitrogenous compounds

It is apparent from Table 6.17 that in the UV/$K_2S_2O_8$ RPR system, nitrogen is the only primary product after the reacting fluid flows through the reactor in one pass. Only 0.58 and 0.18% are nitrite and nitrate, respectively. Hydrazine and hydroxylamine are not detected in the aqueous sample. In addition, nitrogen is the only detected component in the gas sample. Following is the discussion of the reactor model and kinetics model to simulate the product distribution and reaction kinetics

Similar to the UV/H_2O_2 system, the outputs of the C_A/C_{A0} at different residence time θ_H are summarized in Table 6.18 and plotted in Fig. 6.37.

Table 6.18 Summary of the experimental results under different flowrates in the UV/$K_2S_2O_8$ RPR system

Flowrate (ml/min)	**Residence Time θ_H (s)**	**Nitrogen concentration of different species**			
		NH_3	**NO_2^-**	**NO_3^-**	**N_2**
0	0	3.42	0	0	0
195	13.98	2.83	0.0041	0.0038	0.58
85	32.06	2.28	0.020	0.0063	1.11
48	56.78	2.01	0.032	0.029	1.34

Referring to the plug-flow reactor model expressed by Eqn. (6-25) and the curves in Fig. 6.37, it can be concluded that the first-order model is in good agreement with the

experimental results. The reaction rate constant is 0.0112 s^{-1} = 40.32 hr^{-1}. This value is slightly smaller than that for the UV/H_2O_2 system.

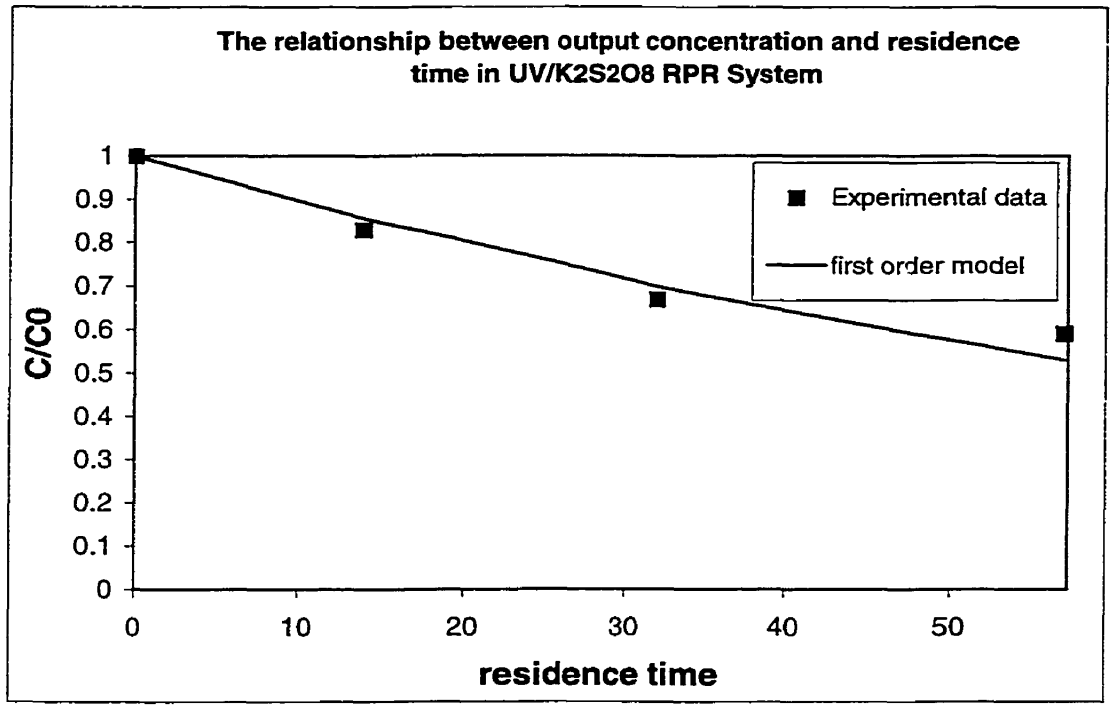

Figure 6.37 The relationship between output concentration and residence time in the $UV/K_2S_2O_8$ RPR system

Overall kinetics model

Table 6.17 indicates that nitrogen is the only primary product in the $UV/K_2S_2O_8$ RPR system. Therefore the same overall kinetics model shown by Eqn. (6-25) can be applied here. The squares and diamonds in Fig. 6.38 are experimental concentrations of ammonia and nitrogen, respectively, while the two solid lines are model data calculated from Eqns. (6-26) and (6-27). It is shown that the model data fits the experimental data well.

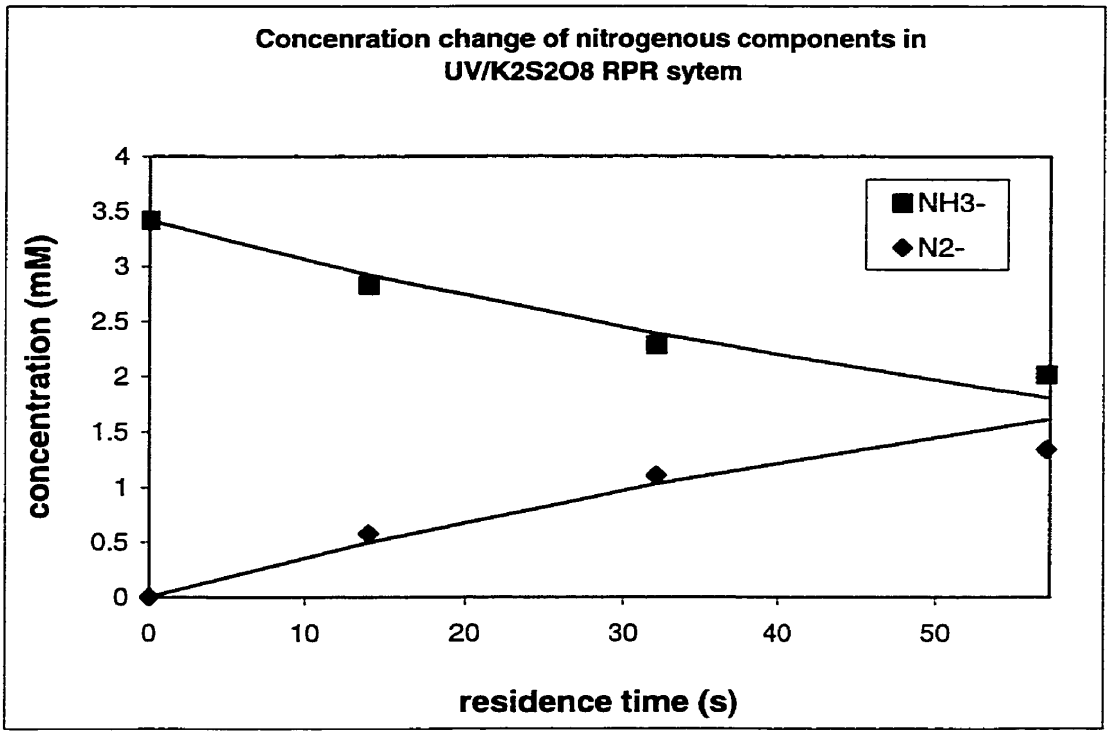

Figure 6.38 The concentration change of the nitrogenous components in the UV/$K_2S_2O_8$ RPR system

Performance comparison of the UV/$K_2S_2O_8$ recirculation and RPR system

To compare the performance of the UV/$K_2S_2O_8$ recirculation and RPR system, the overall kinetic rate constant, the volume of the reacting fluid and the amount of ammonia removed in 0.5 h are presented in Table 6.19.

Table 6.19 Summary of the performance of the recirculation reactor and RPR system in the UV/$K_2S_2O_8$ treatment

Reactor type	**Overall rate constant (hr^{-1})**	**Reaction time (hr)**	**Volume of the reacting fluid (L)**	**Amount of ammonia removed (mmol)**
Recirculation reactor	2.21	0.5	60	145.07
RPR	40.32	0.5	2.55	2.89

It is found from Table 6.19 that the reaction rate constant in the RPR system is higher than in the recirculation reactor, but the amount of ammonia removed in the former system is much less than that in the latter one. Hence it can be concluded that the UV/$K_2S_2O_8$ RPR system may not be energy efficient. However, it is noticed that one advantage of the RPR system is that nitrogen is the only primary product, which is an environmentally benign substance and requires no secondary treatment.

6.3.7 Multi-pass UV/$K_2S_2O_8$ system

As in the UV/H_2O_2 system, the reactor was operated in a multi-pass mode. The operation conditions for every pass were kept constant as input voltage = 250 V, input current = 3.8 A, flow rate of the fluid = 85 ml/min, and the cylinder rotation speed = 7.5 rpm. Every pass lasted for 30 minutes. Samples were taken after the lamp came to steady state. Table 6.19 lists the initial ammonia concentration, average exiting concentration,

average overall removal percentage and average removal percentage per pass. Figure 6.39 demonstrates the change of ammonia removal percentage against time.

It is observed that the ammonia removal percentage goes down with the second and third passes. This may be explained by the consumption of potassium persulphate and the decrease of pH in the system with the increase of the passes.

Table 6.20 Experimental data in the multi-pass UV/$K_2S_2O_8$ RPR system

	Ammonia nitrogen concentration (mM)	**Overall removal percentage (%)**	**Removal percentage per pass (%)**
Initial	3.46	0	0
One pass	2.39	30.89	30.89
Two pass	1.78	48.56	25.56
Third pass	1.38	60.14	22.52

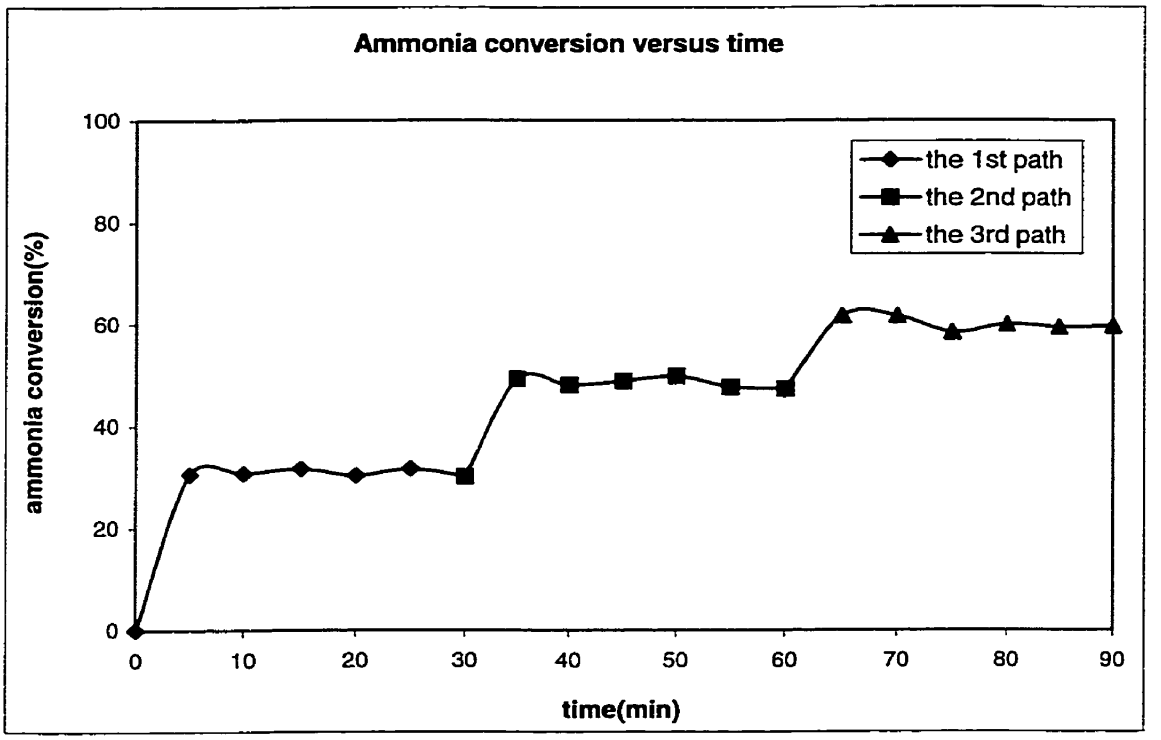

Figure 6.39 Ammonia conversion versus time in the UV/$K_2S_2O_8$ RPR system

6.3.8 Alternative UV lamp in the UV/$K_2S_2O_8$ RPR system

Product identification and quantification

The Hanovia medium-pressure mercury lamp was replaced by Rayox medium-pressure mercury lamp and experiments were conducted for different flowrates. Other operating conditions were taken to be the same as in earlier experiments. It has been noted that the input energy in the Rayox lamp system is slightly different: input voltage = 212 V, input current = 4.11 A. Table 6.21 presents the results obtained under the alternative light source.

Table 6.21 Summary of the experimental results under different flowrates (Rayox lamp)

Flowrate (ml/min)	Resid-Ence Time θ_H (s)	Nitrogen concentration of different species			
		NH_3	NO_2^-	NO_3^-	N_2
0	0	3.33	0	0	0
195	13.98	2.80	0.0057	0.00037	0.42
85	32.06	2.31	0.036	0.0069	0.97
48	56.78	2.01	0.085	0.023	1.32
P[6]		69.5	1.08	0.21	29.2

It is found from Tables 6.17, 6.18 and 6.21 that the concentrations of nitrite and nitrate were slightly higher in the Rayox system than those in the Hanovia system. This observation is similar to that for the UV/H_2O_2 system. This can be attributed to the influence of the differences in the spectral distribution on the reaction pathways, such as on the relative amount of the intermediates, hydrazine and hydroxylamine, and then on the final product distribution. Because nitrogen was still the predominant product, the overall kinetics model expressed by Eqn. (6-25) can be employed. The experimental data and calculated model data are plotted in Fig. 6.40. The rate constant k″ is 0.0101 s^{-1}, which is equal to 36.36 hr^{-1}. From Fig. 6.40, it can be observed that the experimental data are in good agreement with the model data.

[6] P is the percentage of the concentration of various nitrogenous compounds under the flowrate of 85ml/min

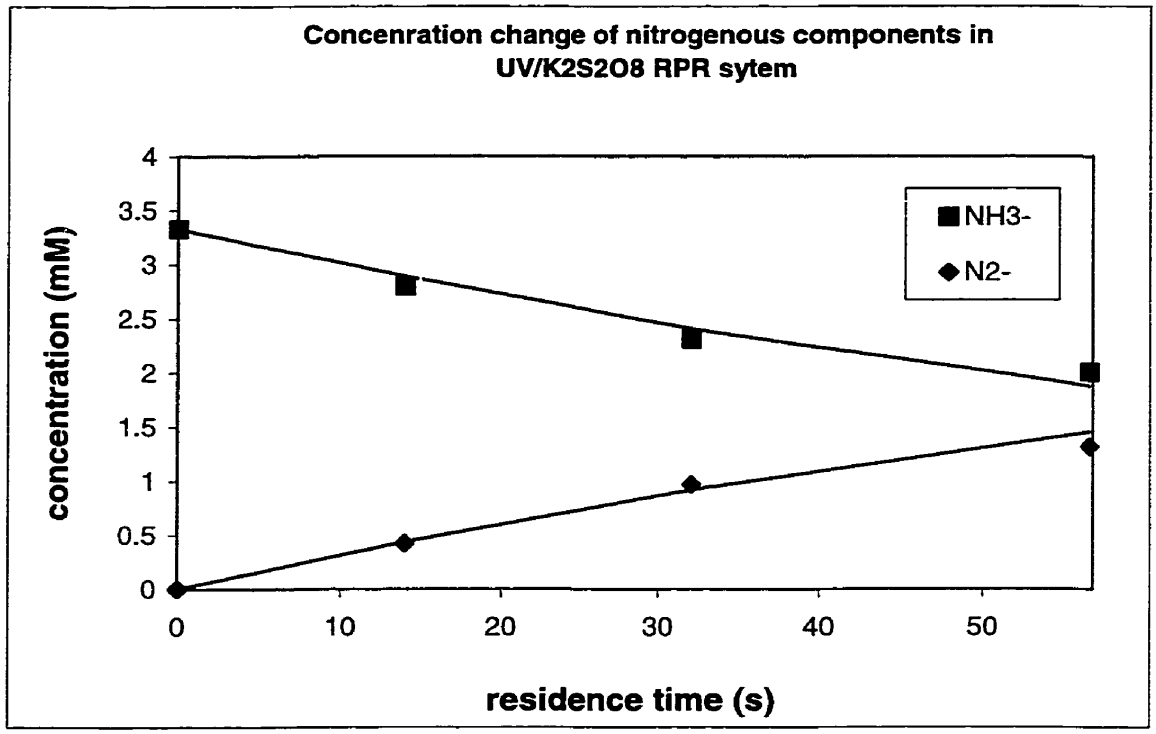

Figure 6.40 The concentration change of the nitrogenous components in the UV/$K_2S_2O_8$ RPR system (Rayox lamp)

Performance comparison of the Hanovia/Rayox lamp in the UV/$K_2S_2O_8$ RPR system

To compare the performance of the Hanovia lamp and Rayox lamp in the UV/$K_2S_2O_8$ RPR system, the performance parameters are summarized in Table 6.22. It can be seen that the rate of ammonia removal is higher and the amount of ammonia removed is greater in the Hanovia lamp system than that in the Rayox lamp system. This observation is consistent with that in the UV/H_2O_2 system and it can be similarly explained by the difference in input power.

Table 6.22 Summary of the performance of the Hanovia lamp and Rayox lamp in the $UV/K_2S_2O_8$ RPR system

Lamp type	**Overall rate constant (hr^{-1})**	**Reaction time (hr)**	**Volume of the reacting fluid (L)**	**Amount of ammonia removed (mmol)**
Hanovia lamp	40.32	0.5	2.55	2.89
Rayox lamp	36.36	0.5	2.55	2.59

Effect of nozzle

As in the UV/H_2O_2 RPR system, the flowrate of nozzle was adjusted to 85, 157, 236, 317 ml/min respectively, and all the experiments were run under the same operating conditions with initial concentration of ammonia nitrogen = 3.78 mM. Table 6.23 presents the amount of ammonia removed under different flowrates in one half hour. The last column is the experimental results obtained without reflector, which will be discussed later.

Table 6.23 demonstrates that the amount of ammonia removed is increased with spray feed augmentation, which is consistent with the observation in UV/H_2O_2 RPR system.

Table 6.23 Summary of the experimental results under different flowrates in the UV/$K_2S_2O_8$ RPR system (Rayox lamp)

Distributor flowrate (ml/min)	**Nozzle flowrate (ml/min)**	**Reaction time (hr)**	**Volume of the reacting fluid (L)**	**Amount of ammonia removed (mmol)**	
				With reflector	**Without reflector**
85	0	0.5	2.55	2.59	2.90
85	85	0.5	5.1	3.89	4.27
85	157	0.5	7.26	3.96	4.32
85	236	0.5	9.63	4.67	5.09
85	317	0.5	12.06	5.19	5.49

Effect of reflector

The effect of reflector was studied by comparing the experimental results with and without the reflector. A typical experiment was carried out under the following operating conditions: initial concentration of ammonia nitrogen = 3.79 mM, input voltage = 212 V, input current = 4.11 A, pH = 10, flow rate via distributor tube = 85 ml/min, and cylinder rotation speed = 7.5 rpm. The flow rate via the nozzle varied as 85, 157, 236, 317 ml/min, respectively. The experimental results are presented in the last column of Table 6.23. From the last two columns of Table 6.23, it can be seen that the amount of ammonia removed is slightly higher without the reflector than with the reflector. As discussed earlier, two counterbalancing factors, light intensity and exposure time are involved.

6.3.9 Effect of turbidity in different reactor systems

Because actual wastewater usually contains a large amount of suspended matter, it is worthwhile to study the effect of turbidity on the removal efficiency of ammonia in different reactors. In the study presented here, feed solution with turbidity is synthesized by the addition of Bentonite. A series of experiments was carried out both in the UV/$K_2S_2O_8$ RPR system and batch reactor as shown in Table 6.24. The experimental results obtained previously without turbidity are also summarized in Table 6.24 to facilitate comparison.

From Table 6.24, it is evident that turbidity imposes significant effect on the ammonia removal in the batch reactor system. With the initial concentration of ammonia nitrogen of about 3.5 mM, the removal percentage of ammonia in a half hour is reduced from 89.32% (without turbidity) to 20.29% (turbidity = 56 NTU) and 8.79% (turbidity = 140 NTU), which are equivalent to reductions of 77 and 90%, respectively.

However, it is found that in the RPR system, the removal percentage of ammonia decreases only slightly. For example, when the turbidity increases from 0 to 56 and 140 NTU, the removal percentage decreases from 30 to 27.89 and 24.98%, respectively, with the initial concentration of ammonia nitrogen of about 3.6 mM and flowrate of 85 ml/min, and with the reflector in the system. The reduction of removal percentage is equivalent to 7 and 17%, respectively, which is much less than that in the batch reactor system. These observations indicate that the RPR system can handle wastewater with high fine suspensions well, which is a significant advantage of the RPR system over other types of reactors.

Table 6.24 Effect of turbidity on ammonia removal in the UV/$K_2S_2O_8$ RPR system and batch reactor (Rayox lamp)

Reactor type	**Initial concentration of ammonia nitrogen (mM)**	**Turbidity (NTU)**	**Reaction time(hr)**	**With (v) or without reflector (×)**	**Volume of reacting fluid(L) or flowrate (ml/min)**	**Ammonia removal percentage (%)**
Batch	3.62	0	0.5	-	30 L	89.32
Batch	3.54	56	0.5	-	30 L	20.29
Batch	3.50	140	0.5	-	30 L	8.79
Batch	7.10	56	0.5	-	30 L	23.10
Batch	7.10	140	0.5	-	30 L	12.01
RPR	3.78	0	0.0089	v	85 ml/min	30.0
RPR	3.59	56	0.0089	v	85 ml/min	27.89
RPR	3.65	140	0.0089	v	85 ml/min	24.98
RPR	3.78	0	0.0089	v	85+85 ml/min	20.18
RPR	3.59	56	0.0089	v	85+85 ml/min	18.90
RPR	3.65	140	0.0089	v	85+85 ml/min	16.98
RPR	3.79	0	0.0089	×	85 ml/min	30.03
RPR	3.61	56	0.0089	×	85 ml/min	28.08
RPR	3.67	140	0.0089	×	85 ml/min	26.78
RPR	7.24	56	0.0089	×	85 ml/min	27.96
RPR	7.36	140	0.0089	×	85 ml/min	25.79
RPR	3.79	0	0.0089	×	85+85 ml/min	22.11
RPR	3.61	56	0.0089	×	85+85 ml/min	20.87
RPR	3.67	140	0.0089	×	85+85 ml/min	18.02
RPR	7.24	56	0.0089	×	85+85 ml/min	20.52
RPR	7.36	140	0.0089	×	85+85 ml/min	17.91

6.3.10 Summary of the performance comparison between different reactor systems

To compare the performance of the different reactor systems using different oxidants and different UV lamps, the performance parameters are presented in Table 6.25.

Table 6.25 Summary of the performance of different reactor systems

Reactor type	**Lamp type**	**Oxidant**	**Overall rate constant (hr^{-1})**	**Reaction time (hr)**	**Volume of the reacting fluid (liter)**	**Amount of ammonia removed (mmol)**
Batch	Rayox	H_2O_2	0.24	6	30	90.97
Recirculation	Rayox	H_2O_2	0.14	6	60	130.87
RPR	Rayox	H_2O_2	36.0	6	30.6	35.68
RPR	Hanovia	H_2O_2	43.92	6	30.6	36.83
Batch	Rayox	$K_2S_2O_8$	4.04	0.5	30	96.87
Recirculation	Rayox	$K_2S_2O_8$	2.21	0.5	60	145.07
RPR	Rayox	$K_2S_2O_8$	36.36	0.5	2.55	2.59
RPR	Hanovia	$K_2S_2O_8$	40.32	0.5	2.55	2.89

From the above table, it can be seen that for either oxidant, H_2O_2 or $K_2S_2O_8$, the overall rate constant of ammonia degradation is the highest in the RPR system, which can be

explained by the high intensity. However, the amount of ammonia that is removed is much lower in the RPR than in batch and recirculation system, suggesting that the energy utilization may not be high in the RPR system.

Chapter 7

Conclusions

7.1 Conclusions

In the work presented here, an advanced photooxidation process for ammonia removal is extended from conventional batch reactor to a custom-modified recirculation reactor and further to a new film-type flow reactor, the Rotospray Photolytic Reactor (RPR). The effects of certain important process parameters have been investigated. Overall kinetics models are built to illustrate the possible mechanisms and the performance characteristics of the different reactors. Performance comparisons are established between these reactors.

It is found that in any kind of reactor, for either oxidant, hydrogen peroxide or potassium persulphate, the photooxidation process occurs significantly only in alkaline solutions. Therefore it is necessary to keep the reacting solution in the basic region to obtain effective removal of unionized ammonia.

Experimental results have provided conclusive evidence that both oxidant type and reactor configuration significantly affect the course of the photooxidation process. The product distributions in the recirculation reactor and the conventional batch reactor show obvious differences. When hydrogen peroxide is used as the oxidant, in the recirculation reactor, the primary products are nitrogen, nitrite and nitrate, among which nitrogen is the predominant product, nitrite is the intermediate and nitrate is the lowest

amount. In the batch reactor, nitrate is the predominant product, while nitrogen is second and nitrite is the lowest amount. Speculative reasons for the differences in product distribution have been advanced which relate the removal of active intermediates from the UV zone as the probable cause.

When potassium persulphate is used as the oxidant, in the recirculation reactor, the primary products are nitrate, nitrogen and nitrite, among which nitrate is the predominant component, followed by nitrogen and then the nitrite. In the batch reactor, nitrogen is the predominant product, with a small amount of nitrate, while the amount of nitrite is negligible. Reaction schemes have been proposed to explain the possible pathways of the photooxidation process of ammonia degradation. The overall kinetics model developed was found to be in good agreement with the experimental results.

The total amount of ammonia removed in the recirculation reactor system was found to be greater than that in batch reactor system, which suggests that the performance of recirculation reactor system is better. However, a complete evaluation of process cost should include a detailed comparison between the different reacting systems on the final product distributions and the resulting cost of subsequent processing, such as back-end denitrification, which is beyond the scope of the study presented here.

The investigation of different operating variables in the RPR system indicated that the reaction rate of ammonia removal is greater at higher input power, which is attributed to the higher light intensity. As mentioned earlier, pH also has a significant effect on the removal efficiency. The other important factor is the flowrate of the reacting fluid. At lower flowrate, the hydraulic residence time of reacting fluid in the UV reactor is longer and the total removal efficiency of ammonia is higher. A plug flow reactor model has

been proposed to simulate the new reactor. Under the assumption of first-order degradation of ammonia, this reactor model can explain the relationship between flowrate and removal efficiency well, under the operating conditions employed in this study.

It has been found that the predominant product in the RPR system is nitrogen, accompanied by only a small amount of nitrite and nitrate, for both the UV/H_2O_2 treatment and the UV/$K_2S_2O_8$ treatment. From the point of view of product distribution, this is a favorable situation because nitrogen is an environmentally benign substance and can be discharged into the air directly. This phenomenon illustrates the effect of reactor configuration on the course of the photooxidation process.

A simplified overall reaction model was found to fit the experimental data well and the kinetic rate constant is quite high in the RPR system. However, design constraints stipulate that the amount of wastewater that can be treated is relatively small compared to that of the recirculation reactor. This indicates that the energy efficiency in the RPR system may not be high. It seems that there is an upper limit on energy utilization, which explains why there is no obvious difference on the removal efficiency of ammonia and product distribution between different oxidants. With a nozzle to provide additional water supply and distribution, it has been confirmed that part of the UV energy does escape from the reacting surface unutilized. More research is required to improve the energy utilization.

The study of the effect of turbidity in different reactor systems has demonstrated that the RPR system has an obvious advantage on the treatment of high turbidity wastewater over other types of reactors.

7.2 Recommendations for future work

The feasibility of the photooxidation for ammonia degradation has been confirmed in the present study. The overall kinetics models for different reacting systems provide good explanation of the product distribution and performance of these systems. Based on the results obtained in the present study, the following additional work are recommended for future research:

The reaction mechanism of photooxidation process is a comprehensive process which involves various reactions between molecules, atoms and radicals. The proposed reaction schemes in this study need to be explored further in detail to elucidate the effect of the nature of the oxidants on the product distribution in different reacting systems.

It is worthwhile to extend the investigation to other oxidants or combination of oxidants, such as ozone plus peroxide, etc. The possibility of finding a homogenous or a heterogeneous catalyst leading to higher removal can not be ruled out either.

The existing overall kinetics model is required to be developed further to incorporate the effect of the spectral distribution of light source, light intensity profile in the reactor, and fluid flow pattern on the photochemical reaction rate and possible change of reaction pathways for a specific reactor type.

The design of the RPR system needs to be optimized to improve its energy utilization. Suggestion on enhancing the energy efficiency includes optimizing the lamp system for the specific design.

Because various UV lamps have significant differences in their spectral distribution and light efficiency, a more detailed performance evaluation of the commercially available lamps needs to be done.

A complete economic analysis of the treatment system should include capital costs, operating costs of the existing process and subsequent processes such as denitrification, that may have to be added on to treat nitrite and nitrate in the final products.

References

1. Department of National Health and Welfare, (1993), Guidelines for Canadian Drinking Water Quality: Water Treatment Principles and Applications, A manual for the Production of Drinking Water, the Canadian Water and Wastewater Association in Cooperation with the Department of National Healthand Welfare, Ottawa, Ontario, Canada, pp.228-229.

2. Ontario Ministry of the Environment (1981), Outline of Analytical Methods, a Guide to the Occurrence, Significance, Sampling and Analysis of Chemical and Microbial Parameters in Water, Toronto, Canada, pp.147-154.

3. Safarzadeh-Amiri, A., Bolton, J.R. and Cater, S.R.(1996), The Use of Iron in Advanced Oxidation Processes, J. Adv. Oxid. Tecnol., 1(1), pp.18-26.

4. Helz, G.R., Zepp, R.G., Crosby, D.G.(ed.), (1994), Aquatic and Surface Photochemistry, Lewis Publishers, Boca Raron, U.S.A.

5. Awadalla, F.T., Striez, C. and Lamb, K., (1994), Removal of Ammonium and Nitrate Ions from Mine Effluents by Membrance Technology, Separation Science and Technology, 29(4), pp. 483-495.

6. Zadorojny, C. , Saxton, S. and Finger, R., (1973), Spectrophotometic Determination of ammonia, Water Pollution Control Federation, 45(5), 1973, pp.905-912.

7. Forsyth, B., Cameron A. and Miller, S., (1995), Explosive and Water Quality, Proceedings of Sudbury '95-Mining and Environment, Vol II, Sudbury, Ontario, Canada, pp. 795-803.

8. Water Environment Research Foundation, (1992), Design of Municipal Wastewater Treatment Plants, Volume I, prepared by Joint Task Force of the Water Environment and the American Society of Civil Engineers, Alexandria, VA, pp.35-43.

9. Health and Welfare Canada, (1982), Municipal Wastewater Disinfection in Canada Need and Application, Prepared by Health Protection Branch, Ottawa, Canada.

10. Metcalf & Eddy, Inc., (1991), Wastewater Engineering, Treatment, Disposal and Reuse, 3rd Edition, McGraw-Hill, Inc., New York, pp.735-742.

11. Kelly, M., (1988), Mining and the Freshwater Environment, Elsevier Science Publishers Ltd, London, England, pp.9-15.

12. Environment Canada, (1992), Status Report on Water Pollution Control in the Canadian Metal Mining Industry (1990 and 1991), Prepared by Mining, Mineral and Metallurgical processes Division, Industrial Programs Branch, Environmental Protection, Conservation and Protection, Report EPS 1/MM/4, Ottawa, Canada.

13. Environment Canada, (1987), Review of the Canadian Fertilizer Industry and Evaluation of Control Technology, Prepared by Industrial Programs Branch, Environment Protection, Conservation and Protection, Report EPS 2/AG/1, Ottawa, Canada.

14. Canadian Council of Resource and Environment Ministers (CCREM), (1987), Canadian Water Quality Guidelines, Prepared by the Task Force on Water Quality Guidelines of CCREM, Ottawa, Ontario, Canada

15. Tchobanoglous, G. and Schroeder, E.D., (1985), Water Quality, Addison-Wesley Publishing Company, Reading, Massachusetts.

16. Pontius, F.W. (ed.), (1990), Water Quality and Treatment, A handbook of Community Water Supplies, 4th Edition, American Water Works Association, McGraw-Hill, Inc., Toronto.

17. Haque, K. E., Mackinnon, D.J., (1996), The Halide Mediated Electro-oxidation of Ammonia, Cyanide, Cyanate and Thiocyanate in Mine/Mill Waste Waters, Bulletin of CIM, Ottawa, Canada, 89(1), pp.104-106.

18. Prosser, J.I.(ed.), (1986), Nitrification, IRL Press Limited, Oxford, England, pp.185-207.

19. Delwiche, C.C.(ed.), (1981), Denitrification, Nitrification, and Atomospheric Nitrous Oxide, John Wiley & Sons, New York, pp.105-125.

20. Payne, W.J., (1981), Denitrification, John Wiley & Sons, New York, pp. 17-32, 162-172.

21. Metcalf & Eddy, Inc., (1972), Wastewater Engineering, Collection, Treatment, Disposal, McGraw-Hill Book Company, New York, pp.662-668.

22. Lin, S.H. and Wu, C.L., (1996), Removal of Nitrogenous Compounds from Aqueous Solution by Ozonation and Ion Exchange, Water Research, 30(8), pp. 1851-1857.

23. Paller, M.H., (1987)The Use of Ozone and Fluidized Biofilters for Water Reuse in Aquaculture, Ph. D thesis, Southern Illinois University at Carbondale, U.S.A.

24. Preston, K. T., (1992), Co-Immobilization of Nitrifying Bacteria and Clinoptilolite, Ph. D Thesis, Purdue University, U.S.A.

25. Doede, C.M. and Walker, C.A., (1955), Photochemical Engineering, Chemical Engineering, 62, pp.159-178.

26. Smith, J.M., (1967), Reactor Design for Photochemical Systems, Lecture Notes delivered under the Sir A. L. Mudaliar Endowment Lectures in Technology at A.C. College of Technology.

27. Mulin, C.R., (1968), Kirk-Othmer Encyclopedia of Chemical Technology, Wiley-Interscience, New York, pp. 331-354.

28. Phillips R., (1983), Sources and Applications of Ultraviolet Radiation, Academic Press Inc. (London) Ltd, London, England.

29. Wayne, R.P., (1988), Principles and Applications of Photochemistry, Oxford University Press, Oxford, England.

30. Harano, Y. and Matsuura, T., (1972), Problems in Designing photochemical Reactors, International Chemical Engineering, 12(1), pp.131-143.

31. Lunak, S. and Sedlak, P., (1992), Photoinitiated Reactions of Hydrogen Peroxide in the Liquid Phase, Journal of Photochemistry and Photobiology, A: Chemistry, 68, pp 1-26.

32. Stefan, M. I., Hoy, A.R. and Bolton, J.R., (1996), Kinetics and Mechanism of the Degradation and Mineralization of Acetone in Dilute Aqueous Solution Sensitized by the UV Photolysis of Hydrogen Peroxide, Environmental Science & Technology, 30(7), pp. 2382-2390.

33. Ogata, Y., Tomizawa, K. and Adachi, K., (1981), Photo-Oxidation of Ammonia with Aqueous Hydrogen Peroxide, Mem. Fac. Eng. Nagoya Univ., 33, pp. 53-65.

34. Yang, X, (1998), Advanced Photo-Oxidation Process For Ammonia Removal From Industrial Wastewater, Masters Thesis, Carleton University, Canada

35. Wang, A., (1991), Photoassisted Oxidation of Aqueous Ammonia with or without Iron-Doped Titanium Dioxide, Masters Thesis, The University of Toledo, Canada

36. Haque, K.E., (1991), Oxidation of Ammonia, Report MSL 91-50(LS), Mineral Sciences Laboratories Division, CANMET, Ottawa, Canada.

37. Rollefson, G. K. and Burton, M., (1939), Photochemistry and the Mechanism of Chemical Reactions, Prentice-Hall, Inc., New York, pp.151-164, pp.181-185.

38. Jolly, W. L., (1964) The Inorganic Chemistry of Nitrogen, W.A. Berjamin, Inc., New York.

39. Glaze, W.H., Kang, J.W. and Chapin, D.H., (1987), The Chemistry of Water Treatment Processes Involving Ozone, Hydrogen Peroxide and Ultraviolet Radiation, Ozone Science & Engineering, 9, pp. 335-552.

40. Neta, P., Maruthamuthu, P., Carton, P.M. and Fessenden, R.W, (1978), Formation and Reactivity of the Amino Radical, The Journal of Physical Chemistry, 82(17), 1875-1878.

41. Okabe, H., (1978), Photochemistry of Small Molecules, John Wiley & Sons, Inc., New York.

42. Fischer, M., (1978), Industrial Applications of Photochemical Syntheses, Angew. Chem. Int. Ed. Engl., 17, pp.16-26.

43. Soroush, M. and Kravaris, C., (1993), Optimal Design and Operation of Batch Reactors. 1. Theoretical Framework, Ind. Eng. Chem. Res., 32, pp.866-881.

44. Roger, M. and Villermaux, J., (1975), Light Distribution in Cylindrical Photoreactors, AIChE Journal, 21(6), pp. 1207-1209.

45. Levenspiel O., (1972), Chemical Reaction Engineering, 2nd Edition, John Wiley & Sons, New York.

46. Cassano, A.E., Silveston, P.L., Smith, J.M., (1967), Photochemical Reaction Engineering, Industrial And Engineering Chemistry, 59(1), pp. 19-38.

47. Tournier, A., Deglise, X., Andre., J.C. and Niclause, M., 0(1982), Experimental Determination of the Light Distribution in a Photochemical Reactor, AIChE Journal, 28(1), pp.156-166.

48. Harris, P.R. and Dranoff, J.S., (1965), A Study of Perfectly Mixed Photochemical Reactors, A.I.Ch.E Journal, 11(3), pp.497-502.

49. Jacob, S. M. and Dranoff, J.S., (1968), Design and Analysis of Perfectly Mixed Photochemical Reactors, Chemical Enigeering Progress Symposium Series, 64(89), pp. 54-63.

50. Dworkin, D. and Dranoff, J. S., (1978), Free Radical Transport in a Photochemical Reactor, AIChE Journal, 24(6), pp. 1134-1137.

51. Isaacson, W. B. and Ting, S. T., (1970), Versatile Constant Transmission Photochemical Reactor, I&EC Fundamentals, 9(1), pp. 171-173

52. Wolfrum, E.J., Ollis, D.F., Lim, P.K. and Fox, M.A., (1994), The UV-H2O2 Process: Quantitative EPR Determination of Radical Concentrations, Journal of Photochemistry and Photobiology, A: Chemistry, 78, pp. 259-265.

53. Calgon Carbon Corporation, (1999), Document #E800019.

54. Calgon Carbon Corportation, The AOT Handbook.

55. Cerda, A., Oms, M.T. and Cerda, V., (1996), Speciation of Nitrogen in Wastewater by Flow Injection, The Analyst, 121(1), pp. 13-17.

56. Greenberg, A.E., Clesceri, L.S. and Eaton, A.D., (1992), Standard Methods for the Examination of Water and Wastewater, American Public Health Assoication.

57. Fishbein, W.N., (1967), Determination of Hydroxylamine with Nessler reagent, Anal. Chem. Acta., 37, pp. 484-489.

58. Vogel, A.I., (1961), A Textbook of Quantitative Inorganic Analysis, John Wiley and Sons Inc., New York, pp. 325-326.

59. Kolthoff, I.M., Sandell, E.B., Meehan, E.J. and Bruckenstein, S., (1969), Quantitative Chemical Analysis, The Macmillan Co., Collier-Macmillan Ltd., London, U.K.

60. Streuli, C.A. and Averell, P.R., (1970), The Analytical Chemistry of Nitrogen and Its Compounds, John Wiley & Sons, Inc., New York.

61. Adams, V.D., (1990), Water and Wastewater Examination Manual, Lewis Publishers, Inc., New York.

62. Weiss, J., (1995), Ion Chromatography, VCH Publishers, Inc., New York, pp. 348 – 361.

63. Varian Company, (1981), Operational Manuals for Vista 6000 Series of Varian Gas Chromatography.

64. Chromatographic Specialties Inc., (1998), Instruction for Column Conditioning for Teflon Column Packed with Porapak Q.

65. Gastec Corporation, (1998), Gastec Nitrogen Oxides Detector Tube, (No. 11 L), Operational Manual.

66. Gould, W.D., Bedard, P., Koren, D. W. and Liang, D., (1992), Removal of Ammonium and Nitrate from Mine Effluent by Sequential Nitrification/Denitrification, Report MSL 92-79(IR), Mineral Sciences Laboratories Division, CANMET, Ottawa, Canada.

67. Sridhar, S., X.Yang, Gould, W.D. and Malaiyandi, M., (1998), Combined Photolytic-Biological Process for Nitrification-Denitrification of Industrial Effluent, in Lu, G.Q., Rudolph, V. and Greenfild, P.F.(eds.), Sustainable Energy and Environmental Technologies-Challenges and Opportunies, Published by The University of Queensland, Brisbane, Australia, pp.259-268.

68. Murov, S. L., Carmichael, I. and Hug, G.L., (1993), Handbool of Photochemistry, Marcel Dekker, Inc., New York.

69. Sridhar, S., (1996), Research Report in Support of ESTAC Proposal, Department of Civil and Environmental Engineering, Carleton University.

70. http://everyday.physics.lsa.umich.edu/106/content/emspectrum/spectrum.html

71. http://www.phs.uiuc.edu/~dbrady/ece469/notes/spectrum.html

72. http://www.h2o2.com/intro/properties.html

73. http://www.jtbaker.com/msds/p6027.htm

74. http://triadsci.com/lamps_uv.html

75. http://www.thekrib.com/TankHardware/glass.html

Appendix A

Fundamental physical constants in photochemistry [29]

Constant	Symbol	Value
Avogadro's number	N	6.022×10^{23} mol^{-1}
Boltzmann constant	k	1.38×10^{-23} $J.K^{-1}$
Charge of electron	e	1.60×10^{-19} C
Gas constant	R	8.31 $J.mol^{-1}.K^{-1}$
Mass of electron at rest	m	9.11×10^{-31} kg
Planck's constant	h	6.63×10^{-34} J.s
Speed of light in vacuum	c	2.998×10^{8} $m.s^{-1}$

Appendix B

Conversion table for energy units [68]

	kJ.mol^{-1}	cm^{-1}	Hz	eV	kcal.mol^{-1}
1 kJ.mol^{-1} =	1	83.593	2.5061×10^{12}	1.0364×10^{-2}	2.3901×10^{-1}
1 cm^{-1} =	1.1963×10^{-2}	1	2.9979×10^{10}	1.2398×10^{-4}	2.8592×10^{-3}
1 Hz =	3.9903×10^{-13}	3.3356×10^{-11}	1	4.1357×10^{-15}	9.5371×10^{-14}
1 eV =	96.488	8065.5	2.4180×10^{14}	1	23.061
1 kcal.mol^{-1} =	4.1840	349.75	1.0485×10^{13}	4.3363×10^{-2}	1

Note: To get the wavelength, λ, of a photon which has an energy in the units shown in the table, it is easy to convert the wavelength either to wavenumber ($\bar{\nu}$ in cm^{-1}) or frequency (ν in Hz) and then use the following equation

$$\lambda = \frac{1}{\bar{\nu}} = \frac{c}{\nu} = \frac{hc}{E}$$

Appendix C

Input voltage = 250 V, input current = 3.8 A, pH = 10, the cylinder rotation speed = 7.5 rpm (Hanovia lamp)

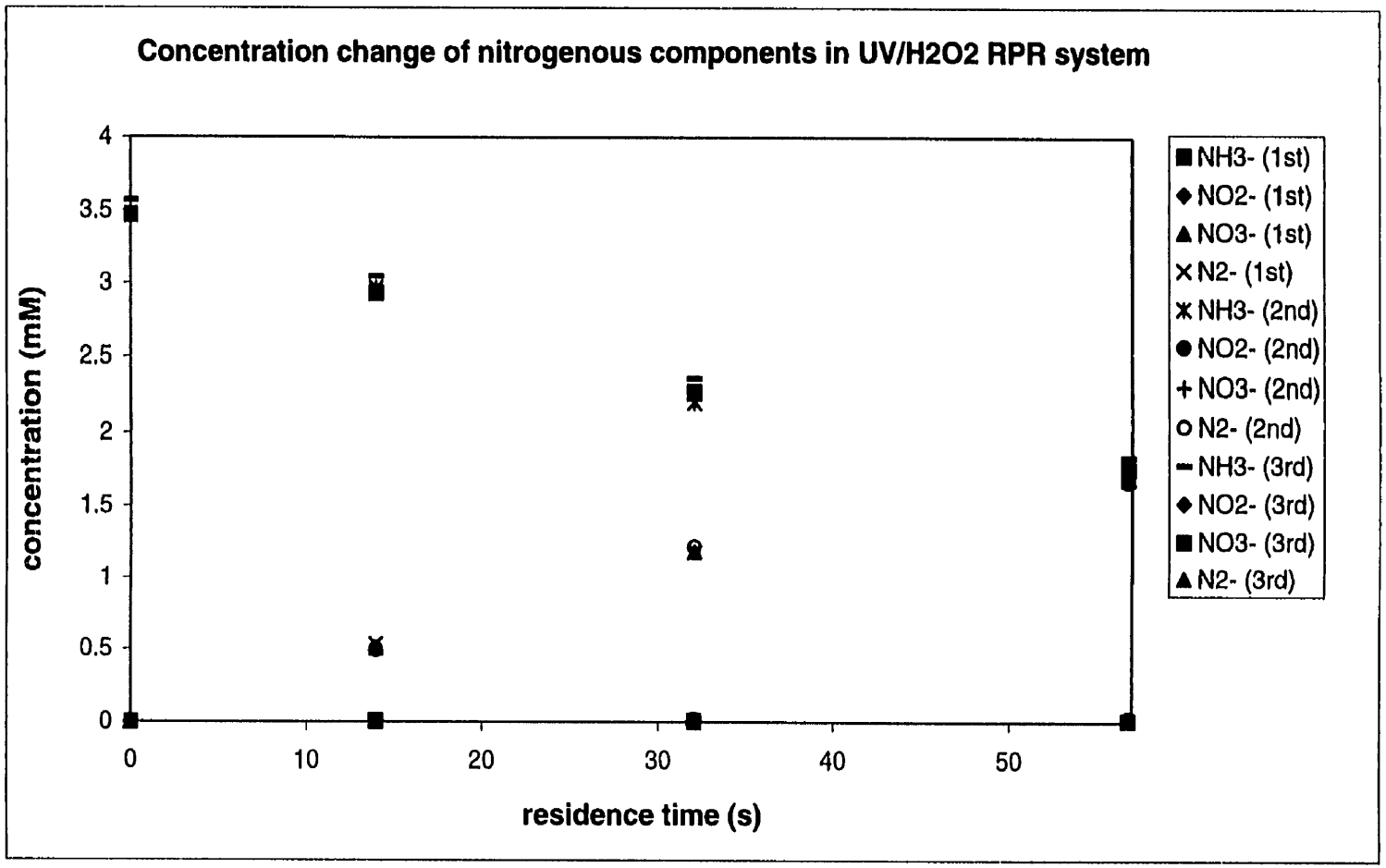

Appendix D

Input voltage = 250 V, input current = 3.8 A, pH = 10, the cylinder rotation speed = 7.5 rpm (Hanovia lamp)

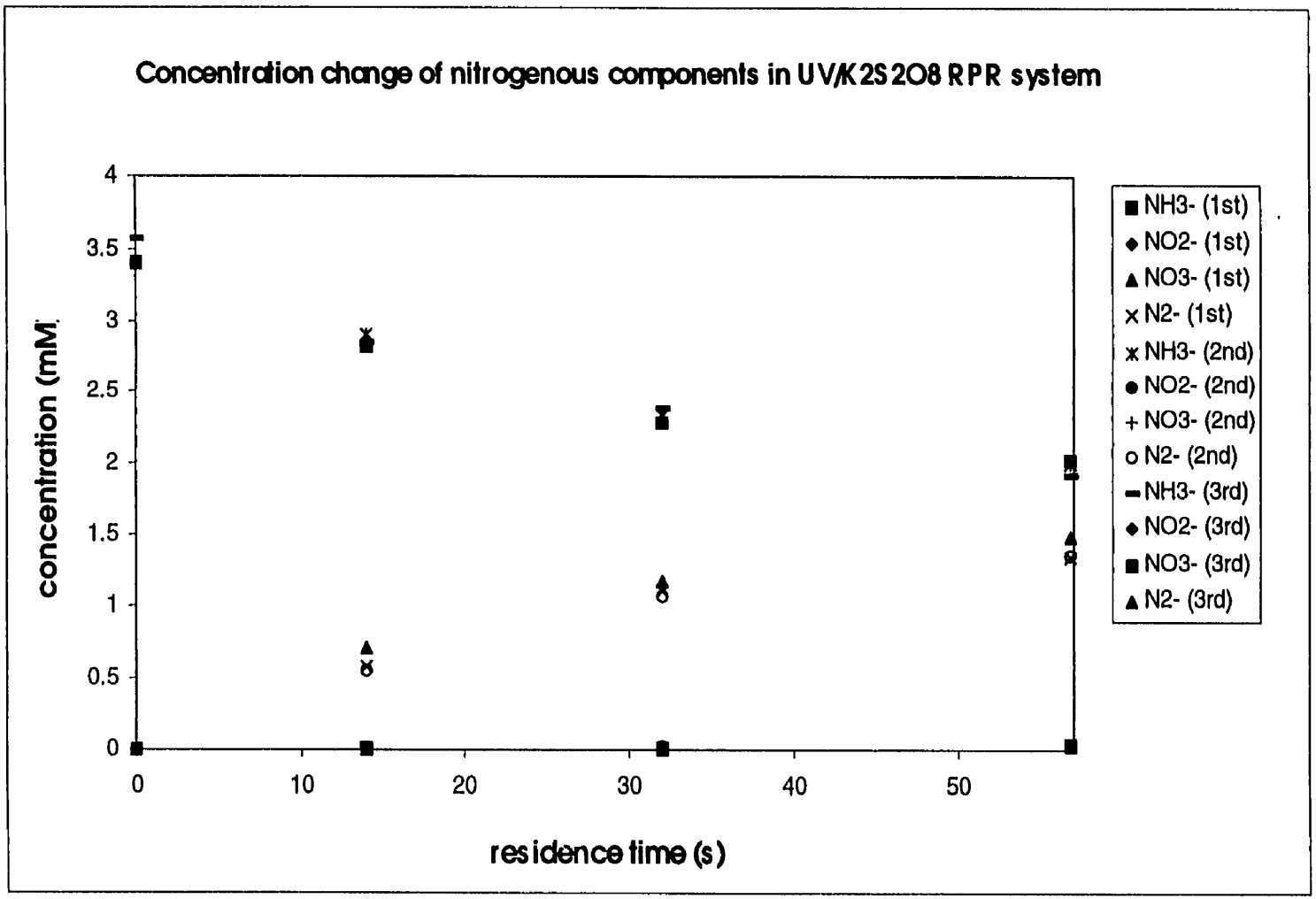

Appendix E

Sample calculation (e.g., Table 6.5, nitrogen concentration of different species after half an hour in UV/$K_2S_2O_8$ recirculation system)

Ammonia nitrogen

The experimental data obtained in ammonia nitrogen determination by colorimetric analysis are shown in the second and third columns of Table E.1.

Table E.1 Experimental data in ammonia nitrogen determination

Solution type	Absorbance	NH_3-N (mg/L)	NH_3-N (mM)
Standard	0	0	-
Standard	0.245	1	-
Standard	0.523	2	-
Standard	0.769	3	-
Sample	0.174	0.69	1.23

Calibration curve is obtained by plotting the absorbance of standard solutions versus their concentrations, which is shown in Figure E.1. The least-squares method is applied to the experimental data by using Microsoft Excel software. r^2 is also given directly by the Excel software, which is 0.9994. Therefore giving the absorbance of the sample solution as 0.174, the concentration of ammonia nitrogen is 0.69 mg/L from the

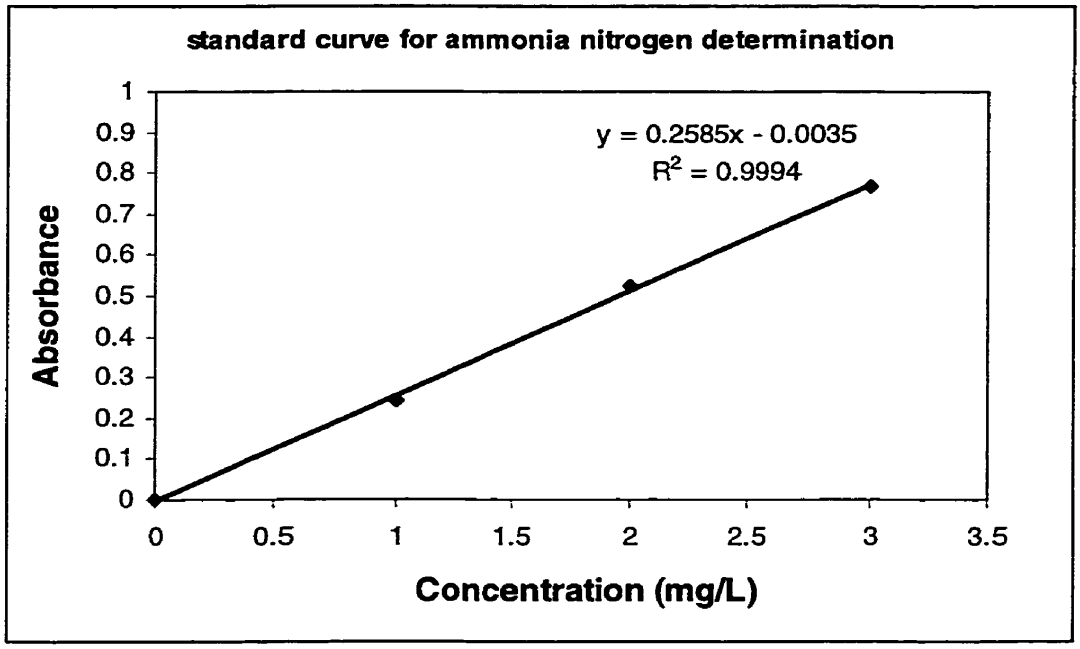

Figure E.1 Standard curve for ammonia nitrogen determination

calibration curve. Because the sample is diluted 25 times, the original concentration of ammonia is $0.69 \times 25 = 17.25$ mg/L, which is equal to $17.25/14 = 1.23$ mM.

Nitrite nitrogen

The experimental data obtained in nitrite determination by ion chromatographic analysis are shown in the second and third columns of Table E.2.

Table E.2 Experimental data in nitrite determination

Solution type	Peak area	NO_2 (mg/L)	NO_2-N (mM)
Standard	945275	1	-
Standard	3416217	5	-
Standard	6882236	10	-
Standard	9882017	15	-
Sample	8687128	13.04	0.28

Calibration curve is obtained by plotting the peak area of standard solutions versus their concentrations, which is shown in Figure E.2. The least-squares method is applied to the experimental data by using Microsoft Excel software. r^2 is also given directly by the Excel software, which is 0.9992. Therefore giving the peak area of the sample solution as 8687128, the concentration of nitrite is 13.04 mg/L from the calibration curve. Because the concentration is in terms of nitrite, it has to be multiplied by a correction factor of 0.304 to convert into the concentration of nitrite nitrogen, which is 3.96 mg/L. Therefore the concentration of nitrite nitrogen in original sample is 3.96/14 = 0.28 mM.

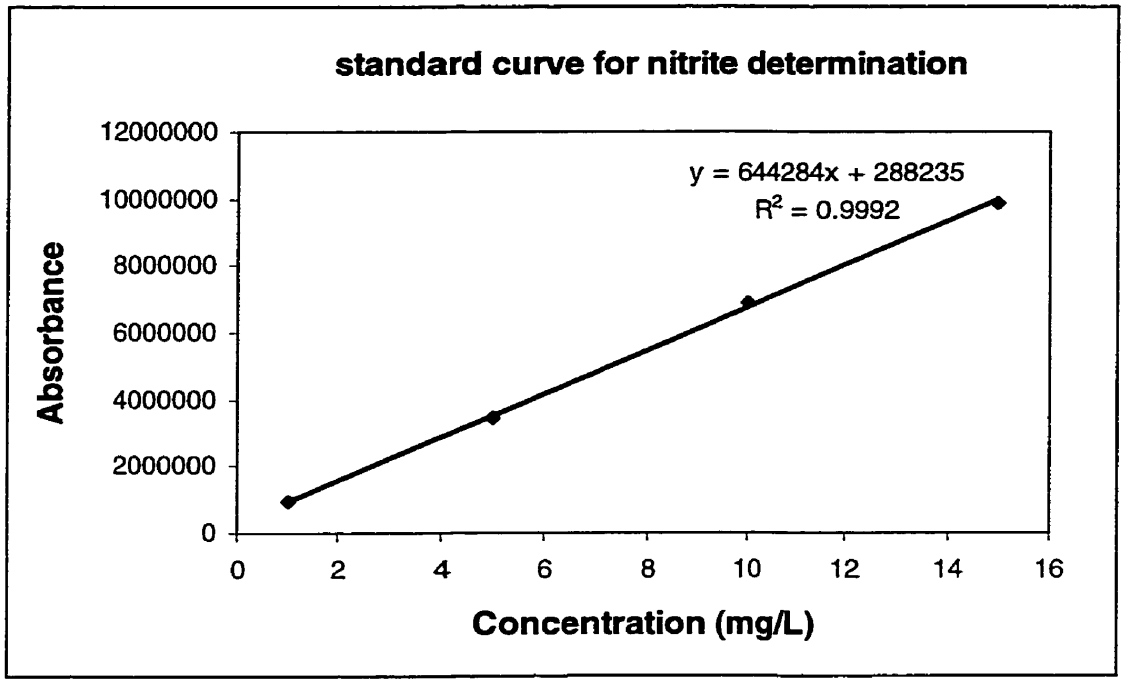

Figure E.2 Standard curve for nitrite determination

Nitrate nitrogen

The experimental data obtained in nitrate determination by ion chromatographic analysis are shown in the second and third columns of Table E.3.

Table E.3 Experimental data in nitrate determination

Solution type	Peak area	NO_3 (mg/L)	NO_3-N (mM)
Standard	503285	1	-
Standard	2831525	5	-
Standard	6101149	10	-
Standard	9466975	15	-
Sample	5439130	8.86	1.43

Calibration curve is obtained by plotting the peak area of standard solution versus their concentrations, which is shown in Figure E.3. The least-squares method is applied to the experimental data by using Microsoft Excel software. r^2 is also given directly by the Excel software, which is 0.9991. Therefore giving the peak area of the sample solution as 5439130, the concentration of nitrate is 8.86 mg/L from the calibration curve. Because the concentration is in terms of nitrate, it has to be multiplied by a correction factor of 0.226 to convert into the concentration of nitrate nitrogen, which is 2.0 mg/L. The sample has been diluted 10 times, therefore the concentration of nitrite nitrogen in original sample is 2.0×10/14 = 1.43 mM.

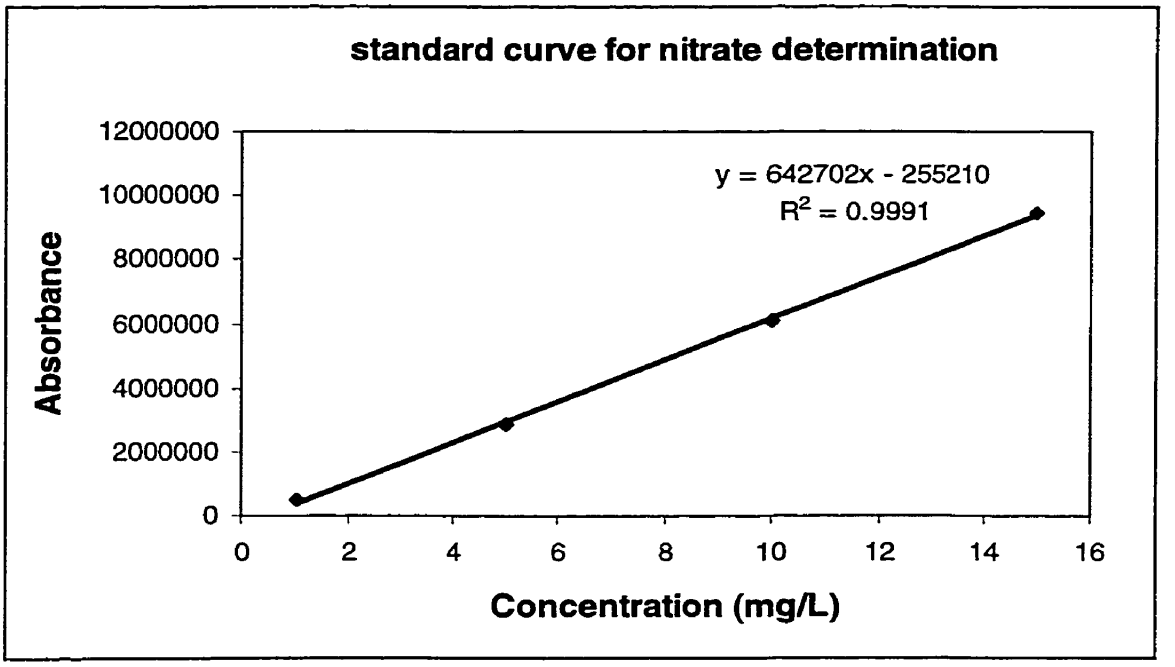

Figure E.3 Standard curve for nitrate determination

Nitrous oxide

Nitrous oxide is measured by gas chromatographic analysis. Experimental data are shown in the second and third columns of Table E.4.

Table E.4 Experimental data in nitrous oxide determination

Solution type	Peak area	N_2O-N (%)	N_2O-N (mM)
Standard	10995.33	0.5	-
Standard	28046.33	1	-
Standard	44909.33	1.5	-
Standard	63424.5	2	-
Sample	0	0	0

Calibration curve is obtained by plotting the peak area of standard gases versus their volumetric concentrations (%), which is shown in Figure E.4. The least-squares method is applied to the experimental data by using Microsoft Excel software. r^2 is also given directly by the Excel software, which is 0.9995. Therefore giving the peak area of the sample gas as 0, the concentration of nitrous oxide is 0% from the calibration curve. Although the gas phase was routinely tested, nitrous oxide nitrogen was never detected for any of the experimental runs.

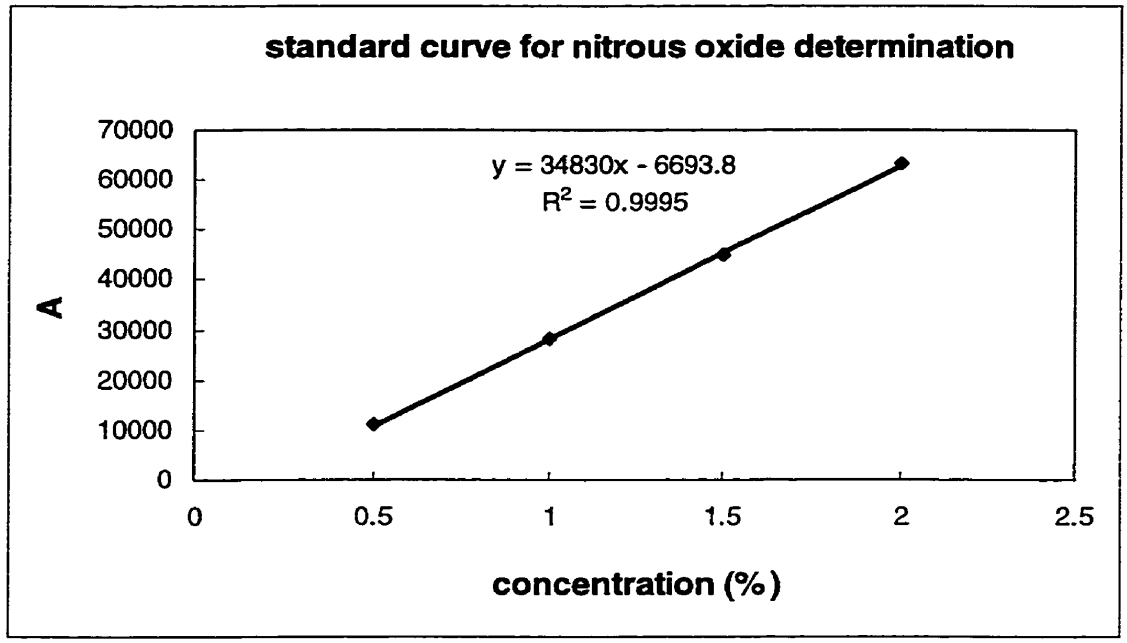

Figure E.4 Standard curve for nitrous oxide determination

Nitric oxide and nitrogen dioxide

Nitric oxide and nitrogen dioxide is measured directly by Gastec Detector Tube in which the concentration is detected in the form of nitrogen dioxide as mg/L. The experimental data is 3.04 mg/L, which is equal to 0.066 mM/L nitrogen in the form of nitrogen dioxide. Because the total volume of gas inside the photoreactor is 10 L, the total amount of nitrogen in the form of nitrogen dioxide is 0.66 mM. Assuming that this amount of nitrogen in gas comes from the photooxidation reaction in aqueous solution (60 L), the corresponding concentration of nitrogen in aqueous solution is 0.66/60 = 0.011 mM.

Nitrogen

The concentration of nitrogen is calculated by the mass balance of nitrogenous compounds, which is 3.64-1.23-0.28-1.43-0.011 = 0.7 mM.